Molecular chaperone regulation in the cellular stress response of proliferating and senescent human mesenchymal stem cells

Jack Llewellyn

A thesis submitted to The University of Manchester for the degree of Doctor of Philosophy in the Faculty of Biology, Medicine and Health

The University of Manchester

Division of Cell Matrix Biology and Regenerative Medicine
School of Biological Sciences
Faculty of Biology, Medicine and Health

2021

Mitigating circumstances

Product recall

An immunostaining study of the post-translational modification of the elongation initiation factor EIF2α in proliferating and senescent cells was carried out, with the results intended to be presented and discussed in Section 3.2. In October 2020 - after the conclusion of this experiment - the following correspondence was received from the manufacturer of the phospho-EIF2α antibody used:

> Your Order ID is: 3559501
>
> We are contacting you because we have very recently reviewed our information on Recombinant Anti-EIF2S1 (phospho S51) antibody [E90] (ab32157) which you had previously purchased from us.
>
> Recent retests of ab32157 have showed that this antibody shows unspecific signal in ICC/IF, therefore we have concluded that this product is unsuitable to be used for ICC/IF and Flow cytometry. We will be happy to send the test results if requested.
>
> [...]
>
> Best regards, Alexandru Mandrut, MSci Biology Scientific Support Specialist www.abcam.com

As a result, the data from this experiment is omitted.

Contents

Word count: 39,280

List of abbreviations

AA amino acid.

ADP adenosine diphosphate.

ALS amyotrophic lateral sclerosis.

ATP adenosine triphosphate.

BAG BCL-2-associated athanogene.

CCT chaperonin-containing tailless [complex].

cDNA complementary deoxyribonucleic acid.

CHIP carboxyl-terminus of HSP70-interacting protein.

DAPI 4',6-diamidino-2-phenylindole.

DDE delay differential equation.

DMEM Dulbecco's Modified Eagle Medium.

DMSO dimethyl sulphoxide.

DNA deoxyribonucleic acid.

DTT dithiothreitol.

ECM extracellular matrix.

EDTA ethylenediaminetetraacetic acid.

EIF2α elongation initiation factor.

EP early-passage.

ER endoplasmic reticulum.

FDR [Benjamini-Hochberg] false discovery rate.

hBM-MSCs primary human mesenchymal stem cells derived from bone marrow.

HEK 293 human embryonic kidney-293 cells.

HK housekeeping.

hMSCs human mesenchymal stem cells.

HSE heat shock element.

HSF1 heat shock transcription factor 1.

HSP heat shock protein.

IF immunofluorescence.

IMS industrial methylated spirit.

kDa kiloDalton.

LP late-passage.

MCF-7 Michigan Cancer Foundation-7 [cell line].

MDA-MB-231 M.D. Anderson metastatic breast cancer [cell line].

MEF mouse embryonic fibroblast.

MFP misfolded protein.

mRNA messenger ribonucleic acid.

MS mass spectrometry.

MSCs mesenchymal stem cells.

ODE ordinary differential equation.

PBS phosphate buffered saline.

PCA principal component analysis.

PES 2-phenylethynesulfonamide.

PMCC Pearson product-moment correlation coefficient ("Pearson's r").

PN proteostasis network.

PPI protein-protein interaction.

PTM post-translational modification.

RNA ribonucleic acid.

RNA-seq ribonucleic acid sequencing.

rRNA ribosomal ribonucleic acid.

RT recovery time.

RT-qPCR reverse transcription quantitative polymerase chain reaction.

SASP senescence-associated secretory phenotype.

sHSP small heat shock protein.

SILAC stable-isotope labelling by amino acids in cell culture.

siRNA short/small interfering RNA.

SSE sum of squared errors.

TCTP tissue culture treated plastic.

TPR tetratricopeptide repeat.

UPS ubiquitin-proteasome system.

List of Figures

List of Tables

Abstract

Cells respond to stress by up-regulating chaperone proteins that correct protein misfolding to maintain function. However, protein homeostasis is lost in ageing, leading to aggregates characteristic of protein-folding diseases. While much is known about how these diseases progress, discovering what causes protein-folding to deteriorate could be key to their prevention. Studying ageing in humans introduces a key temporal obstacle, however results in model organisms suggest ageing has cellular origins.

In this work, primary human mesenchymal stem cells (hMSCs) have been cultured to a point of replicative senescence and subjected to proteotoxic stress, as an *in vitro* model to investigate changes to the stress response during cellular ageing. Through -omic analyses it has been shown that the maintenance of protein homeostasis deteriorated in senescent cells through the attenuation of processes downstream of chaperone transcription. This was coincident with lowered levels of a functional module of chaperone proteins associated with stress-inducible heat shock protein 70 kDa (HSPA1A). Further analysis of the temporal dynamics of the transcriptomic and proteomic stress responses revealed a lack of translational capacity to be a limiting factor in the ability of senescent cells to mitigate proteotoxic stress, leading to a loss of speed, magnitude, and efficacy of the cellular stress response.

Furthermore, here it has been shown that senescent cells experience partial loss of the E3 ubiquitin ligase CHIP. CHIP is known to regulate HSPA1A stability during stress and cooperates with the chaperone to mark misfolded proteins for turnover. By building a mathematical model of the proteotoxic stress response, *in silico* simulations have predicted that a decrease in cellular CHIP leads to a greater accumulation of misfolded proteins during proteotoxic stress. Using a cysteine-reactive label which binds to residues typically buried in correctly folded proteins, this prediction has been validated by showing significant conformational compromise to the proteomes of senescent cells in response to stress, whereas no perturbation was seen in proliferating cell populations. Prime among the conformationally compromised proteins in senescent cells were several cytoskeletal proteins. Here it has been shown that this is likely due to the senescence-associated down-regulation of another functional module of chaperone proteins responsible for maintaining cytoskeletal protein homeostasis, the chaperonin-containing tailless (CCT) complex.

These results demonstrate multiple mechanisms which drive the attenuation of the proteotoxic stress response in cellular ageing. As such, these represent a step forward in our understanding of the underlying link between ageing and a loss of protein homeostasis. Given the therapeutic potential of hMSCs, this work also holds relevance to the emerging field of regenerative medicine. In this context, this study gives a comprehensive evaluation of consequential, but often neglected, changes to the hMSC stress response following extended culture *in vitro*.

Declaration and copyright statement

No portion of the work referred to in the thesis has been submitted in support of an application for another degree or qualification of this or any other university or other institute of learning.

The author of this thesis (including any appendices and/or schedules to this thesis) owns certain copyright or related rights in it (the "Copyright") and s/he has given The University of Manchester certain rights to use such Copyright, including for administrative purposes.

Copies of this thesis, either in full or in extracts and whether in hard or electronic copy, may be made only in accordance with the Copyright, Designs and Patents Act 1988 (as amended) and regulations issued under it or, where appropriate, in accordance with licensing agreements which the University has from time to time. This page must form part of any such copies made.

The ownership of certain Copyright, patents, designs, trademarks and other intellectual property (the "Intellectual Property") and any reproductions of copyright works in the thesis, for example graphs and tables ("Reproductions"), which may be described in this thesis, may not be owned by the author and may be owned by third parties. Such Intellectual Property and Reproductions cannot and must not be made available for use without the prior written permission of the owner(s) of the relevant Intellectual Property and/or Reproductions.

Further information on the conditions under which disclosure, publication and commercialisation of this thesis, the Copyright and any Intellectual Property and/or Reproductions described in it may take place is available in the University IP Policy (see http://documents.manchester.ac.uk/DocuInfo.aspx?DocID=24420), in any relevant Thesis restriction declarations deposited in the University Library, The University Library's regulations (see http://www.library.manchester.ac.uk/about/regulations/) and in The University's policy on Presentation of Theses.

Acknowledgements

Without the advice, support, and obstinate enthusiasm of dedicated supervisors; without the guidance of inexplicably patient mentors who were willing to give time they didn't have; without proof-readers, cake-bakers, and tea-makers, this project would not have been possible. So thanks go to Dr. Joe Swift and Prof. Simon Hubbard; Drs. Hamish Gilbert, Oana Dobre, and Venk Mallikarjun; Alis, Anna, Bel, Ellie, Matt, Melissa, and Rob. I would also like to thank my parents, without whose nagging this thesis would not have been completed on schedule; and my friends Isaac, Lizzie, and Maddie, without whose comic relief this thesis would have been completed much earlier.

Feedback throughout this project has been invaluable, and for that I am grateful to the WTQBB cohort and to all members, past and present, of the Brennan, Gilmore, Hubbard, Swift, and Uçar labs. I would also like to acknowledge the help and expertise of the Bioimaging, Bioinformatics, Biological mass spectrometry, and Genomic technologies core facilities. Additional thanks go to Mr. Mobeen Ismail of Trafford General Hospital (TH) and Prof. Tim Broad of Wrightington Hospital (WH) for the provision of human tissue samples for bone marrow-derived mesenchymal stem cell isolation. Finally, I would like to acknowledge the funding body, the Wellcome Trust, who supported this project financially.

Chapter 1

Introduction

1.1 Overview

Proteins are molecular machines required for cell and tissue function, providing structure and performing vital transport, signalling and enzymatic roles. The proteins expressed by cells, or *proteome*, must be actively regulated to match functional demands and address challenges – a state of protein homeostasis (*proteostasis*). This ensures that proteins are correctly folded, present in the right locations at the appropriate concentrations, and with any necessary post-translational modifications (Balchin et al., 2016; Sala et al., 2017). Due to its importance, proteostasis is safeguarded by a coordinated proteostasis network (PN) that executes several functions: molecular chaperones assist in the folding of newly-synthesised proteins and resolve misfolding events as part of the cellular stress response; and protein degradation machinery allows misfolded or surplus proteins to be removed or recycled. Dysregulation of the PN is a recognised consequence of ageing (Hipp et al., 2019; Kaushik and Cuervo, 2015). Aged cells have decreased chaperone and proteasomal activity, and consequently accumulate oxidatively damaged and misfolded proteins (Koga et al., 2011). The detrimental effects of protein misfolding are two-fold: firstly, that loss of a protein's structure leads to loss of its function; and secondly, that misfolded proteins can form aggregates that are toxic to cells. Protein aggregation is characteristic of diseases such as Alzheimer's, Parkinson's and Huntington's – all disorders where age is considered a major risk factor (Hipp et al., 2014; Labbadia and Morimoto, 2015). Progress in the development of drugs to address diseases such as Alzheimer's has been slow (Cummings et al., 2014), but a better understanding of the PN may inform new therapeutic strategies.

The PN in human cells contains on the order of two thousand component proteins (Klaips et al., 2017). Within this group, ~ 300 chaperone and co-chaperone proteins are associated with protein folding and conformational maintenance (Brehme et al., 2014). Thermodynamically speaking, chaperone proteins function by guiding their unfolded client proteins through a free energy landscape – traversing partially-folded intermediate states at points of local energetic minima – to find the global energetic minimum associated with the native folded state. In mechanistic terms, this process requires that chaperones shield exposed hydrophobic regions of their partially-folded clients, thus preventing unwanted interactions (Hartl et al., 2011). Many proteins within the chaperone are classified as heat shock proteins (HSP) as they are ex-

pressed in response to heat as a prototypic form of stress, and grouped by molecular weight (kDa). Proteins within the HSP60, HSP70, HSP90 and HSP100 families have activity dependent on adenosine triphosphate (ATP) metabolism, whereas the small HSPs (sHSPs) are ATP-independent (Jayaraj et al., 2020). Chaperone function is further regulated by co-chaperone proteins, such as the tetratricopeptide repeat (TPR) proteins that assist the HSP90 system and the HSP40 family of proteins that increase the client-specificity of HSP70 chaperones (H. H. Kampinga & Craig, 2010).

More than one hundred genes related to the PN have been shown to be significantly suppressed with age in humans, including representatives of the chaperone network from HSP40, HSP70 and HSP90 families (Brehme et al., 2014). Correspondingly, chaperone-assisted protein folding and disaggregation processes have been demonstrated to deteriorate with ageing (Calderwood et al., 2009; Koga et al., 2011). The protective response to heat stress was found to deteriorate with ageing in *C. elegans*, concomitant with increased levels of protein unfolding (Ben-Zvi et al., 2009). In the same model, knockdown of heat shock transcription factor 1 (HSF1) – a transcription factor considered to be a master regulator of the heat shock response – was found to amplify age-associated loss of protein function, while its overexpression extended the maintenance of proteostasis and lengthened lifespan (Ben-Zvi et al., 2009; Hsu, 2003). In post-mitotic mouse tissues (heart, spleen, renal and cerebral cortices), basal levels of HSP70 protein were found to be decreased in aged vs. adult animals. Interestingly, however, adult levels of HSP70 were found to be maintained in naturally long-lived animals (Martínez de Toda et al., 2016).

Expression of HSP70 has also been shown to increase in mice during exercise, a response thought to protect against muscle damage; and overexpression of HSP70 reduced age-associated deterioration of muscle function (McArdle et al., 2004). A study of human-derived lymphoblasts has shown that the ability to increase levels of HSP70 gene expression in response to stress was generally decreased by ageing, but that the response was maintained in cells from exceptionally long-lived subjects (Ambra et al., 2004). Taken together, this evidence suggests that dysregulation of PN components with ageing is widely conserved, that age may affect both basal levels of HSPs and their ability to respond to stress, and that prolonged maintenance of proteostasis machinery may benefit both health and longevity. Nonetheless, a systematic survey of how the complex PN responds to stress, and how the response is affected by ageing, remains lacking – particularly in human cells and tissues.

Human ageing varies greatly between individuals due to genetic and environmental diversity, and therefore a lack of longitudinal ageing studies has limited our understanding of the process. Cellular senescence, such as achieved through replication of primary cells, has therefore often been used as an *in vitro* ageing model (Martinez Guimera et al., 2017). Senescence is a cellular response to irreparable DNA damage. To prevent propagation of potentially oncogenic damage the cell cycle is arrested and the cell marked for clearance. Changes to relative rates of cell damage, repair, clearance and renewal mean that aged tissues have disproportionately high numbers of senescent cells compared to young tissues (J. P. Magalhães and Passos, 2018; López-Otín et al., 2013). Senescent cells experience morphological changes, becoming larger, flatter, and more rounded (Biran et al., 2017; Son et al., 2019);

and have been reported to have decreased levels of HSPs (Deschênes-Simard et al., 2014), and lowered proteasomal (Saez & Vilchez, 2014) and mitochondrial activity (Martinez Guimera et al., 2017).

This study focuses on the response of primary human mesenchymal stem cells derived from bone marrow (hBM-MSCs) to heat stress. So-called due to their capacity for tri-lineage differentiation (Burrow et al., 2017), this cell type has been widely studied in the context of tissue engineering and regenerative medicine, with a range of applications currently subject to clinical trials (Pittenger et al., 2019). This study has important implications to this purpose because: (i) how ageing and/or serial expansion in culture impacts on hMSC behaviour is an important consideration when applying autologous treatment strategies to older patients; and, (ii) many medical applications of hMSCs will require that the cells be robust to stress e.g. in tissue repair (Richardson et al., 2016). Replicative senescence has been utilised in this work to model the effects of ageing, comparing early- and late-passage (EP and LP respectively) hMSCs from matched donors to maximise the statistical power of downstream analysis. A combination of proteomic, transcriptomic and imaging methods has been used to construct a systematic, time-resolved characterisation of how senescence affects the speed, magnitude and efficacy of the stress response. Furthermore, applying network and computational analyses has enabled better understanding of the complexity of the PN and modelling of the response to stress. This study reports on the senescence-induced decline of a functional module within the PN, centred around the activity of a heat-inducible protein within the heat shock protein 70 kDa family (the HSPA1A gene product) and attributes a weakening of the responsiveness to stress to depreciation of translational capacity. In summary, this investigation into the nature and cause of the decline of the heat shock response in senescent hMSCs provides mechanistic insight into how proteostasis is lost, and offers a starting point for strategies that could recover it.

1.2 Background

In an ageing population developing treatments against age-associated diseases is imperative - Livingston et al., 2017 report that globally the number of people living with dementia is projected to increase 41% by 2030, and 179% by 2050. However, clinical trials aimed at treating protein-folding diseases have particularly poor success rates (Servick, 2019) - between 2002 and 2012, US clinical trials aimed at improving cognition among Alzheimer's patients had a 99.6% failure rate (Cummings et al., 2014). While inadequate models for studying protein folding diseases contribute to this figure, this also highlights a need to improve basic understanding of how protein folding goes awry during ageing (Becker et al., 2008; Anderson et al., 2017).

Cellular senescence and the loss of proteostasis are two key hallmarks of ageing (López-Otín et al., 2013), with the former linked with a loss of efficacy in certain regenerative medicines (Khan et al., 2011; J. Wang et al., 2013; Choudhery et al., 2014); and the latter seen as a common precursor for several age-associated protein-folding diseases, such as Alzheimer's (Brehme et al., 2014). *In vitro* and *in vivo* studies have shown organismal ageing has cellular origins (Dimri et al., 1995; Chon-

drogianni et al., 2003; Ogrodnik et al., 2017), however proteostasis in senescent cells is largely unexplored. This may have implications in emerging stem cell therapies. While it is well documented how donor age in autologous stem cell transplants can affect treatment outcomes, the mechanism behind this effect is unknown. Similarly, while the mode of action of protein-folding diseases is broadly understood, less is known about the underlying link between ageing and chronic protein misfolding.

1.3 Division of thesis

This thesis will focus on how the speed, magnitude, and efficacy of the cellular proteotoxic stress response - the cell's ability to resolve a sudden influx of protein-misfolding - is attenuated by senescence in hBM-MSCs. A combination of targeted, -omic, and mathematical approaches will be used to form a comprehensive analysis of how proteostasis is impaired by cell ageing.

The thesis has been divided into six chapters:

- **Chapter 1 - Introduction**
  The reader will be introduced to the thermodynamic concepts of protein folding in order to understand why proteins become misfolded, and the role molecular chaperones play in ensuring correct proteome function. The importance and different classes of molecular chaperones will be discussed, as well as how chaperone levels are regulated. The reader will be given a review of the literature concerning the cellular proteotoxic stress response, its interplay with ageing, and proposed mathematical models of the stress response. The value of senescent hMSCs as a model system will be discussed, including case studies of the use of MSCs in regenerative medicine. The aims of the PhD project will also be discussed.

- **Chapter 2 - Materials & methods**
  Full disclosure of all reagents, solutions, equipment, and software used in this study, including manufacturer and product-code/designer and version will be provided. Available information for hMSC donors is detailed and all methods used to obtain forthcoming results are described in full.

- **Chapter 3 - Results: The transcriptomic and proteomic profiles of proliferating and senescent human mesenchymal stem cells before and after stress**
  Biomarkers are used to verify the prevalence of senescent cells in late-passage populations. Transcriptome-wide data from ribonucleic acid sequencing (RNA-seq) will be analysed in tandem with proteome-wide data from label-free mass spectrometry (MS) to show large-scale changes in the profiles of senescent hMSCs compared to their early-passage counterparts. Evidence is presented that the stress response is predominantly post-transcriptional, and a pathway analysis shows late-passage hMSCs are subject to a pronounced reduction in protein translation capacity and in proteins associated with the stress response.

- **Chapter 4 - Results: A functional module based around HSP70 machinery becomes unresponsive to heat stress in senescent human mesenchymal stem cells**
  Tools from mathematical graph theory are used to show that the human chaperone protein network is divided into functional modules, and the stress response of early-passage cells consists of the up-regulation of the module containing the HSP70 machinery - a response which is absent in late-passage cells. Functional inhibition of this module demonstrates that the effects of dysfunctional HSP70 machinery are different in early- and late-passage populations. Immunofluorescence microscopy and reverse-transcription quantitative polymerase-chain-reaction techniques are used to investigate HSP70 dysregulation in senescent cells with higher temporal resolution. The reader will be shown how senescent cells are less able to up-regulate HSP70 protein during proteotoxic stress, and take much longer to return to equilibrium HSP70 transcript levels following stress.
- **Chapter 5 - Results: A mathematical model of early- and late-passage stress response dynamics and prediction of cellular "damage"**
  The case will be made to the reader that insufficient quantities of ribosomal proteins are a limiting factor in the senescent proteotoxic stress response. An ordinary/delay differential equation model of HSP70 regulation during the stress response is designed and fit to *in vitro* data from early-passage cells to challenge current perceptions concerning chaperone regulation in the stress response. Results from immunofluorescence imaging and label-free mass spectrometry will be used to dictate changes to the model to reflect HSP70 regulation in senescent cells. It will then be demonstrated to the reader that factoring in these changes enables the model to predict the *in vitro* kinetics of HSP70 in late-passage cells. The reader will be shown that the model predicts a greater stress-induced accretion of misfolded proteins in senescent cells, and this is verified using monobromobimane-labelling mass spectrometry to analyse changes in protein conformation.
- **Chapter 6 - Conclusions & future work**
  A review of main findings of this study and their impact. Achievement of the aforementioned aims of the study is evaluated, and areas for future research that would build on the findings of this study are discussed.

1.4 Thermodynamic protein folding

The vast majority of proteins need to fold into a well-defined, three-dimensional *native state* to attain functionality (Carver et al., 2003). Protein folding is crucial to the viability of cells and is linked to a broad range of biological processes (Mackenzie, 2017). Incorrect folding results not only in the loss of normal function, but often also in a gain of toxicity. Proteins fold or misfold in an attempt to minimise the *Gibbs free energy* of their local micro-environment, G - the maximum energy which can be reversibly extracted from a system:

$$G = H - TS, \tag{1.1}$$

where H is the enthalpy (a function of the internal energy of the system), T is the temperature, and S is the entropy (a measure of the 'disorder' in the system). Reactions occur spontaneously if they result in a decrease in the Gibbs free energy, i.e. $\Delta G < 0$. Following from Equation 1.1, at thermal equilibrium spontaneous reactions must satisfy

$$\Delta H - T\Delta S < 0. \tag{1.2}$$

Equation 1.2 tells us that favourable reactions at thermal equilibrium must either cause a decrease in enthalpy or an increase in entropy of a protein and its local micro-environment. During folding, proteins transition from an initial unfolded state with thousands of possible folding conformations (high disorder), to a final state with just one conformation (low disorder). This means, seemingly in violation of Equation 1.2, $\Delta S < 0$.

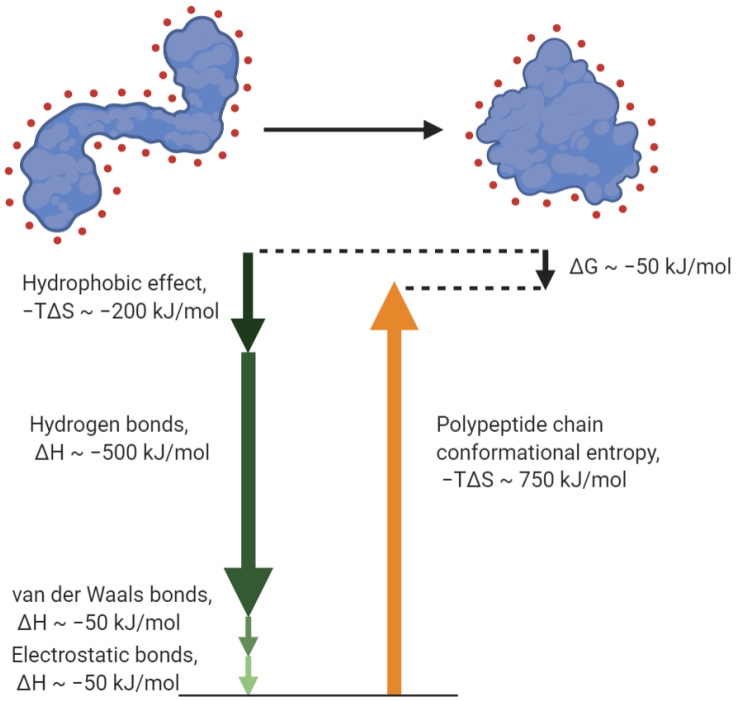

Figure 1.1: A thermodynamic perspective on protein folding. Proteins (blue) fold to form a hydrophobic core. Hydrophobic side chains become exposed to fewer water molecules (red) in the surrounding cytosol, causing the increase in entropy necessary to facilitate folding (top arrow, "hydrophobic effect"). Adapted with *BioRender* from Chou, 2008.

However, the exposed hydrophobic amino acid (AA) side chains of unfolded proteins have an 'ordering' effect on the surrounding cytosol. Water molecules will organise around proteins to minimise contact with the hydrophobic side chains. When these side chains are buried during folding, this ordering effect is removed, which causes an increase in entropy as illustrated in Figure 1.1. In addition, a number of different types of bonds are formed during folding, decreasing the enthalpy of the system (O'Connor & Adams, 2010). The AA sequence of a protein dictates the bonds which can form and thus guides folding conformations. Polar AAs capable

of forming hydrogen bonds, hydrophobic AAs are capable of forming van der Waals bonds, charged AAs are capable of forming electrostatic bonds, and cysteines alone are capable of forming covalent bonds which are much stronger than the previously mentioned ionic bonds. Together, these can offset the negative change in entropy due to the protein's conformational change, allowing protein folding to occur spontaneously (Petsko & Ringe, 2009).

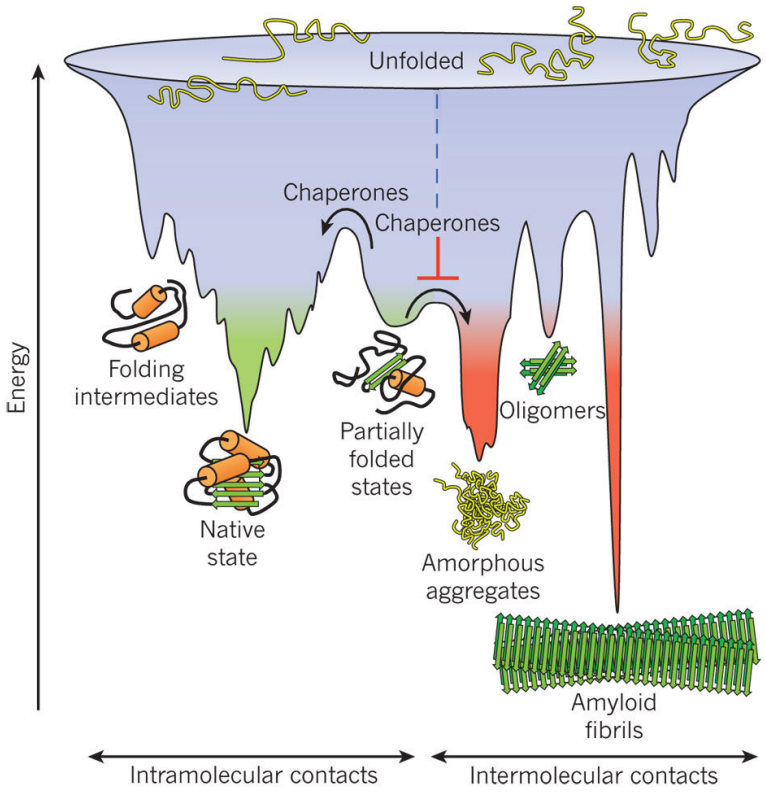

Figure 1.2: The Gibbs free energy surface traversed by proteins. Green regions represent states with proper function while red regions represent toxic folding conformations. From Hartl et al., 2011.

Proteins move through a Gibbs free energy landscape via folding, burying hydrophobic AA side chains within a three-dimensional structure. Proteins may either fold properly and move towards the native state, or they can misfold. Proteins misfold because it is energetically beneficial for them to do so, Figure 1.2 illustrates how a misfolded state with some side chains buried will still have a lower Gibbs free energy than an unfolded state (Hartl et al., 2011). The hydrophobic AA residues which stick out in misfolded proteins can then bind together with other misfolded proteins to form very stable, but toxic, protein aggregates.

Proteins typically fold quickly, transitioning through several folding intermediate states, taking in the range of µs to ms (Tanguay & Hightower, 2015). However, as proteins increase in size, the number of possible conformations increases exponentially and may push equilibrium away from the native state (Petsko & Ringe, 2009). The macromolecule-dense environment inside the cell ($\sim$200 g L^{-1}, Milo, 2013) can also make it difficult for proteins to fold correctly. Indeed, Dobson, 2003 discusses how aggregation begins even before synthesis is completed, with the polypeptide

chain unable to bury its hydrophobic regions until the entire chain leaves the ribosome. Even after reaching the native state, environmental or functional effects expose the hydrophobic regions of a protein and increase susceptibility to aggregation (Malyshev, 2013).

1.5 Molecular chaperones

Perturbations from tissue homeostasis inflict stresses upon cells which upset proteostasis. When cells are subjected to stress, proteins become unstable and their three-dimensional structure begins to break down. Human cells *in vivo* are subjected to multiple different stresses, including thermal, chemical, oxidative, and mechanical stresses, with each having distinct effects on cellular homeostasis and proteostasis. Cells in cardiac muscle tissue, for example, experience a large mechanical stress with every heartbeat, while cells experience thermal stress during febrile diseases, where core body temperature increases by up to 4°C (Evans et al., 2015).

To maintain proteostasis in the face of various cellular stresses, cells express *chaperone* proteins - so called as their function is to mediate proper folding. Chaperone proteins recognise and bind to the hydrophobic AA residues which protrude from misfolded proteins. Thus chaperones improve the efficiency of protein folding by providing a competing reaction to aggregation. Chaperones are also able to bind to folding intermediates, which are proteins stuck in local energy wells such as those illustrated in Figure 1.2. Chaperones change the organisation of the client protein, which 'restructures' their energy landscape, allowing them to fold properly and fall into the native state.

Previous analysis of chaperone workload in yeast by the Hubbard lab (Brownridge et al., 2013) estimates chaperones are responsible for mediating folding of over 60% of cellular proteins, with each individual chaperone responsible for 14-25 client molecules per minute. Work by Brehme et al., 2014 outlines the human chaperone network, consisting of 332 human genes that encode for chaperones or co-chaperones, collated using a combination of several literature sources and genomic databases. Functional classification of these reveals the human chaperone network consists of 88 chaperones and 244 co-chaperones.

1.5.1 The heat shock proteins

The suppression of global protein synthesis in response to stress is well-documented (as reviewed by Advani & Ivanov, 2019). This reduces the workload of molecular chaperones, and allows the cell to respond to stress through the focused synthesis of a particular family of chaperones - the heat shock proteins (HSPs), so named as they were found to increase in abundance following thermal stress. The various HSP subfamilies are identified by their molecular mass, in kDa.

1.5.2 The HSP70 family

Of particular importance is the HSP70 subfamily, which have been found to interact with over 30% of the proteome. Literature studies using the generic term "HSP70

protein" most often refer implicitly to the HSPA1A gene product HSP70α, also termed "stress-inducible HSP70" (for instance: Eftekharzadeh et al., 2019; Wu et al., 2020) - as will be the case in the present study. Other proteins in the HSP70 subfamily are generally given greater specification (for example: "heat shock cognate 70", HSPA8; "mitochondrial HSP70", HSPA9), however clarity in future studies would be beneficial to the field[1].

HSP70 proteins are ubiquitous in the cell and linked to a broad range of protein quality-control functions, including protein translocation, regulation of signalling, protein assembly, and disaggregation (Ryan and Pfanner, 2001; Pratt and Toft, 2003). The three-domain structure of HSP70 molecules includes an ATPase N-domain, which generates energy for folding activity through the hydrolysis of ATP; a substrate domain which is able to bind to hydrophobic residues of proteins; and a flexible C-domain which covers clients to protect against aggregation.

1.5.3 HSP70 co-chaperones

The HSP40 family

The efficiency of ATP hydrolysis by HSP70 is enhanced by members of the HSP40 family, which functions as the main co-chaperones to HSP70. Rather than the traditional chaperone family grouping based on molecular mass, members of the HSP40 family are classified by the presence of a structural J domain which is highly conserved and was first identified in the *Escherichia coli* protein DnaJ (41.1 kDa). As shown by Jiang et al., 2007, the structure of this J domain facilitates interaction with HSP70 family members. Also referred to as "J proteins" due to their wide range of molecular weights, the human HSP40 family consists of $\sim$50 proteins encoded by the DNAJ genes (Qiu et al., 2006). This by far outnumbers the human HSP70 family members, and H. H. Kampinga and Craig, 2010 argue that the diversity of HSP40 proteins drives the multifunctionality of HSP70 proteins. In support of this, Q. Liu et al., 2020 review the function of the ER resident HSP70 family member, HSPA5. This single HSP70 protein has been found to interact with seven different HSP40 family members, with the interaction partner dictating HSPA5 function between protein import, protein folding, and protein degradation.

GRPE proteins

In *Escherichia coli*, the protein GrpE was discovered to promote ADP-ATP exchange at the N-terminus of bacterial HSP70 (as reviewed by Bhandari and Houry, 2015) and is thus termed a nucleotide exchange factor. Bacterial GrpE is well-researched and has long been known to be stress inducible, with GrpE1 mutant strains up-regulating stress response proteins at equilibrium temperature (Straus et al., 1990, as reviewed by Roncarati and Scarlato, 2017). Despite its role in the bacterial

[1] As an example of the confusion this creates, W. Zhang et al., 2016 perform a study of the effect overexpression of HSPA1A has on rat BM-MSCs, while mistakenly referring to this as heat shock cognate 70, and base experiments on literature which uses other members of the HSP70 subfamily (including Hu, 2006, namely HSPA12B; Duffy et al., 2012, namely HSPA8; and Aisha et al., 2014, namely HSPA4), with the authors repeatedly referring to these as if they focus specifically on heat shock cognate 70 - in their case meaning stress inducible HSP70.

stress response, scarce research has been carried out on the mitochondrial GrpE homologs GRPEL1 and GRPEL2. Srivastava et al., 2017 were recently the first to demonstrate the additional GRPE protein GRPEL2 is upregulated in response to GRPEL1 (and *vice versa*) - providing an evolved buffering system in higher eukaryotes. The group also demonstrated that this buffering mechanism takes effect during stress. While GRPEL1 co-chaperone activity is higher than GRPEL2 during equilibrium conditions, GRPEL1 is down-regulated in response to stress, while GRPEL2 is stress-resistant and begins to dominate co-chaperone activity. Harrison, 2003 notes that, while human cells do not contain a ubiquitous homolog of GrpE, HSP70 nucleotide exchange factor function is instead provided in the ER by the SIL1 protein (K. T. Chung et al., 2002), and in the cytosol by the BAG co-chaperone family.

SIL1

A comprehensive review of SIL1 function was recently carried out by Ichhaporia and Hendershot, 2021, due to its role in Marinesco-Sjogren syndrome. The authors make an interesting observation by cross-referencing human protein Atlas data (Uhlen et al., 2015) with literature studies of loss of SIL1 nucleotide exchange factor function - finding that tissues with higher levels of SIL1 are not the most affected by the loss of function. The authors argue that this may indicate a further, undiscovered, function of SIL1 in human tissues requiring further investigation.

BAG proteins

The BCL-2-associated athanogene (BAG) family of proteins provide another mechanism by which cells regulate the chaperone network. Kabbage and Dickman, 2008 outline six ubiquitous BAG family members in humans: BAG1, 2, 3, 4, 5, and 6. BAG1 and BAG5 are well-known to bind to HSP70 (Brive et al., 2001; Arakawa et al., 2010) and stimulate ATP hydrolysis, providing a mechanism to negatively regulate HSP70 activity by releasing client proteins. BAG1 also binds to the proteasome to act as an 'adapter' to mediate the turnover of HSP70 client proteins (as reviewed by Fernández-Fernández et al., 2017). Another family member, BAG3, performs an analogous role in the autophagy pathway. BAG3 is the most studied member of the BAG family, as it plays a role in therapies for several diseases including cancers, myopathies, and neurodegenerative diseases (as reviewed by Behl, 2016). BAG3 gene expression is controlled by heat shock transcription factors, and is essential for growth, with Youn et al., 2008 observing 100% lethality of BAG3-knockout mice within 3 weeks of age.

Gamerdinger et al., 2009 have discovered the BAG proteins dynamically respond to stress through expression of BAG1 and BAG3. Turnover of misfolded proteins at homeostasis is mainly carried out by the ubiquitin-proteasome system (UPS), assisted by BAG1. However during stress or ageing, where the demand on the chaperone network increases, the expression of BAG1 significantly decreases, while the expression of BAG3 significantly increases - suggesting a switch from the proteasomal pathway to the autophagy pathway during stress.

HSPBP1

Finally, HSP70 binding protein 1 (HSPBP1) was first identified by Raynes and Guerriero, 1998 as an inhibitor of HSP70 chaperone activity, based on an experiment where HSPBP1 over-expression reduced HSP70 ATPase activity by 90%. Subsequent studies suggest this inhibitory effect is an artefact of HSPBP1 over-expression. At physiological levels, Shomura et al., 2005 showed that HSPBP1 binds transiently to HSP70 to facilitate ADP dissociation, and found that a deletion of the HSPBP1 ortholog in *S. cerevisiae* resulted in a 50% reduction in protein folding mediated by the yeast HSP70 family compared to wild-type.

Proteins which are unable to utilise the HSP70 chaperone machinery are instead folded by either the HSP60 or HSP90 machinery - depending on the nature of the client protein.

1.5.4 The HSP90 family

To increase the efficiency of protein folding inside the cell, many partially folded proteins which have failed to reach the native state through the HSP70 system are transferred to the HSP90 system (Y. E. Kim et al., 2013, Quintana-Gallardo et al., 2019). The HSP90 subfamily consists of two proteins, stress-inducible HSP90α and constitutively active HSP90β, encoded by genes HSP90AA1 and HSP90AB1, respectively. The HSP90 subfamily is ubiquitous in the cell, and - like HSP70 - is ATP-dependent. Schopf et al., 2017 emphasise the importance of the HSP90 machinery, which makes up 2-5% of cytosolic proteins under non-stressed conditions and mediates the folding of several hundred client proteins. However, HSP90 is selective of its clients. Verified client proteins have a broad range of cellular functions (Backe et al., 2020), but what determines whether a protein is a suitable client for HSP90 is yet to be defined.

1.5.5 Chaperonins

The term *chaperonins* is used to describe the ATP-dependent HSP60 chaperone family and its co-chaperone HSP10. Chaperonins are divided into two classes based on location/mode of action. Type I chaperonin (HSPD1) is exclusive to the mitochondria in eukaryotic cells and is able to fold proteins which cannot be folded by the HSP70 machinery (Y. E. Kim et al., 2013; Spiess et al., 2004). The structure of type I HSP60 consists of two large rings back-to-back with a central cavity. Unfolded proteins bind to the cavity, following which HSP10 acts as a lid for the cavity to form a chaperonin cage, so that the unfolded protein can fold at a much lower macromolecule concentration. Experimental evidence reviewed by Motojima, 2015 that chaperonins also increase the folding rate for some, but not all client proteins suggests there is an additional, unknown, mechanism by which type I HSP60 interacts with unfolded proteins.

Type II chaperonins (CCT1-8) do not require the co-chaperone function of HSP10 and form a barrel-shaped complex consisting of two rings of its 8 member proteins (as reviewed by Ansari & Mande, 2018). The CCT complex (also referred to in the literature as the "TRiC complex") is located in the cytoplasm of eukaryotic cells

and its clients include the cytoskeletal proteins actin and tubulin, which can only fold with the assistance of the CCT complex (Spiess et al., 2004). Due to the sheer abundance of these clients, it has been difficult to elucidate other CCT client proteins (as reviewed by Willison, 2018; Vallin and Grantham, 2019; Grantham, 2020). Some evidence suggests CCT proteins have a role in cell cycle progression - either as individual monomers or as a complex - that extends beyond chaperoning nascent cytoskeletal proteins. In yeast, Camasses et al., 2003 show the cell division cycle protein Cdc20 associates with the CCT complex (an association affirmed by Kaisari et al., 2017), and loss of this association using a CCT mutant led to attenuation of cell cycle progression. This study is particularly noteworthy as Camasses et al., 2003 were able to show this attenuation occurs upstream of cytoskeletal impairment due to loss of function of the CCT complex, by utilising actin/microtubule-depolymerising drugs. In mammalian cells *in vitro*, X. Liu et al., 2005 found coimmunoprecipitation of PLK1 - an early trigger for G2/M transition - with an element of the CCT complex. Furthermore, knockdown of the CCT complex caused a block at the G2/M transition, however an equivalent control was not carried out to confirm that this is not the result of a compromised cytoskeleton. These studies are in agreement with a multitude of evidence linking cell cycle and cytoskeletal pathways (as reviewed by Jones et al., 2019).

Evidence by Brehme et al., 2014 shows several CCT proteins are repressed in aged human brain samples, while Nollen et al., 2004 demonstrate that loss of the CCT complex leads to early protein aggregation in *C. elegans*, and Tam et al., 2006 demonstrate that overexpression of individual CCT proteins in yeast affects the conformation of huntingtin aggregates. While these studies hint at a direct therapeutic application of the CCT complex, Pavel et al., 2016 have more recently shown, both *in vitro* and *in vivo*, that a build up of aggregates following attenuation of the CCT complex occurs because integrity of the CCT complex is essential for the degradation of aggregates via autophagy.

1.5.6 Small heat shock proteins

The 10 genes HSPB1-10 encode the human small heat shock protein (sHSP) system. Tanguay and Hightower, 2015 postulate that while evidence suggests all sHSPs are capable of binding to misfolded client proteins, the lack of structural similarity between the sHSPs implies they have different functions. Of particular importance are the sHSPs corresponding to genes HSPB1, B5, and B8; which are ubiquitous and up-regulated following heat shock (as reviewed by Acunzo et al., 2012; Carra et al., 2013). sHSPs lack ATPase activity, and thus these chaperones are incapable of refolding misfolded client proteins (Haslbeck et al., 2005; Basha et al., 2012; Garrido et al., 2012). Instead, sHSPs bind to prevent aggregation of clients until they can be refolded by ATP-dependent chaperones (colloquially referred to as *holdases* rather than *foldases*). Over-expression of sHSPs (namely B1, H. Kampinga et al., 1994; and B8, Crippa et al., 2016) has been shown to improve clearance of protein aggregates in mammalian cell lines, however it may be the case that up-regulation of these holdases simply reduces the workload of chaperones such as HSP70, allowing more efficient maintenance of proteostasis. Charmpilas et al., 2017 highlight that whilst tissue-specific up-regulation of sHSPs has potential in treatments of age-associated

cardiovascular and neurodegenerative disease, more work is needed to understand the mode of action of sHSPs.

1.5.7 The HSP110 disaggregation machinery

Other key roles of HSPs and other chaperones in maintaining proteostasis are disaggregation of misfolded proteins or, failing this, proteolytic degradation of misfolded proteins. The ability of chaperones to disaggregate proteins is a relatively recent finding, and much is still unclear of the mechanisms by which proteins are rescued from stable aggregates (Sousa, 2014). Unfolding of misfolded proteins is carried out through the HSP100 subfamily in in yeast, bacteria, and plants; but is not encoded by the metazoan genome (Heuck et al., 2016; J. Lee et al., 2017). Interestingly, work by Mosser et al., 2004 has shown that when introducing *Saccharomyces cerevisiae* HSP100 (lacked by metazoa) to human cell lines, the foreign chaperone will cooperate with endogenous HSP70 and improve cell-survival under thermal stress.

Shorter, 2016 argues the protein disaggregation machinery is the least understood aspect of proteostasis, and until recently, observed disaggregation activity in animal cells was left unexplained. Observations of co-localisation of chaperones with protein aggregates had suggested disaggregation activity in animal cells was carried out by HSP70 interacting with another co-chaperone, HSP110 (Rampelt et al., 2012). However, Nillegoda et al., 2015 demonstrated that this mechanism alone in human cells leads to a scarcity of disaggregation activity *in vitro*. Instead, it was shown that the HSP40 subfamily is able to take the place of HSP100 in metazoan cells. Under heat stress, HSP40 subfamily members interact with HSP70 and HSP110 to extract proteins from aggregates, in a mechanism separate from its co-chaperone role in folding. The nature of how HSP70 and HSP40 decide between their multiple functions is still enigmatic, and new disaggregation mechanisms independent of the HSP100 and HSP110 subfamilies are also emerging (den Brave et al., 2020).

1.5.8 Misfolded protein degradation pathways

In the case where the native state of a misfolded protein cannot be rescued, the chaperone machinery marks the protein for degradation by the UPS. Dantuma and Bott, 2014 have shown that the UPS is used to degrade several proteins associated with neurodegenerative diseases. The E3 ubiquitin ligase carboxyl-terminus of HSP70-interacting protein (CHIP), encoded by the STUB1 gene, interacts with HSP70 and HSP90 and inhibits ATP hydrolysis, 'switching off' the folding activity of these chaperones, signalling a transition from refolding to degradation of misfolded proteins (Kriegenburg et al., 2014). CHIP has then been shown to ubiquitinate both chaperone proteins and known chaperone clients, however Qian et al., 2006 demonstrate that when CHIP encounters HSP70 bound to a client misfolded protein, HSP70 acts as an adapter, and the client protein is marked for degradation. This outlines a post-translational regulatory mechanism by which cells up-regulate HSP70 during proteotoxic stress through reduced HSP70 ubiquitination through HSP70-client binding. Furthermore, following the clearance of misfolded proteins, this same mechanism supports a return to equilibrium through increased HSP70 ubiquitination due to a dearth of HSP70-client binding. Morishima et al., 2008 have

shown that while CHIP is not essential for development, CHIP-knockout mice have an increased rate of mortality. Similarly, Tawo et al., 2017 find reduced lifespans in CHIP-deficient worms and mice, and postulate that proteotoxic stress contributes to organismal ageing by detracting from CHIP's ability to regulate insulin receptor levels.

Proteins which have aggregated are too large for degradation by the UPS and are instead removed by autophagy (Y. E. Kim et al., 2013). As aggregates often begin to form several years before the symptoms of protein-folding diseases appear, therapeutic targeting the removal of aggregates is of particular interest (H. Y. Kim et al., 2015; Iaccarino et al., 2016; Lim and Yue, 2015). Mice with impaired autophagy machinery exhibited signs of premature ageing - namely increased rates of protein aggregation and neurodegeneration (Komatsu et al., 2006); whilst Pyo et al., 2013 show that the overexpression of a single autophagy-related gene in mice improved motor function, cellular resilience to oxidative stress, and extended lifespan. In addition to a loss of proteostasis, these studies implicate a failure to clear misfolded proteins as a strong pro-ageing factor and suggest that a build up of misfolded protein within human cells could cause a predisposal to neurodegenerative disease.

1.6 Chaperone regulation

Whether at homeostasis or under stress, chaperone proteins require strict regulation, in terms of both chaperone abundance and chaperone localisation between the nucleus and the cytoplasm. When exposed to stresses which cause proteins to denature, cells must rapidly increase their concentration of HSPs to cope with the increased demand of unfolded proteins.

1.6.1 Transcriptional regulation

Mahat et al., 2016 show that stress triggers rapid changes in transcription. Heat shock transcription factors are consistently acknowledged as the master-regulators of the human chaperone network at the transcriptional level (as reviewed by Takaki and Nakai, 2016; Calderwood et al., 2009; Anckar and Sistonen, 2011).

Heat shock transcription factors

There are a total of 6 human genes which encode heat shock transcription factors: HSF1, HSF2, HSF4, HSF5, HSFX, and HSFY (Åkerfelt et al., 2010). By far, the most extensively studied are HSF2 and, in particular, HSF1, which are both ubiquitous in human tissues. The focus of research on HSF1 is due to its role in tumour progression in cancer (Scherz-Shouval et al., 2014; Mendillo et al., 2012), and deficiency in neurodegenerative disease (Gomez-Pastor et al., 2017). As a result, the mechanism of activation of HSF1 is well-researched, yet not completely understood. A long-standing dogma has been that, at equilibrium, intramolecular binding between three leucine zipper domains keeps HSF1 in an inactive state as a coiled monomer with negligible DNA-binding activity, in a complex with chaperones HSP70 (Shi et al., 1998) or CCT (Neef et al., 2014). This interaction inhibits HSF1 activation, such that this inhibitory complex is disassembled during proteotoxic

stress (Dayalan Naidu & Dinkova-Kostova, 2017)[2]. Following activation, these intramolecular bonds break to allow HSF1 to homotrimerise and achieve its active form, however the mechanism of HSF1 activation has come under scrutiny in recent years.

Proteins denature within minutes when subjected to heat stress, however experimental evidence suggests the cellular heat shock response is triggered much more rapidly (Csermely & Vígh, 2007). This indicates that some element of the response is instigated by the temperature itself, rather than protein denaturation. In support of this, Hentze et al., 2016 demonstrate a heat-induced conformational change in HSF1 which could provide this activation mechanism. For this to be crucial or the sole mechanism of HSF1 activation however, would contradict reports of HSF1 activation in non-thermal forms of stress (Ahn, 2003; Metzler et al., 2003).

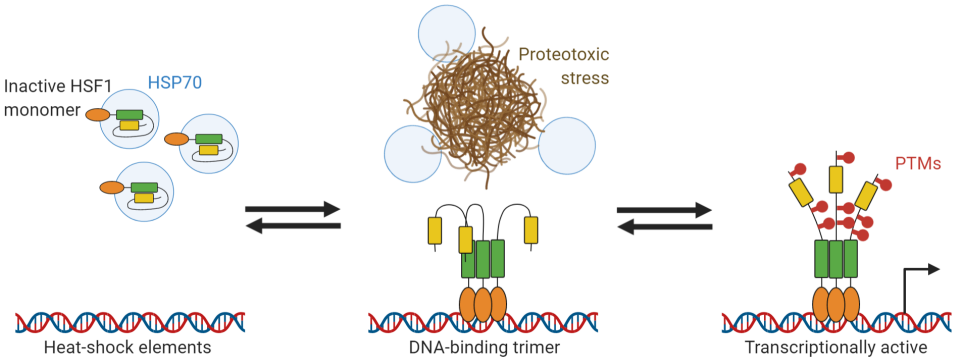

Figure 1.3: The theory of distinct processes of HSF1 activation and initiation of HSP transcription. HSF1 is kept in its inactive monomeric state through HSP70 binding. At the onset of proteotoxic stress, bonds between leucine zippers (green/yellow) break to activate HSF1 binding affinity to DNA. In a theorised separate - but necessary - process, post-translational modifications (red) make HSF1 transcriptionally active at heat shock elements: the promoter regions of genes encoding for HSPs. Adapted with *BioRender* from Takaki and Nakai, 2016.

Active HSF1 trimers rapidly target heat shock elements (HSE), located at the promoter regions of genes corresponding to HSPs. Dissociation from these HSEs and HSF1 monomerisation following the resolution of stress was recently showed to be carried out by HSP70, in cooperation with HSP40 (Kmiecik et al., 2020). Takaki and Nakai, 2016 compile evidence that the acquisition of this binding activity via trimerisation is necessary, but not altogether sufficient to initiate transcriptional activity (Figure 1.3). Instead, it is suggested that transcriptional activity is acquired through various post-translational modifications (PTM), suggesting a high degree of

[2]Dayalan Naidu and Dinkova-Kostova, 2017 cite that HSF1 activity is also repressed through binding to HSP90, however increasing evidence suggests this is a common misconception within the field. Often cited are the observations of Ali et al., 1998 in *Xenopus laevis* oocytes, namely coimmunoprecipitation of HSP90 with HSF1; and increased HSF1 activation following HSP90 inhibition. Hentze et al., 2016 have since found the presence of HSP90 alone does not inhibit activation of recombinant human HSF1. Furthermore Zheng et al., 2016 found no coimmunoprecipitation between HSP90 and HSF1 in yeast strains, and postulate that the common finding of HSF1 activation following HSP90 inhibition (for example J.-H. Lee et al., 2013) is due to the loss of HSP90 function causing higher levels of unfolded proteins and increasing the workload of HSF1-bound HSP70.

control over the transcription of HSPs. This is contested by Zheng et al., 2016, who claim PTMs are not necessary for transcriptional activity, and the purpose of these modifications is not yet known. This is justified by recent work. Budzyński et al., 2015 discovered that a phosphorylation-deficient HSF1 mutant in mouse fibroblast cells was still transcriptionally active during stress. Furthermore, Raychaudhuri et al., 2014 found that acetylation of HSF1 did not affect its transcriptional activity, but rather this PTM prevents HSF1 ubiquitination. This suggests PTMs of HSF1 are a separate mechanism of the stress response which reduce HSF1 turnover.

The lack of a complete understanding of the role of HSF1 is emphasised by the D'Mello lab. A strong neuroprotective effect of HSF1 is thought to stem from this mechanism of inducing chaperone synthesis through HSP70 dissociation, and indeed Verma et al., 2014 find HSF1 knockdown in mouse/rat neuronal cell cultures to be detrimental to cell viability. However, the use of a HSF1 mutant incapable of trimerisation - and thus incapable of HSE binding - suffered no significant loss of viability. Following up on this result, Qu et al., 2018 performed RNA-seq and found a near-complete loss in the transcriptional activation of the HSF1 mutant, showing the neuroprotective effect of monomeric HSF1 is not due to transcriptional activation of non-HSP promoting genes.

Despite the importance of HSF1 in chaperone regulation, the regulation of HSF1 itself also remains poorly defined. Similarly, the mechanisms controlling activation of HSF1's transcriptional activity are not fully-understood, although evidence suggests HSP70 plays an important role. The best-supported theory of how HSF1 activation controls chaperone levels is the *chaperone titration model*.

Under the titration model, HSF1 bound in complex with HSP70 (at its substrate-binding domain) is kept in its inactive state. The chaperone however, has a higher binding affinity for unfolded or misfolded proteins, and is titrated away from HSF1 during proteotoxic stress. The unbound HSF1 is then free to trimerise, and binds to DNA encoding for chaperones such as HSP70 and HSP90. Upon restoring proteostasis, HSP70 molecules will then bind to the free HSF1, deactivating it to complete a negative feedback loop (Sivéry et al., 2016; as reviewed by Gomez-Pastor et al., 2017). Figure 1.4 in Section 1.7.1 illustrates a mathematical model of the titration of HSF1 by Sivéry et al., 2016. Direct experimental evidence of the titration model is presented by Zheng et al., 2016, wherein yeast cells over-express a "decoy" HSF1, with removed DNA-binding and trimerisation domains. HSP70-decoy binding causes a dearth of binding sites for wild-type HSF1 molecules, and the titration model accurately predicts *in silico* an increase in HSF1 activation which is observed *in vitro*.

1.6.2 Post-translational regulation

As noted by Mao et al., 2013, study of chaperone network regulation at the post-translational level is neglected compared to regulation at the transcriptional level. Following proteotoxic stress, cells are left with an excess of HSPs. The E3 ligase CHIP, which works with HSP70 and HSP90 in the UPS, is also partially responsible for the regulation of these chaperones (Kundrat and Regan, 2010; Tawo et al.,

2017; H. Zhang et al., 2015). Qian et al., 2006 found that when CHIP-knockout mouse fibroblasts were exposed to a 42°C heat shock for 30 minutes, HSP70 reached peak levels after 4 hours. The excess HSP70 in the CHIP-knockout cells was much more stable ($t_{\frac{1}{2}} \gg 8$h) than in wild-type cells ($t_{\frac{1}{2}} < 4$h), with HSP90 levels reacting similarly. As discussed in Section 1.5.8, Qian et al., 2006 also showed that CHIP is able to ubiquitinate HSP70 and HSP90, but with less affinity than with misfolded proteins, such that chaperones and chaperone-bound client proteins compete for the ubiquitin ligase activity of CHIP. This mechanism reduces the turnover rate of chaperones while the concentration of misfolded proteins is high, and increases the turnover rate of chaperones during recovery from stress, where misfolded protein concentration is low, but chaperone concentration is elevated.

Mao et al., 2013 found that HSP70 in the immortal human "HeLa" cell line interacts with the ATPase OLA1, and this interaction interferes with CHIP-HSP70 binding. In this way, OLA1 helps to stabilise elevated HSP70 levels during stress. The study showed populations of OLA1-knockout mouse embryonic fibroblast (MEF) cells had significantly lower levels of HSP70, and as a result fewer viable cells than wild-type following a 1 hour, 42°C heat shock. Furthermore, human embryonic kidney-293 cells (HEK 293) with over-expressed OLA1 had significantly more viable cells than wild-type following the same heat shock. Despite these findings, the mechanisms and functions of human OLA1 are poorly understood (Wenk et al., 2012). The extent to which OLA1 is regulated during stress has not been reported, and so it is not known whether OLA1 is integrated into the stress response.

It is well-established (Welch & Feramisco, 1984) that the cell shuttles HSPs to the nucleus during proteotoxic stress, however the reason for this is still uncertain. Whilst referencing this uncertainty, both Kotoglou et al., 2009 and Shibata and Morimoto, 2014 suggest the purpose of translocation of HSPs to the nucleus under stress is to protect ribosomal DNA. In contrast to findings that chaperones are transported to the nucleus during proteotoxic stress, Furuta et al., 2004 and Miyamoto et al., 2004 have reported that active transport pathways into the nucleus are inhibited during heat stress, most likely to block the transport of misfolded or aggregated proteins into the nucleus. This paradox was solved by Kose et al., 2012, who discovered an alternative pathway for nuclear transport during heat stress. The protein dubbed HIKESHI ("firefighter") transports HSP70 into the nucleus, and has been found to increase by up to 3-fold during a 1 hour heat shock of HeLa cells at 43°C. Much of this mechanism remains undetermined, including whether HIKESHI is able to transport chaperones other than HSP70.

1.7 The heat shock response

What we now term the heat shock response was first documented by Goldschmidt, 1935 in *Drosophila melanogaster*, and the mechanisms by which cells counteract stress have continued to garner interest from researchers - more recently in the field of cancer science, where tumour cells are thought to reside in a perpetually stressed state (Graner et al., 2007). A majority of organisms must retain a specific internal temperature, and the heat shock response is heavily conserved throughout organisms with widely varying internal equilibrium temperatures (as reviewed by Morimoto,

1998). A protein's Gibbs energy landscape (Figure 1.2) is highly susceptible to alteration through changes in its physical environment, including pH, pressure, and temperature changes (S.-Q. Liu et al., 2012). At high temperatures, the energy landscape shallows, making transitions from the native state to unfolded or aggregated states more likely. Proteins denature within minutes when subjected to heat stress. However, as discussed in Section 1.6.1, experimental evidence suggests the heat shock response is triggered much more rapidly. This indicates that the unfolded protein response (explained by the titration model) is independent of another mechanism which is activated by the temperature itself, rather than denatured proteins.

While a general response to protein misfolding is observed through any mode of cellular stress which causes proteins to lose their three-dimensional structure, the effects on the cell specifically due to thermal stress stretch far beyond this. For example de Andrade Mello et al., 2017 show that heat stress results in increased membrane fluidity in mammalian cells, while Balogh et al., 2005 note the similarity between the cellular response to hyperfluidisation and the response to heat shock. These results suggest membrane fluidity as a potential trigger of the heat shock response. In agreement with this theory, the temperature at which yeast cells initiate a heat shock response is determined by the ratio of saturated to unsaturated fatty acids in the cell membrane (as reviewed by Verghese et al., 2012), while Török et al., 2003 show that increasing the membrane fluidity of HeLa cells in the absence of proteotoxic stress induces up-regulation of HSPs. Csermely and Vígh, 2007 postulate the heat stress signalling pathway must be activated by the physical state of cell membrane lipids. Calderwood et al., 2009 state the heat stress-signalling pathways are driven by kinase activation cascades, the most notable being the three major mitogen-activated protein kinases (junK, ERK1, and p38) and protein kinase B (PKB). Csermely and Vígh, 2007 discuss how these pathways can lead to both transcription of chaperones and apoptotic functions, depending on factors such as the intensity of the stress.

The link between these signalling pathways and thermosensors such as lipid membrane fluidity is not yet clear. Nadeau and Landry, 2007 suggest the increase in membrane fluidity may lower the activation thresholds of certain membrane receptors, leading to activation of heat stress-signalling pathways. Bromberg and Weiss, 2016 outlines the transient receptor potential channel TRPV1 as a potential candidate for this role. The channel has been shown to be gated by heat, and TRPV1 was up-regulated in rats treated with an adenovirus which caused overexpression of HSP70. Furthermore, blocking the receptor in the breast cancer cell line MCF-7 cells decreased levels of HSP70 and HSP90. The downstream pathways of TRPV1 which lead to activation of the heat shock response have yet to be found. Further study of the consequences of targeting this receptor would be clinically relevant for its potential use to moderate HSP levels without affecting cellular proteostasis or membrane fluidity.

1.7.1 Mathematical models of the heat shock response

Mathematical models of biological processes are a growing tool to provide not only a means to validate a hypothesis, but also a means to generate new hypotheses

(Tomlin & Axelrod, 2007). Reviews by Jeremy Gunawardena (Gunawardena, 2012; Gunawardena, 2013; Gunawardena, 2014) describe in detail several examples of the efficacy of combining mathematical models with biological measurements. Many processes within biology are extremely multifaceted, and a functional *descriptive* model demonstrates a working understanding of a process. Going further, one can then perturb single elements of a system *in silico*, likely with much greater ease than experimentally, and use this *predictive* model to develop a deeper understanding of a system and its dynamics.

Mathematical models of the HSF1-mediated stress response (as introduced in Section 1.6.1) have been designed previously (Rieger et al., 2005; Szymańska and Zylicz, 2009; Petre et al., 2011; Scheff et al., 2015; Magni et al., 2018; Pal and Sharma, 2020), however increasing complexity has led to over-fitting and - perhaps counter-intuitively - limited the usefulness of these models. The value of simplifying models within mathematical biology is commonly advocated for in reviews on the subject. For example Tomlin and Axelrod, 2007 explain that the current complexity of models within developmental biology prevents the establishment of a base of properties that are invariably true, and simpler models are needed. Similarly, Motta and Pappalardo, 2013 discuss how complex mathematical models of biological systems cannot be analysed analytically and lack "extendibility" - losing relevance when new information or data emerges. Gunawardena, 2014 discusses how simpler models have greater capacity for predictiveness, while Torres and Santos, 2015 explain that larger and more complex models are often worse at expressing meaningful details of the systems they describe, citing highly effective simple models such as the three-element model of the NF-κB signalling pathway by Krishna et al., 2006.

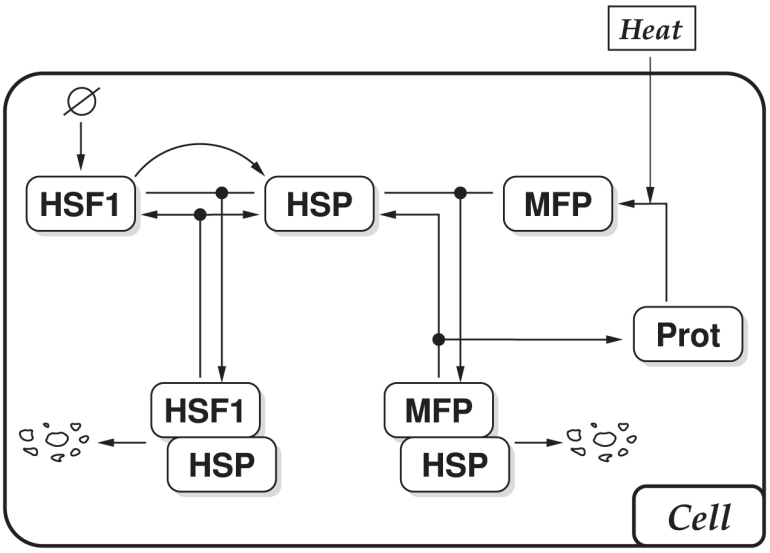

Figure 1.4: The titration model of HSF1 chaperone regulation during proteotoxic stress. Competition for chaperone binding between HSF1 and misfolded proteins creates a negative feedback loop to control proteostasis. From Sivéry et al., 2016.

Sivéry et al., 2016 argue that the complexity and amount of contributing mechanisms in some of the aforementioned models are not justified by experimental data. Furthermore, the choices to fit specific processes describing HSP70 transcription/translation and HSF1 trimerisation/phosphorylation prevent these models from being

able to elucidate the core mechanisms of the stress response. Instead, the "minimal titration model" by Sivéry et al., 2016 and the concurrent "minimal kinetic model" by Zheng et al., 2016 (further developed by Krakowiak et al., 2018) are built around just three protein populations (Figure 1.4): HSP70, HSF1, and misfolded protein (MFP). Binding states between these also exist as pseudo-populations, and population dynamics are evaluated using a coupled ordinary differential equation (ODE) system. As reviewed in Section 1.6.1, the results of these studies have contributed significantly to the understanding of HSF1 activation.

Sivéry et al., 2016 and Zheng et al., 2016 reduce the complexity of their models by constraining HSF1 to two states: active (free) and inactive (HSP70-bound), arguing that HSF1 phosphorylation and trimerisation are transient processes. Instead, a Hill function - designed by A. V. Hill and commonly used to model transcription factor-gene element binding (Bassett, 2002; Bottani and Veitia, 2017) - with a Hill coefficient = 3 was used in both studies to reflect a transcription rate proportional to the HSF1 trimer. In the model by Sivéry et al., 2016, active HSF1 instigates the synthesis of HSP70 mRNA, which in-turn instigates the synthesis of HSP70 with a constant rate of translation. This is redundant, and results in HSP70 protein following a temporal pattern no different to HSP70 mRNA. In the present study, the complexity has been reduced by removing the HSP70 transcript population and replacing this process with a delay differential equation (DDE). A transcript population is also omitted by Zheng et al., 2016, however no delay between HSF1 activation and HSP70 synthesis is incorporated, and as a result much sharper rises in HSP70 are seen in their *in silico* heat shock data relative to their *in vivo* data. Another key way in which the models differ is how a heat shock is simulated. Sivéry et al., 2016 begin with a model converged to a steady state, before increasing the rate at which misfolded protein is introduced $\sim$ 9-fold. Questionably, Zheng et al., 2016 do not use a dynamic system of constantly generated misfolded protein, and instead the system begins with a concentration of unfolded protein which cannot increase, and a higher starting value is used to simulate a heat shock. Zheng et al., 2016 also lacks a mechanism to facilitate HSP70 turnover, such that the chaperone levels can only increase during the simulation. While the studies based around this model by Zheng et al., 2016 and Krakowiak et al., 2018 are much more widely cited (presumably due to their publication in a biological science-based journal), due to these limitations we will instead focus on the results from the model by Sivéry et al., 2016.

Sivéry et al., 2016 found *in silico* that active HSF1 rose rapidly at the onset of heat stress and plateaued after 1 hour. HSP70 protein levels plateau after 10 hours, and remain elevated after 24 hours, with a constant HSP70 turnover rate chosen to fit experimental data of HSP70 dynamics in HeLa cells by Abravaya et al., 1991. This is also open to criticism, as it neglects evidence of a down-regulation of HSP70 half-life during stress (Danxi and Duncan, 1995; Qian et al., 2006; Mao et al., 2013). Another drawback this causes is the model lacks a descriptive processes of stress recovery. Interestingly, an over-correction is seen, where *in silico* misfolded proteins and active HSF1 levels drop below pre-stress levels after six hours due to an excess of HSP70. Under this model of constant HSP70 turnover, this over-correction persisted for the duration of the simulation.

1.7.2 Inhibition of HSP70

In order to correctly fold proteins, HSP70 is required to interact and cooperate with co-chaperones such as HSP40 (Verghese et al., 2012). The small molecule 2-phenylethynesulfonamide (PES) has been shown by Leu et al., 2009 to interact selectively with HSP70 and interfere with its ability to interact with its co-chaperones. Proximity labelling of PES using biotin was used by the authors to reveal binding partners of the drug. Subsequent SDS-PAGE showed just one clear band at $\sim$ 70kDa and mass spectrometry revealed this corresponded to either HSPA1A or HSPA8 (with the detected peptides common to both these proteins). Using antibody tagging methods, the interaction with HSPA1A was confirmed and any possible interaction with HSPA8 was refuted. The same group (Leu et al., 2011) demonstrated in two human cell lines that HSP70 inhibition caused by a 20 μM, 24-hour PES treatment caused a reduction in proteasomal activity and led to an accumulation of protein aggregates relative to solvent-only (dimethyl sulphoxide (DMSO)) controls. A third study using a different human cell line (Leu et al., 2017) showed that PES inhibition (2.5 μM, 48-hour, DMSO controlled) again caused a reduction in proteasomal activity and increase in protein aggregation, whilst also leading to a drop in cellular ATP and rupture of mitochondrial membranes.

This inhibitor allows the study of how cells respond to a prominent feature of ageing, namely the decline in HSP70 activity leading to higher rates of protein misfolding and aggregation (see Section 1.8). Recalling the titration mechanism which is thought to regulate HSP70 levels, we may also expect HSP70 inhibition to interfere with this process. If the ability of HSP70 to bind to HSF1 is compromised, the response could be similar to the misfolded protein response, and more HSF1 would become active, increasing rates of chaperone synthesis.

1.8 Proteostasis in ageing

The breakdown of proteostasis is a key hallmark of ageing. Alzheimer's, Parkinson's, Huntington's, and several other neurodegenerative diseases with characteristic protein aggregation are also strongly age-associated; while chaperone-assisted folding, unfolding (for transport), and disaggregation have all been demonstrated to deteriorate with ageing. An interesting large-scale study by Njemini et al., 2011 compared the serum level of HSP70 in groups of young (23 ± 3 years, $n = 100$); elderly healthy human subjects (74 ± 5 years, $n = 100$); and elderly hospitalised patients (83 ± 6 years, $n = 90$). HSP70 levels in the young group were significantly higher than in both aged groups, and patients suffering afflictions associated with cognitive decline had lower levels of serum HSP70 than the elderly healthy group[3]. It is clear how the loss of proteostasis contributes to ageing, but little is known of the cause of this deterioration. Similarly, while the mechanism of chaperone-mediated protein folding is broadly understood - chaperones such as HSP70 bind to the exposed hydrophobic

[3]The study by Njemini et al., 2011 of HSP70 levels in hospitalised vs healthy elderly subjects also highlights an interesting discrepancy, whereby patients suffering from illnesses associated with chronic inflammation had significantly increased HSP70 levels. As inflammatory pathologies often coincide with ageing (as reviewed by H. Y. Chung et al., 2019), it is unclear what effect, if any, this has on the age-associated decline in proteostasis.

residues of unfolded proteins - less is known of the cellular dynamics of chaperones (as reviewed by López-Otín et al., 2013; Powers et al., 2009; Koga et al., 2011).

The decline of the heat shock response in ageing has been consistently reported (Westerheide et al., 2009; Jolly et al., 2002). In particular, Brehme et al., 2014 find 101 genes related to the proteostasis network are significantly repressed with age, including HSP70, 40, and 90. A study of the heat shock response in *C. elegans* (lifespan 2-3 weeks) by Shemesh et al., 2013 showed that, while 76% of wild-type adults survived a heat shock occurring on day 1 of adulthood, just 13% survived a heat shock occurring instead on day 2 of adulthood. Work by McArdle et al., 2004 has shown that rapid synthesis of the key chaperone HSP70 (attributed to the rise in temperature during exercise) functions to protect against muscle damage in mice. Furthermore, the study shows that overexpression of HSP70 reduces deterioration of muscle function due to ageing. Investigating the nature and cause of the decline of the heat shock response will give valuable insights into how proteostasis is lost and, potentially, how it could be recovered.

The root cause of the age-associated decline in proteostasis leading to aggregation-associated diseases has yet to be found (Lackie et al., 2017). Ageing is associated with cell membrane defects (Csermely & Vígh, 2007) which may contribute to attenuating the response of aged cells to heat stress. In an analysis of postmortem *substantia nigra* tissue, Hauser et al., 2005 identify the stress-response as one of the main pathways altered in cases of Parkinson's Disease. *In vitro* studies in human neuroblastoma SH-SY5Y cells by Roodveldt et al., 2009 confirmed that treatment with HSP70 suppresses the toxicity of α-synuclein aggregates. Ben-Zvi et al., 2009 have observed in *C. elegans* that both the rate of protein misfolding and the strength of the response to heat shock are age-dependent. In the same study, HSF1 knock-down increased protein loss-of-function with age, while proteostasis was maintained during ageing when HSF1 was overexpressed. Kaushik and Cuervo, 2015 attribute the decline in chaperone activity to a limited amount of ATP in aged cells due to reduced cellular metabolism and mitochondrial function. This is supported by findings from Brehme et al., 2014, that aged human brain cells repress ATP-dependent chaperones, but induce ATP-independent chaperones and co-chaperones, with these changes to the human chaperone network emphasised in brain cells from sufferers of Alzheimer's, Huntington's, or Parkinson's disease.

In addition to a decline in chaperone activity, Schmidt and Finley, 2014 and Tanaka and Matsuda, 2014 review evidence that the UPS and autophagy pathways also begin to fail in aged cells, contributing to the onset of widespread protein aggregation. Furthermore Vilchez et al., 2014 discuss how the increased level of aggregates due to deterioration of the UPS and proteasome actually feed back and disrupt these systems further. Recent studies have focused on observations of buffering between the UPS and autophagy machineries. Gavilán et al., 2015 disrupted the proteasome in the hippocampus of both young and aged rats, and observed that the UPS machinery compensated for the loss of proteasome function in young rats only. Klaips et al., 2017 highlighted this cross-talk as a key area of proteostasis requiring better understanding. The role of the proteasome in ageing is emphasised by a study by Chondrogianni et al., 2000, which showed fibroblasts from human donors

who lived to 100 years have levels of proteasome activity much more similar to young fibroblasts than aged. Koga et al., 2011 comment that, although experiments over-expressing autophagy genes have yielded positive results in invertebrate model systems (as reviewed by Chondrogianni et al., 2015; Madeo et al., 2015), analogous studies in mammals are much more sparse. A study by Pyo et al., 2013 showed that aged mice over-expressing Atg5, which enhances autophagy, had improved motor function and extended lifespans.

Beyond neurodegenerative diseases, recent studies suggest the ability to maintain the potency of the stress response through ageing has potential applications in organ transplantation. Naesens, 2011 compiles evidence that the success of kidney transplants is largely reliant on donor age, while Milisav, 2011 cites several cases where targeting stress response proteins increases the viability of grafts, underlining the potential of developing methods to up-regulate human HSPs in clinical practice.

1.8.1 Human Mesenchymal Stem Cells as a model system to study cellular ageing

Labbadia and Morimoto, 2015 propose that more understanding of the spatial and temporal dynamics of the proteostasis network are necessary to develop effective treatments for protein aggregation diseases. Ageing studies are most commonly done in model organisms such as *Caenorhabditis elegans*, *Drosophila melanogaster*, and *Mus musculus*; due to the long duration of the human life-cycle. Use of these model organisms in ageing research has come under scrutiny, with Valenzano et al., 2017 commenting that the former two of these organisms are largely post-mitotic in adulthood and have held back studies of stem cell function within the context of ageing; while neurodegenerative diseases such as Alzheimer's do not occur naturally in mammalian models such as *Mus musculus* (as reviewed by King, 2018; Dawson et al., 2018; Cohen, 2018) - or even aged nonhuman primates (as reviewed by Heuer et al., 2012). Vilchez et al., 2014 stress the need for more studies of proteostasis in ageing in humans to pave the way for treatments of age-related protein aggregation diseases. Studies in these model organisms have shown ageing at the cellular level contributes to ageing of the organism (as reviewed by J. Magalhães, 2004), leading to increasing numbers of studies using human cells in prolonged culture to study ageing in humans.

Mesenchymal stem cells (MSCs) can be derived from mammalian tissue from brain, spleen, liver, kidney, lung, muscle, thymus, pancreas, and heart (da Silva Meirelles, 2006); but are most commonly harvested from bone marrow. BM-MSCs are multipotent, isolable, and expandable *in vitro*; and are already being applied in clinical practice (as reviewed by F. Gao et al., 2016). As stated by Shatrova et al., 2016, MSCs are becoming increasingly useful in the field of tissue engineering, and are becoming a more commonly used cell source to study the cellular stress response (Swift et al., 2013; Cho et al., 2016; Gilbert et al., 2019; Rühle et al., 2020).

1.8.2 Senescence provides a model for cell ageing

The main obstacle of studying the effects of ageing in humans is donor matching. A scarcity of human donors will donate tissue both early and late in life, and the high genetic and environmental diversity between human donors prevents young and old tissue from different donors being comparable. Instead, a model system of ageing in human cells is required. The use of senescent cells as a cell culture model for *in situ* ageing is well-documented (as reviewed by Phipps et al., 2007; Martinez Guimera et al., 2017; van Deursen, 2014). To this end, proliferating cultures can be split, with some cells cryogenically stored in this proliferative state to serve as a control for the remaining cells kept in culture until the widespread onset of senescence. *In vitro* cellular senescence in MSCs can be easily triggered through persistent passage and replication (see Chapter 2). The time taken for human MSCs to reach replicative senescence *in vitro* is weeks-months, which is relatively short compared to the human life cycle and thus provides a good model to study human cell ageing. Studies in multiple mammals (Martinello et al., 2011; de Moraes et al., 2016) have compared fresh and thawed mesenchymal stem cells and demonstrated cryopreservation had no effect on the characteristics of the cells, allowing valid comparisons between donor-matched early- and late-passage cultures.

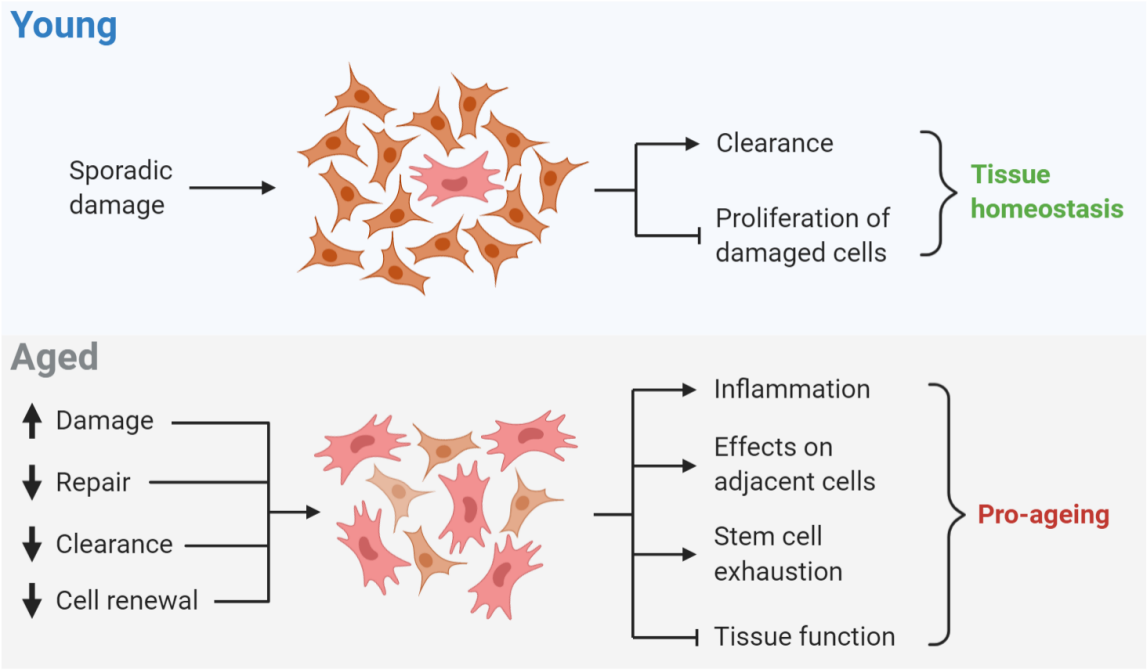

Figure 1.5: The cellular senescence mechanism to maintain tissue homeostasis. As tissue gets older, the rate of cell damage increases, while the rates of cell repair, removal, and renewal all decrease. The result is a disproportionately high number of senescent cells in aged tissue. Adapted with *BioRender* from López-Otín et al., 2013.

Senescence is a cellular response to contracting irreparable DNA damage, and striving to mitigate the propagation of this damage. The cell responds by arresting its cell cycle, to halt division, and by triggering the autophagy system to remove the cell (Figure 1.5). However, two other hallmarks of ageing (López-Otín et al., 2013)

are the increased rate of accumulation of senescent cells, and the decline in activity of the autophagy system. Thus aged tissue consists of disproportionately high numbers of senescent cells compared to young tissue. Early work by Dimri et al., 1995 took skin samples from 10 human donors < 40 years old and 10 human donors > 69 years old and, using the senescence marker β-galactosidase (see Section 1.8.3), showed negative dermal staining in each donor from the younger group, and positive dermal staining from all but one of the aged group.

Given the temporal difficulty of using human samples in ageing studies, most of the research on the correlation between senescence and ageing has been done in mouse tissues. Hewitt et al., 2012, using telomere-associated DNA-damage foci as a marker for senescence, found a strong ($r = 0.96$) positive correlation between the age of mice and the percentage of senescent cells in gut tissue sections. Baker et al., 2016 also found an increase in β-galactosidase positive cells with age in mouse heart tissue. The group were able to induce apoptosis in the senescent cells only in wild-type mice and found evidence this prevented an age-associated loss of cardiomyocytes; and led to increased resilience to cardiac stress.

Use of senescent cells as an ageing model is further justified by several studies which report changes in senescent cells which mirror changes in more established models of ageing. Chondrogianni et al., 2003 report a decline in proteasome activity in senescent cells from human lung tissue, which reflects the decline seen by Carrard et al., 2003, who investigated blood lymphocytes from 20-63 year old human donors. In another example, Ogrodnik et al., 2017 show senescent hepatocytes from the livers of wild-type mice experience a decrease in the mitochondrial efficiency of fatty acid metabolism. Interestingly, it had been suggested by Petersen, 2003 over a decade earlier that increased fat accumulation in the liver tissue of humans aged over 65 may be due to an age-associated loss of mitochondrial activity. Importantly, Passos et al., 2007 also demonstrate mitochondrial dysfunction *in vitro* after sorting for β-galactosidase-positive cells in an early-passage population of human lung fibroblasts, decoupling the effects of senescence from the effects of extended culture. These studies mirror the long-known concurrence of mitochondrial dysfunction and human ageing (Cortopassi & Arnheim, 1990).

A recent study followed on from the finding of Dimri et al., 1995, namely aged skin consists of high numbers of senescent cells. Weinmüllner et al., 2020 induced senescence in a 3D *in vitro* model of skin using primary human keratinocytes, and demonstrated a decrease in epidermal thickness which is phenotypic of *in vivo* skin ageing (Mine et al., 2008). Of particular relevance is another recent study, by X. Chen et al., 2019 on the characteristics of senescent hBM-MSCs. Donors were grouped according to age (15-25, $n = 10$; 26-45, $n = 12$; 46-65, $n = 15$; and > 65 years, $n = 12$) and the incidence of cellular senescence (measured using β-galactosidase staining) continued to increase significantly with each group over the last.

1.8.3 β-galactosidase as a biomarker for cellular senescence

β-galactosidase activity, detected using the chromogenic substrate X-gal at pH 6.0 is a widely used and highly specific marker for cellular senescence (Dimri et al., 1995). As reviewed by Kiernan, 2007, cleavage of X-gal by the enzyme β-galactosidase forms a product which undergoes dimerisation and oxidation resulting in insoluble 5,5'-dibromo-4,4'-dichloro-indigo which has a distinct blue colouring that can be easily detected via microscopy. Kurz et al., 2000 demonstrated that β-galactosidase activity was between three- to six-fold higher following the serial passaging of human endothelial cells when compared to first passage.

B. Y. Lee et al., 2006 verified that the senescence marker is specifically lysosomal β-galactosidase, driven by overexpression of the GLB1 gene. This was done by by testing human fibroblasts which had undergone replicative senescence from patients lacking lysosomal β-galactosidase activity only. This result also demonstrates that lysosomal β-galactosidase activity is merely a product - and not a cause - of cellular senescence. Debacq-Chainiaux et al., 2009 postulate that this increase is due to the accumulation of damaged non-degradable macromolecules in senescent cells. This is an idea supported by long-standing data from Robbins et al., 1970 showing that senescent human cells contain larger and a greater number of lysosomes. More recently, Piechota et al., 2016 found lysosomal mass to correlate with increasing numbers of divisions in murine neuronal cultures.

Several reviews such as Hernandez-Segura et al., 2018 and de Mera-Rodríguez et al., 2021 echo the sentiment that β-galactosidase activity is up-regulated in senescent cells due to increased lysosomal mass, however very little work has been done to corroborate the theory that this is due to the accumulation of damaged non-degradable macromolecules in senescent cells. Furthermore, these reviews do not question or discuss why this lysosomal enzyme alone is indicative of senescence over several other lysosomal enzymes which are also up-regulated to a lesser extent in senescent cells (Kurz et al., 2000). Studies in murine models by Ho et al., 2003 and Cui et al., 2004 have established that the administration of galactose negatively affects lifespan and leads to increased neurodegeneration. Following the results of these studies, Elzi et al., 2016 demonstrated that administration of galactose induces senescence in human fibroblast cultures. Work by Rossignol et al., 2004 and Marroquin et al., 2007 suggests that intracellular galactose levels change the pH and respiratory capacity of mitochondria, which may lead to the generation of cytotoxic reactive oxygen species, however more work is needed to understand the link between ageing, intracellular galactose levels, and senescence.

1.8.4 Chaperone function in senescent cells

There is a surprising lack of research into changes to proteostasis in senescent primary cells. Perhaps still the most comprehensive study is Gutsmann-Conrad et al., 1998, using human skin fibroblasts from donors from two age groups, 27-44 ($n = 7$) and 78-92 ($n = 6$) years old, further split into early- and late-passage groups. The cultures were heat shocked at 45°C for one hour before being returned to 37°C for 4 hours. A decrease in HSF1, HSP70, and HSP70 mRNA was reported in the pre-stressed cells from aged donors; and the amount of HSP70 induced following stress

was shown to decline with donor age and, interestingly, decline in late-passage cells independent of donor age. In contrast, while Bonelli et al., 1999 concurrently reported a dampening of HSP70 up-regulation in late-passage human lung fibroblasts following a similar heat shock, it was reported that HSP70 mRNA levels and the degree of HSF1-HSE binding were unchanged between early- and late-passage cells before and after stress, pointing to "an impairment in the post-transcriptional processing of the HSP70 mRNA" in senescent cells.

Regarding degradation of misfolded proteins, Cuervo and Dice, 2000 argue senescent cells accumulate damaged proteins due to a decline in chaperone-mediated autophagy, and demonstrate a decline in the degradation rates in the isolated lysosomes of 3 and 22 month old rats. More recently, Sisoula and Gonos, 2011 focus on levels of CHIP in senescent cells, claiming short/small interfering RNA (siRNA) knockdown of CHIP in human lung fibroblasts *in vitro* caused premature cell ageing. Widespread growth arrest occurred one population doubling after treatment, while control cells continued to proliferate beyond 6 population doublings. 21 days following CHIP knockdown, the % of senescent cells (defined using β-galactosidase staining) was $\sim 100\%$, compared to $\sim 20\%$ in control cells.

G. Kim et al., 2012 study the skin fibroblasts of patients with segmental progerioid Werner syndrome, of interest because these cells accumulate DNA damage and undergo premature senescence; and therefore it can be argued this study decouples the effects of senescence from chronological age. It was found that these cells (taken from three patients aged between 19 and 30 years) had a dampened response to a 35 minute heat shock at 43°C (observed following 6 hours of recovery at 37°C) compared to cells from age-matched healthy controls. While there was no detectable difference (via immunoblotting) in HSP70 levels in unstressed cells, there was a stark decrease in the amount of HSP70 induced due to stress in the prematurely senescent cells. It was further shown that cell cycle arrest alone was not the cause of impairment of the heat shock response, by demonstrating that HEK 293 growth arrested at G1 showed no change in HSP70 induction relative to controls, suggesting the accumulation of DNA-damage associated with senescence is key to the impairment of proteostasis. This was supported by showing that up-regulation of three different elements of the DNA-damage signalling pathway each caused a dampening in the heat shock response.

Of particular relevance is a recent study by Sabath et al., 2020, analysing the proteostasis decline in senescent human lung fibroblasts from the WI-38 cell line. Given the relevance of this work to the present study - despite differences including a lack of proteomic or primary cell data - it has been closely analysed. Passage 24 proliferating cells and passage 36 senescent cells (verified using β-galactosidase staining) were exposed to heat shock at 44°C for 2 hours ($n = 3$). Using RNA-sequencing, transcripts were clustered into groups following similar patterns between passage 24 and passage 36 cells, before and after stress. While the method of clustering isn't explicitly stated, the study focuses on a group of 161 transcripts which it claims are up-regulated in the proliferating stress response, but less so in the senescent stress response. This claim is dubious however, as the clustering performed is based upon absolute transcript values, rather than stress-induced changes in transcript values.

Pathways analysis of this cluster found enrichment of terms relating to the HSP70 family, chaperone binding, and protein ubiquitination. 157 chaperone proteins are manually chosen by the authors, who show the expression of these chaperone transcripts follows a 1:1 relationship (with a goodness of fit $p = 1$) between unstressed proliferating and senescent cells - a surprising result as this included the cell-cycle regulatory chaperone family, CCT, which has been repeatedly shown to decrease in ageing (as reviewed in Section 1.5.5). In reference to this and other results which contradict the literature on WI-38 cells (such as that of Chondrogianni et al., 2003), the authors note that their system differs from others in that "cells have just fully entered senescence" - though the practical meaning of this is ambiguous.

Ribosomal profiling was also performed to analyse the translational profile of these proliferating and senescent cells. A large overlap was found between chaperone transcriptional and translational behaviour, such that chaperone translation was again similar between unstresssed proliferating and senescent cells. Important to the present study which focuses in particular on the HSPA1A gene product, supplemental data showed senescence-associated loss of stress-induced HSPA1A transcription was overshadowed by the loss of stress-induced HSPA1A translation.

Chaperone function in quiescent cells

Most studies on cellular senescence (including the present study) focus on the differences between proliferating and senescent cells, neglecting the quiescent state which, as described by Alekseenko et al., 2018, "is the prevailing state of many cell types under homeostatic conditions". The authors compare proliferating and quiescent cells exposed to heat shock and show that, surprisingly, quiescent cells have a more effective DNA-damage response, are more resilient to heat shock, and see a reduction in stress-induced premature senescence. However, it could be argued that cell quiescence induced through serum starvation contradicts the authors' strive for physiological relevance; and perhaps these findings reflect similar results showing nutrient deprivation/calorie restriction in a range of cells/organisms leads to overexpression of HSPs and thus a more effective stress-response (Ehrenfried et al., 1996; Hall et al., 2000; de Cabo et al., 2003; Colotti et al., 2005; Allard et al., 2008; Novelle et al., 2015; Q. Wang et al., 2019). Increasing work is being done on the differences between proliferating, quiescent, and senescent cells, in particular by the Schosserer lab (G. Yang et al., 2020). In the present study investigating the cellular stress response, it was deemed that the use of quiescent cells would be detrimental, while the use of actively proliferating MSCs has additional relevance to the emerging field of regenerative medicine.

1.8.5 Mesenchymal stem cells in regenerative medicine

MSCs are frequently used in stem cell therapies in the emerging field of regenerative medicine. Development of these therapies began in animal models and became widely used in the effective treatment of companion/sport animals; and more recently MSC treatments are translating to clinics for human injuries and disease. Most commonly, these therapies consist of autologous transplantation using MSCs expanded on tissue culture treated plastic (TCTP), following which MSCs migrate

to the site of injury and improve tissue health through paracrine signalling (Figure 1.6a, as reviewed by Lukomska et al., 2019; Pittenger et al., 2019).

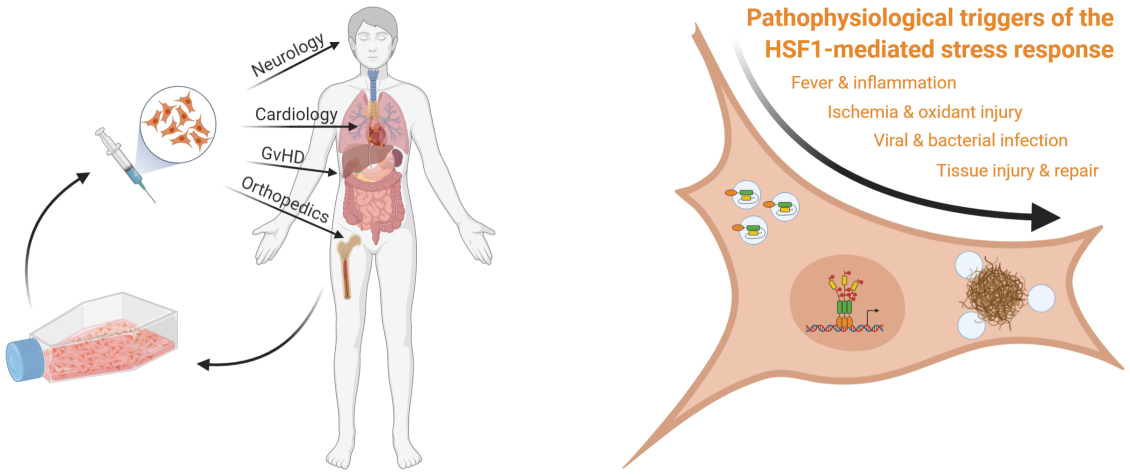

(a) (b)

Figure 1.6: Typical procedure for autologous hBM-MSC transplants. (1.6a) MSCs are extracted from bone marrow under sterile conditions, following which these cells are expanded *in vitro* before re-injection near to the target site. Adapted with *BioRender* from Lukomska et al., 2019 and MS Society UK, 2019. (1.6b) The transplant procedure carries an inherent risk of triggering a stress response in MSCs. Adapted with *BioRender* from Morimoto, 2008.

Ullah et al., 2015 review MSCs as a prominent cell source in pre-clinical treatments for neurodegenerative diseases. In a rat model of the neurodegenerative disease amyotrophic lateral sclerosis (ALS), injection of MSCs modified to express nerve growth factors by Suzuki et al., 2008 has improved motor neurone loss, delayed disease progression, and extended lifespan. A characteristic of Parkinson's disease is the substantial loss of neurons. In rat models of Parkinson's disease, Danielyan et al., 2014 nasally administered MSCs and found the cells were able to migrate and survive in several regions of the brain, prompting further research into the potential use of this method to treat the disease. In a mouse model of Alzheimer's disease, Shin et al., 2014 found administration of MSCs enhanced autophagy pathways, reduced levels of Alzheimer's characteristic amyloid-β protein in the brain, and increased survival rates of neurons. Interestingly, while most studies focus on the reparative qualities of MSCs within the brain in terms of protein-folding disease, Soria et al., 2019 investigate potential protective effects in the context of radiotherapy treatment for brain cancer. Human MSCs were expanded on TCTP and used at passages 4-7, with a dose of 5×10^5 cells intranasally administered to mice one day following radiation-induced brain injuries, with MSC doses repeated weekly for 4 weeks. The treatment was shown to promote brain injury repair and improve neurological function in agreement with the previously mentioned studies, which the authors suggest demonstrates the promise of human MSCs to treat diseases involving cognitive deterioration.

As reviewed by Markoski, 2016, therapeutic use of MSCs is most commonly applied to veterinary medicine. Work by Smith et al., 2013 isolated MSCs from the bone

marrow of racehorses with career-ending tendon injuries. BM-MSCs were grown for 3-4 weeks on TCTP (including one 1:9 passage) and 10^7 cells were implanted (autologously) into the damaged tendons. Compared to controls implanted with an equal volume of saline, the BM-MSC-treated tendons had improved functional outcomes including significantly improved stiffness, vascularity, cellularity, and matrix organisation; leading to the resemblance of normal, uninjured tendon rather than fibrous scar tissue formed in the naturally repairing controls. In another study (Marx et al., 2014), both autologous ($n = 4$) and allogeneic ($n = 5$) MSCs were used to treat canine hip dysplasia in cases where established drug therapies proved ineffective. MSCs isolated from either patients or a healthy canine donor were cultured on TCTP for between 3 and 6 passages before transplantation of $\sim 10^6$ cells via injection near the infected joint. 8 of 9 patients showed improvement of range of motion, lameness, and pain on manipulation within one month, with the most beneficial results seen in the autologous treatments.

The success of the allogeneic treatments highlights another important feature of MSCs: the ability to modulate the immune system. This was first demonstrated in humans *in vivo* by Lazarus et al., 2005 during a clinical trial of hematologic malignancy patients, spawned from the need to overcome the delay caused by autologous MSC expansion (31-day culture on TCTP). Human *in vitro* studies (Di Nicola et al., 2002; Klyushnenkova et al., 2005) have shown MSCs suppress lymphocyte proliferation, while producing antibacterial agents to prevent the drawback of causing infection (Németh et al., 2009; Krasnodembskaya et al., 2010). These features have led to clinical trials of the integration of MSCs to ameliorate the effects of graft-vs-host disease (GvHD, Munneke et al., 2016).

An intriguing emerging application of the regenerative potential of MSCs is in animal husbandry - specifically the treatment of disease or injury in bovine species. As reviewed by Hill et al., 2019, mesenchymal stem cell therapies have potential economic and animal welfare benefits through the treatment of bone/joint injuries, diabetes, and in particular mastitis (Sharma & Jeong, 2013) through their anti-inflammatory effects (Y. Gao et al., 2014). A study by Olde Riekerink et al., 2007 shows the incidence of bovine mastitis increases during hot climates; while S. Chen et al., 2018 found bovine species exposed to high temperatures suffered increased incidence of disease and reduction of milk quality. Crucial to these potential therapies would therefore be the ability of MSCs to withstand thermal stress, however Shimoni et al., 2020 show that bovine MSCs exposed to high, but physiological, temperatures *in vitro* experience stress induced premature senescence. As such, a comprehensive study of the MSC response to heat shock, and how this changes in senescence, would be of great interest (Roberts et al., 2009).

Human mesenchymal stem cell therapies

Translation of MSC therapies has been set back several years by the now retracted study by Rubio et al., 2005, which appeared to demonstrate the transformation of hMSCs into cancerous cells following long-term *in vitro* culture on TCTP. It was later found that this phenomenon could not be replicated and was likely due to cross-contamination with a human fibrosarcoma cell line also being cultured in the lab ("Retraction", 2010). To date, this study remains one of the top 10 most-cited

retracted articles of all time, however the widespread successful use of MSC therapies in large animal models is now beginning to facilitate translation into human therapies.

Kabat et al., 2020 review over 350 clinical trials involving BM-MSCs between 2004-2018, with phase 3 trials most common in GvHD and neurological, joint, and cardiovascular conditions. The dose of MSCs used is most commonly of the order 10^8 cells (typically chosen by extrapolating numbers effective in murine models based on body weight), and the authors comment that trials utilising a dose of $< 0.7 \times 10^8$ MSCs are more likely to be ineffective, possibly highlighting a need for extended MSC culture *in vitro* prior to treatment. The authors also note a lack of standardisation among culture protocols in clinical trials and highlight a need for more research into the optimisation of this process. Due to the relatively recent emergence of MSC-based therapies, understanding of the long-term effects of MSC transplantation is lacking. J. S. Lee et al., 2010 performed an interesting 5-year follow-up study of patients with ischemic stroke who received BM-MSC-based therapies, compared to controls who did not. The clinical trial was open-label and observer-blinded; with patients randomly allocated between the two groups. Autologous BM-MSCs were cultured on TCTP for 4-6 weeks prior to transplantation. 3.5 years after treatment, neurological ability had significantly improved in the MSC-treated group ($p = 0.046$), compared with no change in the control group ($p = 0.257$); and the five-year survival rate in the MSC-treated group was 72% compared with 34% in the control group ($p = 0.058$).

With increasing culture time comes the inevitability of increasing senescent cells through telomere shortening. In senescent MSCs, the paracrine signalling which promotes tissue repair is replaced with a senescence-associated secretory phenotype (SASP). Consisting of inflammatory, extracellular matrix-modifying, and tumourigenic factors (as reviewed by Neves et al., 2015; Faget et al., 2019), the SASP also includes several factors which induce senescence in healthy cells. The Gil lab (Acosta et al., 2008; Acosta et al., 2013) exposed human fibroblasts to 7-day culture medium from either healthy or senescent cultures. While the former grew normally, the latter showed a much higher proportion of β-galactosidase-positive cells after 4 days, demonstrating a positive feedback loop of senescence in late-passage cultures and aged tissues. In support of this, the group also find that senescent cells cluster together *in vivo*. Furthermore Basisty et al., 2020 demonstrate a significant correlation between SASP proteins and markers of ageing in human plasma. These studies exemplify that, while pharmacological methods of senescent cell clearance are in development and appear promising (Guerrero et al., 2020; Pignolo et al., 2020), the detrimental effect senescent cells have on surrounding cells/tissue within days cannot be neglected.

J. Liu et al., 2020 review the 15 clinically approved MSC treatments at the time of writing and find that no information on cell passage number is given for any of the treatments. Khan et al., 2011 compare the efficacy of MSC treatments in a mouse model of myocardial infraction when using young (2 months) and aged (18 months) donor MSCs. MSCs were cultured on TCTP for one week prior to transplantation and while young cultures were not devoid of senescent cells (identified

using β-galactosidase staining), a much higher proportion of senescent cells were present in the aged cultures. Mice treated with the young MSC population experienced a significant improvement in heart function compared with aged-treated mice. While the authors conclude the capacity for MSC-mediated tissue repair declines with donor age, the mechanism which causes this drop in efficacy is not explored. This is a common theme in the literature on MSC-based therapies (for example: J. Wang et al., 2013; Choudhery et al., 2014), and underpins an enduring incomplete understanding of how the MSC expansion procedure affects MSC behaviour. The need for increased basic science research in this area is further highlighted by a recent report by the BBC on extreme cases of side effects in clinically approved stem cell therapies (Montague, 2019).

Morimoto, 2008 (Figure 1.6b) reviews the triggers of the heat shock response, including several factors such as inflammation, infection, and tissue damage which are risks in MSC transplantation. Similarly, Mohyeddin Bonab et al., 2012 and Oh et al., 2015 discuss fevers as one of the most common adverse effects induced by MSCs transplants which may well cause a local heat shock environment around transplanted cells. Choudhery et al., 2014 discuss how treatment efficacy is dependent on MSC resilience to the post-transplant environment. The authors demonstrate that MSC cultures from aged human donors (> 50 years, $n = 6$) contained more senescent cells (verified via β-galactosidase staining) than young donors (< 40 years, $n = 5$) and this resulted in increased cell death when exposed to a hypoxic environment reflective of the post-transplant environment in ischemic patients.

Thus a study of the effects that both senescence and prolonged culture on TCTP have on the stress response of hBM-MSCs would be extremely beneficial to the field of regenerative medicine. Volk et al., 2012 advocate the need for better characterisation of MSC behaviour, showing young ($n = 10$; 4.9 ± 1.9 months) canine BM-MSCs change markedly following two cell passages 12-14 days apart *in vitro*, while in aged canines ($n = 8$; 89.5 ± 20.9 months), the same behavioural differences are found after just one cell passage. Regarding the practicality of scaling up therapeutic MSC use, Bronzini et al., 2012 demonstrate senescence is induced by a short shipping time of canine and equine MSC samples.

1.9 Aims

The primary aim of the PhD project was to comprehensively define how the proteotoxic stress response changes as a result of cellular ageing. To this end, a multi-omics level analysis comparing proliferating and senescent human cells *in vitro* was carried out to identify targets to investigate with higher temporal resolution approaches. These targets would then be used to evaluate cellular age-associated changes to the stress response, in terms of the speed, magnitude, and efficacy of the response. Finally, this study aimed to challenge the long-standing paradigm of chaperone regulation in the stress response. Current models theorise HSF1 activation is solely sufficient to drive the urgent and substantial up-regulation of highly abundant heat shock proteins in response to stress. To test this, this study aimed to design the first *in silico* model of the heat shock response which incorporates dynamic post-translational regulation machineries.

The realisation of these aims would provide mechanistic insight into reports in the literature that demonstrate an age-associated loss of proteostasis. As such, this would add to the basic science understanding of proteostasis and its implication in several as-yet incurable protein folding diseases. Human BM-MSCs were utilised for this study in order to simultaneously contribute to the emerging field of stem cell therapies. At a time when both clinical and pre-clinical BM-MSC treatments follow ambiguous and inconsistent protocols with varying degrees of success, this study aimed to elucidate the effects of long-term cell culture on the HSF1-mediated stress response triggered in the post-transplant environment.

Chapter 2

Materials & methods

2.1 Reagents & solutions

- Acetonitrile (Thermo Fisher scientific, #10629112)
- Ammonium bicarbonate (Sigma-Aldrich, #09830)
- Bovine serum albumin (Sigma-Aldrich, #A3294)
- Calcium chloride dihydrate (Sigma-Aldrich, #C3306)
- Copper(II) sulphate (Sigma-Aldrich, #12852)
- Custom designed real-time PCR assay primers (Primerdesign)
- 4',6-diamidino-2-phenylindole (DAPI) (Sigma-Aldrich, #D9542)
- Dimethylformamide (Cell Signaling Technology, #12767)
- Dithiothreitol (Roche, #10197777001)
- Dulbecco's Modified Eagle Medium (DMEM), low glucose, pyruvate (Gibco, #31885-023)
- Dimethyl sulphoxide (Sigma-Aldrich, #D2650)
- Dulbecco's phosphate buffered saline (Sigma-Aldrich, #D8537)
- Ethanol (Thermo Fisher scientific, #E/0650DF/P17)
- Fluorescence mounting medium (Agilent, #S3023)
- Foetal bovine serum (Labtech)
- Formaldehyde, methanol-free (Thermo Fisher Scientific, #28908)
- Formic acid (Sigma-Aldrich, #695076)
- Glycerol (Thermo Fisher scientific, #G/0650/08)
- High-Capacity RNA-to-cDNA Kit (Applied Biosystems, #4388950)
- Hydrochloric acid (Thermo Fisher scientific, #10294190)

- Industrial methylated spirit (IMS) (Thermo Fisher scientific, #M/4450/17)
- Iodoacetamide (Sigma-Aldrich, #I1149)
- Immersion Oil (Zeiss, #518F)
- L-Glutathione reduced (Sigma-Aldrich, #G4251)
- Liquid nitrogen (BOC Ltd)
- Monobromobimane (Sigma-Aldrich, #B4380)
- Penicillin-Streptomycin (Sigma-Aldrich, #P0781)
- 2-phenylethynesulfonamide (PES) (Sigma-Aldrich, #P0122)
- Phalloidin (Invitrogen, #A12379)
- Phosphotase inhibitor cocktail (Sigma-Aldrich, #P0044)
- Protease inhibitor cocktail (Sigma-Aldrich, #P8340)
- R3 reversed-phase resin (Thermo Fisher Scientific, #1-1339-03)
- RNase free water (Invitrogen, #10977-035)
- RNase-Free DNase Set (QIAGEN, #79254)
- RNeasy Mini Kit (QIAGEN, #74904)
- Senescence β-Galactosidase Staining Kit (Cell Signaling Technology, #9860)
- Sodium deoxycholate (Sigma-Aldrich, #D6750)
- Sodium dodecyl suplphate (Sigma-Aldrich, #75746)
- Sodium hydroxide (Sigma-Aldrich, #S8045)
- Sodium laurate (Sigma-Aldrich, #L9755)
- SYBR Select Master Mix (Applied Biosystems, #4472903)
- Trifluoroacetic acid (Sigma-Aldrich, #302031)
- Triton (Sigma-Aldrich, #93443)
- TruSeq Stranded mRNA assay (Illumina, Inc., #20020594)
- Trypsin-ethylenediaminetetraacetic acid (EDTA) solution (Sigma-Aldrich, #T3924)
- Trypsin resin (Thermo Fisher Scientific, #60109)
- Ultrapure water (Millipore)

2.2 Equipment

- 0.2, 0.5, and 1.5 mL tubes (Starlab Ltd.)
- 1.5 mL Protein LoBind microcentrifuge tubes (Eppendorf, #022431081)
- 1.6 mm diameter steel beads (Next Advance)
- 0.2 mL microcentrifuge (VWR, #521-2845)
- 15 mL and 50 mL Screw cap tubes (SARSTEDT)
- 96-well collection plates (Thermo Fisher Scientific, #AB0796)
- 96-well filter plates with 0.2 µL PVDF membrane (Corning, #3504)
- Aspirator (Charles Austen Pumps Ltd)
- Block heater (Techne)
- cBot (Illumina Inc.)
- Cell scraper (Grenier Bio-One, #541070)
- Class II Biological Safety cabinet (Thermo Fisher Scientific)
- Microcentrifuge (Eppendorf, #5424)
- Centrifuge, refrigerated, with 15 mL, 50 mL, and plate attachments (Eppendorf, #5810R)
- Charged surface hybrid C_{18} analytical column (Waters)
- CO_2 incubator (New Brunswick)
- Coverslips (Deltalab, #D102222)
- Cryo-gloves (Tempshield)
- Cryovials (STARLAB, #E3370-6122)
- Direct Detect Assay-free Cards (Millipore, #DDAC00010)
- Dry incubator (Genlab)
- Fast optical 96-well reaction plates (Applied Biosystems, #4346906)
- Fluorescence microscope (Zeiss, Axioimager.D2)
- Fluorescence microscope camera (Photometrics, Coolsnap HQ2)
- Forceps (Thermo Fisher scientific)
- Freezer, −80°C (New Brunswick)
- Fume cupboard (S+B UK Ltd.)

- Gel-loading tips (Starlab Ltd., #I1022-0600)
- Gel polish (Collection)
- Hemocytometer (NanoEntek)
- HiSeq 4000 Sequencing System (Illumina Inc.)
- Howie lab coat
- Infrared spectrometer (Millipore, #DDHW00010)
- Laboratory wrapping film (Bemis, #PM992)
- Lint-free laboratory wipe (Northwood, #PP1280)
- Liquid chromatography system (Dionex Corporation)
- Liquid nitrogen storage system (Thermo Fisher Scientific)
- Mass spectrometry certified vials (Thermo Fisher Scientific)
- Microscope (Olympus, CKX31 inverted)
- Quadrupole/orbitrap mass spectrometer (Thermo Fisher Scientific)
- Microscope slides (Starfrost - KNITTEL)
- NanoDrop 2000 Spectrophotometer (Thermo Fisher Scientific, #ND2000)
- Nitrile gloves (STARLAB)
- Objective lenses (Zeiss, 0.5 EC Plan-Neofluar)
- pH meter (Hanna Instruments)
- Pipette 0.5–10 µL, 2–20 µL, 20–200 µL, 100–1000 µL (Gilson)
- Pipette controller (STARLAB)
- Pipette tips 10 µL, 20 µL, 200 µL, 1000 µL (STARLAB)
- Precision balance (0.0001 g, Denver Instrument)
- Q Exactive Oribtrap Mass Spectrometer (Thermo Fisher Scientific)
- Real-Time PCR System (Applied Biosystems)
- Serological pipettes (SARSTEDT)
- TapeStation 2200 (Agilent Technologies)
- TC-treated culture flasks (Corning, #430641U)
- Thermal cycler (Applied Biosystems)
- Tissue culture-treated culture dishes (Corning, #430641U)

- Tissue homogeniser (Next Advance)
- Vacuum concentrator (Thermo Fisher Scientific, #SPD1010)
- Vortex mixer (Thermo Fisher scientific)
- Water bath (Grant Instruments)

2.3 Software

- Affinity Designer (Serif, version 1.9.0.932)
- bcl2fastq (Illumina Inc., version 2.20.0.422)
- CellProfiler (Kamentsky et al., 2011, version 2.2.0)
- Cytoscape (Shannon, 2003, version 3.6.1)
- DESeq2 (Love et al., 2014, version 1.20.0)
- Direct Detect Spectrometer software (Millipore)
- FastQC (unpublished, http://www.bioinformatics.babraham.ac.uk/projects/fastqc/)
- Fiji (Schindelin et al., 2012, version 2.0.0)
- Mascot Daemon (Matrix Science UK)
- MATLAB (MathWorks, R2017a)
- MaxQuant (Cox & Mann, 2008, version 1.6.17.0)
- Micro-Manager (Edelstein et al., 2014, version 1.4.23)
- MultiQC (Ewels et al., 2016, version 1.8)
- NanoDrop 2000 software (Thermo Fisher Scientific, version 1.6.198)
- PANTHER Classification System (Mi et al., 2021, version 16.0)
- Prism (GraphPad, version 7)
- Progenesis QI (Nonlinear Dynamics, version 4.1)
- R (R Core Team, version 3.4.1)
- Reactome Pathway Database and Overview (pathway browser version 3.7, database version 74, Fabregat et al., 2017)
- STAR (Dobin et al., 2013, version 2.7.2b)
- STRING (Szklarczyk et al., 2019, version 11.0)
- Trimmomatic (Bolger et al., 2014, version 0.36)
- Xcalibur (Thermo Fisher Scientific, version 4.1.31.9)

2.4 Acquisition of human mesenchymal stem cells

Human mesenchymal stem cells (hMSCs) were isolated from bone marrow following the total knee or hip replacements of male and female donors of varying ages using established methodology (Strassburg et al., 2010). Fully informed consent was obtained from all donors. All work was performed in accordance with guidelines and regulations from the WMA Declaration of Helsinki and the UK Human Tissue Authority; and with approval from the NHS Health Research Authority National Research Ethics Service (approval number 10/H1013/27) and The University of Manchester. Details of individual donors and the passage numbers at which hMSCs were used are provided in Table 2.1.

Donor ID	Gender	Source	Age	Passage # (proliferating)	Passage # (senescent)
WH176	F	Hip	64	2	7
WH211	F	Hip	36	7	18
TH223	M	Knee	64	4	7
WH226	F	Hip	54	2	9
TH191	F	Hip	61	4	9
TH270	M	Knee	72	1	7
TH305	M	Knee	67	3	7
TH309	F	Knee	69	4	10
WH230	M	Hip	43	3	7
WH143	M	Hip	58	2	7
TH296	M	Hip	68	2	7
TH194	M	Knee	65	3	8
TH215	M	Knee	73	3	5

Table 2.1: Disclosed information on primary human mesenchymal stem cell donors.

Sets of donors used for experiments were chosen blinded to the information in Table 2.1. Despite evidence of functional differences between female and male MSCs (Siegel et al., 2013; Tajiri et al., 2014; Zanotti et al., 2014; Y. Li et al., 2014), it was concluded that variance due to genetic and environmental factors outside of the disclosed donor information would dominate over variance due to gender and source. The generally high age of donors was also deemed appropriate and reflective of the

ages of patients who receive autologous stem cell therapies (Schimke et al., 2015). A deliberate attempt was made to not frequently use cells derived from the same donors for multiple experiments. This decision was taken in order for the results to represent a general behaviour amongst hMSCs.

2.5 Cell culture

All cell culture was carried out within a Class II Biological Safety cabinet (Thermo Fisher Scientific), using nitrile gloves (STARLAB) to prevent contamination and following proper aseptic technique with all equipment sterilised and cleaned using 70% (v/v) IMS in MilliQ ultrapure water (Millipore) prior to use. Human MSCs were cultured on tissue culture-treated polystyrene (TCTP, Corning) in low-glucose DMEM with pyruvate (Gibco, #31885-023) supplemented with 10% (v/v) fetal bovine serum (FBS, Labtech.com) and 1% (v/v) penicillin/streptomycin cocktail (PS, Sigma-Aldrich, #P0781) - herein referred to as complete medium. Cultures were incubated (New Brunswick) in a humid environment at 37°C and 5% CO_2. Unless otherwise stated, all solutions in contact with cells were warmed to 37°C in a water bath (Grant Instruments) prior to use.

2.5.1 Cell culture contaminant testing and prevention

Copper sulphate solution (Sigma-Aldrich, #12852) was used to keep incubators free from microbial contamination. Cell cultures were thoroughly checked for microscopic contaminants 2-3 times weekly using a brightfield microscope (Olympus). Cultures were also frequently checked for strains of nanoscopic mycoplasma contaminants by Eurofins Genomics, with infected cultures immediately disposed of.

2.6 Cell expansion

Human MSCs were expanded in culture within vented T25, T75, T150, or T225 tissue culture flasks (Corning, #430641U), according to the quantity of cells needed. Cells in T75 flasks were cultured in 10 mL of medium. Unless otherwise stated, all volumes used were scaled for differently sized flasks or dishes according to the surface area of the base. Old medium was fully removed via aspiration and replaced every 2-3 days. Treatment for experiments was generally carried out upon $\sim$ 80% confluency, at this point expanding cells were also passaged to facilitate further growth.

2.7 Passaging of cells

Following the aspiration of old medium, 5 mL of Dulbecco's phosphate-buffered saline (PBS, Sigma-Aldrich, #D8537) was briefly added to T75 flasks and then aspirated (herein referred to as washing with PBS) in order to remove any remaining medium. Following this, 5 mL of 1x porcine trypsin-EDTA (Sigma-Aldrich, #T3924) was added and flasks were incubated at 37°C for 5 minutes. Detachment of cells was verified under a brightfield CKX31 inverted microscope (Olympus) and trypsin was inactivated by the addition of an equal volume of the serum-containing complete medium. This cell solution was centrifuged (Eppendorf, #5810R) at an

angular acceleration of $400g$[1] at room temperature for 5 minutes. The supernatant was aspirated to leave a cell pellet. To remove any remaining trypsin-EDTA the pellet was vortexed (Thermo Fisher scientific) in 5 mL of PBS and the centrifuge and aspiration steps were repeated. For further growth, this cell solution was typically split 1:3, with two shares seeded and cultured in new T75 flasks and the third share prepared for cryogenic storage.

2.8 Cryogenic storage and recovery of cells

Cell numbers were counted using disposable hemocytometers (NanoEntek) and $\sim 5 \times 10^5$ cells were mixed in a solution of complete medium with 10% (v/v) dimethyl sulphoxide (DMSO, Sigma-Aldrich, #D2650) to prevent ice crystals forming during the freezing process and damaging cells. For short-term storage ($\leq$3 months), 1 mL of this cell solution was stored in a cryovial (Starlab Ltd., #E3370-6122) at $-80°$C (New Brunswick), whilst for long-term storage ($>$ 3 months), the vial was stored in liquid nitrogen (BOc Ltd) at $-185°$C in a Cryolus Storage System (Thermo Fisher Scientific).

To optimise the conditions of the culture for survival following removal from cryogenic storage, vials were rapidly thawed to 37°C in a water bath (Grant Instruments) and seeded at a high density ($\leq$ 75cm^2), with medium replaced the following day to remove DMSO from the culture medium. For the purpose of recording cultures' number of passages, cryogenic storage and subsequent recovery were treated as one passage.

2.9 Intra-donor pairing of early- and late-passage cells

Following acquisition, cells were seeded into tissue culture flasks. At this stage, the cells were referred to as being at "passage 1", and this number was incremented with every passage of the cells. Cultures consisting of mostly proliferating, fibroblastic cells were regarded as early-passage (EP) and cultures consisting of mostly growth-arrested, enlarged cells were regarded as late-passage (LP). Experiments requiring late-passage cells were carried out when cells in these cultures were exhibiting clear morphological changes such as increases in size and circularity, and cell growth had slowed such that the confluency required for passaging had not been achieved within 1 month of the previous passaging. Experiments requiring both early- and late-passage cells were performed by culturing late-passage cells until they met the conditions previously outlined, and then recovering early-passage cells from the same donor. Once these early-passage cells had reached 80% confluency experimental treatments were performed on both early- and late-passage cells concurrently.

[1]Throughout this document, 1 g refers to the unit of mass, while $1g$ refers to the constant of acceleration due to gravity, $g = 9.81\,\mathrm{m\,s^{-2}}$.

2.10 β-galactosidase staining of senescent cells

All reagents and solutions introduced in this section are (unless otherwise stated) supplied with the Senescence β-Galactosidase Staining Kit (Cell Signaling Technology, #9860).

1.67×10^5 hMSCs were seeded into T25 culture flasks. The culture medium was aspirated and cells were washed using PBS. 3 mL of 1x Fixative Solution was added and cells were incubated and left to fix at room temperature for 15 minutes, followed by two 5 minute PBS washes. β-Galactosidase Staining Solution was pH adjusted using hydrochloric acid (Thermo Fisher scientific, #10294190) and sodium hydroxide (Sigma-Aldrich, #S8045) to within the range 5.9-6.1 and 3 mL was added to the culture flasks. The flasks were sealed using parafilm (Bemis, #PM992) to prevent solution evaporation and crystal formation, and incubated at 37°C for 24 hours in a dry incubator (Genlab) to prevent high CO_2 levels affecting the solution pH. The Staining Solution was removed and two 5 minute PBS washes were carried out. Cells were overlaid with 70% glycerol (Thermo Fisher scientific, #G/0650/08) in ultrapure water.

Images were collected on an Olympus CKX31 inverted microscope using x5, x10, and x20 magnification lenses. All samples under comparison in the same experiment were incubated with the same batch of Staining Solution, in the same incubator at the same time, and images had matched exposure and contrast settings.

2.11 Seeding of cells onto single well plates

For microscopy experiments requiring low quantities of cells and several differing concurrent treatments, cells were seeded onto single-well 35 m diameter dishes (Corning). Coverslips (Deltalab, #D102222) were submerged in 70% ethanol (Thermo Fisher scientific, #E/0650DF/P17) in ultrapure water for 30 minutes, then rinsed in ultrapure water, and placed in the dishes (1 per dish). Cells were counted as in Section 2.8 and $\sim 10^4$ cells were seeded onto each coverslip-containing dish in 2 mL of complete medium.

2.12 Heat shock of cells

Heat shock of cells was carried out by quickly moving cultures to an identical incubator pre-heated to 42°C. Cells in dishes or flasks were incubated at this temperature for either 1 or 2 hours before being harvested or being returned to a 37°C incubator for heat shock recovery. While perhaps on the border of physiological relevance (Evans et al., 2015), an elevated thermal stress *in vitro* may better represent the compound of environmental stresses cells experience *in vivo*.

2.13 Cell fixation, permeabilisation, and blocking for microscopy

35 m dishes of hMSCs were aspirated of medium and washed with PBS. Cells were fixed with the addition of 1 mL of 4% (w/w) methanol-free formaldehyde (Thermo Fisher Scientific, #28908) in PBS for 10 minutes, incubated at 37°C. Following removal of the formaldehyde and two washes in PBS for 5 minutes each, cells were permeabilised in 1 mL of 1% Triton X-100 (Sigma-Aldrich, #93443) in PBS for 10 minutes at room temperature. Following removal of Triton and PBS washing, cells were blocked in a 1 mL solution of 2% bovine serum albumin (Sigma-Aldrich, #A3294) and 0.1% Triton X-100 in PBS (herein referred to as blocking buffer) for 1 hour at 37°C.

2.14 Primary and secondary antibody staining

Blocking buffer was replaced with fresh blocking buffer containing one of the primary antibodies (see Table 2.2): anti-HSPA1A (abcam, #ab181606), anti-HSF1 (abcam, #ab52757), or anti-STUB1 (abcam, #ab134064). Cells were incubated for 1 hour at 37°C and then washed in PBS five times for 5 minutes each. Cells were then incubated in fresh blocking buffer containing 0.2% (v/v) $1\,\mathrm{mg\,mL^{-1}}$ $\lambda = 461$nm DAPI (Sigma-Aldrich, #D9542), 0.2% (v/v) $\lambda = 488$nm Phalloidin (Invitrogen, #A12379), and $\lambda = 594$nm secondary antibody (Invitrogen, #A21207), for 1 hour at 37°C, followed by five PBS washes for 5 minutes each. From the introduction of fluorescent antibodies, all work was done whilst obscured from direct light.

Antibody	Host	Species	Concentration (v/v)	Catalogue #
Monoclonal [EP1710Y] α-HSF1	Rabbit	Human	0.1%	abcam, #ab52757
Monoclonal [EPR16892] α-HSPA1A	Rabbit	Human	0.1%	abcam, #ab181606
Monoclonal [EPR4447] α-STUB1	Rabbit	Human	0.1%	abcam, #ab134064
$\lambda = 594$nm IgG (H+L)	Donkey	Rabbit	0.1%	Invitrogen, #A21207

Table 2.2: Details of primary and secondary antibodies.

Primary and secondary antibody concentrations were optimised from a range of concentrations suggested by the supplier, such that a viable signal was obtained whilst mitigating background signal. The same antibodies and concentrations have been used for all comparisons between fluorescence signals.

2.15 Immunofluorescence microscopy

A drop of Dako anti-fade fluorescence mounting medium (Agilent, #S3023) was placed on microscope slides. Stained coverslips were removed from dishes, rinsed in water to remove PBS salt crystals, inverted and placed on microscope slides such that mounting medium coated the cell-side. Mounted slides were left at room temperature overnight for mounting medium to dry, before being sealed with a thin layer of Crystal Clear 1 gel polish (Collection).

Images were collected on a Zeiss Axioimager.D2 upright microscope using 0.5 EC Plan-Neofluar objective lenses and captured using a Coolsnap HQ2 camera (Photometrics) with Micro-Manager software (version 1.4.23). Band pass filter sets for DAPI, FITC and Texas red were used to prevent bleed between channels. Images were taken from 20 frames of view per treatment.

2.16 Fluorescence quantification

Images were processed using Fiji and ImageJ (Schindelin et al., 2012, version 2.0.0). Images were corrected for background fluorescence by subtracting the mean intensity per pixel of a cell-free area from each pixel. All images under comparison in the same experiment had matched exposure and contrast settings. CellProfiler (Kamentsky et al., 2011, version 2.2.0) was used to quantify cellular and nuclear morphometric parameters, using DAPI-filtered images to identify nuclear areas, and using FITC-filtered images to identify cellular areas (Figure 2.1). Cytoplasmic areas were defined as the cellular area, excluding the nuclear area. Using the Texas red-filtered images, relative quantification of the concentration of the antibody-tagged protein was measured using the mean pixel intensity in these areas.

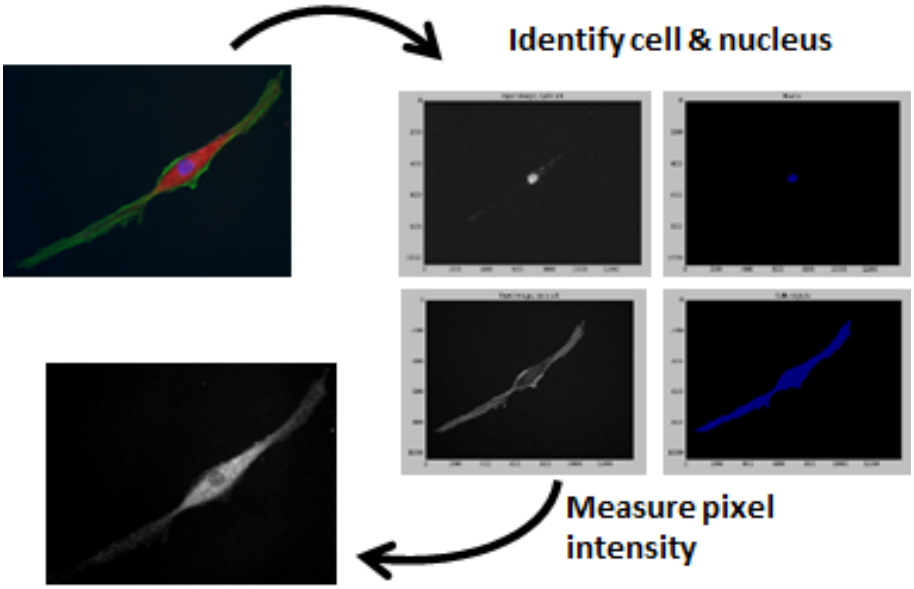

Figure 2.1: Relative protein quantification using fluorescence microscopy. Distinct channels are used for nuclear marker DAPI, cytoskeletal marker phalloidin, and secondary antibody staining.

2.17 Analysis of microscopy data

All microscopy experiments were performed using three biological replicates (i.e. cells from three different donors, see Table 2.1). Measurements from 20 frames of view from each of these biological replicates were used to apply a multi-way analysis of variance (ANOVA). This enabled treatment effects to be isolated from donor effects, as donor effects incur large amounts of data variance in human cell experiments due to high genomic and environmental variability between donors (Mallikarjun et al., 2020; Brodin et al., 2015). This was carried out using the MATLAB function `fitlm.m` to set out a categorical linear regression model:

$$Measured\,value = \beta_0 + \vec{\beta_1} \cdot [\vec{Donor}] + \vec{\beta_2} \cdot [\vec{Time}] + \epsilon \tag{2.1}$$

to evaluate the significance of changes with time; and

$$Measured\,value = \beta_0 + \vec{\beta_1} \cdot [\vec{Donor}] + \vec{\beta_2} \cdot [\vec{Passage}] + \epsilon \tag{2.2}$$

to evaluate the significance of changes with passage. Here β_0 is the intercept value corresponding to an arbitrarily chosen donor and the control treatment; $\vec{\beta_1} = (\beta_{1,i}, \beta_{1,j}, \beta_{1,k})^\intercal$ is the effect size of each donor on the measured value; $\vec{\beta_2}$ is defined similarly and gives the effect size of each treatment on the measured value; the binary arrays $[\vec{Donor}]$, $[\vec{Time}]$, and $[\vec{Passage}]$ represent the donor, time-point, and passage of interest, respectively; and ϵ is the error variable of the model.

In graphical representations of microscopy data, $\beta_0 + \vec{\beta_2} \cdot [\vec{Time}]$ or $\beta_0 + \vec{\beta_2} \cdot [\vec{Passage}]$ values are normalised to β_0 to illustrate treatment effects relative to the control treatment whilst discounting donor effects. The marker size for each data point in these graphical representations is proportional to the p-value for the t-statistic of the hypothesis test that the corresponding $\vec{\beta_2}$ element is equal to zero or not. Filled data points indicate treatment effect sizes which are non-zero at the 5% significance level.

2.18 RNA isolation

All reagents and solutions introduced in this section are (unless otherwise stated) supplied with the RNeasy Mini Kit (QIAGEN, #74904).

hMSCs were seeded onto 35 mm dishes with $\sim 10^5$ cells per dish. Following heat shock/recovery, the culture medium was aspirated and cells were washed using chilled (4°C) PBS to ensure no complete medium remained to potentially inhibit lysis. Cells were lysed in 0.7 mL Buffer RLT for 2 minutes. The solution was then collected in a 1.5 mL tube (Starlab Ltd.) - detachment and collection were assisted using a cell scraper (Grenier Bio-One, #541070). The cell lysate was homogenised by vortexing for one minute. One volume of 70% ethanol in ultrapure water was added and mixed into the homogenised lysate by pipetting. 700 µL was transferred into an RNeasy Mini Spin Column fitted with an RNeasy Mini Collection Tube. The column was centrifuged in a microcentrifuge (Eppendorf, #5424) at 20000g for 15 seconds. The flow-through was discarded from the collection tube and this step was repeated with the final 700 µL of homogenised lysate.

2.18.1 DNase treatment

Due to the sensitivity of RT-qPCR to off-target DNA binding, a DNase digestion was performed. DNase I stock solution and Buffer RDD were supplied with the QIAGEN RNase-Free DNase Set, #79254. 350 µL Buffer RW1 was added to the spin column containing the homogenised lysate. The column was centrifuged in a microcentrifuge at 20000g for 15 seconds and the flow-through was discarded. 5 µL of DNase I stock solution was added to 35 µL Buffer RDD in a 0.5 mL tube (Starlab Ltd.) and mixed by inverting to prevent denaturation of the DNase. This solution (40 µL) was added by gently pipetting directly onto the membrane of the spin column containing the homogenised lysate and was left to incubate at room temperature for 15 minutes. The wash step immediately prior to the addition of DNase I stock solution was then repeated to conclude DNase digestion.

500 µL of reconstituted Buffer RPE was added to the spin column containing the homogenised lysate. The column was centrifuged at 20000g for 15 seconds and the flow-through was discarded. This step was then repeated with a further 500 µL Buffer RPE, and instead centrifuged at 20000g for 2 minutes. The column was then centrifuged again at 20000g for 1 minute in order to dry the column membrane. The collection tube was replaced with a 1.5 mL tube and 30 µL of RNase-free water (Invitrogen, #10977-035) was added by gently pipetting directly onto the column membrane. To elute the purified RNA into the 1.5 mL tube, the column was centrifuged at 20000g for 1 minute.

2.18.2 RNA quantification

RNA concentration was measured using a NanoDrop 2000 spectrophotometer (Thermo Fisher Scientific, #ND2000) on the Nucleic Acid setting. A blank was established using 1.2 µL of RNase-free water, before the absorbance of light at a wavelength $\lambda = 260\,\text{nm}$ by 1.2 µL of the purified RNA sample was measured. The sample stage was cleaned prior to use and between samples using lint-free laboratory wipes (Northwood, #PP1280). The absorbance was converted to nucleic acid concentration using the Beer-Lambert equation, with an extinction coefficient of $40\,\text{ng cm}\,\mu\text{L}^{-1}$ for RNA. High RNA yield and low protein or salt contamination in all samples used was verified with absorbance ratios $\frac{260\,\text{nm}}{280\,\text{nm}}, \frac{260\,\text{nm}}{230\,\text{nm}} \geq 2$.

2.19 Reverse transcription

Enzyme Mix (containing MuLV and RNase inhibitor protein) and reverse transcription Buffer Mix (containing dNTPs, random octamers, and oligo dT-16) were supplied with the High-Capacity RNA-to-cDNA Kit (Applied Biosystems, #4388950). Buffer Mix was warmed to 37°C in a water bath, whilst Enzyme Mix was kept on ice until use.

RNA samples were diluted using RNase-free water, such that 9 µL of solution contained 350ng of RNA (to yield well over the 30ng of RNA needed for each of the 8 primers used in Section 2.20). A negative control containing 9 µL of RNase-free water only was also included. Enzyme Mix was mixed by pipetting, before adding

1 µL of Enzyme Mix to 10 µL of reverse transcription Buffer Mix in 0.2 mL tubes (Starlab Ltd.) and mixing by pipetting. 9 µL of RNA sample solution was added to the 11 µL Enzyme-Buffer solution and tubes were centrifuged (MiniStar microcentrifuge, VWR, #521-2845) momentarily to push all liquid to the bottom of the tube. Samples were reverse-transcribed using a Veriti Thermal Cycler (Applied Biosystems) as shown in Table 2.3.

Step	Temperature	Duration
Incubation	37°C	60 minutes
Reverse transcription	95°C	5 minutes
Inactivation	4°C	∞

Table 2.3: Thermal cycler settings for reverse transcription reactions.

Under the assumption the reverse-transcription reaction yielded an approximately equal mass of complementary deoxyribonucleic acid (cDNA), the solution was transferred to a 0.5 mL tube and diluted in RNase-free water to a cDNA concentration of 5 ng μL^{-1}.

2.20 Quantitative Polymerase Chain Reaction

Reverse transcription quantitative polymerase chain reaction (RT-qPCR) was performed in triplicate using the SYBR Select Master Mix, containing SYBR GreenER dye, AmpliTaq DNA Polymerase UP, dNTPs with dUTP/dTTP blend, heat-labile UDG, ROX passive reference dye, and optimized buffer components (Applied Biosystems, #4472903). Custom designed and validated primers (PrimerDesign Ltd) were used as in Table 2.4. In addition to primers for 7 genes of interest, an endogenous control primer for the housekeeping (HK) gene PPIA was also included. For an evaluation of the expression stability of PPIA in hMSCs, see X. Li et al., 2015. Further, see R.-H. Jeon et al., 2019, where it has been shown that PPIA RNA levels in primary hBM-MSCs remain stable across 20 passages on TCTP. Finally, Silva et al., 2013 carried out the heat shock of bovine cells *in vitro* at 41°C for 6 hours and evaluated the suitability of several common housekeeping genes, finding PPIA as the most stable in response to heat shock.

Target gene	Sense	Anti-sense
Peptidyl-prolyl isomerase A (PPIA)	ATG CTG GAC CCA ACA CAA	TTT CAC TTT GCC AAA CAC CA
Heat shock 70 kDa protein 1A (HSPA1A)	CCA CCA AGC AGA CGC AGA T	CCC TCT CGC CCT CGT ACA T
Heat shock factor protein 1 (HSF1)	CCA CCT CCA CCC CTG AAA A	GGA GTC CAT AGC ATC CAA GTG
Lamin-B1 (LMNB1)	CCT TCT TCC CGT GTG ACA GTA	CTA CTC GCC TCT GAT TCT TCC A
ATM	TTT CTA CAT TTT ATC CAG CAT TTC TCT	TTC CAC TTC TAC CTA TGT ATC AAA CT
HSPA2	TCG CTC GCC TTT CAG TCA G	TGA TCT CCA CCT TGC CAT GTT
DnaJ homolog subfamily B member 1 (DNAJB1)	AAT CTC CCA CAA GCG GCT AA	GGT CTG GTC TCC TTC CTT GG
Heat shock protein beta-1 (HSPB1)	GCC GCC AAG TAA AGC CTT A	CTT TGA ACT TTA TTT GAG AAA AAC AGA

Table 2.4: Custom designed and validated primers used (supplied by Primerdesign).

Primers were warmed on a block heater (Techne) to 37°C prior to use. For each PCR reaction to be carried out, 2 µL of sample (10 ng cDNA) was pipetted into the wells of a fast optical 96-well reaction plate (Applied Biosystems, #4346906). 5 µL of SYBR Select Master Mix was mixed with 2.5 µL RNase-free water and 0.5 µL of the appropriate primer; the resulting 8 µL was also added to each well. The plate was covered and briefly centrifuged up to 1500 rpm to push all liquid to the bottom of the wells. The qPCR reaction was carried out using a StepOnePlus Real-Time PCR System (Applied Biosystems) following the conditions outlined in Table 2.5.

Step	Temperature	Duration	Cycles
1: UDG Activation	50°C	2 minutes	Hold
2: AmpliTaq Fast DNA Polymerase, UP Activation	95°C	2 minutes	hold
3: Denature	95°C	3 seconds	40
4: Anneal/Extend	60°C	30 seconds	

Table 2.5: Thermal cycler settings for qPCR reactions.

2.21 Analysis of RT-qPCR data

Data was analysed using the $2^{-\Delta\Delta C_T}$ method (Livak & Schmittgen, 2001), where C_T is the cycle at which the sample fluorescence reaches a fixed threshold. All RT-qPCR experiments were performed in triplicate and using four biological replicates (i.e. cells from four different donors, see Table 2.1). Within each biological replicate, a mean C_T value and corresponding standard deviation, σ_{C_T}, was calculated from the triplicate values (with any results more than 3 standard deviations from the mean considered an outlier and removed). These values were then normalised to the corresponding values of firstly the housekeeping gene PPIA, and secondly the control treatment, with the errors propagated accordingly[2]:

$$\sigma_{\Delta C_T} = \sqrt{\sigma^2_{C_T} + \sigma^2_{C_T(HK)}}\,, \tag{2.3}$$

$$\sigma_{\Delta\Delta C_T} = \sqrt{\sigma^2_{\Delta C_T} + \sigma^2_{C_T(Control)}}\,, \tag{2.4}$$

$$\sigma_{2^{-\Delta\Delta C_T}} = \mid -ln(2) \cdot 2^{-\Delta\Delta C_T} \mid \cdot \sigma_{\Delta\Delta C_T}\,. \tag{2.5}$$

The mean $2^{-\Delta\Delta C_T}$ value, representing the relative change in RNA expression; and corresponding standard deviation calculated in Equation 2.5 from the triplicate values for each biological replicate $i \in [1, 4]$; were used to give a weighted mean μ and weighted standard deviation σ for each treatment such that more consistent triplicate values would hold higher weight:

[2]Livak and Schmittgen, 2001 set a precedent which continues to reverberate in published qPCR data, whereby $\sigma_{C_T(HK)}$ is neglected. This may be intentional - in Schmittgen and Livak, 2008 the authors assert their method of data analysis is correct. As an example of the overestimation of significance this causes, if the reader so chooses to repeat the worked example of how to calculate standard deviation in qPCR data from the aforementioned 2001 article (Figure 2, purple box), the correct standard deviation of the authors' data is more than 5-fold larger than quoted in the article.

$$\mu = \frac{\sum \frac{2_i^{-\Delta\Delta C_T}}{\sigma_{2_i^{-\Delta\Delta C_T}}}}{\sum \frac{1}{\sigma_{2_i^{-\Delta\Delta C_T}}}}, \tag{2.6}$$

$$\sigma = \sqrt{\frac{1}{\sum \frac{1}{\sigma_{2_i^{-\Delta\Delta C_T}}}}}. \tag{2.7}$$

In graphical representations of RT-qPCR data, the μ values calculated in Equation 2.6 are shown. The marker size for each data point is proportional to the p-value for the t-statistic of the hypothesis test that $\mu - 1$ is equal to zero or not, using the σ values calculated in Equation 2.7. Filled data points indicate changes in relative RNA expression which are non-zero at the 5% significance level.

2.22 RNA-sequencing

All reagents and solutions introduced in this section are (unless otherwise stated) supplied with the TruSeq Stranded mRNA assay (Illumina, Inc.,#20020594).

Total RNA from five biological replicates (i.e. cells from five different donors, see Table 2.1) was prepared as in Section 2.18 and was submitted to the Genomic Technologies Core Facility (GTCF). Quality and integrity of the RNA samples were assessed using a TapeStation 2200 (Agilent Technologies) and then libraries were generated as follows. Briefly, total RNA (0.1–4 µg) was used as input material from which polyadenylated mRNA was purified using poly-T, oligo-attached, magnetic beads. The mRNA was then fragmented using divalent cations under elevated temperature and then reverse transcribed into first strand cDNA using random primers. Second strand cDNA was then synthesised using DNA Polymerase I and RNase H. Following a single 'A' base addition, adapters were ligated to the cDNA fragments, and the products then purified and enriched by PCR to create the final cDNA library. Adapter indices were used to multiplex libraries, which were pooled prior to cluster generation using a cBot instrument (Illumina Inc.). The loaded flow-cell was then paired-end sequenced ($76 + 76$ cycles, plus indices) on a HiSeq4000 instrument (Illumina Inc.). Finally, the output data was demultiplexed (allowing one mismatch) and BCL-to-Fastq conversion was performed using bcl2fastq software (Illumina Inc., version 2.20.0.422).

2.23 Analysis of sequencing data

The quality of RNA-sequencing data was assessed using Phred quality scores (Q, Ewing and Green, 1998):

$$Q = -10Log_{10}P, \tag{2.8}$$

where P is the base calling error probability. Unmapped paired-end sequences from an Illumina Hiseq4000 sequencer were assessed by FastQC (unpublished). Sequence

adapters were removed and reads were quality trimmed (to the threshold $Q \geq 20$) using Trimmomatic (Bolger et al., 2014, version 0.36). The reads were mapped against the reference human genome (hg38) and counts per gene were calculated using annotation from GENCODE 36 (http://www.gencodegenes.org/) using STAR (Dobin et al., 2013, version 2.7.2b). Normalisation, principal component analysis, and differential expression was calculated in DESeq2 (Love et al., 2014, version 1.20.0) using default settings. This was treated as a standard 2x2 design and data was fitted to a linear regression model as in Equation 2.2. Where figures containing -omic data are windowed for ease of interpretation, all plots contain $\geq 99\%$ of data points.

2.24 HSP70 inhibition

In experiments with HSP70 inhibition, complete medium was replaced with an equal volume of fresh complete medium containing 0.01% dimethyl sulphoxide (Sigma-Aldrich, #D2650) and 10 µM 2-phenylethynesulfonamide (Sigma-Aldrich, #P0122) 30 minutes prior to heat shock. In the subsequent analysis of these experiments, comparisons were made to vehicle-only controls where complete medium was instead replaced with fresh complete medium containing just 0.01% dimethyl sulphoxide.

2.25 Cell lysis for mass spectrometry

hMSCs were harvested and pelleted as in Section 2.7, with the exception that, following the detachment of cells, centrifugation steps were performed at 4°C and a separate PBS solution pre-chilled to 4°C was used. 30 µL of Lysis Buffer (see Table 2.6 for full composition) containing detergents and protease and phosphotase inhibitors was mixed into the cell pellet by pipetting, and the cell solution was transferred to a 1.5 mL protein LoBind tube (Eppendorf, #022431081). Detergents sodium laurate and sodium deoxycholate were chosen for their proficiency in lysing cell membranes (Y. Lin et al., 2013) and effectively solubilising cellular proteins and aiding trypsin digestion (Y. Lin et al., 2008).

Buffers used for the preparation of samples for mass spectrometry were made up in 25 mM ammonium bicarbonate (Sigma-Aldrich, #09830) due to its volatility - to allow samples to dry quickly - and pH $\approx$ 7.8 which facilitates peptide reduction and alkylation via dithiothreitol (Roche, #10197777001) and iodoacetamide (Sigma-Aldrich, #I1149), respectively.

Six 1.6 mm diameter steel beads (Next Advance) were added to the cell pellet tube and cell lysis was carried out by homogenisation in a Bullet Blender Tissue Homogeniser (Next Advance) at 4°C at maximum speed for 2 minutes. To remove cell debris, the cell homogenate was centrifuged at 10,000 rpm for 5 minutes and the supernatant was transferred to a fresh 1.5 mL LoBind tube.

Constituent	Concentration (w/w)	Supplier
Sodium laurate	1.1%	Sigma-Aldrich, #L9755
Sodium deoxycholate	0.3%	Sigma-Aldrich, #D6750
Protease inhibitor cocktail	0.1%	Sigma-Aldrich, #P8340
Phosphotase inhibitor cocktail	0.1%	Sigma-Aldrich, #P0044
25 mM Ammonium bicarbonate in ultrapure water	98.4%	Sigma-Aldrich, #09830

Table 2.6: Composition of the buffer used in cell lysis for mass spectrometry. The buffer was kept on ice until use to aid the stability of protease and phosphotase inhibitors.

2.25.1 Protein quantification by infrared spectrometry

A calibrated Direct Detect Infrared Spectrometer (Millipore, #DDHW00010) was used to quantify the amount of protein in each sample. This was done by pipetting a 2 µL blank of Lysis Buffer onto a Direct Detect Assay-free card (Millipore, #DDAC00010), followed by 2 µL from each sample. To form proteins or peptides, amino acids are covalently linked via amide bonds. These amide bonds absorb strongly in the mid-IR range 1600-1690cm^{-1}. The spectrometer was run on the AM1 setting, intended for samples in buffers such as ammonium bicarbonate with low absorbtion at 1600-1700cm^{-1}. For each sample it was verified that no absorbance peak occurred in the 1600-1690cm^{-1} range in the blank absorbance spectrum, and that a clear absorbance peak did occur in this range in the sample absorbance spectrum (Figure 2.2). These readings were used to dilute each sample to a concentration of 2 µg µL^{-1}.

2.26 Protein digestion

175 µL of 1.33 mM $CaCl_2$ (Sigma-Aldrich, #C3306) in 25 mM ammonium bicarbonate, and 50 µg of protein (25 µL) were mixed together in a 500 µL tube containing immobilised trypsin beads. As shown by Kotormán et al., 2003, calcium ions increase the stability of trypsin without compromising enzyme activity. Protein samples were digested into tryptic peptides overnight ($>$ 8 hours) using a thermal cycler (Applied Biosystems) running at 1,400 rpm, 37°C.

2.27 Peptide reduction and alkylation

The reduction and alkylation of cysteine residues improves peptide yield and protein sequence coverage in mass spectrometry. Figure 2.3 demonstrates the mechanism of action of dithiothreitol, a reducing agent which breaks disulphide bonds that have

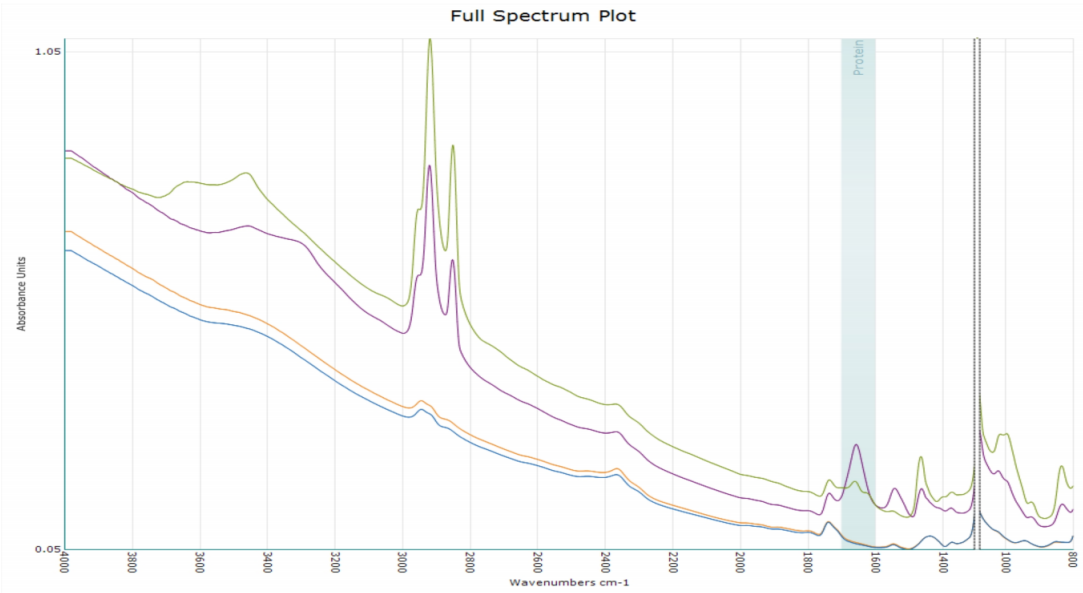

Figure 2.2: Protein quantification of whole-cell lysates using infrared spectrometry. The green line indicates the absorption spectrum of the blank (lysis buffer); the purple line indicates the absorption spectrum of a whole-cell lysate; while the blue and orange lines correspond to unused card slots. The shaded region indicates the region of protein absorption wavelengths.

formed between cysteine residues in peptides, converting these into free sulphydryl groups (Gundry et al., 2009). Following sample digestion, 4 µL of 500 mM dithiothreitol in 25 mM ammonium bicarbonate was added and the samples were run on the thermocycler for 10 minutes at 1,400 rpm, 60°C. The temperature of the thermocycler was increased to 60°C in order to increase the efficiency of the dithiothreitol, by encouraging denaturation and increasing the accessibility of disulphide bonds in the sample.

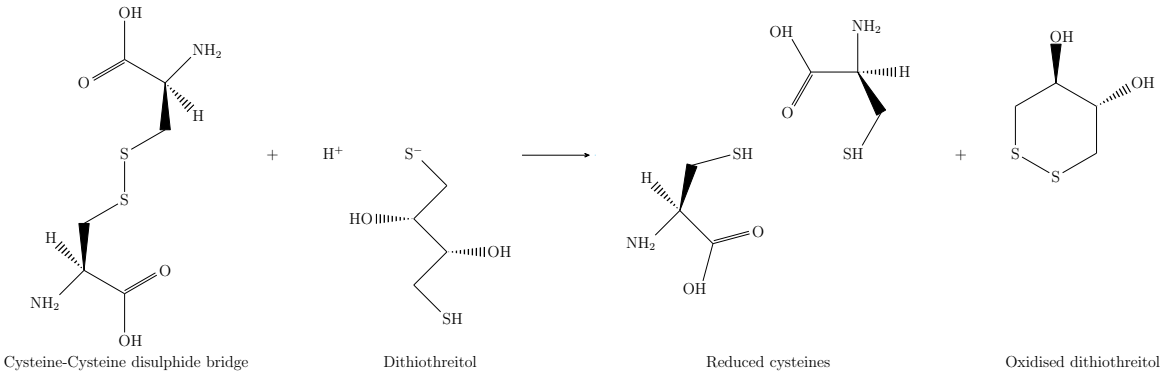

Figure 2.3: Reduction of cysteine-cysteine disulphide bridges using alkaline dithiothreitol.

Iodoacetamide (Figure 2.4) is an alkylating agent which reacts with the free sulphydryl groups of cysteine residues (induced by peptide reduction) to form S-carboxyamidomethyl-cysteine, which cannot be reoxidised to form disulphide bonds (Gundry et al., 2009). The thermocycler was cooled to 25°C and 12 µL of 500 mM iodoacetamide in 25 mM ammonium bicarbonate was added and the samples were

ran on the thermocycler for 30 minutes at 1,400 rpm. During the alkylation, the thermocycler was covered due to the light-sensitivity of iodoacetamide (Crestfield et al., 1963).

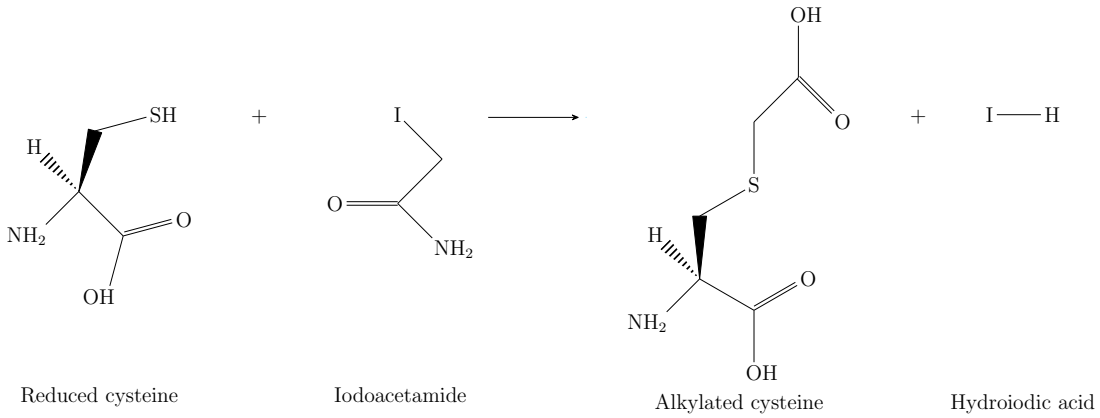

Figure 2.4: Alkylation of reduced cysteine using iodoacetimide.

While reduction and alkylation of peptide samples for mass spectrometry is typically carried out prior to protein digestion to allow trypsin maximal access to protein cleavage sites, studies such as Boja and Fales, 2001 and Guo et al., 2015, have shown the detrimental effects of prolonged exposure of samples to alkylating agents. Thus these steps were carried out following overnight digestion.

Samples in 500 µL tubes containing immobilised trypsin beads were centrifuged (Eppendorf, #5810R) at 20000g for 10 minutes at room temperature, and the supernatants (200 µL) were transferred to 1.5 mL LoBind tubes.

2.28 Biphasic extraction of peptides

To quench any further trypsin digestion and facilitate the removal of hydrophobic molecules - such as lipids and detergents - by biphasic extraction, the sample solution was acidified by adding 5 µL of 10% trifluoroacetic acid (Sigma-Aldrich, #302031) in ultrapure water. An equal volume (200 µL) of ethyl acetate was added to the samples and the solution was vortexed for 1 minute to thoroughly mix the organic compound into the solution. The solution was separated into two phases by centrifuging at 20000g for 5 minutes at room temperature. Gel-loading tips (Starlab Ltd., #I1022-0600) were used to carefully aspirate the organic epiphase and the process of adding ethyl acetate, vortexing, centrifuging, and aspirating was repeated twice more.

Peptide samples were dried down to a minimal volume using a SpeedVac (Thermo Fisher Scientific, #SPD1010) on a manual run at room temperature for 3 hours. Dried samples were stored overnight at 4°C.

2.29 Peptide desalting

Because mass spectrometry measures charged ions, salts must be removed prior to analysis (Thermo Fisher Scientific, 2017). Salts in the peptide samples were removed

by reversed-phase chromatography. A 120 µL volume of OLIGO R3 reversed-phase resin (Thermo Fisher Scientific, #1-1339-03) was added to the wells of a 96-well filtration membrane plate (Corning, #3504). The resin was rinsed in 50 µL 50% (v/v) acetonitrile (Thermo Fisher scientific, #10629112) in ultrapure water by pipetting up and down, taking care to avoid piercing the filter membrane. This equilibrates the beads in a buffer compatible with peptide attachment as the binding of peptides to hydrophobic bead resins is most effective at high ionic strength. A 96-well collection plate (Thermo Fisher Scientific, #AB0796) was fitted under the filtration membrane plate and the plate was centrifuged (Eppendorf, #5810R) at 200g for 1 minute. The flow-through into the collection plate was discarded and the rinsing and centrifugation steps were repeated. Following this, two rinse and centrifuge steps were also performed using 50 µL of 0.1% (v/v) trifluoroacetic acid in ultrapure water. The purpose of the acidic buffer is to prevent peptides precipitating through the membrane.

Dried samples were mixed by pipetting into 200 µL 5% (v/v) acetonitrile, 0.1% (v/v) trifluoroacetic acid in ultrapure water. The bead resin was then rinsed using 100 µL of the sample solution, the plate was centrifuged at 200g for 1 minute, the flow-through into the collection plate was discarded, and these steps were repeated for the final 100 µL of sample solution. In these steps, hydrophobic molecules in the sample solution interact with the C_{18} chains of the resin.

To wash out hydrophillic salts, the resin-bound sample was rinsed in 50 µL of 0.1% (v/v) trifluoroacetic acid in ultrapure water and the plate was centrifuged at 200g for 1 minute, the flow-through into the collection plate was discarded, and these rinse and centrifugation steps were repeated. To prepare for peptide elution, the wells of the collection plate were rinsed using 100 µL 50% (v/v) acetonitrile in ultrapure water, which was then discarded. The desalted, resin-bound sample was then rinsed in 50% (v/v) acetonitrile in ultrapure water and the plate was centrifuged at 200g for 1 minute and these rinse and centrifugation steps were repeated. The increased percentage of acetonitrile reduces hydrophobic interaction and allows for elution of the desalted peptide samples from the bead resin (Ciborowski & Silberring, 2016).

Desalted peptide samples were transfered to mass spectrometry certified vials (Thermo Fisher Scientific) and dried down to a minimal volume using a SpeedVac on a manual run at room temperature for 1 hour. Dried samples were stored at $-20°C$ until mass spectrometry was performed.

2.30 Liquid chromatography-Mass spectrometry

Dried samples were reconstituted in 5% acetonitrile and 0.1% trifluoroacetic acid in ultrapure water. The peptide concentration was measured, again using a Direct Detect spectrophotometer, and samples were diluted to 300 ng µL^{-1}. Samples were analysed by liquid chromatography-MS/MS using an UltiMate 3000 RSLC (Dionex Corporation) coupled to a Q Exactive HF (Thermo Fisher Scientific) mass spectrometer. Peptide mixtures were separated using a multistep gradient from 95% A (0.1% formic acid (Sigma-Aldrich, #695076) in ultrapure water) and 5% B (0.1% formic acid in acetonitrile) to 7% B at 1 minute, 18% B at 58 minutes, 27% B in 72 minutes,

and 60% B at 74 minutes at 300nL/minute, using a 75 mm × 250 µm inner diameter 1.7 µM charged surface hybrid C_{18} analytical column (Waters). Peptides were automatically selected for fragmentation by data dependent analysis; mass spectrometers were operated using Xcalibur software (Thermo Fisher Scientific, version 4.1.31.9).

2.31 Peptide quantification

Mass spectrometry results files were imported into Progenesis QI (Nonlinear Dynamics, version 4.1). Ion intensity maps were quality-control checked according to Nonlinear Dynamics guidelines before being aligned automatically. Where automatic alignment failed, manual alignment (Figure 2.5) was carried out until an alignment score of $\geq 70\%$ was achieved.

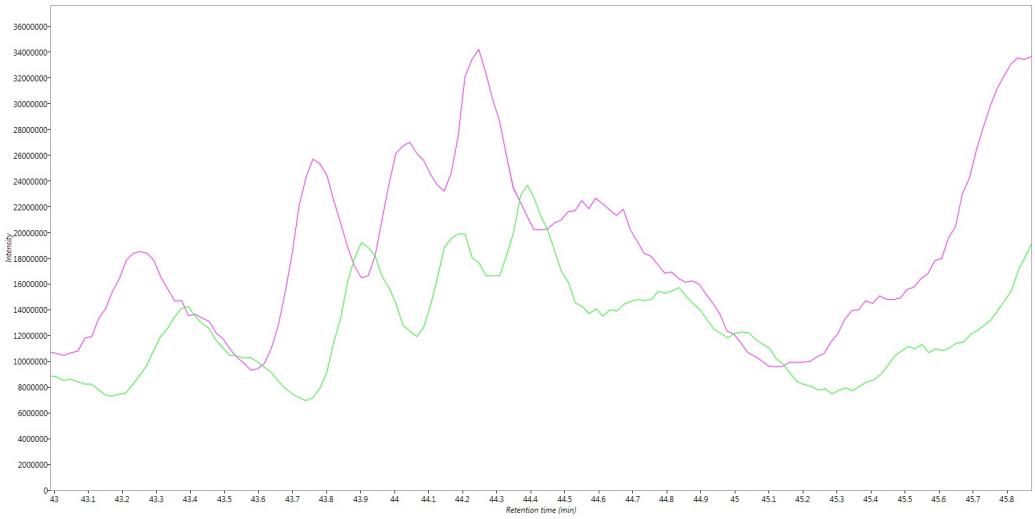

Figure 2.5: Manual alignment of mass spectrometry ion-intensity maps. A reference spectrum (purple) was chosen based on intensity, and peaks in other spectra (green) were aligned to the reference peaks.

Peptide quantification and filtering was carried out in Progenesis QI using the settings detailed in Table 2.7.

Quantification method	Relative quantification using non-conflicting peptides
Peal picking sensitivity limit	4
Charge filtering	Include +1 to +4
# isotopes filtering	Exclude ≤ 2
Batch inclusion options	Exclude rank > 3

Table 2.7: Settings used for peptide quantification and filtering in Progenesis QI (ver. 4.1, Nonlinear Dynamics).

2.32 Peptide identification

Quantified peptides were then exported and identification was carried out using Mascot Daemon (Matrix Science UK) against the SWISS-Prot and TREMBL human databases and filtered to only include sequences from reviewed protein annotations (The UniProt Consortium, 2019). The peptide database was modified to search for alkylated cysteine residues (monoisotopic mass change, 57.021 Da), oxidized methionine (15.995 Da), hydroxylation of asparagine, aspartic acid, proline or lysine (15.995 Da), and phosphorylation of serine, tyrosine, threonine, histidine or aspartate (79.966 Da). A maximum of 2 missed cleavages was allowed. The search results were imported back into into Progenesis QI and the final peptide signal intensities and identifications were exported.

2.33 Relative protein quantification

Protein-level relative quantifications were calculated using the `BayesENproteomics` family of functions (Mallikarjun et al., 2020) written in MATLAB using the Statistics and Machine Learning toolbox (MathWorks, version R2017a). Raw peptide intensities from proteins with fewer than 3 unique peptides per protein were excluded from quantification. Peptide lists were filtered leaving only those peptides with a Mascot score corresponding to a Benjamini-Hochberg false discovery rate (FDR) < 0.2 (Benjamini & Hochberg, 1995). Raw peptide intensities were $\log_2$ transformed to ensure a normal distribution and normalised by equalising sample medians.

To account for the inherent high genetic and environmental variability between human donors, relative quantifications of proteins were fit to a linear regression model that considers donor variability at both the peptide and protein levels. For each protein the following model was fitted:

$$y_{fgd} = \beta_0 + X_f\beta_f + X_g\beta_g + X_d\beta_g + \epsilon_{fgd} \tag{2.9}$$

where y_{fgd} corresponds to the observed $\log_2$ intensity for peptide f under experimental condition g from donor d. Predictor variables β_f, β_g, and β_d correspond to the effect sizes of peptide f, group g, and donor d, respectively. β_0 represents the intercept term. ϵ corresponds to a Gaussian error term centered on 0 with a variance specific to each protein (for a full description of the method of relative protein quantification, see Mallikarjun et al., 2020). Where protein fold-changes are plotted graphically, the error bars shown are the standard error in the treatment effect size, β_g. Where figures containing -omic data are windowed for ease of interpretation, all plots contain $\geq 99\%$ of data points.

2.34 Monobromobimane (mBBr) labelling

mBBr labelling was carried out either immediately prior to heat shock, immediately following a 2 hour heat shock, or 4 hours following a 2 hour heat shock. Medium was removed and cells in T75 flasks were washed using PBS. Cells were then labelled by incubation at 37°C with 6 mL of 400 µM mBBr (Sigma-Aldrich, #B4380) for

10 minutes. Following labeling, 6 ml of 2 mM L-glutathione reduced (GSH, Sigma-Aldrich, #G4251) in PBS was added to quench the mBBr reaction. The quenched mBBr solution was removed and cells were washed with PBS.

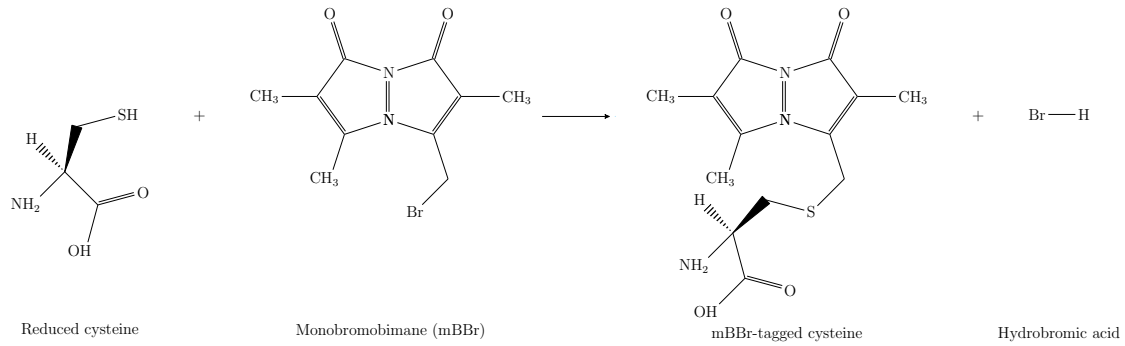

Figure 2.6: Labelling of reduced cysteine using monobromobimane

In experiments in which reduced cysteine residues were labelled with mBBr, the modification was searched for in two possible oxidation states (133.053 and 150.056 Da). Labelled peptides with missed cleavages were summed with their fully tryptic counterparts. The Log_2 fold-change in labelling across samples was normalised to the respective Log_2 fold-change in the respective protein abundance. As both an increase (misfolding) and decrease (aggregation) in mBBr-labelling can be interpreted as the native state of a protein being compromised, a non-parametric test must be used to evaluate the significance of any labelling changes. A Wilcoxon signed-rank test was used to determine whether the mBBr-labelling profile changed between samples at the 95% confidence level.

2.35 Pathway analysis

Statistical enrichment analysis of the Reactome pathway database (version 74, Fabregat et al., 2017) was carried out using the PANTHER gene list analysis tool (Mi et al., 2021) to identify over- or under-enriched pathways with an FDR-corrected p-value ≤ 0.05. Statistically significant enrichments clearly due to common mass spectrometry contaminants (e.g. "keratinisation") were excluded. Clear false-positives due to strong overlaps with other pathways (e.g. a 95% overlap of identified proteins between the "eukaryotic translation and elongation" and "influenza viral RNA transcription and replication" pathways) were treated with an Occam's razor principle and kept or excluded respectively. Where chains of hierarchical pathways are enriched, for simplicity, only the parent pathway in the chain is included. For example, where the pathway "rRNA processing" and its descendant pathway "rRNA processing in the nucleus and cytosol" (99% overlap of identified proteins) are both enriched, only the former would be included.

2.36 Chaperone network analysis

The human chaperone network, consisting of 332 proteins (as characterised by Brehme et al., 2014) was designed using STRING (STRING Consortium, version

11.0, Szklarczyk et al., 2019). Interactions between these chaperone proteins were filtered on the STRING database to only include those of the highest confidence (score ≥ 0.9) and proteins with no known interactions within the network at this level were discounted from further analysis. The remaining chaperone proteins were used as nodes and interaction scores between chaperone proteins were used as weighted edges for the network. This data was used to construct an adjacency matrix for the network:

$$A_{ij} = \begin{cases} a & \text{if } a \geq 0.9 \\ 0 & \text{otherwise} \end{cases} \tag{2.10}$$

where a is the interaction score between chaperones i and j.

The adjacency matrix for the chaperone network was used as the input for the MATLAB Brain Connectivity Toolbox created by Rubinov and Sporns, 2010 (based on methods proposed by Newman, 2006a). Using default settings, a community structure for the network which maximises the modularity score, $Q \in [-0.5, 1]$ was generated:

$$Q = \frac{1}{2m} \sum_{ij} \left(A_{ij} - \frac{k_i k_j}{2m} \right) \delta(c_i, c_j) \tag{2.11}$$

where m is the total number of edges in the network, k_i is the degree of node i, c_i is the community node i belongs to and δ is the Kronecker delta function,

$$\delta(c_i, c_j) = \begin{cases} 1 & \text{if } c_i = c_j \\ 0 & \text{otherwise.} \end{cases} \tag{2.12}$$

2.37 Ordinary/Delay Differential Equation (ODE/DDE) modelling

A mathematical model of the stress response was designed and simulated using MATLAB R2017a (MathWorks). Building on previous models (Sivéry et al., 2016, Zheng et al., 2016), the model consisted of four populations: the chaperone protein HSP70, the transcription factor HSF1, the E3 ubiquitin ligase CHIP (the product of the STUB1 gene), and intracellular misfolded proteins (MFP). Reaction rates were included to represent seven well-defined biological processes between these populations and are defined in Table 2.8 and illustrated in Figure 2.7.

HSP70 synthesis was modelled using a Hill function,

$$k_1 = k \frac{HSF^n}{K_d^3 + HSF^n} \tag{2.13}$$

where the Hill coefficient, $n = 3$, is chosen to reflect HSF1 trimerisation (as in Sivéry et al., 2016) prior to HSP70 synthesis; $k = \lim_{HSF \to \infty} k_1$ is the maximal transcription rate; and K_d is the dissociation constant.

Reaction rate	Reaction(s)	Description
k_1	$[\text{HSF1}] \xrightarrow{k_1} [\text{HSF1}] + [\text{HSP70}]$	HSP70 synthesis
k_2	$[\text{HSF1}] + [\text{HSP70}] \xrightarrow{k_2} [\text{HSF1} \cdot \text{HSP70}]$	HSF1 inactivation
k_3	$[\text{HSF1} \cdot \text{HSP70}] + [\text{MFP}] \xrightarrow{k_3} [\text{HSF1}] + [\text{HSP70} \cdot \text{MFP}]$ $[\text{HSP70}] + [\text{MFP}] \xrightarrow{k_3} [\text{HSP70} \cdot \text{MFP}]$	HSP70 titration to misfolded protein
k_4	$[\text{HSF1} \cdot \text{HSP70}] + [\text{CHIP}] \xrightarrow{k_4} [\text{HSF1}] + [\text{CHIP}]$ $[\text{HSP70}] + [\text{CHIP}] \xrightarrow{k_4} [\text{CHIP}]$	Turnover of HSP70
k_5	$[\text{HSP70} \cdot \text{MFP}] \xrightarrow{k_5} [\text{HSP70}]$	HSP70-mediated refolding
k_6	$[\text{HSP70} \cdot \text{MFP}] + [\text{CHIP}] \xrightarrow{k_6} [\text{HSP70}] + [\text{CHIP}]$	Turnover of misfolded protein
k_7	$\emptyset \xrightarrow{k_7} [\text{MFP}]$	Protein misfolding

Table 2.8: Reactions and rate constants of the mathematical model of the stress response.

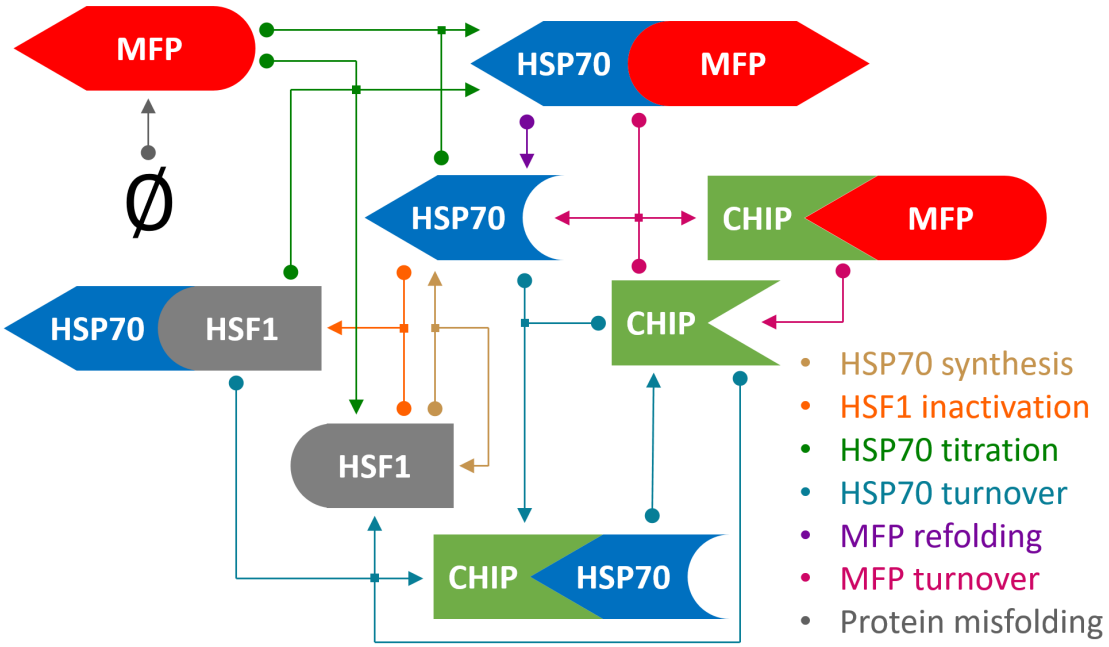

Figure 2.7: Schematic of the titration model of HSP70 regulation, with the inclusion of CHIP-mediated post-translational regulation. Each arrow colour represents a process defined in Table 2.8. Arrows begin at the process reactants and end at the process products.

The reactions in Table 2.8 were used to design the following system of ODE/DDEs:

$$\frac{d}{dt}[HSF1] = k_3[HSF1 \cdot HSP70][MFP] + k_4[HSF1 \cdot HSP70][CHIP] - k_2[HSF1][HSP70] \tag{2.14}$$

$$\frac{d}{dt}[HSP70] = k_1[HSF1]_{t-\tau} + k_5[HSP70 \cdot MFP] + k_6[HSP70 \cdot MFP][CHIP] - k_2[HSF1][HSP70] - k_3[HSP70][MFP] - k_4[HSP70][CHIP] \tag{2.15}$$

$$\frac{d}{dt}[CHIP] = 0 \tag{2.16}$$

$$\frac{d}{dt}[MFP] = k_7 - k_3[HSP70][MFP] - k_3[HSF1 \cdot HSP70][MFP] \tag{2.17}$$

$$\frac{d}{dt}[HSF1 \cdot HSP70] = k_2[HSF1][HSP70] - k_3[HSF1 \cdot HSP70][MFP] - k_4[HSF1 \cdot HSP70][CHIP] \tag{2.18}$$

$$\frac{d}{dt}[HSP70 \cdot MFP] = k_3[HSF1 \cdot HSP70][MFP] + k_3[HSP70][MFP] - k_5[HSP70 \cdot MFP] - k_6[HSP70 \cdot MFP][CHIP] \tag{2.19}$$

where τ is drawn randomly from a uniform distribution of times between one and three hours, i.e. $\tau \sim U[60, 180]$ (Jarnuczak et al., 2018), and represents the delay between the onset and conclusion of HSP70 synthesis. That is, $\frac{d}{dt}[HSP70]$ at time t is dependent on $[HSF1]$ at time $t - \tau$.

2.37.1 Initial conditions

Population units are concentrations and initial conditions are chosen relative to the concentration of HSF1 in the system, quasi-arbitrarily set at 0.1 µM based on the estimate of cellular molecular density by Milo, 2013. To ensure reproducibility and optimisation (see Section 2.37.2), the random number generator is seeded prior to the start of the simulation. Populations are recalculated after every time interval dt (minutes), such that $[HSP70]_{t+dt} = [HSP70]_t + \frac{d}{dt}[HSP70]_t$. The value of dt is fixed at 0.01 minutes, such that the time interval is sufficiently small for the system to remain stable, while minimising running time. Following selection of initial conditions, the system is given an extensive period of time for populations to reach an equilibrium. Following this, a proteotoxic stress comparable with heat shock (Section 2.12) is simulated by multiplying the reaction rate k_7 by a value $\alpha > 1$ for 120 minutes.

2.37.2 Parameter optimisation

Parameters which could not be inferred from theory, experimental results, or literature evidence: $(k, K_d, k_2, k_4, k_5, k_7)$ were chosen to optimise the model's ability to replicate *in vitro* HSP70 protein dynamics in response to a 2 hour heat shock and 24 hour recovery period (see Section 4.5.2). This was done by recording the change in HSP70 concentration *in silico* at the same time points as those used for *in vitro* experiments and totaling the sum of squared errors (SSE) between these. The MATLAB function `fminsearch` was then used to find the parameter set which best replicated HSP70 protein dynamics by minimising the SSE between *in vitro* and *in silico* data. The MATLAB script used to carry out these simulations is detailed in full in Appendix A.1

Chapter 3

The transcriptomic and proteomic profiles of proliferating and senescent human mesenchymal stem cells before and after stress

The primary aim was to characterise the intracellular transcriptomes and proteomes of proliferating early-passage (EP) and senescent late-passage (LP) primary human mesenchymal stem cells (hMSCs) under control conditions (culture at 37°C) and immediately following proteotoxic stress (2 hour heat shock at 42°C). The use of RNA-sequencing (RNA-seq) and mass spectrometry (MS) to create -omic level data has provided a comprehensive overview of the changes LP cells experience. The application of proteotoxic stress will be used to test whether literature reports of an organismal age-associated loss of proteostasis is also experienced at the cellular level. Utilising high-throughput methods to analyse both mRNA and protein levels allowed the additional study of the interaction between the two, giving insight into the mechanisms by which proliferating and senescent cells respond to stress.

3.1 β-galactosidase staining validates senescence in late-passage populations

The principle of comparisons between EP and LP cells as a model of cellular ageing is that the LP populations will contain disproportionately high numbers of senescent cells compared to proliferating EP populations. To verify this, passage 3 and passage 16 cells from the same donor were stained for the senescence marker β-galactosidase using an X-gal assay (Figure 3.1). As expected, positive staining is seen in a majority of cells in LP as opposed to a scarcity of cells in EP. While the influence of long-term culture on cell behaviour alone is important from a regenerative medicine perspective as discussed in Section 1.8.5, Figure 3.1 couples the behavioural changes seen with the consequences of cellular senescence.

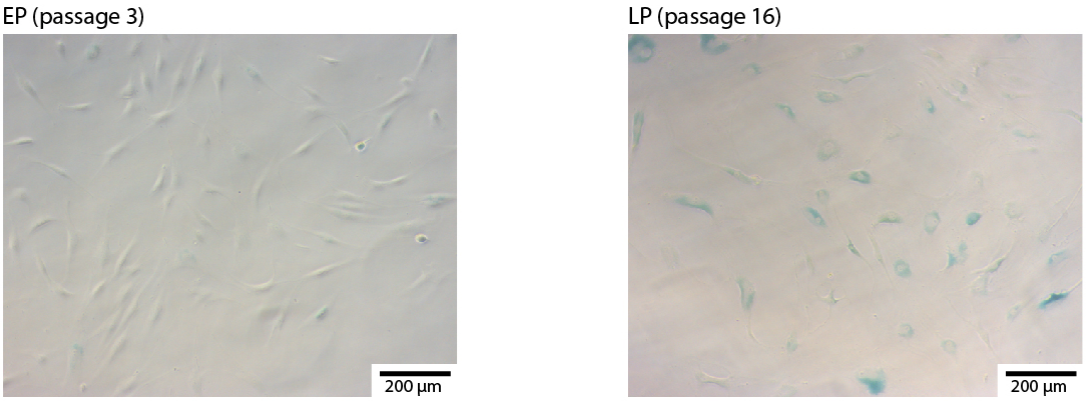

(a) (b)

Figure 3.1: X-gal assay of early- and late-passage human mesenchymal stem cells derived from bone marrow. Blue staining indicates the presence of the senescence biomarker β-galactosidase (see Section 1.8.3). (3.1a) Early-passage (passage 3) donor-matched hMSCs. (3.1b) Late-passage (passage 16) donor-matched hMSCs.

3.2 Label-free mass spectrometry

Log_2 fold-changes in protein levels were quantified in whole cell lysates using liquid chromatography-coupled tandem mass spectrometry (Mallikarjun et al., 2020). Label-free mass spectrometry was carried out on four donor-matched EP and LP populations, comparing hMSCs subjected to a 2-hour treatment at 42°C to matched cells under control conditions. 1,811 proteins were identified with ≥ 3 peptides-per-protein across all samples. The validation of widespread cellular senescence in LP populations was confirmed in Figure 3.2 by the overexpression of β-galactosidase (the product of the GLB1 gene), and loss of lamin B1 (the product of the LMNB1 gene), another marker of senescence demonstrated by Shimi et al., 2011.

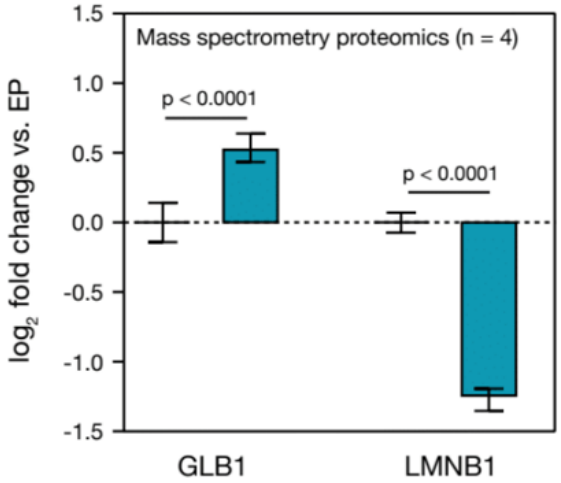

Figure 3.2: Changes in the GLB1 and LMNB1 protein products between unstressed early- and late-passage populations in mass spectrometry data ($n = 4$ donors). Statistical significance is assessed as detailed in Section 2.33.

3.3 RNA-sequencing

EP and LP populations of cells from five paired donors were sequenced with and without a 42°C heat shock, matching the conditions used for mass spectrometry. Figure 3.3 displays the Q scores of RNA fragments calculated using equation 2.8. A Phred (Q) score of 30 is generally achieved, indicating a base call accuracy of 99.9%.

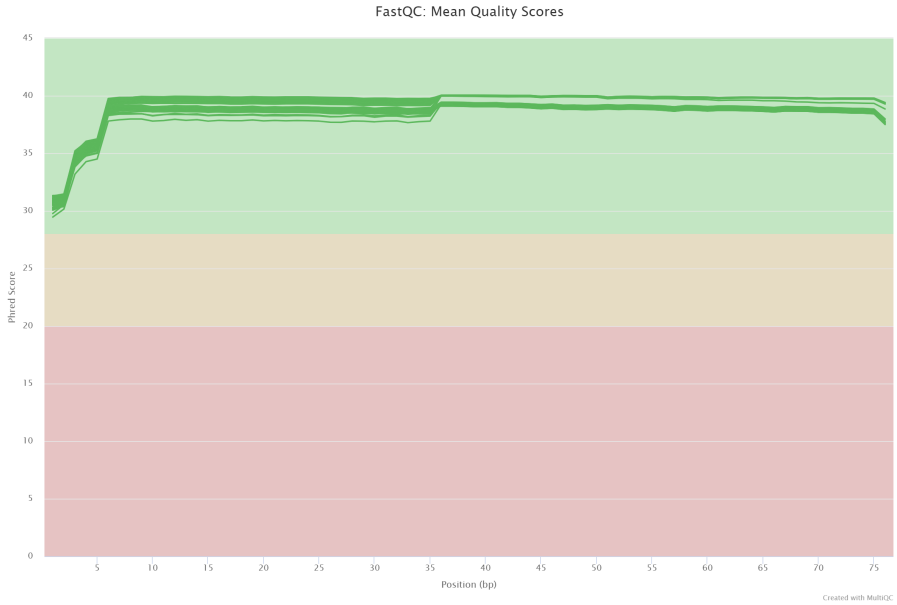

Figure 3.3: Quality control of RNA-sequencing data ($n = 5$ donors), showing the base call accuracy of RNA fragments as a Q score (Section 2.23, Equation 2.8). Plot generated using MultiQC (Ewels et al., 2016, version 1.8).

Figure 3.4 shows the results of a principal component analysis (PCA) on RNA-seq data. PCA is a linear dimensionality reduction technique, the aim of which is to describe the majority of a high-dimensionality dataset (in this case, 20 dimensions detailing RNA signal intensities in 20 different samples) using a lower number of dimensions, or "principal components", which can be visualised. In an example of two-dimensional data, the first principal component axis (PC1) is obtained by drawing the line with the most data variance along itself - in this case, by definition, this would be the line of best fit. To find the second principal component axis (PC2), one would discount the first principal component and repeat the process, in the case of two-dimensional data, PC2 would be the line perpendicular to the line of best fit. In this simplified example, a majority of the two-dimensional data can be described by plotting each data point's position on the PC1 axis only. For a visual representation of a two-dimensional principal component analysis, see Lever et al., 2017. For n-dimensional data, the process is homogeneous, with each principal component axis being an n-dimensional line of best fit rather than two-dimensional. The utility of a principal component analysis is that it allows us to identify any features in our experimental design which introduce variance into the resultant data. For example, if our data points are heavily clustered on PC1 according to some sample characteristic X (e.g. replicate, passage, temperature), then we may conclude that PC1 describes the variance between samples due to characteristic X, which is the largest source of variance in the experiment.

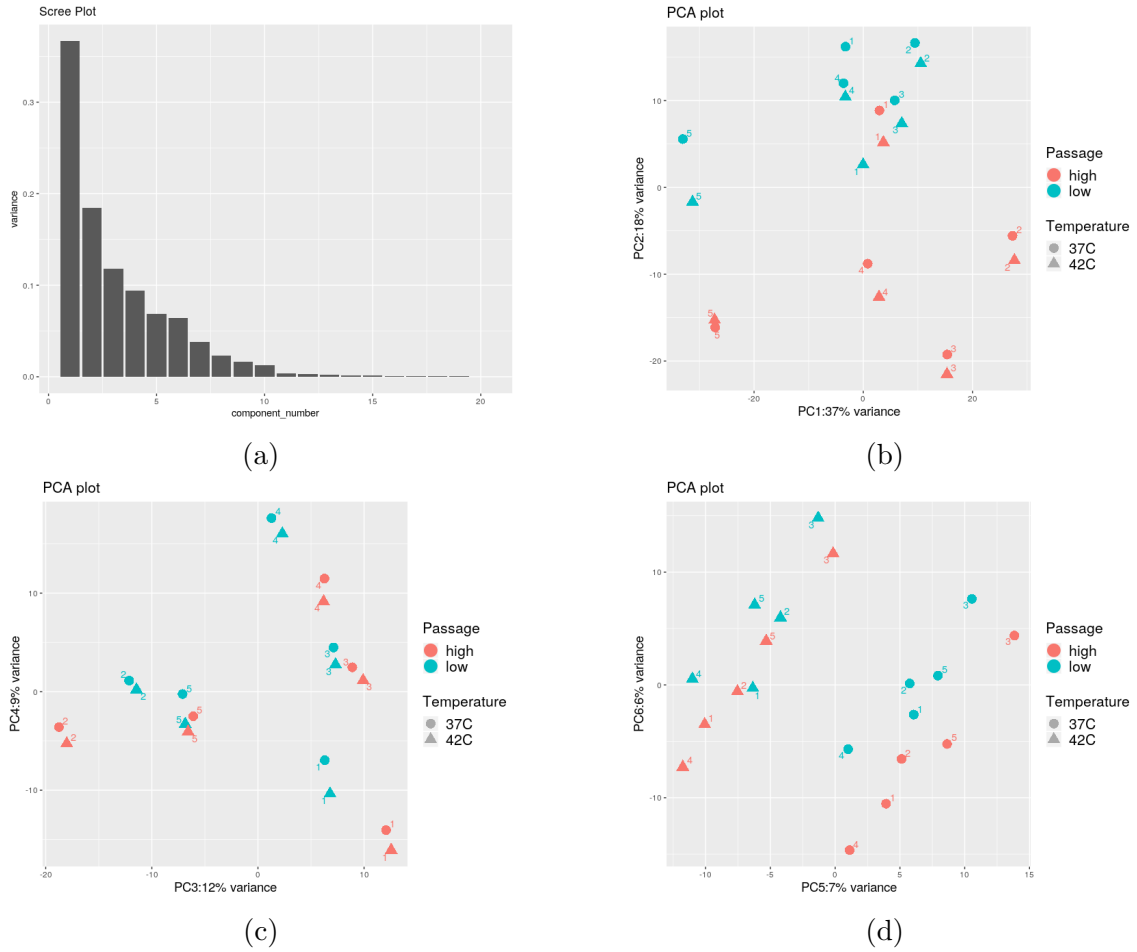

Figure 3.4: Principal component analysis of RNA-sequencing data ($n = 5$ donors), showing the percentage contribution of each principal component to the total variance in the dataset, and the distribution of samples along each principal component axis. (3.4a) Scree plot showing the proportion of total variance encompassed by each principal component. (3.4b) Principal components 1 and 2. (3.4c) Principal components 3 and 4. (3.4d) Principal components 5 and 6.

Figure 3.4a shows the proportion of the total variance in RNA-seq data accounted for by each principal component, with the first six principal components accounting for 89% of the total variance in the data. The highest contribution to the total variance in the data comes from the variation between donors, with samples from different donors mostly separated on the PC1 (37%) axis in Figure 3.4b and the PC3 (12%) axis in Figure 3.4c. This illustrates the importance of the linear modelling approaches used in this study to account for inter-donor variation in human data (see Sections 2.17 and 2.33). The second highest contribution to the total variance in the data is due to differences between EP and LP cells, with these samples separated on the PC2 (18%) axis in Figure 3.4b and the PC4 (9%) axis in Figure 3.4c. Following these, the next highest source of variance is cellular stress. Figure 3.4d shows samples clearly separated on the PC5−PC6 plane (7% and 6% respectively) into two groups consisting exclusively of either stressed or unstressed populations.

3.4 The -omic proteotoxic stress response in early- and late-passage cells

3.4.1 Transcript and protein regulation analysis

Firstly, we will examine the transcriptomic and proteomic responses of EP and LP cells to heat stress treatment. Figure 3.5 shows the correlation between the EP and LP stress responses, using the product-moment correlation coefficient (PMCC, "Pearson r") to assess the percentage of correlation, with r^2 giving the fraction of variance in either condition explained by the other.

In Figure 3.5a, a reasonably strong correlation is seen between the two transcriptomic stress responses, with $100r^2 = 46\%$ explained variance (i.e. $\sim 46\%$ of transcript regulation in the LP stress response is related to transcript regulation in the EP stress response). By far, the most regulated transcript in response to stress is the A-disintegrin-and-metalloproteinase family member ADAMDEC1 (EP Log_2 fold-change 18.5; LP Log_2 fold-change -0.05). This sharp fold change is seen because ADAMDEC1 is not detected in any of the five EP, unstressed samples, but is detected in one EP, stressed sample. This is partially in agreement with Human Protein Atlas data (Uhlen et al., 2015) which shows ADAMDEC1 is not native to bone-marrow. It is worth noting however, that the Human Protein Atlas data is not compiled using aged or stressed tissues, so the significant up-regulation of ADAMDEC1 cannot conclusively be dismissed as a false positive. ADAMDEC1 was also detected in nine out of ten LP samples, and may constitute an additional biomarker of senescent hBM-MSCs. Indeed, Yako et al., 2018 demonstrate that the secretion of ADAMDEC1 in Madin-Darby Canine Kidney cells positively regulates the elimination of neighbouring cells and may therefore also constitute a member of the SASP discussed in Section 1.8.5. Conversely however, ADAMDEC1 is not identified in the proteomic data of either this study, or the recent proteomic atlas of senescence-associated secretomes by Basisty et al., 2020 - therefore more research is needed to verify the existence of ADAMDEC1 in stressed and senescent hBM-MSCs, and hypothesise its purpose in these cells.

Following ADAMDEC1, the most highly up-regulated transcripts common to both EP and LP cells correspond to the HSP70 chaperone family members HSPA6 (EP Log_2 fold-change 9.68; LP Log_2 fold-change 12.3) and HSPA7 (EP Log_2 fold-change 9.20; LP Log_2 fold-change 10.6). In a review of HSP70 family members by Radons, 2016, it is discussed that HSPA6 and HSPA7 are stress-inducible, highly homologous to the better-researched stress-inducible HSPA1A (EP Log_2 fold-change 5.57; LP Log_2 fold-change 6.16), and have low expression levels at equilibrium. The latter of these points is most likely to account for the high fold-changes seen at the transcriptional level. The most-downregulated protein in EP cells is the nuclear pore complex protein RGPD1 which is implicated in nuclear export pathways (Vetter et al., 1999) and, interestingly, is unchanged in LP cells in response to stress (EP Log_2 fold-change -5.88; LP Log_2 fold-change -0.14). The next-strongest down-regulation in EP transcript data corresponds to microtubule-associated-protein MAP10, which is connected to cell division (Fong et al., 2013) and is also strongly down-regulated in the LP stress response (EP Log_2 fold-change -3.11; LP Log_2 fold-change -3.14).

Figure 3.5b shows the same correlation plot for proteomic data. Here the PMCC is just -0.0700 (i.e. a correlation of $100r^2 = 0.49\%$). The most up-regulated protein in both EP and LP cells in response to stress is prolactin-induced protein (PIP, EP Log_2 fold-change 1.87; LP Log_2 fold-change 1.23) - a secreted protein which remains poorly understood (as reviewed by Urbaniak et al., 2018). Notably, the calcium-binding proteins S100A7 (EP Log_2 fold-change 1.17; LP Log_2 fold-change 0.29) and S100A9 (EP Log_2 fold-change 0.94; LP Log_2 fold-change 1.04) are the next most up-regulated proteins in EP and LP cells, respectively. Xia et al., 2018 review how these proteins act as a "danger signal" secreted in response to stress.

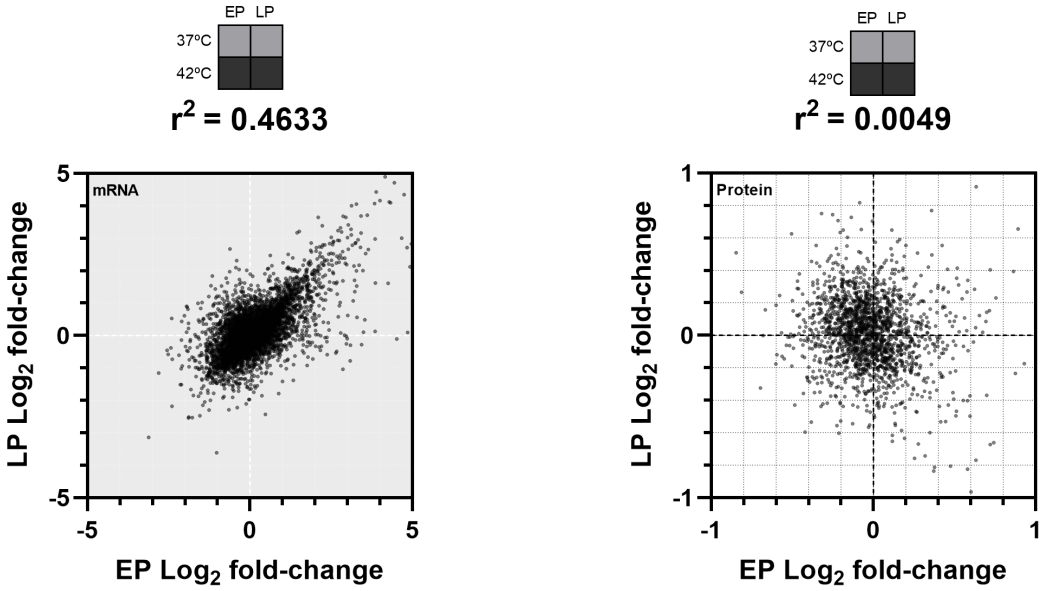

(a) (b)

Figure 3.5: Product-moment correlation coefficients between the EP and LP stress response for transcriptomic and proteomic data. For ease of interpretation, plots are windowed, with $> 99\%$ of data points shown. (3.5a) Correlation of RNA fold-changes due to stress in EP and LP populations. (3.5b) Correlation of protein fold-changes due to stress in EP and LP populations.

Figure 3.5 shows a clear disparity in the PMCCs between EP and LP cells in response to stress in transcriptomic and proteomic data. While there is a strong overlap between the EP and LP transcriptional response to stress, no relationship exists between the EP and LP proteomic response to stress. It was important to confirm that Figure 3.5b does not merely represent the higher statistical noise present in MS data compared to RNA-seq data. A more stringent protein identification cutoff was trialled, with the hypothesis that signals from the most abundant proteins would be subject to the least statistical noise, and highlight whether the PMCC value in Figure 3.5b was an accurate reflection of the relationship between the EP and LP stress responses. Accepting only proteins with ≥ 30 peptides identified, rather than ≥ 3, in fact decreased the PMCC further ($r^2 = 0.0004$, 57 proteins) - validating the low PMCC value seen in Figure 3.5b.

A perhaps over-simplified interpretation of these datasets is that the transcriptome reflects how the cell is attempting to respond to stress, while the proteome reflects how the cell actually is responding to stress. In this view, the disparity shows that while EP and LP cells are attempting to carry out a very similar stress response, the actual response achieved differs greatly. The reasonably strong correlation in the transcriptomic stress response of EP and LP cells also demonstrates that there is no senescence-associated attenuation of the stress response upstream of transcription (for example, thermosensing).

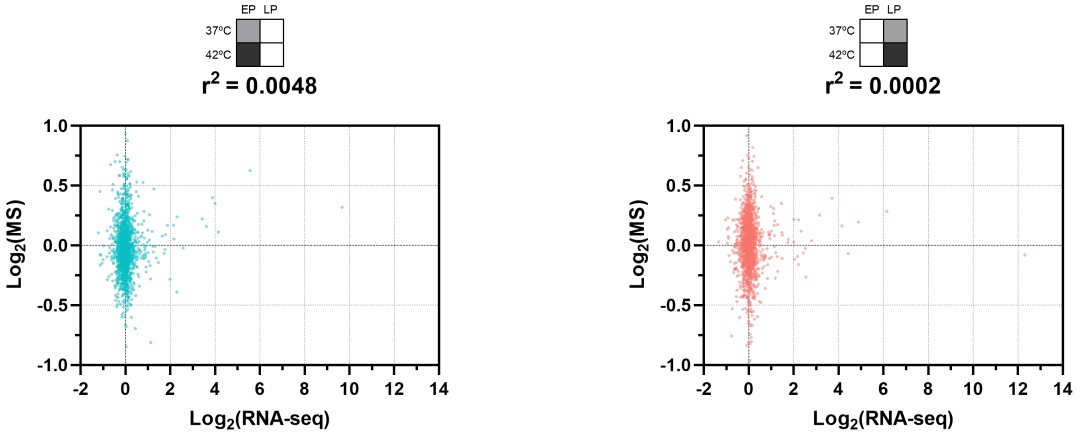

(a) (b)

Figure 3.6: The product-moment correlation coefficients of the fold-changes between unstressed and stressed populations in RNA-sequencing and mass spectrometry data. Data is plotted from the fold-changes between early- (3.6a, 1731 gene products) and late-passage (3.6b, 1729 gene products) populations.

These plots also show that, in general, changes to the transcriptome are much more dynamic than changes to the proteome. The differences in the shape and scale of Figures 3.5a and 3.5b foreshadow a poor correlation between mRNA and protein fold-changes in response to stress. Figure 3.6 shows that while a higher correlation between mRNA and protein is seen in the EP response to stress than in the LP response ($100r^2 = 0.48\%$, 0.02% respectively), both are surprisingly low. The physical interpretation of these PMCC values is that a majority of the short-term regulation of the proteomes of hMSCs in response to stress is carried out downstream of transcription, with transcription accounting for $< 1\%$ of changes to protein levels within two hours of proteotoxic stress. Coupled with the difference in the scale of each axis, it is highly likely that a strong transcriptional response is required to produce any meaningful short-term response at the protein level. Even in the case of strong mRNA up-regulation, this does not invariably render[1] into a corresponding protein up-regulation. HSPA6, previously identified as the most strongly up-regulated transcript in response to stress (HSPA7 was not detected by mass spectrometry), experiences a comparatively small change at the protein level due to stress (EP Log_2 fold-change 0.32; LP Log_2 fold-change -0.08). Conversely, both the transcript and protein products of the HSPA1A gene show relatively strong up-regulation in

[1]avoiding use of the term "translate" to prevent any potential misinference with regard to protein translation.

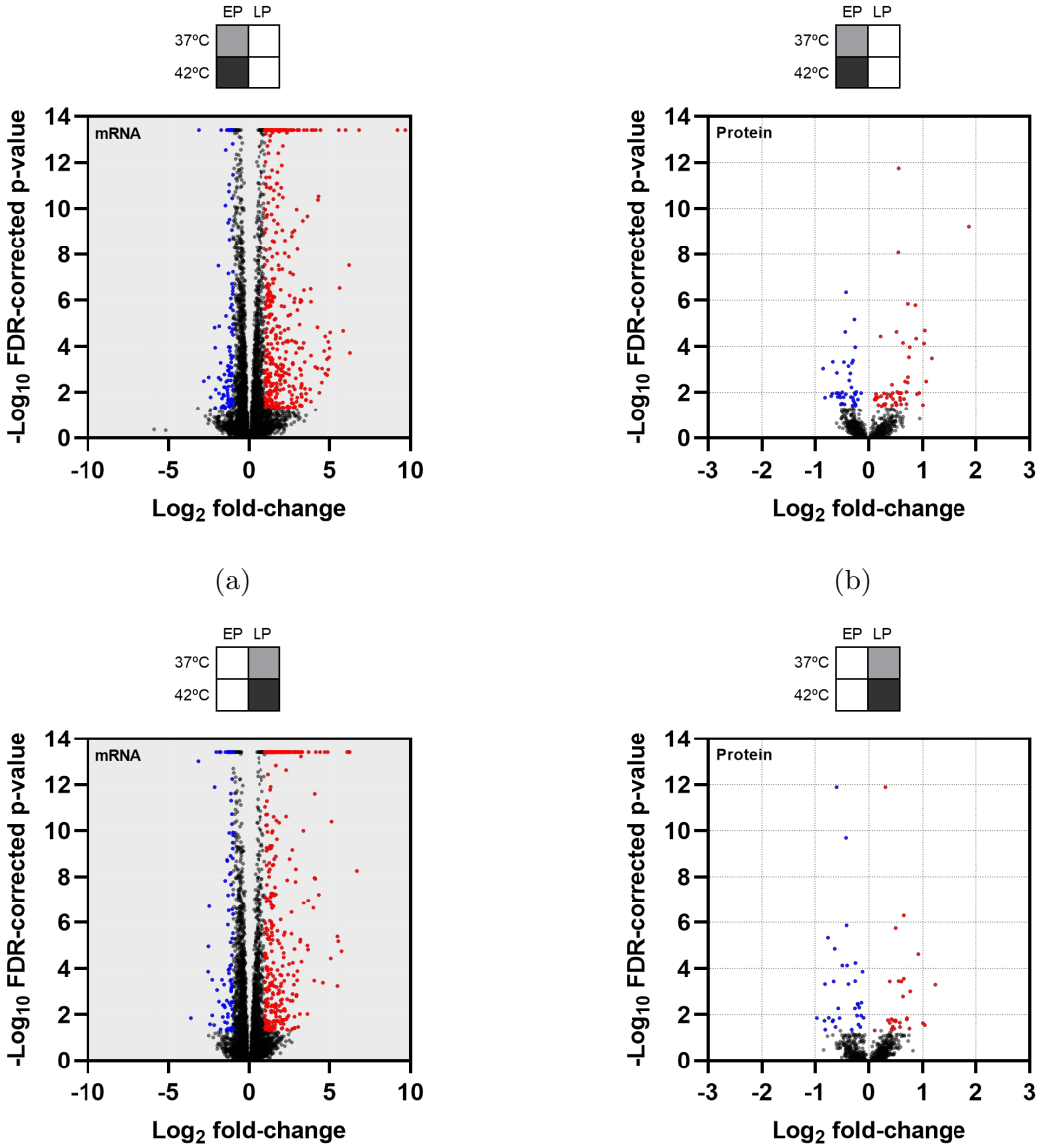

Figure 3.7: Significance of mRNA and protein fold-changes in response to stress in RNA-sequencing and label-free mass spectrometry data. Transcripts satisfying $|\text{Log}_2 \text{ fold-change}| \geq 1$ and FDR-p ≤ 0.05 are coloured blue/red corresponding to down-/up-regulation, with proteins satisfying FDR-p ≤ 0.05 coloured likewise. (3.7a) Fold-changes of 17,243 transcripts in response to stress in early-passage populations. (3.7b) Fold-changes of 1,811 proteins in response to stress in early-passage populations. (3.7c) Fold-changes of 16,550 transcripts in response to stress in late-passage populations. (3.7d) Fold-changes of 1,811 proteins in response to stress in late-passage populations.

response to stress in EP (mRNA Log_2 fold-change 5.57; protein Log_2 fold-change 0.62) and, to a lesser extent, LP populations (mRNA Log_2 fold-change 6.16; protein Log_2 fold-change 0.28).

Figure 3.7 shows volcano plots of the significance of transcript and protein regulation in response to stress. Proteins are assessed for significance at the 5% level using the

Benjamini-Hochberg false-discovery-rate adjustment (Benjamini & Hochberg, 1995, see Section 2.33); while significantly regulated transcripts were assessed with the additional criteria of $|\text{Log}_2 \text{ fold-change}| \geq 1$, such that mRNA levels must double or halve. To emphasise the disparity between the transcriptomic and proteomic responses to stress, Figure 3.8 shows the transcript Log_2 fold-changes of the significantly regulated proteins in Figures 3.7b and 3.7d. From these plots, it is clear that the majority of protein regulation in response to stress over the short time window analysed (two hours) is downstream of transcription.

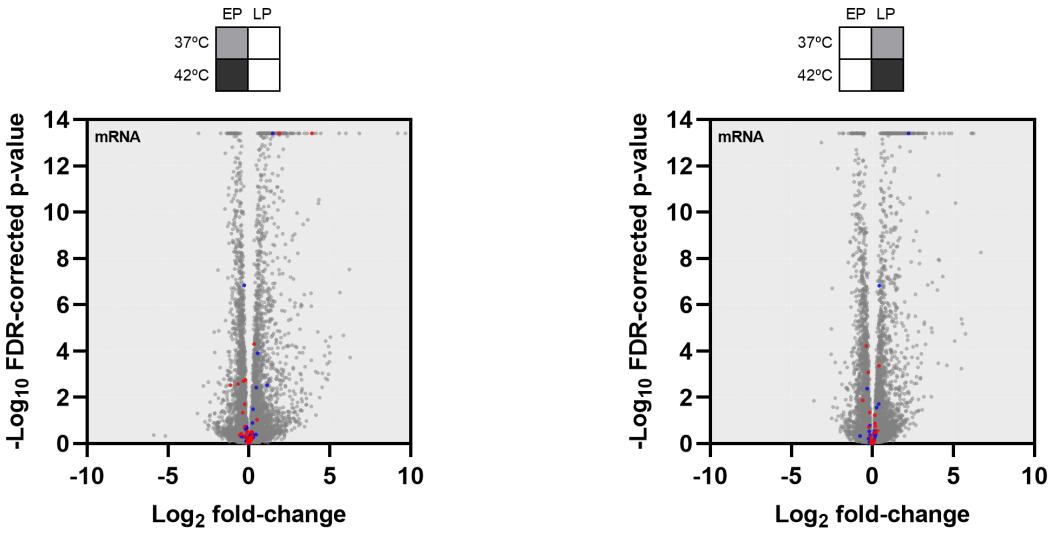

(a) (b)

Figure 3.8: mRNA fold-changes in response to stress in RNA-sequencing data, with significantly up- (red) and down-regulated (blue) protein products in the same conditions highlighted. (3.8a) Fold-changes of 17,243 transcripts in response to stress in early-passage populations. (3.8b) Fold-changes of 16,550 transcripts in response to stress in late-passage populations.

Using the chosen constraints, just 3.23% of transcripts were significantly differentially regulated in response to stress in EP cells (Figure 3.7a), with 447 up-regulated and 110 down-regulated transcripts. The response of LP cells (Figure 3.7c) was slightly lower in magnitude, with 2.81% of transcripts significantly differently regulated, consisting of 367 up-regulated and 98 down-regulated transcripts. A strong overlap is seen in the transcripts significantly regulated in both conditions, with 295 up-regulated and 53 down-regulated transcripts common to both the EP and LP stress responses. Among those commonly up-regulated, transcripts from the HSP70 chaperone family already discussed in this section feature prominently, with 10 family members represented.

Comparing protein levels in stressed versus unstressed EP cells (Figure 3.7b), the vast majority (95%) of proteins were unchanged at the 5% FDR-corrected level of significance, with 46 up-regulated and 40 down-regulated proteins. The proteomes of LP cells were less responsive to stress (Figure 3.7d, with 97% of proteins unchanged (26 up-regulated and 33 down-regulated). Following the lack of correlation seen in Figure 3.5b, there is an overlap of just three proteins between the significantly up-

regulated proteins in EP and LP cells in response to stress: the calcium exporting ATPase, ATP2B4 (Adamo et al., 1995); LIMCH1, which suppresses cell migration (Y.-H. Lin et al., 2017); and the previously discuss secreted extracellular matrix (ECM) protein, PIP. In the down-regulated proteins, only four are seen to overlap between the EP and LP stress response: collagens CO1A1 and CO1A2, fibronectin (FN1), and TPM4. The former three of these proteins are ECM proteins, whose secretion may impose a considerable burden on chaperone proteins, explaining their consistent down-regulation during stress. Regarding the latter - in agreement with LIMCH1 up-regulation in these cells, Jeong et al., 2017 and X. Zhao et al., 2019 report TPM4 promotes cell migration, however a consensus has not been agreed (R. Yang et al., 2018).

3.4.2 Pathway enrichment analysis

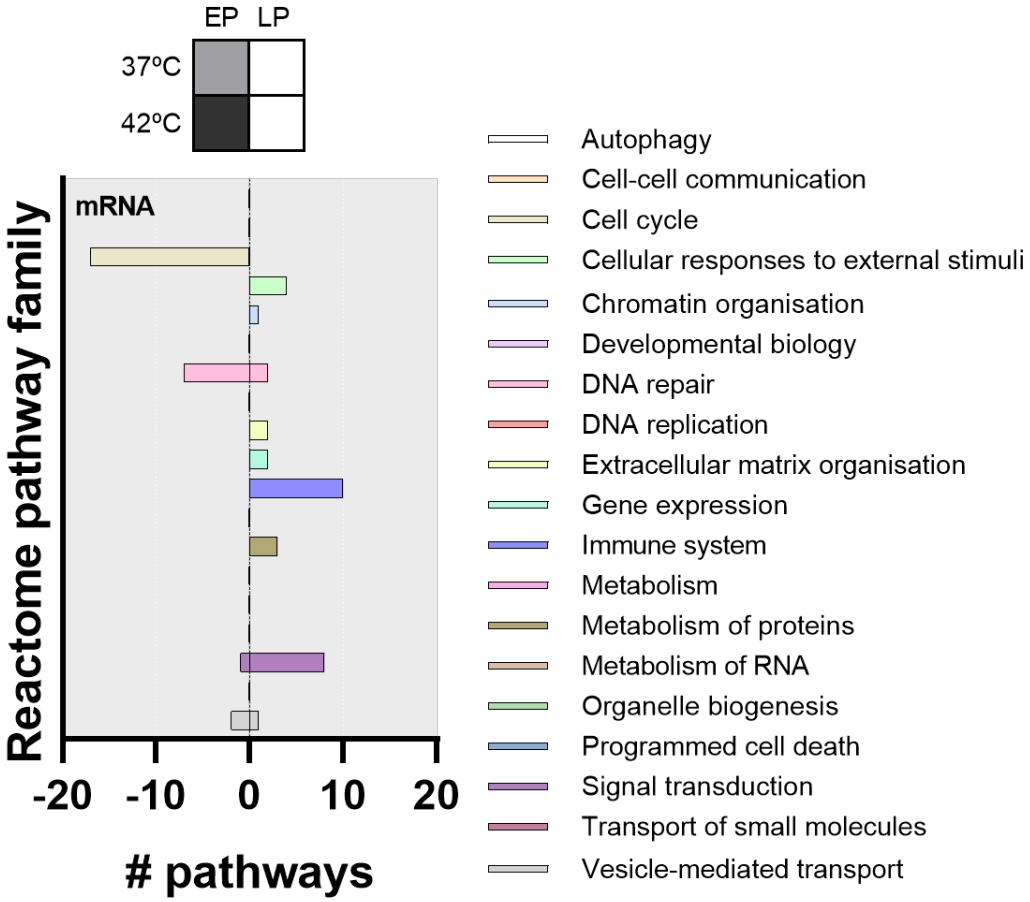

Figure 3.9: Results of a PANTHER statistical enrichment analysis of the fold-changes in the early-passage transcriptome in response to stress. 60 pathways are significantly enriched across 12 Reactome top-tier pathways. Positive values indicate over-enriched pathways while negative values indicate under-enriched pathways.

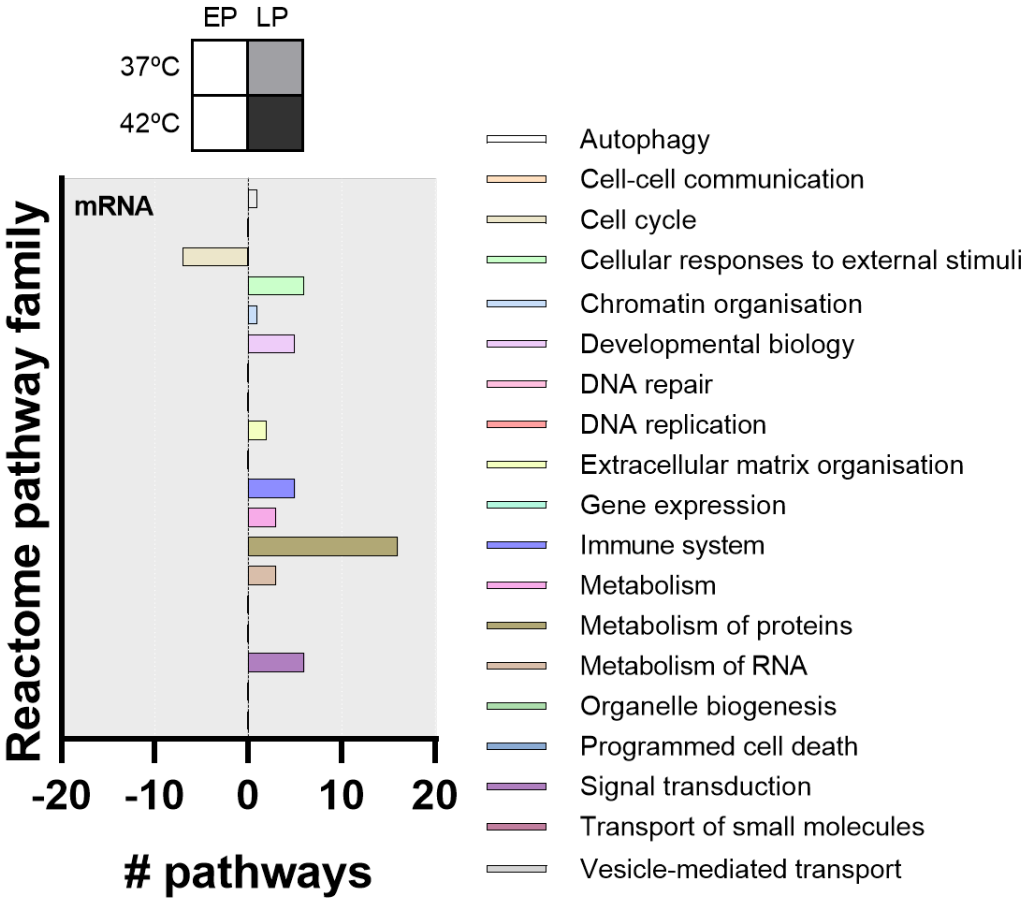

Figure 3.10: Results of a PANTHER statistical enrichment analysis of the fold-changes in the late-passage transcriptome in response to stress. 55 pathways are significantly enriched across 12 Reactome top-tier pathways. Positive values indicate over-enriched pathways while negative values indicate under-enriched pathways.

A statistical enrichment analysis of Reactome pathways (Fabregat et al., 2017, pathway browser version 3.7, database version 74) using the PANTHER classification system (Mi et al., 2021, version 16.0) was performed in order to identify the mechanistic consequences of the transcripts/proteins which are up- and down-regulated in response to stress. The Reactome pathway network sorts all pathways into several hierarchies. For example, "eukaryotic translation elongation" is a descendant of "translation" which in turn is a descendant of "metabolism of proteins"; and as such the proteins implicated in "eukaryotic translation elongation" are a subset of the proteins implicated in "translation", which in turn are a subset of the proteins implicated in "metabolism of proteins". Pathway analysis data is given in terms of the number of pathways significantly over- or under-enriched in each of these hierarchies, referred to by their top-tier pathway (for a visual and interactive representation of the pathway hierarchy structure used, see https://reactome.org/PathwayBrowser). Over-enriched pathways are displayed on the positive axis, while under-enriched pathways are displayed on the negative axis. Where low numbers of pathways are significantly enriched, the data is instead displayed in table format, with under-enriched pathways coloured in blue and over-enriched pathways coloured in red.

Figure 3.9 shows the results of this analysis for the transcriptomes of EP cells in response to stress. The clearest result is the under-enrichment of 17 "cell cycle" pathways. This demonstrates the well-researched and evolutionarily conserved process of cell cycle arrest in response to stress (as reviewed by Mikhailov & Rieder, 2002, who discuss how this arrest can be independent of DNA damage). Surprisingly, the next hierarchy with the most down-regulated pathways is "DNA repair", however a strong coupling between "cell cycle" and "DNA repair" pathways due to the overlap of DNA polymerases should be noted and, conversely, the sub-pathway "DNA double strand break response" is significantly over-enriched (FDR-p = 0.0337). 10 "immune system" pathways are significantly over-enriched in the transcriptomes of EP cells in response to stress, as well as eight "signal transduction" pathways and four "cellular responses to external stimuli" pathways. Regarding the application of hMSCs in stem cell-based therapies, it is important that cells are able to withstand and respond to environmental stress, whilst inducing a minimal immune response.

In the LP populations (Figure 3.10), fewer pathways related to the cell cycle are significantly down-regulated in the transcriptional response to stress (seven). This is intuitive, as the senescent cells within the LP populations have already undergone cell cycle arrest prior to the application of stress. Similarly, fewer "immune system" and "signal transduction" pathways are over-enriched in the LP populations, as the senescent cells are most likely already engaged in pro-inflammatory signalling. While "cellular responses to external stimuli" pathways are again over-enriched, no enrichment of "DNA repair" pathways is seen. The largest enrichment of pathways in LP populations at the transcript level is the over-enrichment of "metabolism of proteins" pathways, with "translation"(FDR-p < 0.0001) being one of the most significantly over-enriched among the 16 pathways regulated in this hierarchy.

Reactome pathway	Hierarchy	# proteins	FDR-p
Interferon alpha/beta signalling	Immune system	12	0.0274
Eukaryotic translation initiation	Metabolism of proteins	90	0.0064
Nonsense-mediated decay	Metabolism of RNA	75	0.0116
Eukaryotic translation termination	Metabolism of proteins	69	0.0106
Response of EIF2AK4 (GCN2) to amino acid deficiency	Cellular responses to external stimuli	80	0.0099
Selenoamino acid metabolism	Metabolism	82	0.0098
Eukaryotic translation elongation	Metabolism of proteins	70	0.0221
SRP-dep. cotranslational protein targeting to membrane	Metabolism of proteins	78	0.0211
rRNA processing	Metabolism of RNA	76	0.0305
Regulation of expression of SLITs and ROBOs	Development	109	0.0316
Transport of mature transcript to cytoplasm	Metabolism of RNA	15	0.0439
ECM proteoglycans	Extracellular matrix organisation	20	0.00339

Table 3.1: Pathway enrichment analysis of changes in the early-passage proteome in response to stress. Red pathways indicate over-enrichment, whilst blue pathways indicate under-enrichment following stress.

Tables 3.1 and 3.2 show the pathways significantly under- and over-enriched in the proteomes of EP and LP populations in response to stress. In contrast to the very little agreement seen between the significantly up-regulated proteins, much more overlap is seen in the pathways enriched in response to stress between EP and LP populations."Interferon alpha/beta signalling", a descendant pathway of the immune system is up-regulated in EP populations while no change is seen in LP populations, echoing the earlier suggestion that immune response signalling is tak-

Reactome pathway	Hierarchy	# proteins	FDR-p
Eukaryotic translation elongation	Metabolism of proteins	70	0.0161
Selenoamino acid metabolism	Metabolism	82	0.0098
Non-integrin membrane-ECM interactions	Extracellular matrix organisation	15	0.0385
SRP-dep. cotranslational protein targeting to membrane	Metabolism of proteins	78	0.0215
Nonsense-mediated decay	Metabolism of RNA	75	0.0161
Eukaryotic translation termination	Metabolism of proteins	69	0.0181
Cellular responses to stress	Cellular responses to external stimuli	206	0.0234
Axon guidance	Development	210	0.0203
rRNA processing in the nucleus and cytosol	Metabolism of RNA	73	0.0465
Eukaryotic translation initiation	Metabolism of proteins	90	0.0489
Integrin cell surface interactions	Extracellular matrix organisation	22	0.0491
ECM proteoglycans	Extracellular matrix organisation	20	0.0478

Table 3.2: Pathway enrichment analysis of changes in the late-passage proteome in response to stress. Red pathways indicate over-enrichment, whilst blue pathways indicate under-enrichment following stress.

ing place in these cells prior to the application of stress. A dearth of over-enriched pathways in both populations may show a bias in the method of analysis, as the volcano plots in Figure 3.7 are symmetrical by MS signal intensity. This is most likely caused by a greater depth of research in down-regulated proteins - such that they appear in more pathways - than in the up-regulated proteins. With pathways related to ECM organisation under-enriched in both populations, this suggests cells attempt to decouple themselves from their surroundings in response to heat shock. In support of this idea, EP cells experience a significant downregulation of SUN2 (FDR-p = 0.0329), a nuclear envelope protein which Gilbert et al., 2019 have shown is responsible for decoupling the nucleus from the cytoskeleton during mechanical stress. LP cells however, do not regulate SUN2 during stress (FDR-p = 0.9420). Alternatively, as discussed in the previous section, this data may demonstrate that coordinating secretion for the purpose of ECM remodelling creates a considerable burden on chaperone machineries.

Figure 3.11 illustrates the contradiction seen in the regulation of protein synthesis pathways between the transcriptome and proteome during stress, with the disparity most evident in data from LP populations. While transcription of these pathways is over-enriched, in general, pathways associated with protein synthesis are under-enriched in proteomic data from both populations. It is likely that this is indicative of both populations carrying out the global suppression of protein synthesis reviewed in 1.5.1, to prioritise the synthesis of stress response proteins. The speed and extent to which both populations are able to instigate global synthesis arrest in response to stress was investigated further through immunostaining for the phosphorylation of the elongation initiation factor EIF2α. The phosphorylation mechanism by which EIF2α suppresses protein synthesis in response to stress is comprehensively defined by the Pavitt lab (Adomavicius et al., 2019), while D. Lee et al., 2019 show that EIF2α phosphorylation also induces stress-associated cell cycle arrest, such as that seen in Figure 3.9. However due to manufacturer error (see mitigating circumstances), the data gathered for this study has been redacted.

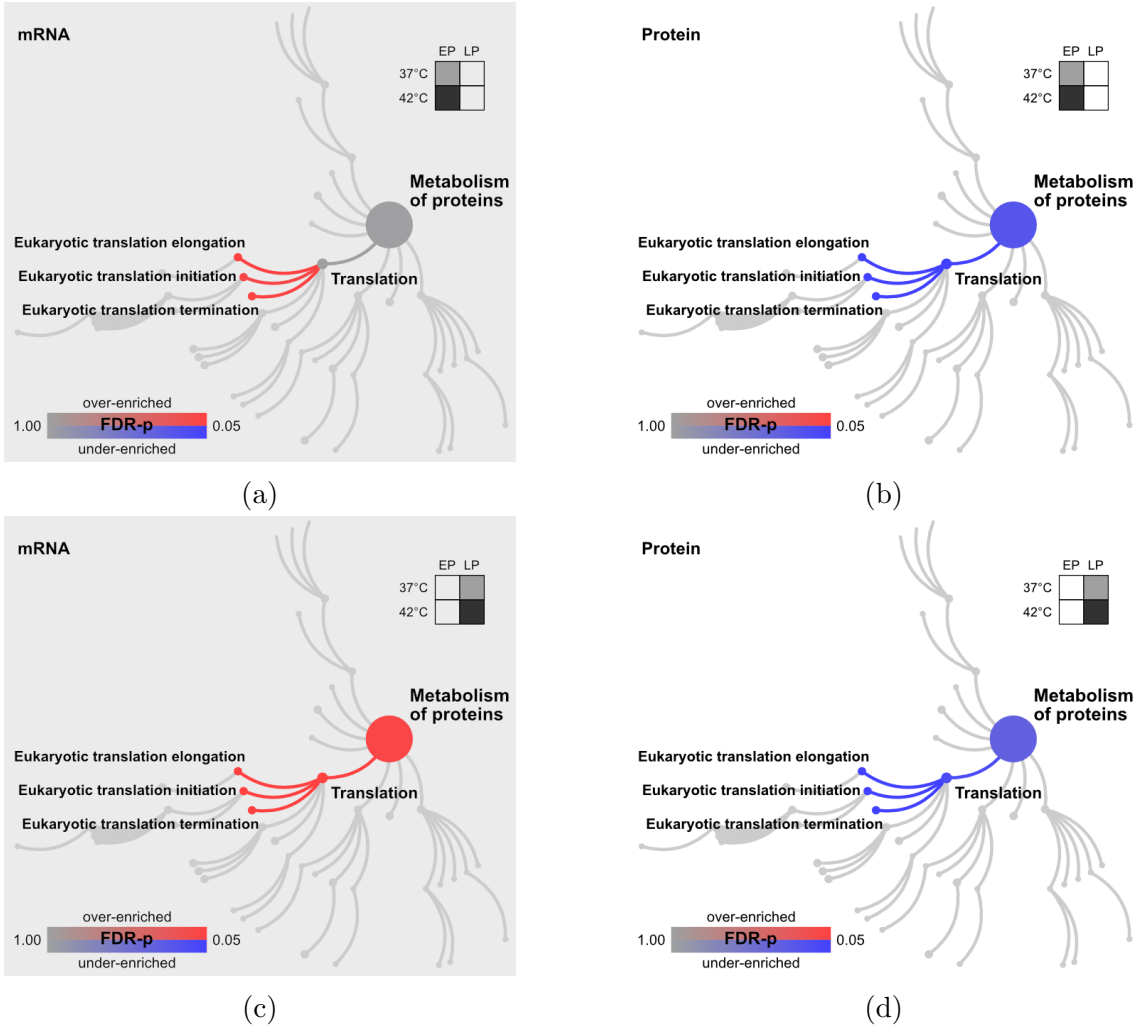

Figure 3.11: Changes to the "metabolism of proteins" Reactome pathway family in response to stress in early- and late-passage populations. The five coloured pathways of interest are subjected to an FDR-corrected PANTHER significant enrichment analysis. (3.11a, 3.11b) Early-passage transcript and protein data in response to stress, respectively. (3.11c, 3.11d) Late-passage transcript and protein data in response to stress, respectively.

Interestingly, the list of significantly under-enriched pathways in proteomic data from LP populations includes the top-tier Reactome pathway "cellular responses to external stimuli". In Figure 3.12, the enrichment statistics of the descendant terms related to the HSF1-mediated heat shock response are plotted, for both transcript and protein data. The transcriptional stress response pathways are highly over-enriched among both EP and LP populations, however the extent to which these render into a proteomic response varies. In stressed LP cells, significant under-enrichment is seen in the "cellular responses to stress" pathway. In EP cells, positive enrichment is seen in the "cellular response to heat stress" (FDR-p = 0.744), "HSF1 activation" (FDR-p = 0.825), and "regulation of HSF1-mediated heat shock response" (FDR-p = 0.689) pathways; while negative enrichment is seen in these pathways in LP cells (FDR-p = 0.713, 0.671, 0.751 respectively).

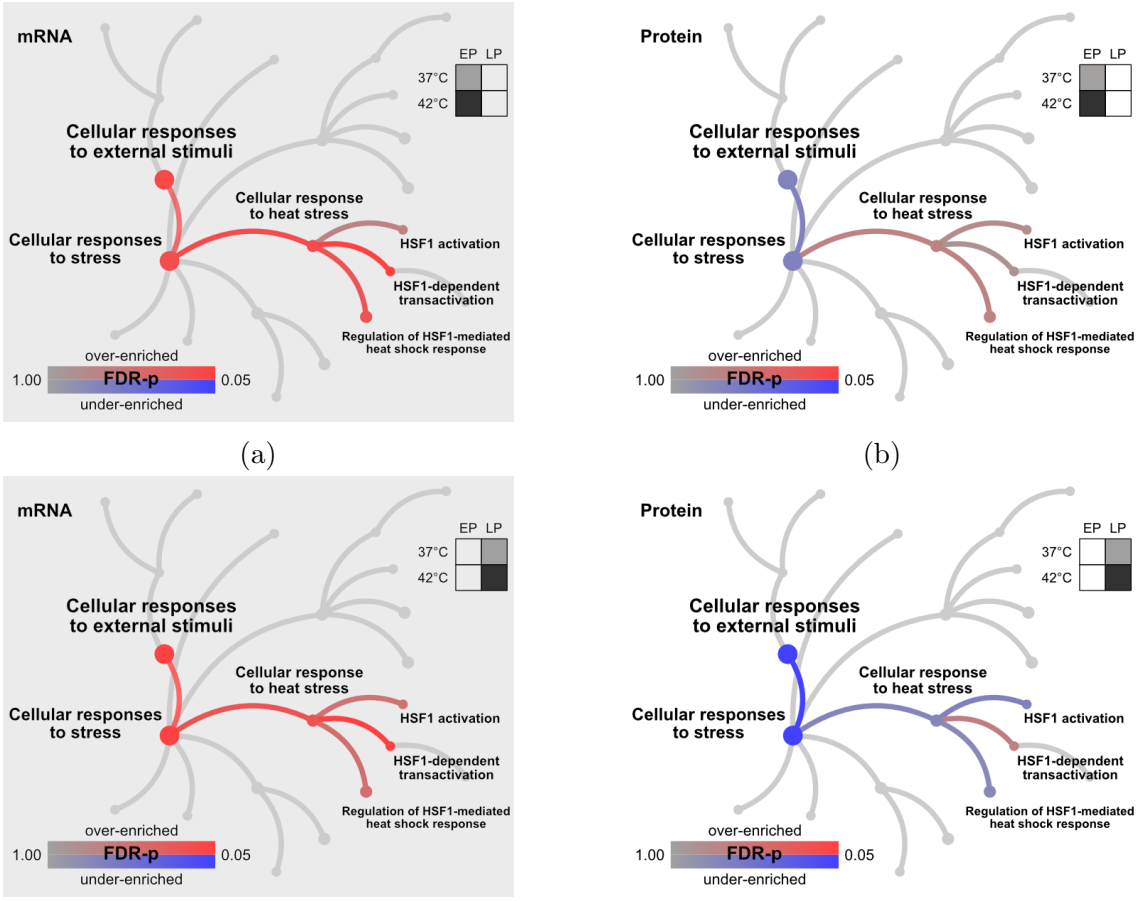

Figure 3.12: Changes to the "cellular responses to external stimuli" Reactome pathway family in response to stress in early- and late-passage populations. The six coloured pathways of interest are subjected to an FDR-corrected PANTHER significant enrichment analysis. (3.12a, 3.12b) Early-passage transcript and protein data in response to stress, respectively. (3.12c, 3.12d) Late-passage transcript and protein data in response to stress, respectively.

3.5 Functional differences of the early- and late-passage proteomes under stress

Following the result in Figure 3.5b that there is no correlation at the level of individual proteins between the changes to the proteome in response to stress between EP and LP cells, perhaps the most important comparison is the functional differences in the stressed transcriptomes and proteomes of EP and LP cells. As discussed earlier in this section, transcriptomic data from RNA-seq will highlight the cellular processes being prioritised in response to stress; while proteomic data from MS will show what processes are in fact being carried out by cells in response to stress, and how this changes in LP populations. It is this comparison which will be focuses on for the remainder of this section.

3.5.1 Transcript and protein regulation analysis

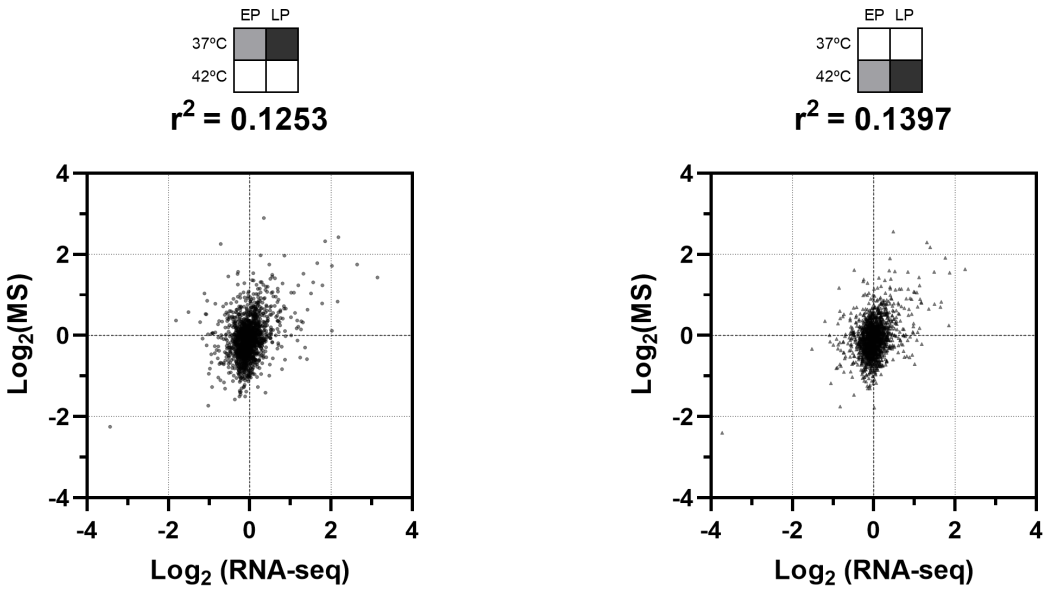

(a) (b)

Figure 3.13: The product-moment correlation coefficients of the fold-changes between early- and late-passage populations in RNA-sequencing and mass spectrometry data. For ease of interpretation, plots are windowed, with $> 99\%$ of data points shown. Data is plotted from the fold-changes of 1726 gene products between unstressed (3.13a) and stressed (3.13b) early- and late-passage populations.

In Figure 3.13, transcript-protein correlation plots have now been made between unstressed/stressed EP and LP cells. In contrast to the correlations seen in Figure 3.6, a much stronger relationship is seen, with and $100r^2 = 14\%$ of changes to the proteome in stressed LP cells explained by transcriptional changes. This demonstrates how changes to the transcriptome influence long-term changes to the proteome, which in most cases do not come into effect over the course of a short proteotoxic stress, but over a prolonged culture period. This more gradual change is reflected in the fact that the absolute RNA fold-changes are not as large as in the response to stress. By far, the most strongly down-regulated among mRNAs and proteins in LP cells are the POSTN gene products (RNA Log_2 fold-change -3.72; protein Log_2 fold-change -2.40). POSTN encodes for periostin, a secreted protein which promotes the migration of hMSCs (Tang et al., 2017) and is involved in the regulation of cell proliferation (as reviewed by González-González & Alonso, 2018).

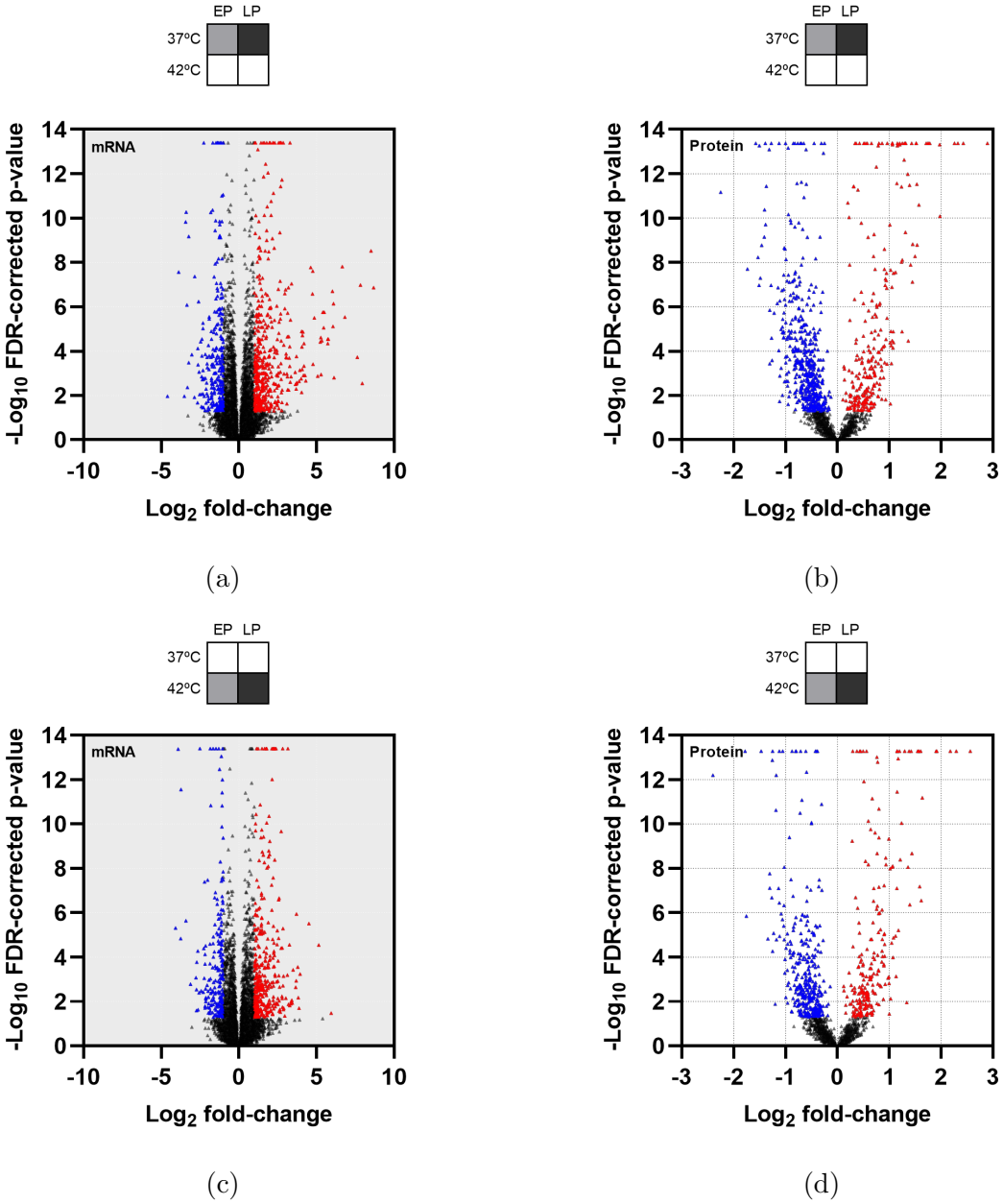

Figure 3.14: Significance of mRNA and protein fold-changes in response to extended passaging in RNA-sequencing and label-free mass spectrometry data. Transcripts satisfying $|\text{Log}_2 \text{ fold-change}| \geq 1$ and FDR-p ≤ 0.05 are coloured blue/red corresponding to down-/up-regulation, with proteins satisfying FDR-p ≤ 0.05 coloured likewise. (3.14a) Fold-changes of 15,782 transcripts in response to stress in early-passage populations. (3.14b) Fold-changes of 1,811 proteins in response to stress in early-passage populations. (3.14c) Fold-changes of 15,378 transcripts in response to stress in late-passage populations. (3.14d) Fold-changes of 1,811 proteins in response to stress in late-passage populations.

The volcano plots in Figure 3.14 show that - particularly at the protein level - far more significant changes are seen when comparing EP versus LP populations rather than changes induced by stress. In RNA-seq data, 5% of 15,782 transcripts are significantly regulated between unstressed EP and LP populations (Figure 3.14a;

262 down-regulated, 471 up-regulated), and 6% of 15378 transcripts between stressed EP and LP populations (Figure 3.14c; 201 down-regulated,353 up-regulated). In MS data, 43% of 1,830 proteins are significantly regulated between unstressed EP and LP populations (Figure 3.14b; 520 down-regulated, 266 up-regulated) and 32% of 1,830 proteins between stressed EP and LP populations (Figure 3.14d; 354 down-regulated, 235 up-regulated). Figure 3.14 highlights the long-term changes to the proteome that have occurred in LP cells due to senescence, in comparison with short-term protein regulation induced by stress. As a result, we would expect strong differences in many aspects of cell behaviour between EP and LP cells.

3.5.2 Pathway enrichment analysis

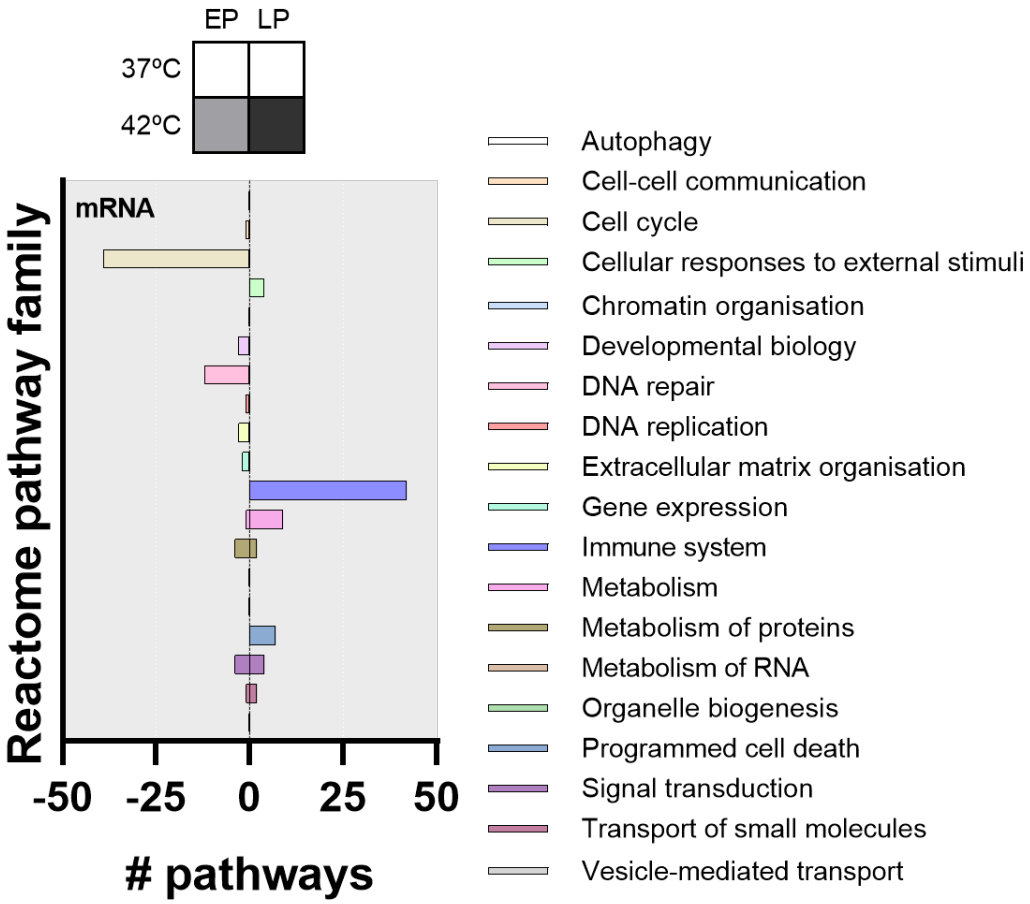

Figure 3.15: Results of a PANTHER statistical enrichment analysis of the fold-changes between the stress transcriptomes of early- and late-passage populations. 141 pathways are significantly enriched across 12 Reactome top-tier pathways. Positive values indicate over-enriched pathways while negative values indicate under-enriched pathways.

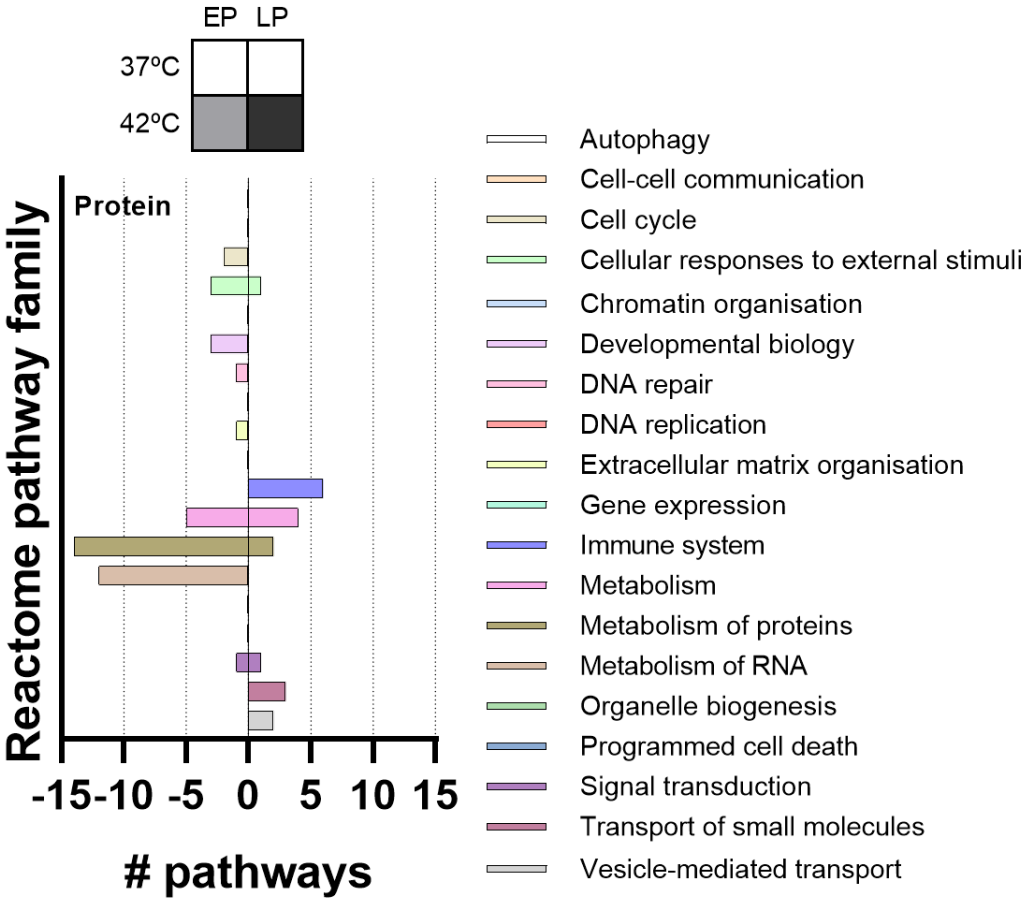

Figure 3.16: Results of a PANTHER statistical enrichment analysis of the fold-changes between early- and late-passage proteomes following stress. 61 pathways are significantly enriched across 12 Reactome top-tier pathways. Positive values indicate over-enriched pathways while negative values indicate under-enriched pathways.

A PANTHER statistical enrichment analysis of Reactome pathways was again carried out, here comparing RNA-seq and MS data between stressed EP and LP populations. Significant enrichment was found in 141 pathways in transcriptional data (Figure 3.15) and 61 pathways in proteomic data (Figure 3.16). In the transcriptional analysis, 39 cell cycle pathways were detected as under-enriched in LP populations as well as 2 pathways in the protein analysis, with no cell cycle pathways over-enriched. This is a further proof of the principle that these LP populations consist of high numbers of senescent cells which have undergone cell cycle arrest. 42 transcriptional and 6 protein pathways associated with the immune system are significantly over-enriched in LP populations following stress, compared with EP populations. As discussed earlier and in Chapter 1, paramount to the use of hMSCs in regenerative medicine is their immunosuppressive capability, which Figures 3.15 and 3.16 suggest is compromised in LP cells.

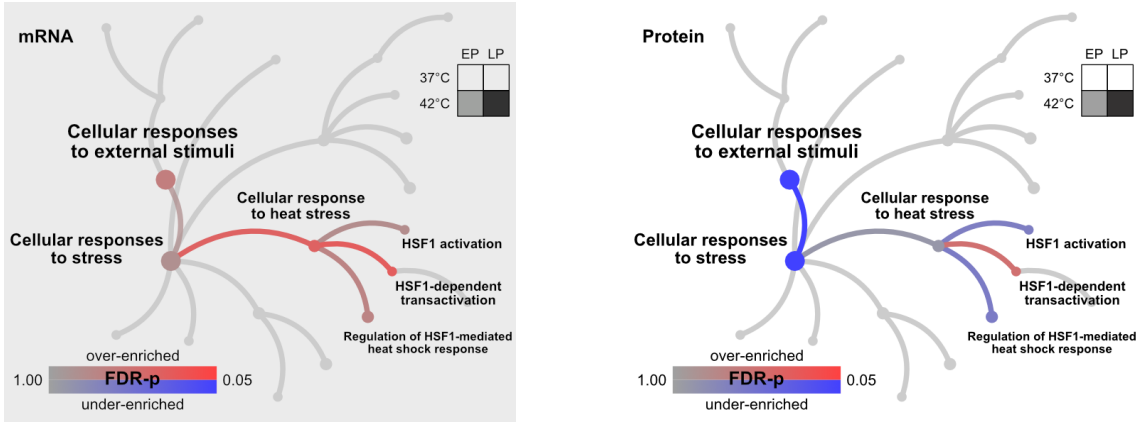

(a) (b)

Figure 3.17: Changes to the "cellular responses to external stimuli" Reactome pathway family between stressed early- and late-passage populations. The six coloured pathways of interest are subjected to an FDR-corrected PANTHER significant enrichment analysis. (3.17a, 3.17b) show the enrichment statistics of transcript and protein data, respectively.

Also discussed in Chapter 1 was the need for cells to be resilient to the stressful post-transplant environment, however Figure 3.15 shows the over-enrichment of transcriptional pathways associated with programmed cell death; under-enrichment in transcriptional and proteomic pathways associated with DNA repair; and under-enrichment in proteomic pathways associated with cellular responses to external stimuli, despite over-enrichment at the transcriptional level. As shown in Figure 3.17b, the top-tier pathway "cellular responses to external stimuli" and sub-pathway "cellular responses to stress" are both positively enriched (FDR-p = 0.655, 0.836 respectively) in transcriptomic data but significantly under-enriched (FDR-p = 0.026, 0.015 respectively) in proteomic data from LP populations following stress compared to EP. Furthermore, the sub-pathways "cellular response to heat stress", "HSF1 activation", and "regulation of HSF1-mediated heat shock response" show contradictory enrichment statistics between transcriptomic and proteomic data. Figure 3.17b indicates that during proteotoxic stress, LP cells do not have the same capability to carry out an efficient and effective stress response as EP cells. Figure 3.17a demonstrates that this attenuation is not caused by a lack of transcription of stress response proteins or upstream thermosensing. On the contrary, transcription of stress response proteins is elevated in LP populations compared to EP, which may indicate that the extent to which proteostasis is compromised is greater in senescent cells.

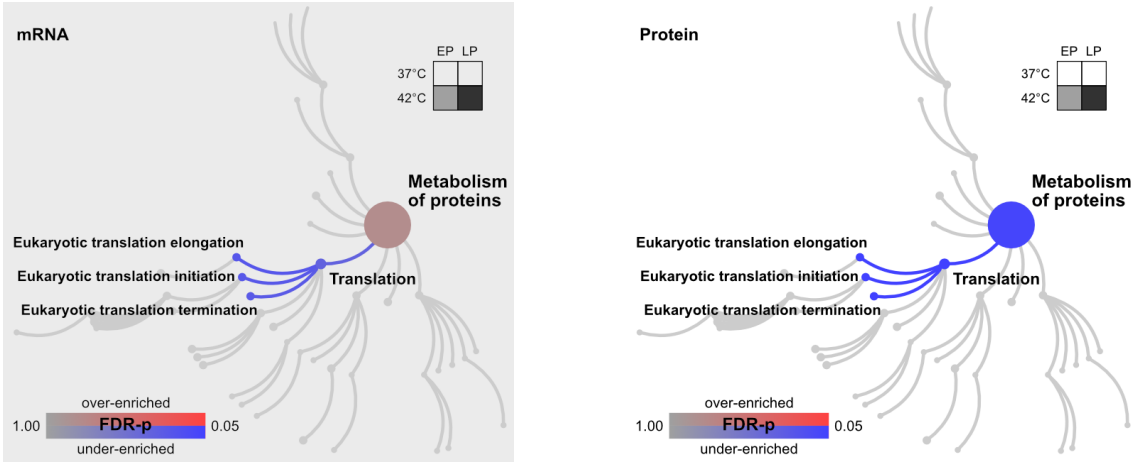

(a) (b)

Figure 3.18: Changes to the "metabolism of proteins" pathway family between stressed early- and late-passage populations. The five coloured pathways are subjected to an FDR-corrected PANTHER significant enrichment analysis. (3.18a, 3.18b) show the enrichment statistics of transcript and protein data, respectively.

Compared to EP populations of proliferating cells, Figure 3.16 shows that several RNA (12) and protein (14) metabolism pathways are under-enriched in LP populations. Figure 3.18 shows the enrichment statistics of pathways related to protein translation. At the transcriptional level, significant under-enrichment is seen in the pathway "eukaryotic translation initiation" (FDR-p = 0.0277) in LP cells. This pathway, as well as "eukaryotic translation elongation", "eukaryotic translation termination", and "translation" as a whole (FDR-p = 0.263, 0.297, and 0.375 respectively) are still negatively enriched in LP populations compared to EP, despite the strong over-enrichment of these pathways in response to stress seen in Figure 3.11c. The four translation pathways are all significantly under-enriched in the stressed proteomes of LP cells compared to EP, showing that - despite a strong transcriptional response to up-regulate these pathways, LP populations have a far lower capacity to synthesise new protein.

3.6 Summary

We have begun this chapter with comprehensive evidence that late-passage TCTP cultures of hMSCs exhibit a senescent phenotype. This was shown through a combination of microscopy and mass spectrometry data (Sections 3.1 and 3.2), and reinforced using pathway analysis results later in the chapter (Section 3.5.2). Due to the use of these cells in regenerative medicine, it was then asked what behavioural changes are exhibited by these cells.

RNA-seq and MS data was collected from four conditions: early- and late-passage cells with and without a two hour proteotoxic stress. In Section 3.3, a PCA was used to rank how these conditions contributed to the difference between samples. This showed that the largest source of variation between samples was, predictably, the use of primary human donors. Following this, the PCA showed that the difference

between early- and late-passage cells contributes much more to the total experimental variance than the difference between stressed and unstressed cells. This finding is echoed by comparisons between the changes due to stress in Figure 3.7; and changes due to passage in Figure 3.14, with a far higher magnitude effect being seen in the latter.

Unexpectedly, the RNA-seq data suggested that transcript from the metalloproteinase ADAMDEC1 may represent a new marker for senescence in hBM-MSCs. As discussed in Section 3.4.1, ADAMDEC1 displays characteristics similar to the senescence-associated secretory phenotype (SASP), however ADAMDEC1 is not currently recognised as a member of the SASP. This may be because ADAMDEC1 may not be sufficiently abundant to be identifiable through label-free techniques, as the protein was undetected in the MS data presented here. Nonetheless, ADAMDEC1 mRNA was undetected in 9 of 10 early-passage samples and detected in 9 of 10 late-passage samples, suggesting this could be used in transcriptional experiments in addition to more established markers of senescence. In any case, more work is needed to conclude this is not an artefact of long-term TCTP culture and, following this, to determine whether ADAMDEC1 RNA undergoes translation and whether this is up- or down-stream of cellular senescence.

Results in Section 3.4.1 also showed that transcriptional changes in response to stress do not carry through to correlating proteomic changes. Conversely a much greater correlation was later seen in transcriptomic and proteomic changes between early- and late-passage cells (Section 3.5.1). This suggests that proteomic changes due to stress are dictated post-transcriptionally, and uncovered a disparity between how cells attempt to respond to stress through protein synthesis; and the changes that actually occur at the protein level. Figure 3.6 shows this disparity is greatest in late-passage cells. While both early- and late-passage cells mount similar transcriptional stress responses, very little correlation was seen between the proteomic stress responses (Figure 3.5). Coherent with this result, a pathway analysis of MS data (Figure 3.18b) showed that several pathways relating to protein translation are significantly under-enriched in late-passage cells compared to early-passage. Again, this is in contrast to transcriptomic data, where protein translation pathways are significantly over-enriched in response to stress in late-passage cells (Figure 3.11c). Notably despite this, MS data shows that late-passage cells experience an under-enrichment in protein translation pathways in response to stress (Figure 3.11d). Thus a key result of this chapter is that late-passage cells have less translational capacity than their early-passage counterparts, and a strong drive to increase this capacity during stress is not effective.

This result raises the question of what this increased translational machinery during stress is needed for, in contrast to the canonical arrest of translation in response to stress. Figure 3.12 shows that significant over-enrichment of stress response pathways was seen in transcriptional data from both early- and late-passage cells, but did not result in significant over-enrichment at the protein level in either case. This suggests that cells may be striving to increase their translational machinery to synthesise additional stress response proteins. Indeed, Figure 3.17b shows that stress response pathways are under-enriched in late-passage populations compared to early-passage,

and a more severe proteotoxic stress being experienced in these cells may be driving the greater transcriptional response seen in Figure 3.17a. To investigate this, the next chapter will focus on the regulation of stress response proteins in early- and late-passage populations.

Chapter 4

A functional module based around HSP70 machinery becomes unresponsive to heat stress in senescent human mesenchymal stem cells

Through ontological analysis, we have observed that the cellular stress response is attenuated in LP cells, despite stress-response proteins being strongly prioritised for up-regulation at the transcriptional level. In light of this, in the following chapter attention will be devoted more specifically to chaperone protein regulation in the cellular stress response. As the breaking of intramolecular non-covalent bonds drives protein misfolding during heat shock (see Section 1.4), the workload of individual chaperone proteins greatly increases, and the up-regulation of these chaperones is necessary to restore proteostasis. Literature discussed in Chapter 1 has shown the age-associated loss of proteostasis coincides with the age-associated accumulation of senescent cells. An analysis of changes in the chaperone network which maintains proteostasis in LP - predominantly senescent - cells may reveal the root of the proteostasis decline in ageing cells and tissues.

4.1 The human chaperone network

In order to better understand the consequences of suppressed stress response in senescent cells, the roles of individual functional modules within the human chaperone network were characterised. An extensive analysis of the literature, domain structures and annotations of the human genome by Brehme et al., 2014 identifies 332 human chaperone proteins which help maintain cellular proteostasis. They define the human chaperone network, consisting of 38 ATP-independent chaperones, 50 ATP-dependent chaperones, and 244 co-chaperones. In the same study, the authors group these proteins into nine chaperone families, somewhat ambiguously based on "chaperone properties". In this study, a more objective method to group chaperone proteins has been used, in order to analyse the stress response in relation to these groupings. STRING (Szklarczyk et al., 2019, version 11.0) was used to gather all published interactions between the 332 human chaperone proteins. This

information was used to build a human chaperone network, with network nodes representing chaperone proteins, and each edge representing a protein-protein interaction (PPI), weighted by its STRING interaction confidence score. A STRING enrichment analysis found that this network was over-enriched ($p < 0.0001$) in terms of PPIs - meaning the network in Figure 4.1 has significantly more edges than would be expected of 332 random human proteins - indicating a high degree of chaperone cooperation. Low-confidence interactions in the STRING database are more likely to be predicted from gene coexpression, protein homology etc., as opposed to physical methods that directly map a PPI (for example, affinity purification mass spectrometry, as reviewed by Meyer and Selbach, 2015). In Figure 4.2, interactions were therefore filtered using STRING's 'highest confidence' cutoff, resulting in the high quality network displayed in Figure 4.3, which formed the basis for further analysis

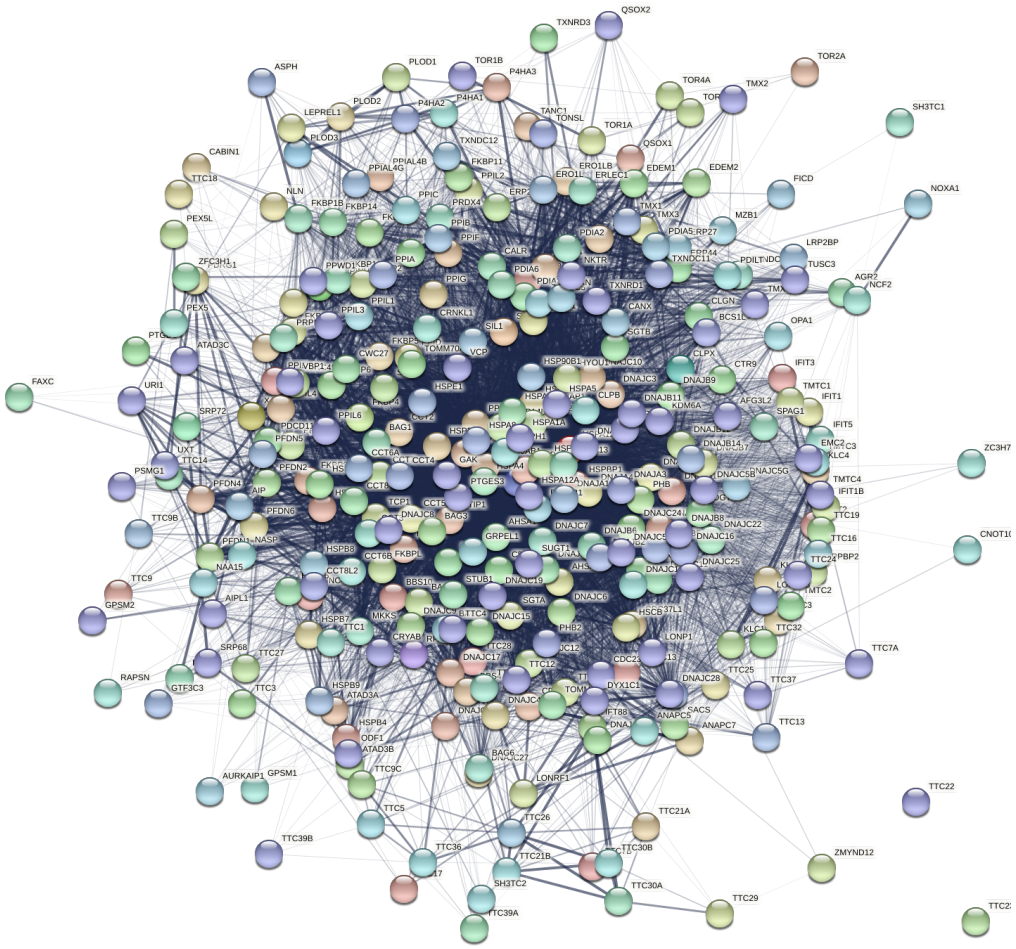

Figure 4.1: The 332 protein human chaperone network curated by Brehme et al., 2014, with nodes connected by published interactions. Created using STRING (Szklarczyk et al., 2019, version 11.0).

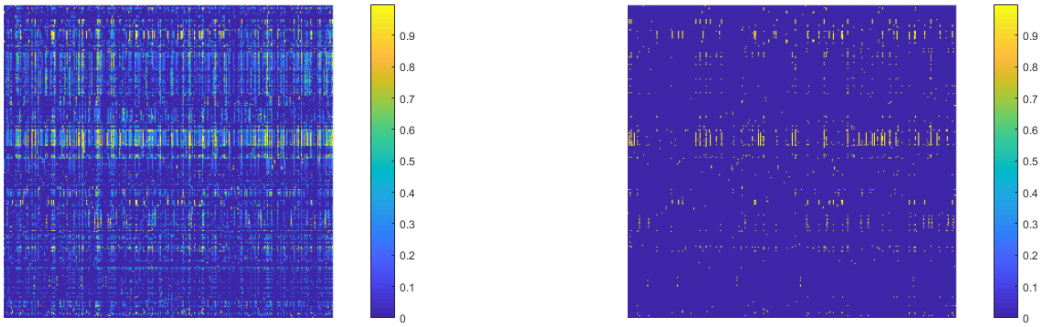

(a) (b)

Figure 4.2: The network adjacency matrix of the 332 protein chaperone network. Each row and column represents an (alphabetically sorted) chaperone node, with the intersection between row i and column j coloured according to the STRING interaction score between chaperones i and j. (4.2a) shows the unfiltered adjacency matrix, while in (4.2b) a cutoff of 0.9 has been applied.

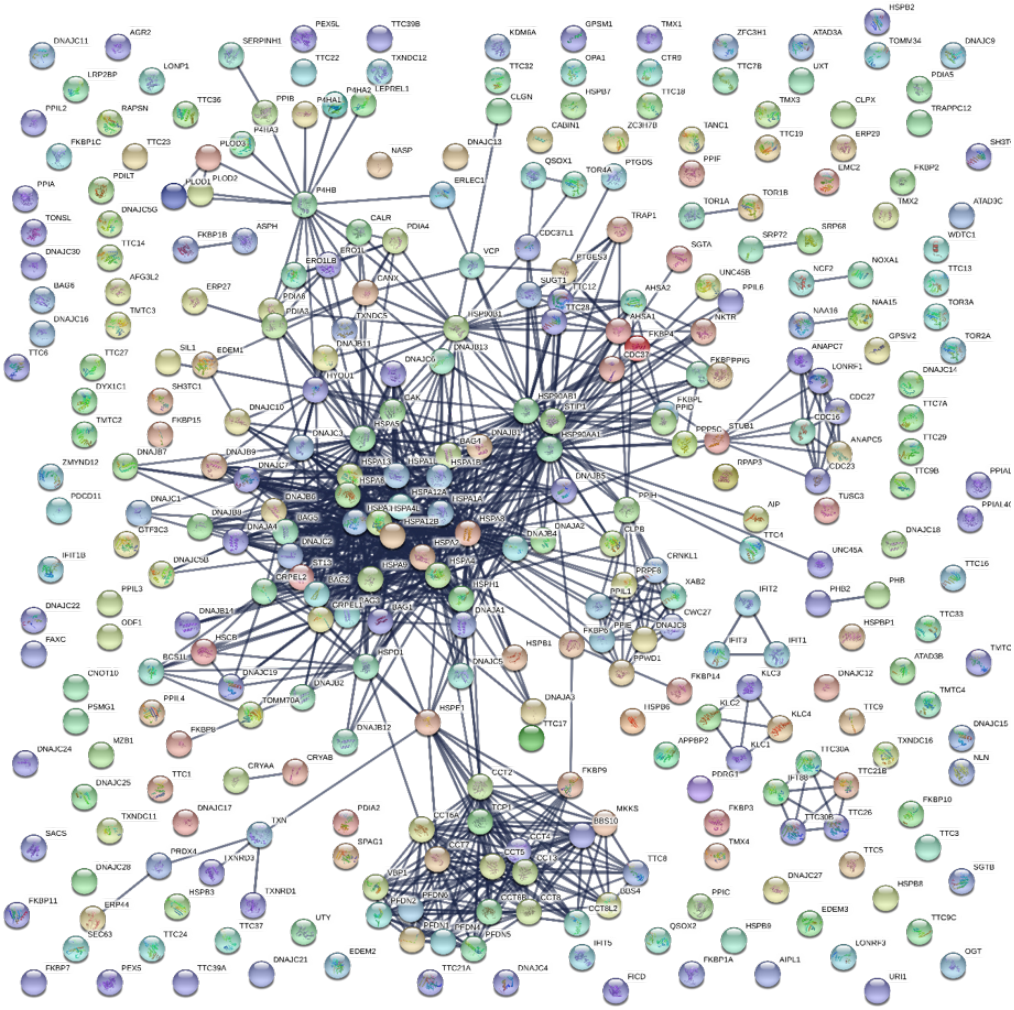

Figure 4.3: The 332 protein human chaperone network curated by Brehme et al., 2014, with nodes connected by published interactions satisfying the "highest confidence" cutoff for STRING interaction confidence scores. Created using STRING (Szklarczyk et al., 2019, version 11.0).

4.1.1 Establishing functional modules of the human chaperone network

With the aim of identifying functional groups of cooperating chaperones, Newman's highly cited modularity algorithm (Newman, 2006b) has been utilised. The algorithm, which aimed to improve on the objectivity of hierarchical clustering methods which are more common within biology, seeks to assign a community structure to the network, such that the number of intracommunity PPIs is maximised while the number of intercommunity of PPIs is minimised. One of the benefits of this algorithm is an objective quantitation of whether a network has sufficient community structure for a modularity analysis to be appropriate, preventing instances of "over-fitting" which can occur when using more common hierarchical clustering methods. The question the modularity analysis serves to answer is – in physical terms – whether all chaperones had the broad remit of maintaining proteostasis as a collective (i.e. low modularity), or whether chaperones could be separated into communities that perform more specialised tasks (i.e. high modularity). To this end, the value $Q \in [-0.5, 1]$ discussed in Section 2.36 gives a measure of the strength of a network's modularity, with $Q > 0$ indicating the presence of a community structure within the network. Using the highest-confidence (PPI) data taken from the STRING database, a modularity analysis of the human chaperone network reveals a highly modular structure ($Q = 0.53$), with the network dividing into 19 deeply intraconnected modules (Figure 4.4).

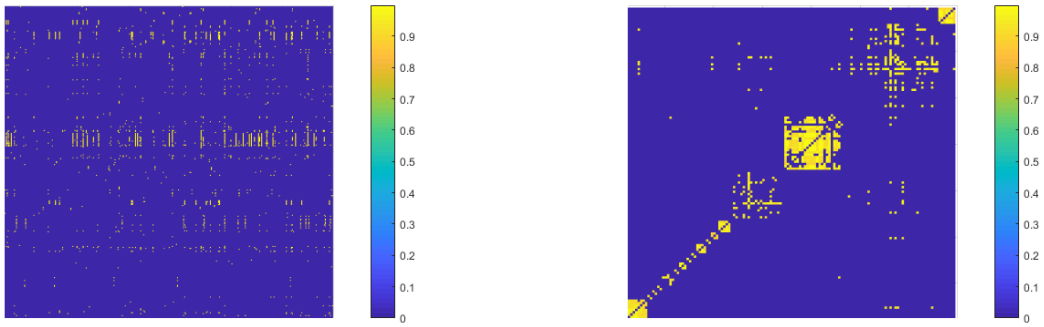

(a) (b)

Figure 4.4: The adjacency matrix of the 332 protein chaperone network The unsorted matrix (4.4a) is subjected to a modularity analysis to identify any existing community structure (4.4b; Newman, 2006b) within the network. Coloured according to STRING interaction score.

Next, functional annotations within the individual interacting communities were analysed, focusing on the five communities that contained the most proteins detected in mass spectrometry data (Figure 4.6). Figure 4.5 displays the constituents of the chaperone modules identified. These communities did indeed seem to be dedicated to specific tasks within the maintenance of proteostasis. For instance, nearly all members of the HSPA and DNAJ families of proteins were grouped together into one module, which we will refer to in this study as the "HSP70 machinery". Similarly, a module containing the two human HSP90 proteins and several documented HSP90 co-chaperones (as reviewed by Dean & Johnson, 2021)) is herein referred to

as the "HSP90 machinery". Chaperones localised in the endoplasmic reticulum (ER) were grouped together in a module containing members of the P4HA and PLOD families of proteins ("ER-specific chaperones"); while all CCT proteins were contained within one module ("cytoskeleton-specific chaperones" - see Section 1.5.5). Another module consisted of the reductases TXN, TXNRD1, TXNRD3, PRDX4, and ERP44 which protect against oxidative stress (as reviewed by Hirota et al., 2002) and has been named as such ("oxidative stress response machinery") - however the Grant lab (Rand & Grant, 2006) have shown that these proteins also protect ribosomes against stress-induced aggregation.

Interestingly, the spring-embedded layout in Figure 4.5 highlights proteins such as STUB1 (grey) and HSPE1 (purple) as key links between different chaperone modules. The latter of these encodes the mitochondrial HSP60 (HSPD1) co-chaperone HSP10 (see Section 1.5.5), and links the CCT/TRiC complex to the HSP70 and HSP90 machineries. Predictably, both HSPD1 and HSPE1 have a strong connection to the HSP70 machinery through interaction with mitochondrial HSP70 (HSPA9); while is has been shown by Young et al., 2003 that HSP70 and HSP90 proteins are directly involved in the transport of native HSPD1/E1 to mitochondria. More surprisingly, HSPE1 exhibits several highly-evidenced interactions with the CCT/TRiC complex (evidence of HSPD1-CCT/TRiC interaction was also present on the STRING database but did not meet the strict confidence cut-off applied in this analysis). While intuitively we would expect the localisation of these two complexes to be mutually exclusive, Lau et al., 2012 identify both CCT/TRiC and HSPD1/E1 as interactors of the tumor suppressant (and cytosol-localised) protein ATF2 - with the authors suggesting these interactions occur at the outer membranes of mitochondria. Similarly, Hein et al., 2015 identify both chaperonin sub-classes as interactors of striatin-3, which has been identified both in the nucleus of human lung carcinoma cells (Petta et al., 2017), and in the cytosol of HeLa cells (Nader et al., 2020). Further to these studies, Vilasi et al., 2014 review several literature studies of the roles of HSPD1/E1 outside of mitochondria. These results suggest any interaction between the two chaperonin sub-classes likely takes place outside of mitochondria, however further work utilising either co-immunofluorescence or proximity labelling techniques is needed to verify any cross-talk between these machineries.

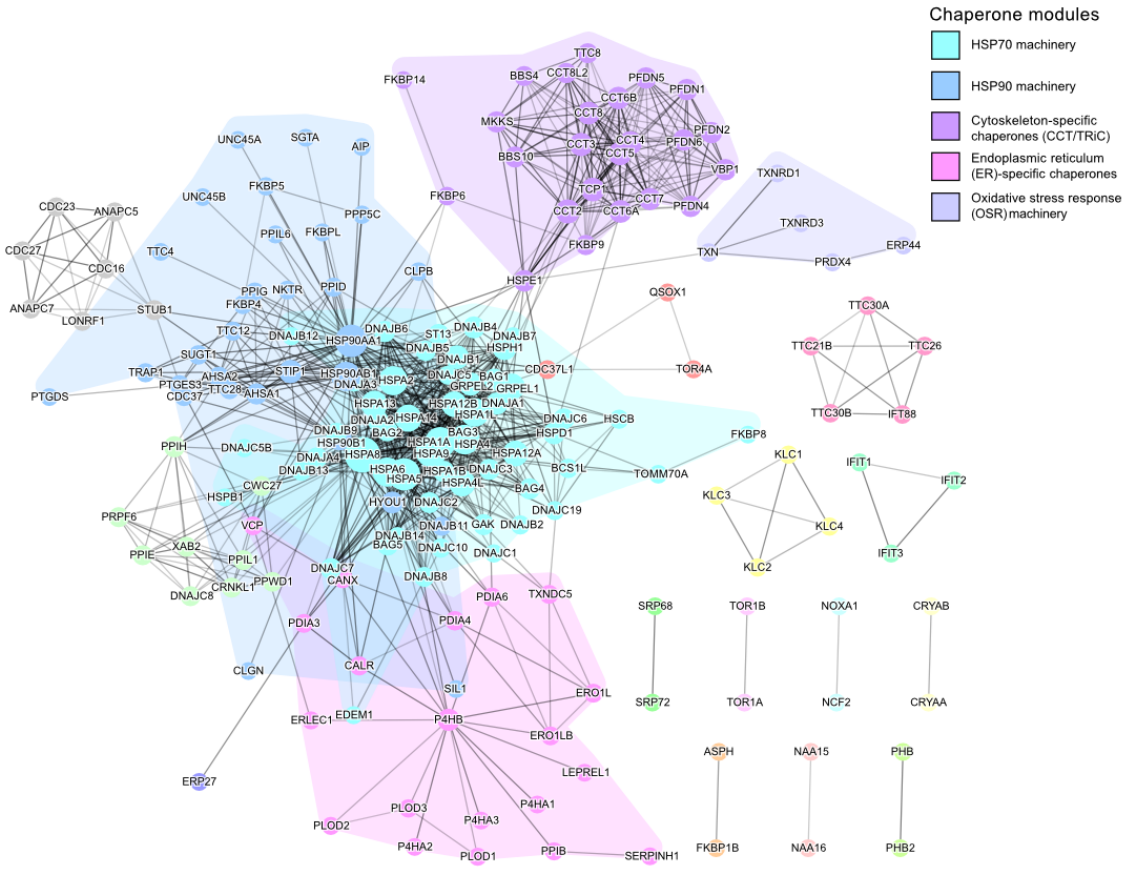

Figure 4.5: The modular structure of the human chaperone network (Brehme et al., 2014). Created using Cytoscape (Shannon, 2003, version 3.6.1). Node size is proportional to node degree, and edge weight is proportional to interaction confidence.

4.2 The modular response to proteotoxic stress

Having established how the chaperone network could be subdivided into interacting functional groups, transcriptomic and proteomic characterisations of the proteotoxic stress response in EP and LP hMSCs were reanalysed. The transcripts detected in the RNA-seq dataset and proteins detected with ≥ 3 peptides-per-protein in the MS dataset gave reasonably representative coverage of the five main chaperone modules identified by modularity analysis (minimum coverage of 43%, Figure 4.6b).

Analysis of the data comparing LP versus EP hMSCs in the absence of heat stress (Figures 4.7a and 4.7b) showed no significant regulation at the transcriptional level, but significant downregulation of two functional chaperone protein modules in senescence: HSP90 machinery ($p = 0.0365$), and cytoskeleton-specific chaperones (CCT/TRiC; $p < 0.0001$). The former of these observations, crucially, shows the changes to the HSP90 and cytoskeletal chaperone machineries in LP populations is not transcriptionally driven. The fact that none of the modules in Figure 4.7a significantly change is surprising in itself. Furthermore, comparing the modular regulation between the stressed transcriptomes/proteomes of EP and LP populations, Figure 4.7c shows the regulation of just two of the five modules of interest. This is in striking contrast to the data previously seen in Figure 3.17a, whereby all stress response pathways are positively enriched in LP populations in the same RNA-seq

dataset. This underlines the existence of partially independent modules within the network which maintains proteostasis. Down-regulation of the module consisting of cytoskeletal chaperones is also seen in Figure 4.7d. Given the role of proteins constitutive of the CCT/TRiC module in maintenance of the cytoskeleton, its substantial downregulation in senescence may be of consequence to the mechanical changes that occur to cells and tissues during ageing (as reviewed by Phillip et al., 2015). Applying Occam's razor however, it may be that the data in Figures 4.7a and 4.7b lend further support to the evidence that the CCT complex serves to chaperone several clients implicated in cell cycle regulation, as discussed in Section 1.5.5.

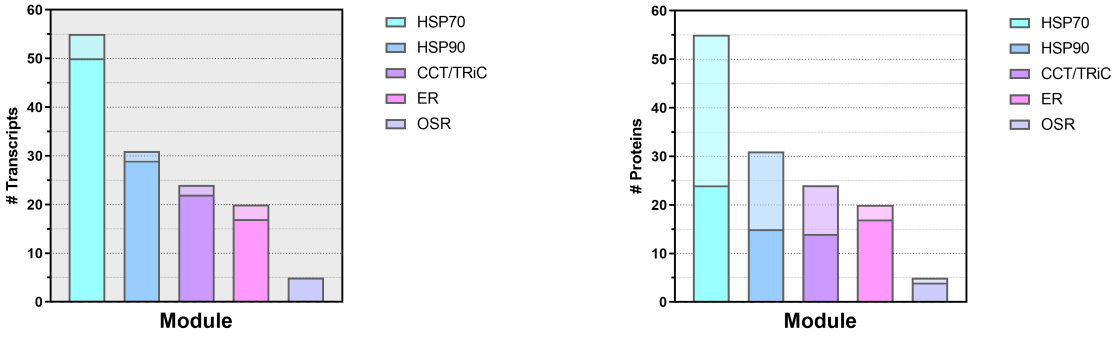

(a) (b)

Figure 4.6: The transcripts (4.6a) and proteins (4.6b) identified per module for the five best-represented chaperone modules in mass spectrometry data.

When the response of EP and LP hMSCs to heat stress was examined, Figures 4.7e and 4.7g show four of the modules of interest were up-regulated at the transcript level. As we have seen evidenced in Chapter 3, these instances of transcriptional regulation are more likely to influence long-term changes to the proteome than short-term. At the protein level, only the module associated with HSP70 machinery is significantly up-regulated in EP populations (Figure 4.7f). This can therefore be regarded as the healthy, functioning, response to stress, whereby up-regulation of the HSP70 machinery is sufficient to resolve the proteotoxic insult induced upon heat shock. The same response however, is not seen in LP populations in response to stress where the mean Log_2 fold-change of chaperones within the HSP70 machinery is just 0.0053 (Figure 4.7h; $p = 0.8821$).

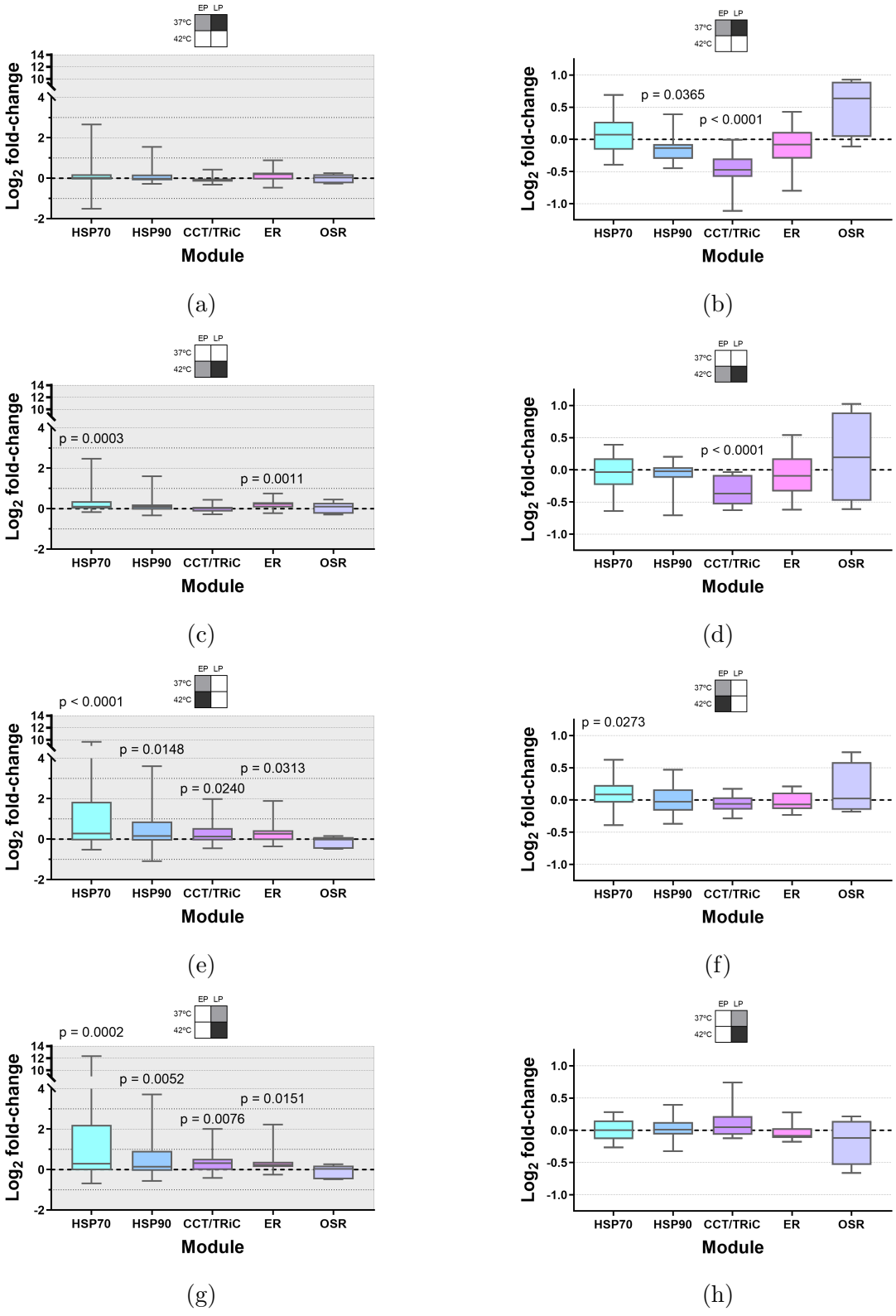

Figure 4.7: mRNA (4.7a, 4.7c, 4.7e, 4.7g; $n = 5$ donors) and protein (4.7b, 4.7d, 4.7f, 4.7h; $n = 4$ donors) fold-changes within chaperone modules across the four comparisons of interest. p-values are calculated using unpaired, two-tailed t-tests.

4.3 The HSP70 machinery

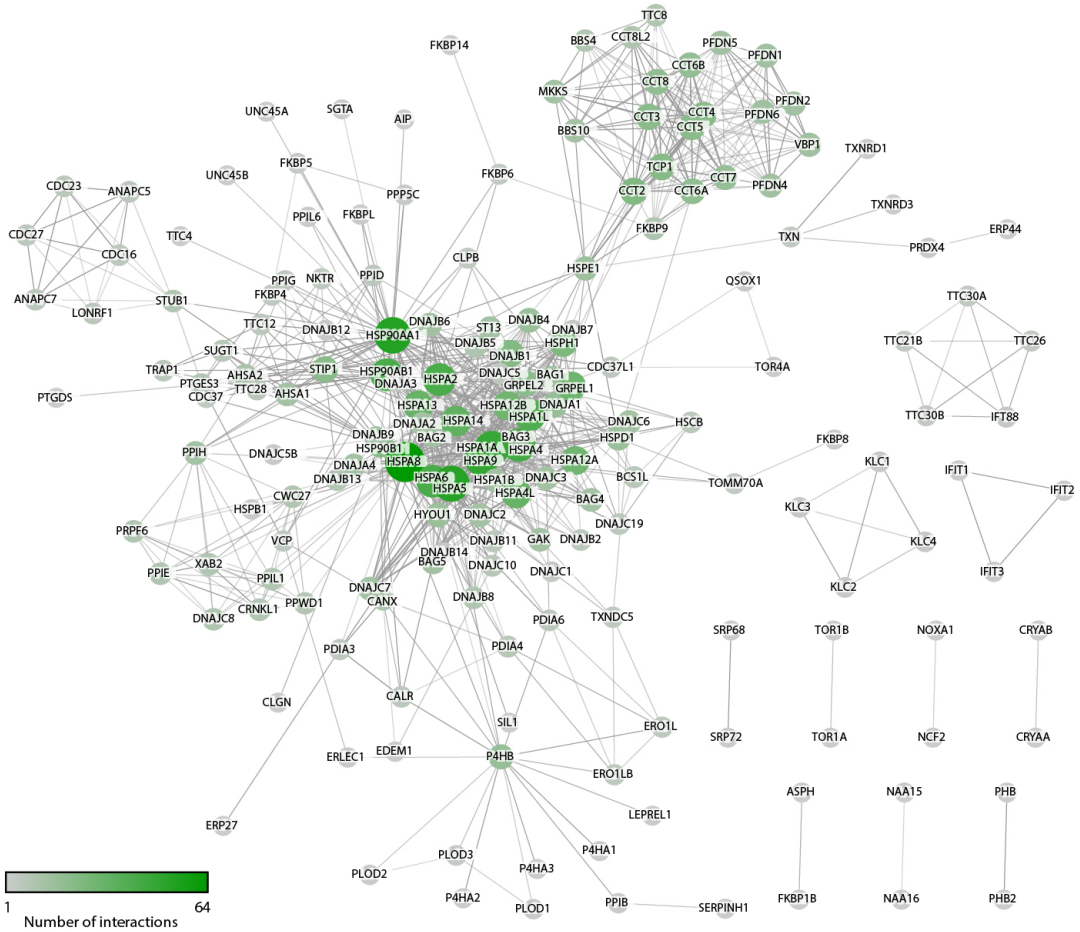

Figure 4.8: The node degree of proteins in the human chaperone network. Node size is proportional to node degree, and edge weight is proportional to interaction confidence. Created using Cytoscape (Shannon, 2003, version 3.6.1).

The results in Figure 4.7 show that the proteotoxic stress response is dictated by the up-regulation of the HSP70 machinery, and LP populations lose the ability to carry out this response. In Figure 4.8, the degree of each node (or more simply, the number of PPIs involving each chaperone; see Section 2.36) in the network is illustrated. As discussed by Rubinov and Sporns, 2010 and Song and Singh, 2013, the degree of each node reflects its importance to the functioning of the network, a feature which Ghosh et al., 2013 and Ghosh et al., 2015 demonstrated can be used to identify treatment targets. In this example, the authors similarly curated network of proteins related to neural apoptosis in Chandipura Virus (CHPV), and found caspase-3 (Casp3) and the Fas-associated Death Domain (Fadd) protein amongst the five highest degree nodes in the network. The authors also showed that Casp3 was significantly up-regulated in a CHPV-infected mouse neuroblastoma cell line; and inhibition of Fadd significantly reduced apoptotic death in these cells. Following this example, Table 4.1 shows the highest degree nodes in the human chaperone network.

Rank	Node	Degree	Rank	Node	Degree
1	HSPA8	64	16	HSPA12B	29
2	HSP90AA1	53	17	HSPH1	25
3	HSPA5	52	18	CCT2	24
4	HSPA9	48	19	DNAJB1	23
5	HSPA1A	47	20	HSP90B1	23
6	HSPA4	43	21	TCP1	22
7	HSP90AB1	41	22	CCT3	21
8	HSPA2	41	23	CCT4	21
9	HSPA6	41	24	CCT5	21
10	HSPA1L	39	25	GRPEL2	21
11	HSPA14	34	26	STIP1	21
12	HSPA13	32	27	CCT6A	19
13	HSPA4L	32	28	CCT8	19
14	GRPEL1	30	29	CCT6B	18
15	HSPA12A	29	30	CCT7	17

Table 4.1: Network degree of nodes within the human chaperone network, coloured according to each node's associated functional module as defined in Figure 4.5.

The HSP70 machinery module contains proteins from the HSPA family that were found to rank highly in terms of node degree, indicating that they are the key proteins within the chaperone network. Figure 4.9 gives a more detailed inspection of the behaviour of the HSP70 machinery. Figure 4.9a shows that, prior to stress, chaperone levels within the HSP70 machinery are generally slightly higher in LP populations than in EP. Figure 4.9b provides a stark contrast however, despite initially higher levels, most chaperones within the HSP70 machinery are down-regulated in the stressed proteomes of LP populations compared to EP. Comparing the response to stress in EP and LP cells (Figures 4.9c and 4.9d respectively), we again see evidence of the attenuation of the stress response in LP populations, with fold changes to proteins constitutive of the HSP70 machinery module generally suppressed. Emphasising again that Figure 4.9c represents the functioning stress response in healthy cells, it is important to note that HSPA1A, or "stress-inducible HSP70" as discussed in Section 1.5.1, is the most stress-sensitive protein within the module, but its up-regulation is dampened in LP cells. HSPA1A is also one of the most influential elements of the human chaperone network with 47 chaperone interactions (as seen in Table 4.1), and it is this particular chaperone we will focus on for the remainder of this chapter.

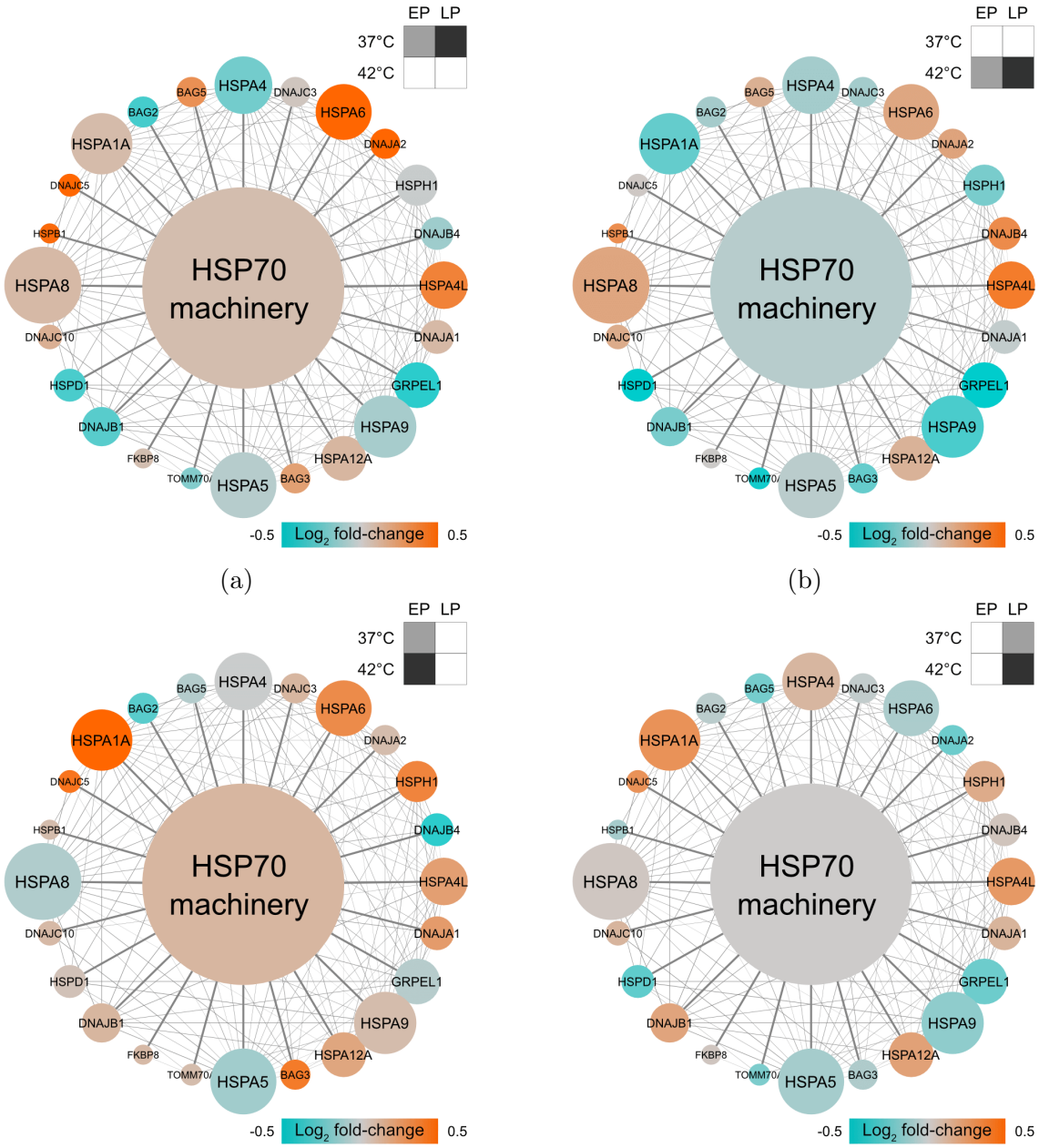

Figure 4.9: Protein fold-changes of nodes within the HSP70 machinery in the four comparisons of interest. (4.9a, 4.9b) From early- to late-passage unstressed and stressed populations, respectively. (4.9c, 4.9d) From before to after stress in early- and late-passage populations, respectively. Node size is proportional to node degree, and edge weight is proportional to interaction confidence. The central node shows the mean fold-change of proteins within the module. Created using Cytoscape (Shannon, 2003, version 3.6.1).

4.4 PES functional inhibition of HSP70

Figure 4.9 shows how the up-regulation of the HSP70 machinery in response to proteotoxic stress is attenuated in LP populations. Next, HSPA1A was targeted for functional inhibition, seeking to investigate the consequences of a compromised HSP70 machinery, and whether any buffering mechanisms exist in EP or LP populations. The small molecule 2-phenylethynesulfonamide (PES) has been shown to bind selectively to the C-terminus (client-binding domain) of HSP70 and prevent interaction with its co-chaperones (Leu et al., 2009). 10 µM PES (efficacy verified in 11 different cell lines by Leu et al., 2009; Leu et al., 2011; Leu et al., 2017), reconstituted in DMSO, was applied to EP and LP cultures 30 minutes prior to heat shock. Both populations were then incubated at either 37°C or 42°C and analysed using label-free mass spectrometry, with the results in each of the four conditions compared to an equivalently treated DMSO-only control.

4.4.1 Protein regulation analysis

Figure 4.10 shows volcano plots for the changes to the proteome due to HSP70 functional inhibition. As in Chapter 3, these plots give a glimpse of the magnitude of the effect PES inhibition has on cells. It is clear from Figures 4.10a and 4.10b therefore, that there is no drastic impact of 10 µM PES treatment in unstressed cells, with totals of 52 differentially regulated proteins in EP populations and 40 differentially regulated proteins in LP populations at the 5% confidence level. In the stressed cells (Figures 4.10c and 4.10d) the impact of HSP70 inhibition is much more visible. In EP populations, 87 proteins are significantly up-regulated and 26 proteins are significantly down-regulated; whereas in LP populations, 92 proteins are significantly up-regulated and 125 proteins are significantly down-regulated. The main point of interest here is that more than twice as many proteins are differentially regulated in LP populations than in EP - showing that LP cells are more strongly affected by HSP70 inhibition. In each of the four conditions, positive regulation of the mitochondrial polyadenylate binding protein PABPC1 is seen (Figure 4.10a, fold-change 0.1383; 4.10b, fold-change 0.3810; 4.10c, fold-change 0.3558; 4.10d, fold-change 0.3976), while Leu et al., 2017 demonstrate the significant up-regulation of PABPC1 transcript in RT-qPCR data as a human cell line marker for HSP70 inhibition.

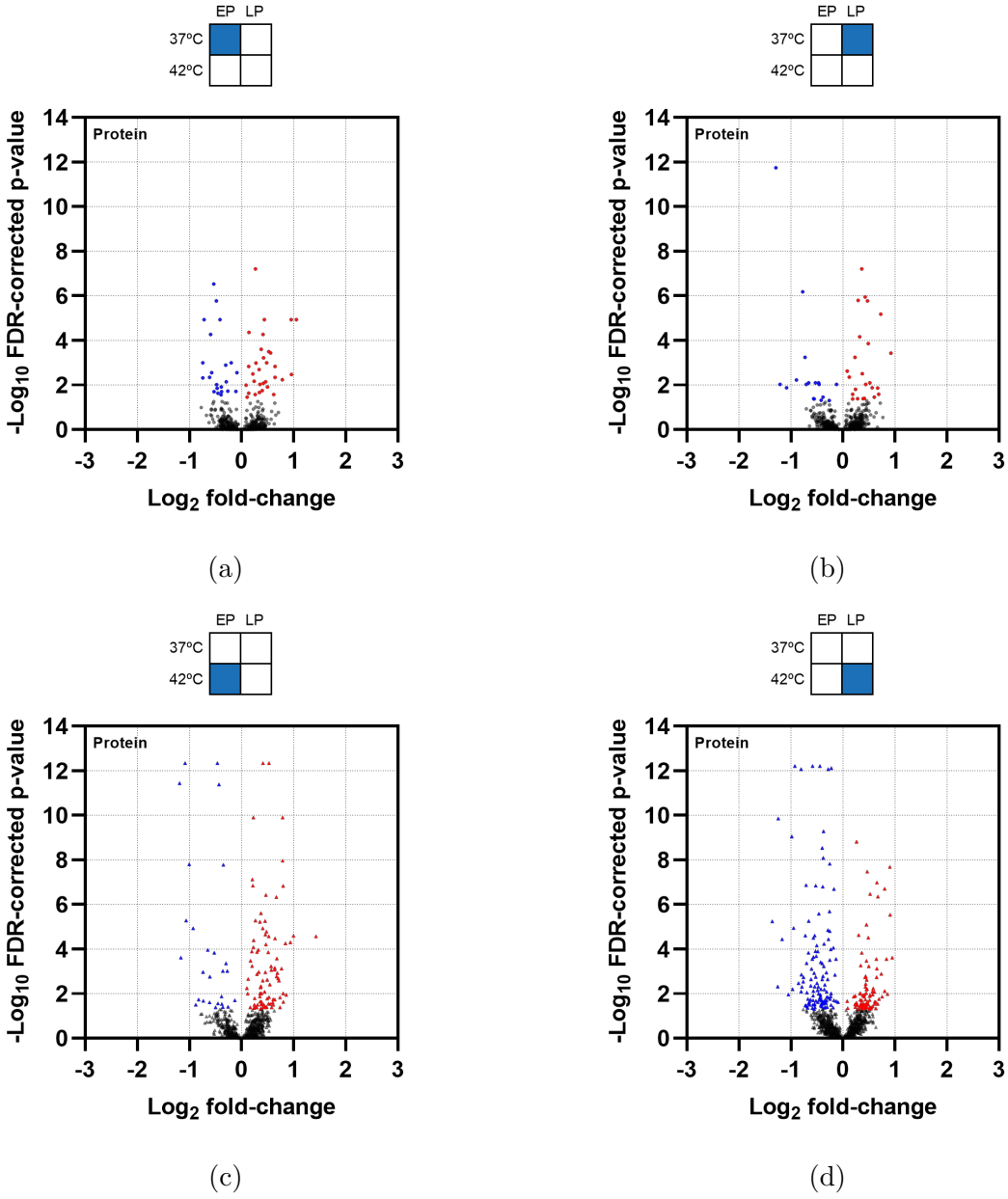

Figure 4.10: Significance of protein fold-changes in response to 10 µM PES treatment in label-free mass spectrometry data (1811 proteins, $n = 4$ donors) across the four mass spectrometry conditions. Proteins satisfying FDR-p ≤ 0.05 versus vehicle-only control are coloured blue/red corresponding to down-/up-regulation.

Surprisingly low PMCC values are seen across all comparisons of HSP70-inhibited data. Figures 4.11a and 4.11b compare the protein fold-changes in response to HSP70 inhibition (versus vehicle-only controls) in unstressed and stressed cells. While there is a clearly higher level of correlation in the EP protein fold-changes than in LP, there is very little similarity in how cells at equilibrium and cells under proteotoxic stress respond to HSP70 inhibition. Figures 4.12a and, particularly, 4.12b also show a complete lack of correlation between the EP and LP responses to HSP70 inhibition.

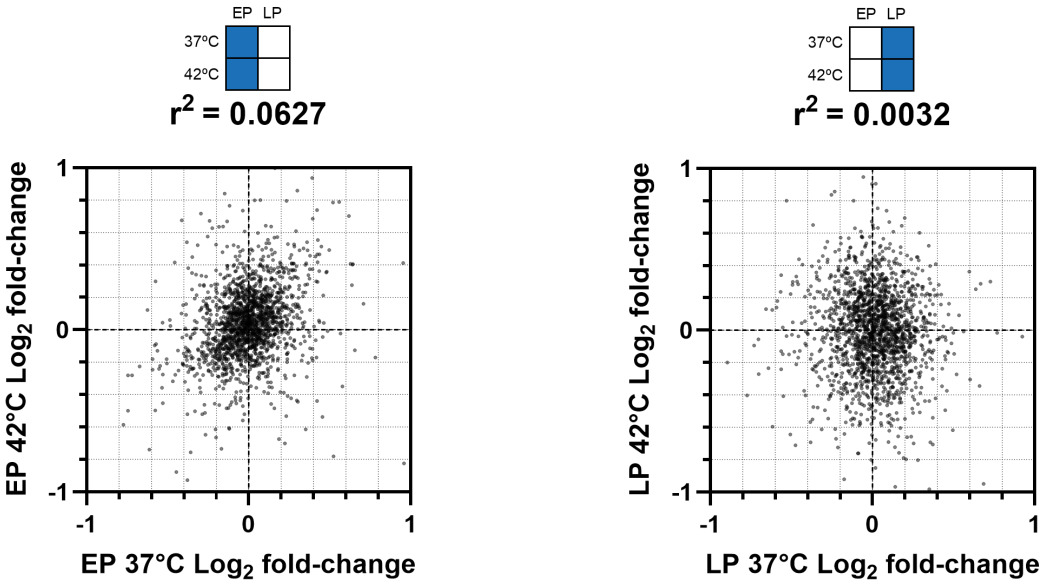

(a) (b)

Figure 4.11: The product-moment correlation coefficients of the fold-changes in response to 10 µM PES treatment between unstressed and stressed populations in mass spectrometry data (1811 proteins, $n = 4$ donors). (4.11a) Early-passage populations. (4.11b) Late-passage populations. For ease of interpretation, plots are windowed, with $> 99\%$ of data points shown.

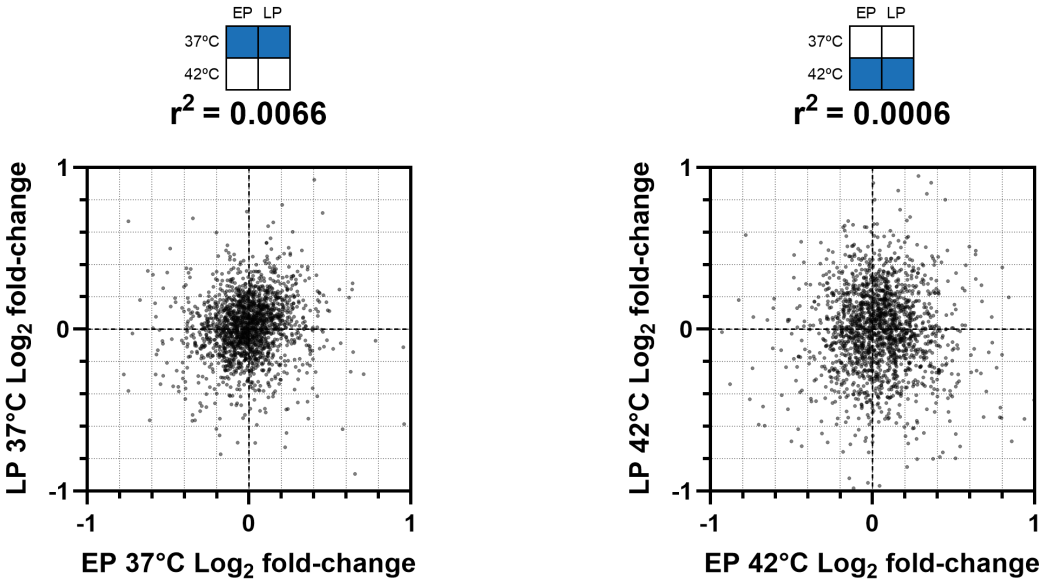

(a) (b)

Figure 4.12: The product-moment correlation coefficients of the fold-changes in response to 10 µM PES treatment between early- and late-passage populations in mass spectrometry data (1811 proteins, $n = 4$ donors). (4.12a) Unstressed populations. (4.12b) Stressed populations. For ease of interpretation, plots are windowed, with $> 99\%$ of data points shown.

4.4.2 Pathway enrichment analysis

Section 4.4.1 repeats the now-familiar result of LP populations failing to emulate the stress response of healthy, EP populations - here in response to HSP70 functional inhibition. The data was next analysed in the same vein as the label-free mass spectrometry data in Chapter 3. A statistical enrichment analysis of Reactome pathways (Fabregat et al., 2017, pathway browser version 3.7, database version 74) using the PANTHER classification system (Mi et al., 2021, version 16.0) was performed for the four inhibitor-versus-control datasets. At the FDR-corrected 5% level of significance, no pathways were significantly under- or over-enriched in either EP or LP unstressed cells. This underlines the data illustrated in Figures 4.10a and 4.10b, where few significant changes in individual proteins are seen in unstressed cells.

Reactome pathway	Hierarchy	# proteins	FDR-p
M phase	Cell cycle	99	0.0499
Eukaryotic translation elongation	Metabolism of proteins	71	0.0402
SRP-dep. cotranslational protein targeting to membrane	Metabolism of proteins	79	0.0428
rRNA processing	Metabolism of RNA	77	0.0427
Formation of a pool of free 40S subunits	Metabolism of proteins	78	0.0486
Nonsense mediated decay independent of the EJC	Metabolism of RNA	72	0.0459

Table 4.2: Pathway enrichment analysis of changes in the early-passage stressed proteome in response to HSP70 functional inhibition. Red pathways indicate over-enrichment, whilst blue pathways indicate under-enrichment in HSP70-inhibited populations.

Reactome pathway	Hierarchy	# proteins	FDR-p
Translation	Metabolism of proteins	144	0.0295
Immune system	Immune system	425	0.0297

Table 4.3: Pathway enrichment analysis of changes in the late-passage stressed proteome in response to HSP70 functional inhibition. Red pathways indicate over-enrichment, whilst blue pathways indicate under-enrichment in HSP70-inhibited populations.

The pathways significantly enriched in the stressed proteomes of EP and LP populations in inhibitor-versus-control comparisons are shown in Tables 4.2 and 4.3. In the EP pathway analysis, it is surprising to see significant over-enrichment in a cell cycle pathway in response to HSP70 inhibition, and this may have some relation to the positive enrichment of the aforementioned pathway associated with the CCT complex. Other significantly enriched pathways are in line with the pathway enrichment seen in response to stress in EP populations in Chapter 3, with the under-enrichment of pathways associated with RNA and protein synthesis. This suggests that EP cells interpret HSP70 inhibition as an exacerbation of the stress condition induced by heat shock. On the other hand, LP populations show over-enrichment of protein translation and under-enrichment of the immune system compared to vehicle-only control - showing differences in the ways LP cells respond to stress and stress-plus-HSP70 inhibition. As in Section 4.2, this demonstrates that LP populations of senescent cells deviate from the "healthy" response of EP populations of proliferating cells - here in response to the compromise of the HSP70 machinery.

4.4.3 Human chaperone network analysis

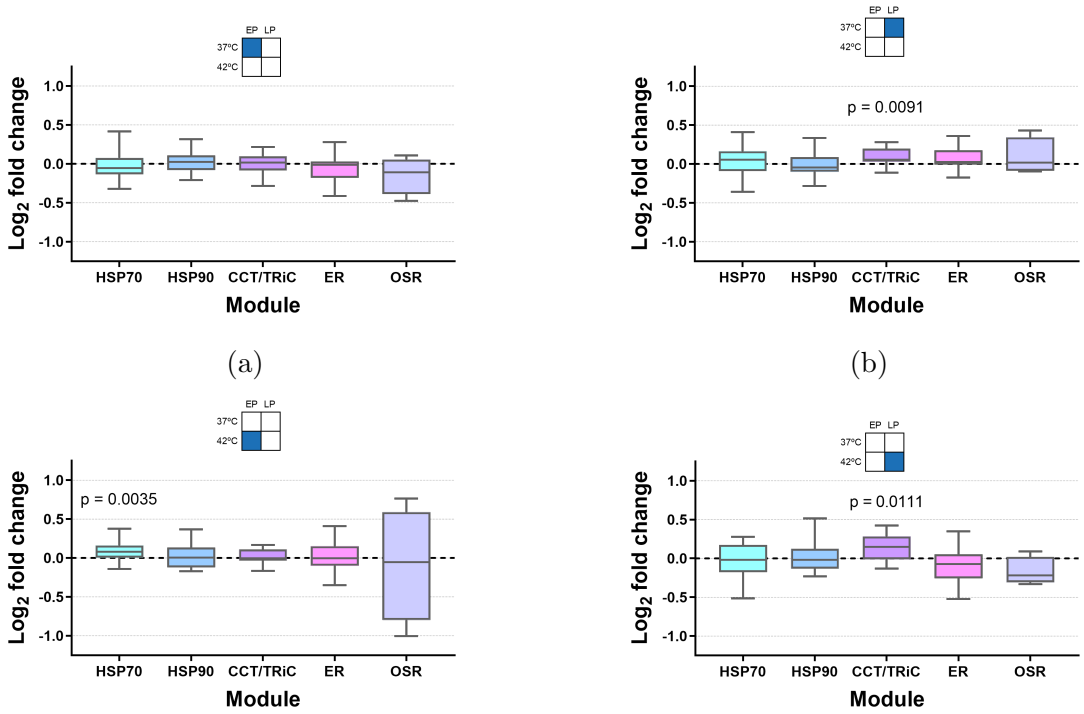

Figure 4.13: Protein fold-changes within chaperone modules in response to 10 µM PES treatment in label-free mass spectrometry data across the four conditions of interest ($n = 4$ donors). p-values are calculated versus vehicle-only controls, using unpaired, two-tailed t-tests.

Focusing on how the chaperone network responds to the compromise of HSP70 function, Figure 4.13 shows how the functional modules identified in Section 4.1 are affected by HSP70 inhibition. Similarly to the previous results in this section, little difference is found between the HSP70-inhibited and control cells in EP, unstressed populations (Figure 4.13a), with no modules significantly regulated. In LP unstressed populations exposed to the HSP70 inhibitor (Figure 4.13b), we find significant up-regulation of the module representing chaperones associated with the CCT complex. Similar positive regulation (p = 0.1273) of this module was seen in the heat stress response of LP populations in Figure 4.7h, and may suggest that while EP cells are largely unaffected by 10 µM PES at 37°C, LP cells show a chaperone profile reflective of cells exposed to proteotoxic stress. In Section 4.2, it was discussed whether the down-regulation of the CCT complex in LP populations was due to the attenuation of cytoskeletal chaperoning, or a reduction of cell cycle proteins in these populations. The up-regulation of the CCT complex in HSPA1A-inhibited LP populations gives support to the former of these two possibilities, and may suggest cytoskeletal proteins are among those most affected by HSP70 inhibition in LP populations. Notably, no regulation of this module was seen in EP populations, such that any compromise of cytoskeletal proteostasis which Figure 4.13 is indicative of in LP populations, does not occur in EP populations.

In cells exposed to proteotoxic stress, the inhibitor led to up-regulation of proteins associated with the HSP70 machinery in EP populations versus controls (Figure 4.13c), indicating cells responding to an influx of misfolded proteins due to a compromised chaperone network. This further supports the inference from pathway analysis results (Section 4.4.2) that EP cells interpret HSP70 inhibition as an exacerbated version of the 42°C stress condition. Presumably the same influx of misfolded proteins occurs in LP cells exposed to stress (Figure 4.13d), however no such response was found.

Of considerable interest is Figure 4.14, which shows the responses of individual members of the HSP70 machinery to functional inhibition of one element of the machinery, namely HSPA1A. In three of the four conditions versus controls, positive regulation of the inhibited element HSPA1A itself is observed. This is not altogether surprising; even in the condition of unstressed EP cells (Figure 4.14a) where aforementioned evidence suggests proteostasis is not compromised by PES treatment, we would expect the inhibitor to compromise HSPA1A-HSF1 binding. Under the titration model of HSF1 activation discussed in Section 1.6.1, increased competition for the substrate-binding domain of HSPA1A will result in a higher rate of HSE binding and subsequent chaperone synthesis. Interestingly, HSPA6 has the highest Log_2 fold-change of proteins within the HSP70 machinery (Log_2 fold-change 0.4176; FDR-p = 0.7773). As reviewed in Section 3.4.1, HSPA6 is a stress-inducible chaperone highly homologous to HSPA1A, but with a substrate-binding domain which is incompatible with PES. Whether the up-regulation of HSPA6 is indicative of a mechanism by which cells are able to recognise the functional inhibition of HSPA1A is unclear.

There is also a clear similarity in the behaviour of the HSP70 machinery between Figures 4.14b and 4.14c, that is, between LP unstressed and EP stressed populations. Furthermore, a PMCC analysis of the entire proteomic dataset between these two conditions revealed a correlation of $r^2 = 0.0450$ (Figure 4.15) which, while low, is more than 10-fold higher than between LP unstressed and stressed populations (Figure 4.11b; $r^2 = 0.0032$). This is unexpected, given the wide-ranging changes that take place in the proteome between EP and LP cells (as discussed in Chapter 3). It would appear that EP cells are largely unaffected by HSP70 inhibition at 37°C, but LP cells show behaviour not unlike cells under proteotoxic stress.

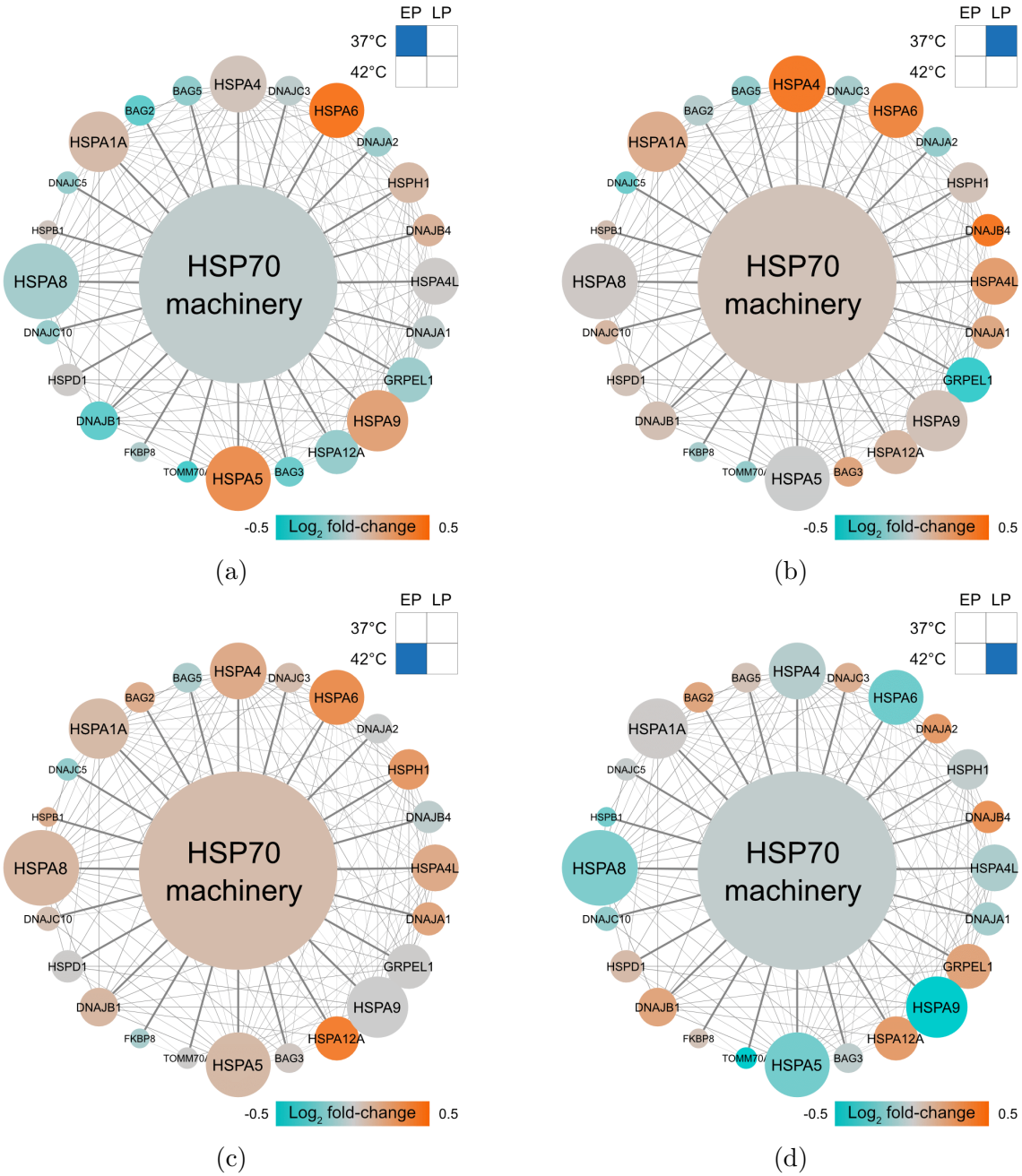

Figure 4.14: Protein fold-changes of nodes within the HSP70 machinery in response to 10 µM PES treatment in the four conditions of interest, compared to vehicle-only controls. Node size is proportional to node degree, and edge weight is proportional to interaction confidence. The central node shows the mean fold-change of proteins within the module. Created using Cytoscape (Shannon, 2003, version 3.6.1).

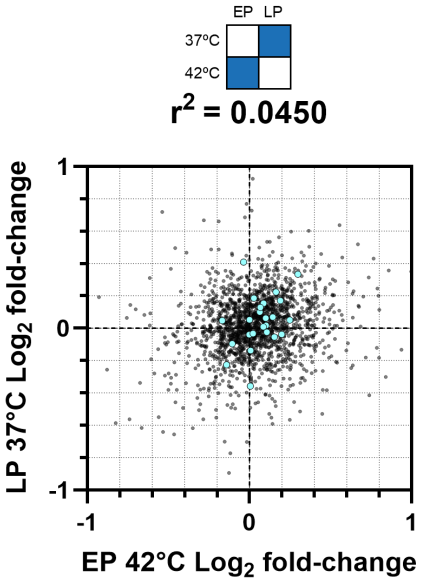

Figure 4.15: The product-moment correlation coefficient of the fold-changes in response to 10 µM PES treatment between late-passage unstressed populations and early-passage stressed populations. Chaperone proteins systematically grouped into a functional module with HSPA1A are overlaid in cyan. For ease of interpretation, plots are windowed, with $> 99\%$ of data points shown.

Perhaps the most meaningful result is the disparity between the response to HSP70 inhibition in stressed EP and LP populations (Figures 4.14c and 4.14d respectively). The HSP70 machinery is significantly up-regulated ($p = 0.0035$) in HSP70-inhibited, stressed EP populations compared to vehicle only controls, demonstrating a clear chaperone buffering mechanism (similar to that seen in *S. cerevisiae* hsp70 mutants; Jarnuczak et al., 2018) within the HSP70 machinery whereby several other elements of the machinery are positively regulated to counter the drop-off in HSPA1A-misfolded protein binding. In LP populations however, very much the opposite response is seen. This is the only one of the four conditions where clear positive regulation of HSPA1A is not seen, and several other HSPA chaperones which provide a compensatory mechanism in EP cells (namely HSPA4, HSPA4L, HSPA5, HSPA6, HSPA8) are negatively regulated in LP cells.

4.5 Temporal dynamics of the HSP70 machinery in response to stress

Thus far in this chapter we have found that the response to stress in healthy hBM-MSCs is dictated by the up-regulation of a functional chaperone module consisting of the HSP70 machinery, among which HSPA1A is stress-inducible and one of the most influential chaperones within the module. We have also seen how this response is attenuated in LP populations consisting of high numbers of senescent cells, and that proteostasis in these cells is far more dependent on HSP70 function than their EP counterparts. Next, the dynamics of HSPA1A in response to stress were analysed using targeted methods with higher temporal resolution than could

be achieved using RNA-sequencing or mass spectrometry, with time points taken before, halfway through, and immediately after heat shock at 42°C; and further time points distributed logarithmically through a 24 hour recovery period at 37°C. This high temporal resolution analysis of HSPA1A dynamics was employed to elucidate the mechanism driving the up-regulation of HSP70 machinery in response to proteotoxic stress; and discover the limiting factor in this process in senescent cells.

4.5.1 Transcriptional dynamics of the HSP70 machinery

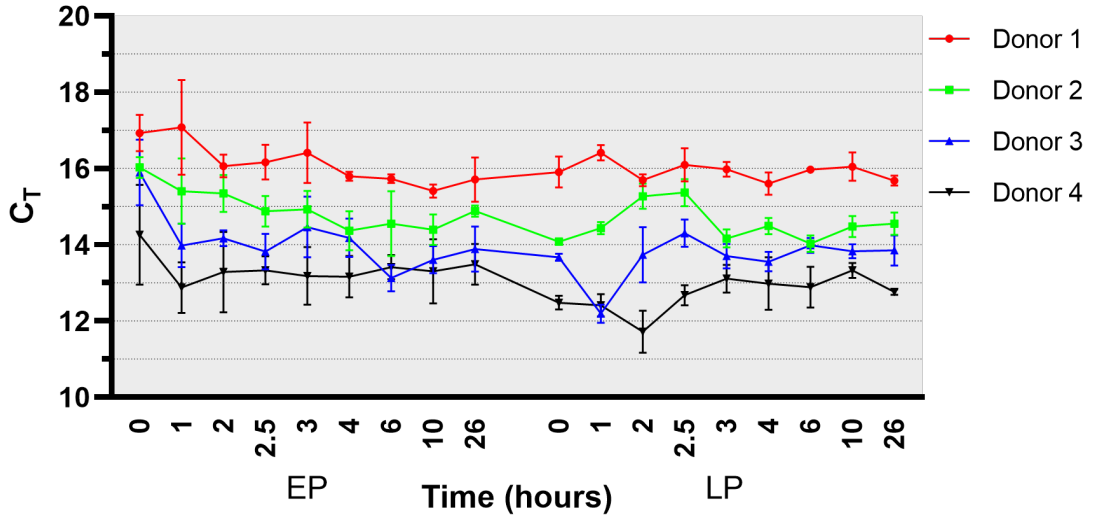

Figure 4.16: PCR cycles at which the fluorescence of the housekeeping gene, PPIA, reaches the threshold for detection in each sample. Mean ± standard deviation of three technical replicates is shown.

Primers for the housekeeping (HK) gene PPIA (X. Li et al., 2015); and the target genes HSPA1A, HSF1, LMNB1, HSPA2, DNAJB1, and HSPB1 were chosen to investigate the regulation of the HSP70 machinery using RT-qPCR. Figure 4.16 demonstrates the steady expression level of the HK gene which other targets are normalised against. Figure 4.17 shows the analysis of of these transcript levels in EP and LP populations at equilibrium. Most noticeably, all seven target transcript levels are lower at equilibrium in LP than in EP. It is important to note that, like the -omic approaches used in Chapter 3, sample quantities in RT-qPCR are normalised such that Figure 4.17 shows representative changes rather than absolute changes. In other words, Figure 4.17 does not imply that transcript levels are lower in LP cells in general, but does show that the seven mRNA targets are less represented in the transcriptomes of LP cells than EP cells.

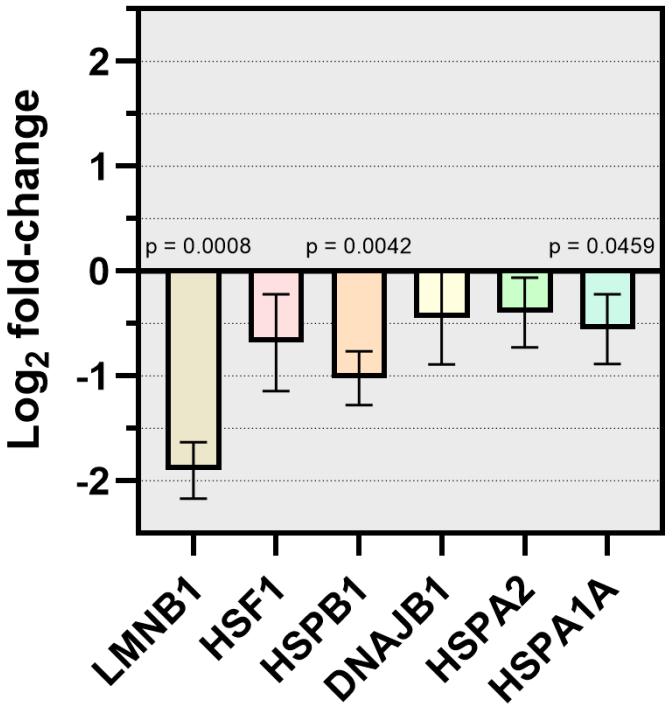

Figure 4.17: Fold-changes of equilibrium levels of RT-qPCR target transcripts between early- and late-passage populations ($n = 4$ donors). Mean ± standard deviation for each target is shown, with p-values versus no change calculated using a two-tailed, one-sample t-test.

Figure 4.17 shows significant down-regulation in transcript levels of lamin B1. Loss of lamin B1 is a marker of senescence (Shimi et al., 2011), and accordingly Figure 4.18a shows transcript levels for lamin B1 are down-regulated in LP populations relative to EP across all time points. This demonstrates that the populations of LP cells used in this RT-qPCR dataset consisted of higher numbers of senescent cells than their donor-matched EP populations. Due to the strong up-regulation of transcripts corresponding to HSPs seen in Figure 3.6, it was first investigated whether this coincides with increased transcription of HSF1, which binds heat shock elements to drive the up-regulation seen in Figure 3.6. However, Figure 4.18b shows no significant change in HSF1 transcript levels in EP or LP populations at a majority of the time points taken. Interestingly, at the end of the 24 hour recovery period following stress, LP HSF1 transcript levels almost doubled to equal EP transcript levels.

The next targets were members of two co-chaperone families represented in the HSP70 machinery functional module attenuated in the stress response of senescent cells, namely the small heat shock protein HSPB1 (Figure 4.18c) and the HSP40 family member DNAJB1 (Figure 4.18d). At equilibrium, HSPB1 transcript levels were significantly lower in LP populations than in EP, but were significantly up-regulated in response to stress in LP populations, before returning to pre-stress equilibrium levels. Surprisingly, HSPB1 mRNA was stress-inducible in LP popu-

lations only, with levels remaining unchanged in EP populations for a majority of the time points taken. Furthermore, levels were significantly down-regulated at the conclusion of the recovery period such that the level of HSPB1 transcript in EP cells following proteotoxic stress resembled the level in LP cells. DNAJB1 transcriptional regulation showed a strong heat shock response (Figure 4.18d, with EP levels increasing almost eight-fold, and LP levels increasing more than 16-fold. These rises show that, as with HSPB1 (and as seen previously in Figure 3.17), the transcriptional response to stress is considerably stronger in LP populations. The DNAJB1 curve for EP transcript levels peaks at the 2 hour time point, before dropping significantly below equilibrium level prior to the 6 hour time point, and returns to a level slightly below equilibrium. As with HSPB1, the level of DNAJB1 mRNA following stress more closely resembles the level in LP populations. The LP DNAJB1 curve peaks slightly later, at the 2.5 hour time point; and also drops below equilibrium level later than in EP populations, following the 6 hour time point, before returning to the pre-stress equilibrium. Extrapolating, Figure 4.18d also shows the recovery time (RT), that is the time at which DNAJB1 transcript levels return to pre-stress levels. As DNAJB1 transcription is downstream of HSF1-HSE binding, which in turn is downstream of HSF1 activation, we may postulate that transcript levels returning to baseline coincides with the HSF1 inactivation and the resolution of proteostasis. This postulate is simplified in that it assumes transient mRNA turnover, but taking it as true, Figure 4.18d suggests that EP populations recover from a 2 hour 42°C proteotoxic stress several hours faster than LP populations.

Focusing on HSP70, transcripts for HSPA1A were analysed as well as, for comparison, the constitutively expressed HSPA2 which, as reviewed by Radons, 2016, is the HSP70 family member most homologous to HSPA1A. Figure 4.18e shows that HSPA2 mRNA is significantly down-regulated in EP populations in response to stress, before returning to equilibrium. Whilst this seems counter-intuitive for a constitutively active protein, this more likely reflects how global (that is, total cellular) transcription rates change in response to stress. Under this postulate, Figure 4.18e shows a global transcriptional arrest in response to stress which agrees with the under-enrichment of RNA metabolism pathways in response to stress seen in Tables 3.1 and 3.2, however the regulation in Figure 4.18e is relatively modest. Evidence of stress-induced global suppression of transcription is supported by results in *Drosophila melanogaster*, however conclusive research on global transcription patterns in response to stress in mammalian cells is lacking, as reviewed in detail by Kantidze et al., 2015 and Goenka et al., 2018. This result would imply that the lifting of transcriptional arrest, which would signal the resolution of the proteotoxic stress, occurs between the 6 hour and 10 hour time points. In LP populations, HSPA2 transcript levels are significantly up-regulated at the 10 hour and 26 hour time points. Regarding HSPA2 mRNA levels as a proxy for global transcription rates, Figure 4.18e may suggest, in contradiction with the response of healthy cells, global transcription is up-regulated in the senescent response to stress. As Figure 4.17 shows, prior to stress, HSPA1A mRNA is significantly down-regulated in LP populations as compared to EP. In both cases transcripts rose rapidly during heat treatment, and reached a similar maximum level $\sim$ 3 hours following the onset of stress.

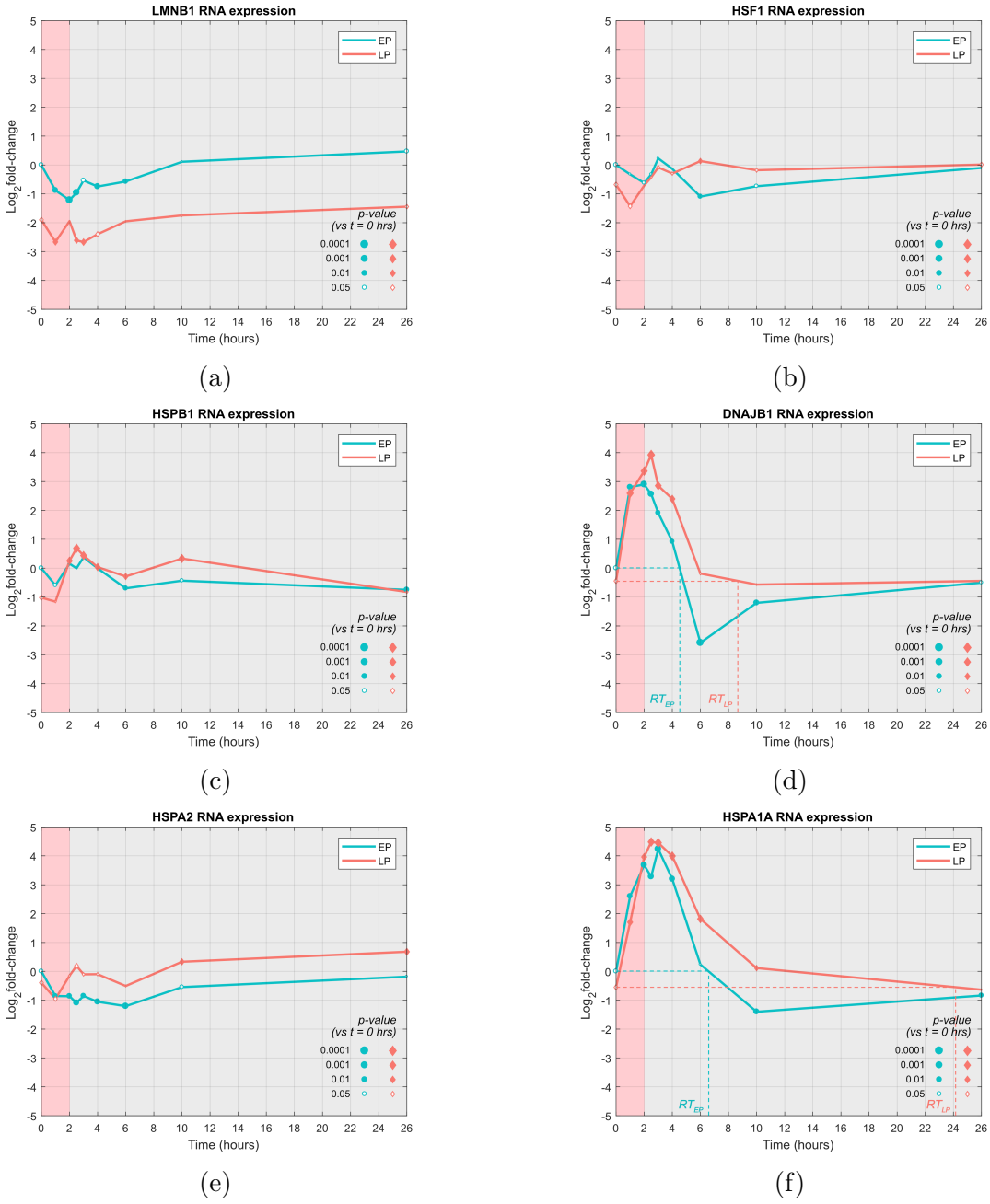

Figure 4.18: RT-qPCR data from early- (blue) and late-passage (red) populations ($n = 4$ donors). Populations are exposed to 42°C heat shock from t = 0 hrs to t = 2 hrs and then kept at 37°C from t = 2 hrs to t = 26 hrs. Time points were taken at t = 0, 1, 2, 2.5, 3, 4, 6, 10, 26 hrs. (4.18a) LMNB1 (lamin B1, senescence marker). (4.18b) HSF1 (heat shock transcription factor). (4.18c) HSPB1 (HSP27). (4.18d) DNAJB1 (HSP40). (4.18e) HSPA2 (constitutive HSP70). (4.18f) HSPA1A (stress-inducible HSP70). p-values are calculated separately for early- and late-passage cells using a weighted, two-tailed t-test (see Section 2.21). Marker sizes are proportional to p-value versus the t = 0 hrs time point, with filled markers representing significant changes at the 5% confidence level.

The primary difference between the behaviour of EP and LP populations was the time required to return to the pre-stress transcript level (RT_{EP} vs RT_{LP}, indicated on Figure 4.18f): in EP cells, HSPA1A was insignificantly different from the initial level at the 6 hour time point; in LP cells, this recovery time extended beyond the 10 hour time point. Intriguingly, the dynamics seen here, whereby HSP70 mRNA drops below pre-stress levels shortly after the 6 hrs time point, mirrors the *in silico* prediction by Sivéry et al., 2016 (as discussed in Section 1.7.1) that active HSF1 drops below pre-stress levels 6 hours following the onset of stress.

4.5.2 Analysis of the dynamics of stress-inducible HSP70 protein through immunofluorescence microscopy

Figure 4.18f emphasises the similarity in the transcriptional response to stress seen previously in Figure 4.7. To further investigate the mechanism by which the HSP70 machinery is attenuated at the protein level in LP populations, immunofluorescence (IF) was used to analyse antibody-tagged HSPA1A protein abundance and localisation in donor-matched EP and LP cells from three hBM-MSC donors, with representative images shown in Figure 4.19.

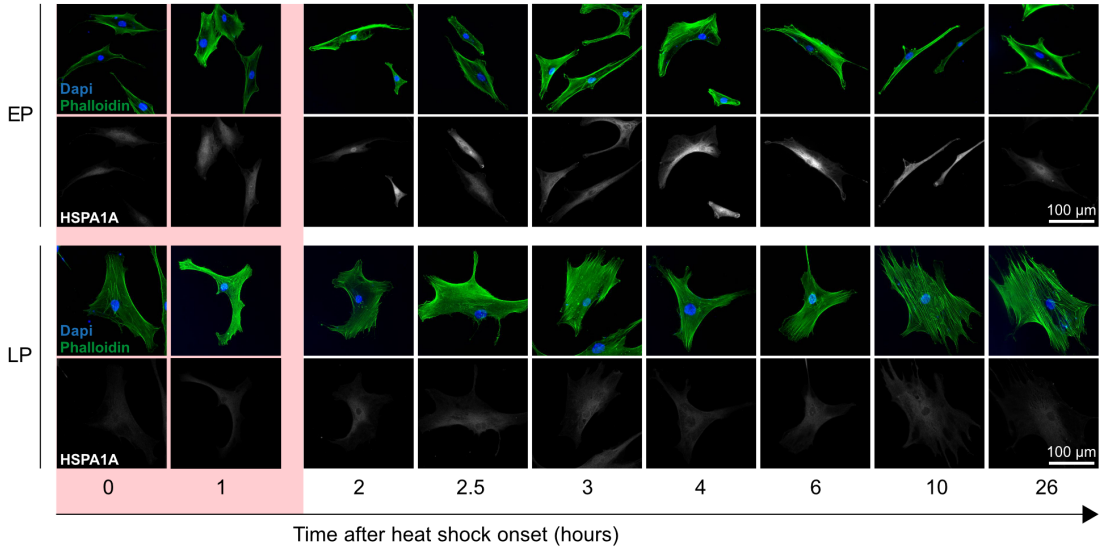

Figure 4.19: Representative images of HSPA1A antibody staining in early- and late-passage cells, with DAPI and phalloidin tags used to identify nuclear and cellular regions, respectively.

Morphological markers of cellular senescence

As reviewed by Hernandez-Segura et al., 2018 and as discussed in Section 1.1 the onset of cellular senescence is accompanied by morphological changes including increased cell area and circularity. Figure 4.20 shows that this is reflected in the LP populations of hBM-MSCs used in this study. Significantly larger cell areas were seen in LP cells compared to EP in each donor, and cell eccentricity, $e \in [0, 1]$, where 0 represents a circle and 1 represents a line, was significantly lower in LP cells from each donor. Due to these limits, the data in Figure 4.20b does not fit to

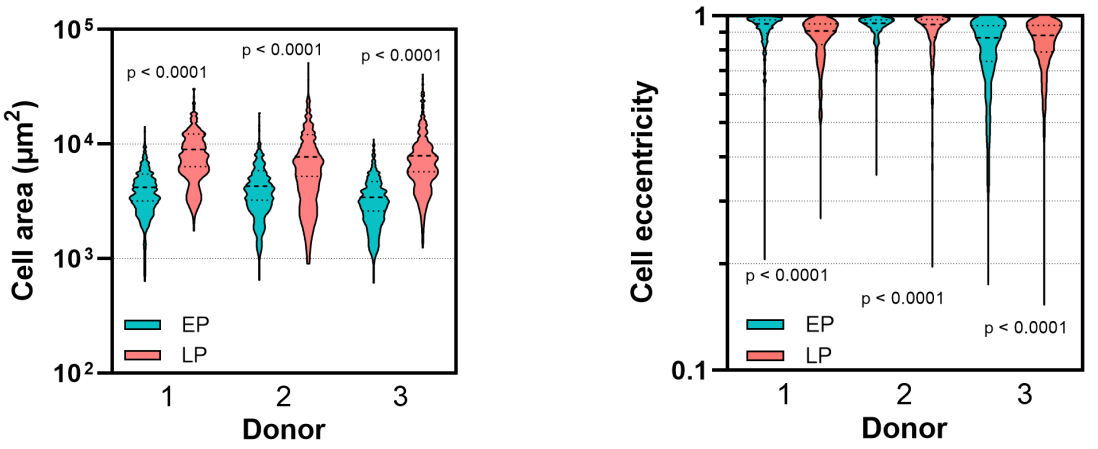

(a) (b)

Figure 4.20: Immunofluorescence microscopy data showing the distribution of morphological parameters of hBM-MSCs from donor-matched early- (blue) and late-passage (red) cells ($n = 3$ donors, ≥ 318 cells per data column). (4.20a) Cell areas, with statistical significance determined via unpaired, two-tailed t-tests. (4.20b) Cell eccentricities, with statistical significance determined via a non-parametric Wilcoxon signed-rank test.

a normal distribution, and as such a non-parametric Wilcoxon signed-rank test was performed to evaluate the statistical significance of changes in cell eccentricity.

Donor variance within immunofluorescence imaging data

In the previous chapter, PCA analysis (Figure 3.4) revealed that the largest source of variance within RNA-seq was inter-donor variation. Furthermore, reanalysing Figure 4.20 between donors, we find significantly different cell areas between each donor (donor 1 vs donor 2, $p = 0.0222$; donor 1 vs donor 3, $p < 0.0001$; donor 2 vs donor 3, $p < 0.0001$). As with RNA-seq and MS data, and as detailed in Section 2.17, microscopy data was fitted to a linear regression model to account for the inter-donor effects seen in human data. Figure 4.21 demonstrates the use of the model across three donors and nine time points, where the full data set is used to determine the "effect size" due to each donor and, donor-independently, the effect size due to each time point and corresponding p-value representing the statistical likelihood that the effect size is nonzero. In other words, a linear model is fitted to the entire dataset with donors and time points forming the predictor variables, and microscopy data the response variable. Hypothesis tests are then performed to assess whether each predictor variable has an effect on the response variable after taking into account the contribution of the other variables. This enables us to separate the effects due to time from the influence of donor variation.

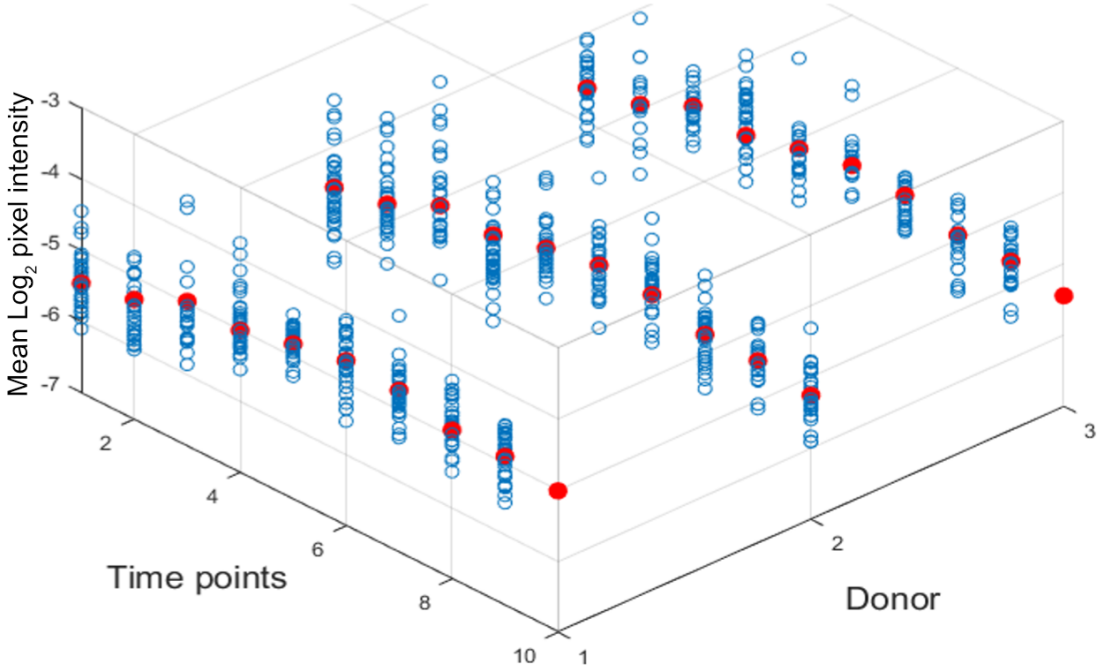

Figure 4.21: Demonstration of effect size calculations (red) from linear models of immunofluorescence microscopy data points (blue). As discussed in detail in Section 2.17, all data points are analysed to determine what effects can be attributed to the variance between donors, in order to isolate treatment-specific effects.

HSPA1A protein spatial and temporal dynamics

As with RT-qPCR analysis, HSPA1A protein was visualised by IF microscopy before, halfway through, and immediately following a 2 hour heat treatment at 42°C, and at time points logarithmically spread over a 24 hour recovery period. Relative protein concentrations of HSPA1A in EP and LP populations were recorded (Figure 4.22). The images taken were two-dimensional, and thus Figure 4.20 shows that LP cells have an inflated cell area, but cannot make any inferences regarding changes to cell volume. As a result it was deemed more appropriate to detail HSPA1A protein concentration (mean IF pixel intensity), rather than HSPA1A protein abundance (integrated IF pixel intensity).

Subsequent quantification of relative HSPA1A concentration (nuclear region, Figure 4.22a; whole cell, Figure 4.22c) showed that the protein concentration increased significantly during the heat treatment, reached a maximum 6 hrs following the onset of stress, and then slowly began to decrease, with HSP70 concentrations remaining elevated above baseline levels throughout the duration of the recovery period. This was the case in both EP and LP hMSCs, with the concentration of HSPA1A prior to stress not differing significantly (nuclear region, Figure 4.22b; whole cell, Figure 4.22d). However, the quantity of HSPA1A induced in the LP stress response was significantly lower, and maximum levels in LP hMSCs were significantly lower than those in EP. An interesting property of HSPA1A is that it is known to be rapidly and reversibly translocated to the nucleus in cells subjected to thermal stress (Velazquez and Lindquist, 1984; Welch and Feramisco, 1984). This process, mediated

by the transport protein HIKESHI (meaning "firefighter"), is thought to protect the contents of the nucleus from proteotoxic damage (Kose et al., 2012). By separately quantifying HSPA1A levels in the nucleus and cytoplasm (demarcated by DAPI and phalloidin staining, Figure 4.19), Figures 4.22a and 4.22b show that nuclear HSPA1A levels mirrored those characterised in the rest of the cell: they reached a maximum after 6 hrs, and levels were generally lower in LP than EP hMSCs. P values in the EP data points demonstrated invariably more confident results, indicating greater heterogeneity in the stress response of LP cells. The ratio between nuclear and cytoplasmic HSPA1A concentrations was also examined, showing significant differences between the behaviours of EP and LP cells, both during and in the two hours following heat treatment (Figures 4.22e and 4.22f). This is suggestive of changed patterns of client proteins, or regulation of transport processes, and consequently that senescence may affect how chaperone resources are directed.

Figure 4.22c - the change in whole-cellular concentration of HSP70 - shows the greatest disparity between the EP and LP stress responses, with the difference in HSPA1A protein concentrations statistically significant from the 2.5 hrs time point to the 10 hrs time point (Figure 4.22d). This is in direct contrast to the HSPA1A transcript dynamics seen in Figure 4.18f, where the HSPA1A stress response showed greater magnitude in LP populations across these time points. In Figure 4.23 HSPA1A data from RT-qPCR and IF microscopy are shown together for temporal comparison. Figure 4.23 also shows recent data from the Grant and Hubbard labs (Jarnuczak et al., 2018), who discovered a lag between the transcriptional and proteomic stress responses in *S. cerevisiae*. Figure 4.23 shows the authors found a three hour time difference between their peak mRNA and protein levels, while the data in the present study shows a remarkably similar mRNA-protein lag. This suggests that within this lag, the regulation of HSPA1A the stress response is predominantly downstream of transcription. This is in agreement with data from the previous chapter (Figure 3.6) where the transcriptional stress response seldom resulted in a proteomic stress response in the two hour time frame analysed. Moreover, this would imply that the 3 hrs time point onward is the period wherein the transcriptional HSPA1A stress response begins to dominate at the protein level. It is this same time period where LP cells see the greatest attenuation of HSPA1A protein up-regulation. Therefore, we may conclude that HSPA1A up-regulation in the stress response is attenuated, at least in part, at a stage which involves HSPA1A mRNA but is downstream of transcription - most likely either in the regulation of HSPA1A translation, or the regulation of HSPA1A turnover.

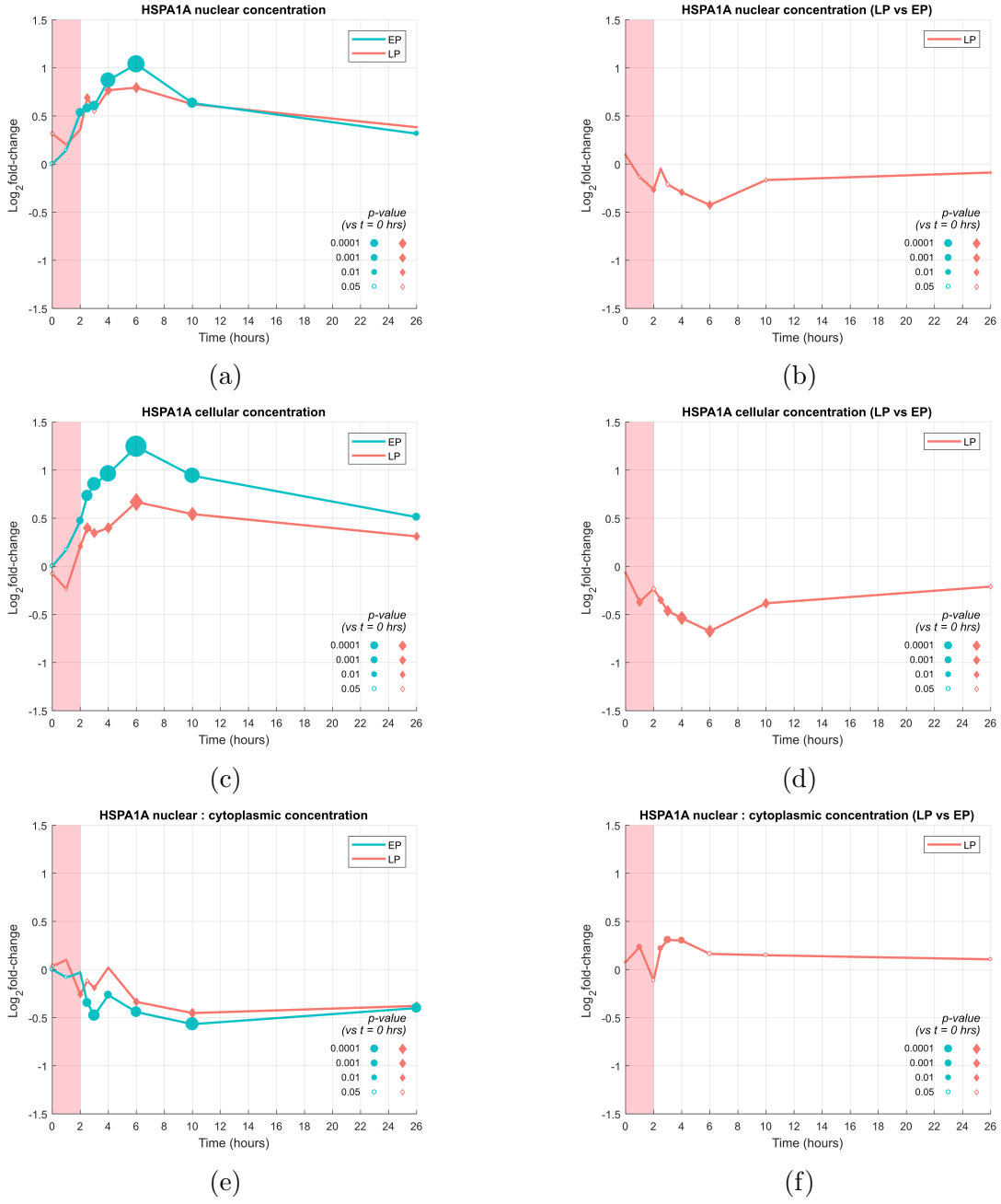

Figure 4.22: Immunofluorescence microscopy data tracking HSPA1A protein concentration dynamics in donor-matched populations of early- (EP, blue) and late-passage (LP, red) hBM-MSCs ($n = 3$ donors). Populations are kept at 42°C from t = 0 hrs to t = 2 hrs and then kept at 37°C from t = 2 hrs to t = 26 hrs. Data is fit to a linear model assessing time point effects for each passage (4.22a, 4.22c, 4.22e); or passage effects for each time point (4.22b, 4.22d, 4.22f). (4.22a/4.22b) Mean/Change in mean antibody fluorescence intensity per nuclear pixel. (4.22c/4.22d) Mean/Change in mean antibody fluorescence intensity per cellular pixel. (4.22e/4.22f) Ratio/Change in ratio of nuclear to cytoplasmic mean antibody fluorescence intensity per pixel. p-values are the statistical significance in linear model effect sizes (see Section 2.17). Marker sizes are proportional to the confidence of a significant change from the 0 hrs time point (4.22a, 4.22c, 4.22e); or from EP (4.22b, 4.22d, 4.22f), with filled markers representing significant changes at the 5% confidence level.

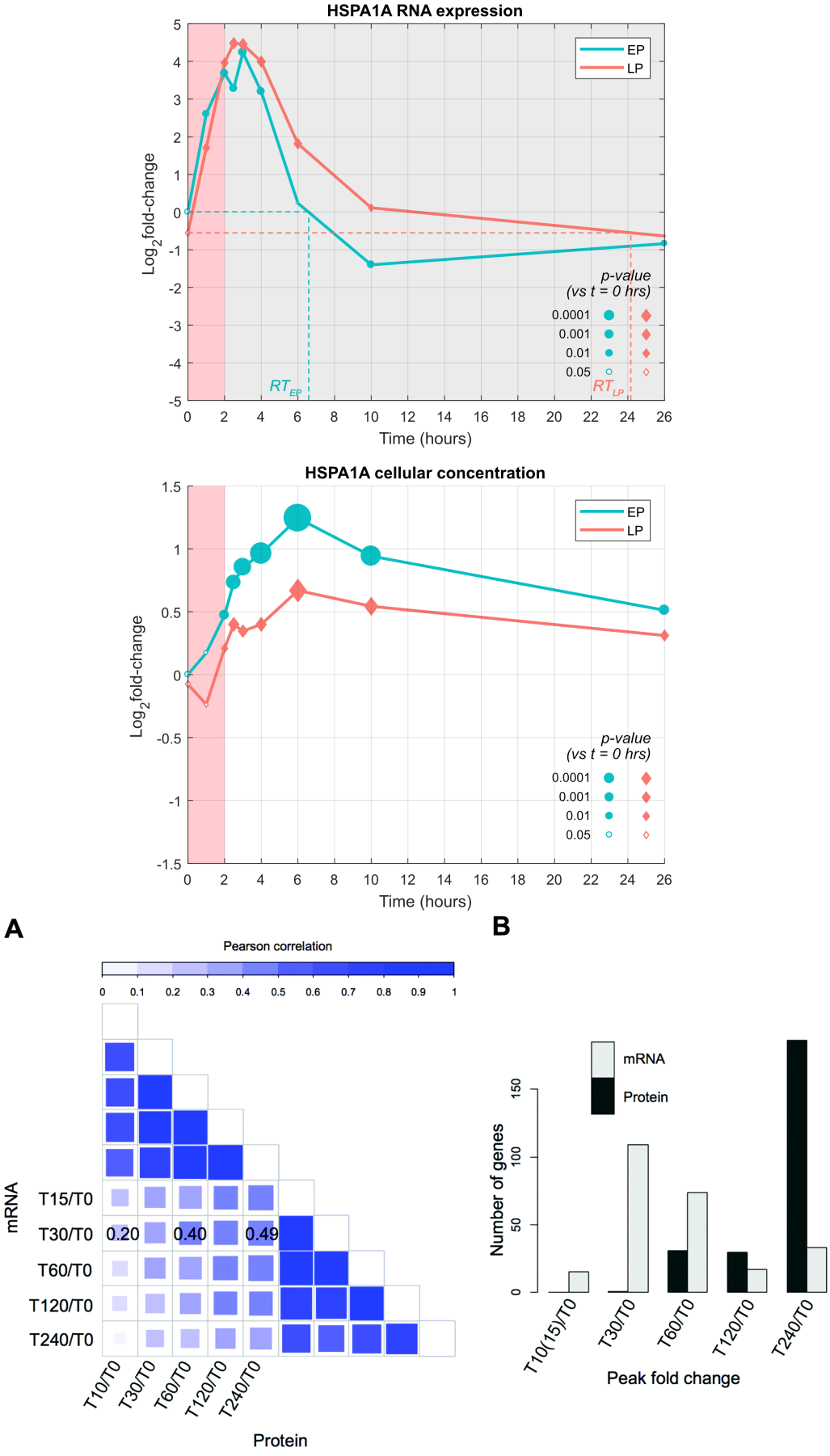

Figure 4.23: HSPA1A mRNA and protein temporal dynamics (from RT-qPCR and IF microscopy) compared with data from Jarnuczak et al., 2018 (bottom).

4.6 Summary

In this chapter an objective and systematic clustering method has been applied to protein-protein interaction data to identify functional modules of proteins within the human chaperone network (Section 4.1.1). Of the modules identified, five were well represented in MS data, namely HSP70 machinery, HSP90 machinery, the CCT/TRiC complex, ER-specific chaperones, and oxidative stress response chaperones (Figure 4.6). In late-passage populations, this analysis revealed that the CCT/TRiC complex is significantly down-regulated compared to early-passage cells (Figure **??**). This down-regulation may be related to the cell-cycle arrest of these late-passage cells with evidence suggesting cell cycle proteins are clients of the CCT/TRiC complex. It remains to be seen what effect this has on the other clients of the CCT/TRiC complex, cytoskeletal proteins.

In response to stress, the HSP70 machinery alone is significantly up-regulated in early-passage cells, indicating this is a key component of the normal functioning stress response. Figure 4.9 shows that the protein within this machinery which was most stress-responsive was that encoded by the HSPA1A gene. In contrast, no overall change was seen in the HSP70 machinery of late-passage cells in response to stress, and up-regulation of HSPA1A was dampened. These results show that late-passage cells lose the ability to correctly regulate the HSP70 machinery in response to stress.

To determine the consequences of a dysfunctional HSP70 machinery, in Section 4.4 HSPA1A was functionally inhibited and mass spectrometry was carried out on early- and late-passage cells with and without proteotoxic stress. Volcano plots (Figure 4.10) demonstrated that the inhibitor has a greater magnitude of effect in stressed late-passage populations than in stressed early-passage populations, while Figure 4.12 showed there was very little correlation between the early- and late-passage proteomic responses to HSPA1A inhibition. Focusing on the HSP70 machinery (Figure 4.14), MS data showed that the effect of the inhibitor is minimal in both early- and late-passage cells kept at 37°C. A more pronounced response was seen in populations exposed to proteotoxic stress. In early-passage populations, evidence of a clear compensatory mechanism was seen, with most elements of the HSP70 machinery up-regulated in the presence of the inhibitor in comparison to vehicle-only controls. This compensatory mechanism was not replicated in late-passage cells however, rather several chaperone levels were reduced compared to vehicle-only controls. These results show that the up-regulation of HSP70 machinery represents normal functioning of the stress response, however late-passage cells are unable to carry out this response, and are more vulnerable to compromise of the HSP70 machinery.

Having found HSPA1A as the most stress-responsive protein in the HSP70 machinery, and having analysed the effects of HSPA1A inhibition, in Section 4.5 HSPA1A regulation during stress was investigated using RT-qPCR and IF microscopy. Time points were taken before, during, and immediately following proteotoxic stress, plus logarithmically spaced time points during a 24 hour recovery period. Across six transcripts, evidence was seen of a general arrest of protein synthesis, however strong significant up-regulation was seen in the transcripts of HSPA1A ($\sim$ 16-fold) and the co-chaperone DNAJB1 ($\sim$ 8-fold) in response to stress in both early- and late-

passage populations (Figure 4.18), with these transcripts reaching peak levels approximately three hours following the onset of stress. As was seen in Chapter 3, the transcriptional regulation of mRNA related to the stress response was greater in late-passage populations than in early-passage populations, however the higher temporal resolution methods utilised in this chapter showed that stress response transcripts return to equilibrium following stress several hours faster in early-passage populations.

In Section 4.5.2, IF data following HSPA1A protein was contrasted against transcript data. At the protein level, HSPA1A is at a similar concentration in both early- and late-passage cells prior to stress. Figure 4.22 shows that the protein is significantly up-regulated in response to stress, peaking 6 hours following the onset of stress in both early- and late-passage cells. Crucially, Figures 4.22c and 4.22d highlight the difference in HSP70 regulation in early- and late-passage cells, with the magnitude of the response far greater in early-passage cells. Paradoxically, late-passage cells carry out a much stronger up-regulation of HSPA1A transcript, but exhibit a much weaker up-regulation of HSPA1A proteins. A temporal lag between the peaks of HSPA1A transcript and protein, approximately 3 hours, with previous work suggesting that this may be the time taken for transcriptional changes to take effect at the protein level. This implies a dual-phase stress response where early post-transcriptional regulation of HSPA1A is carried out prior to the synthesis of additional HSPA1A to resolve proteotoxic stress. In late-passage cells however, where HSPA1A proteins remain significantly lower than in early-passage cells from the 3 hour time point, this reinforces the finding from Chapter 3 that senescent cells experience a loss of translational machinery which is detrimental to the stress response. The current best descriptions of HSP70 regulation during stress are based around new chaperone synthesis alone. Therefore in the next chapter the potential of a dual-phase stress response, and its implications, were evaluated.

Chapter 5

A mathematical model of early- and late-passage stress response dynamics and prediction of cellular "damage"

To investigate how senescence changes the proteotoxic stress response, and predict the consequence of these changes, a system of ordinary/delay differential equations (ODE/DDE) was used to model the protein concentrations key to the stress response. Based around HSP70 the model is informed using data from IF and MS experiments.

5.1 Regulation of model populations and parameters in late-passage cells

5.1.1 HSF1

HSF1 was included as a population in the model to dictate dynamic HSP70 synthesis as per the chaperone titration model reviewed in Section 1.6.1. As in Section 4.5.2, time points were taken before, halfway through, and immediately following a 2 hour thermal stress, in addition to logarithmically spaced out time points during a 24 hour recovery period: 2 hrs, 2.5 hrs, 3 hrs, 4 hrs, 6 hrs, 10 hrs, and 26 hrs. Cellular and nuclear protein concentrations of HSF1 were recorded (Figure 5.1). This data was used to identify whether HSF1 itself is regulated as part of the stress response.

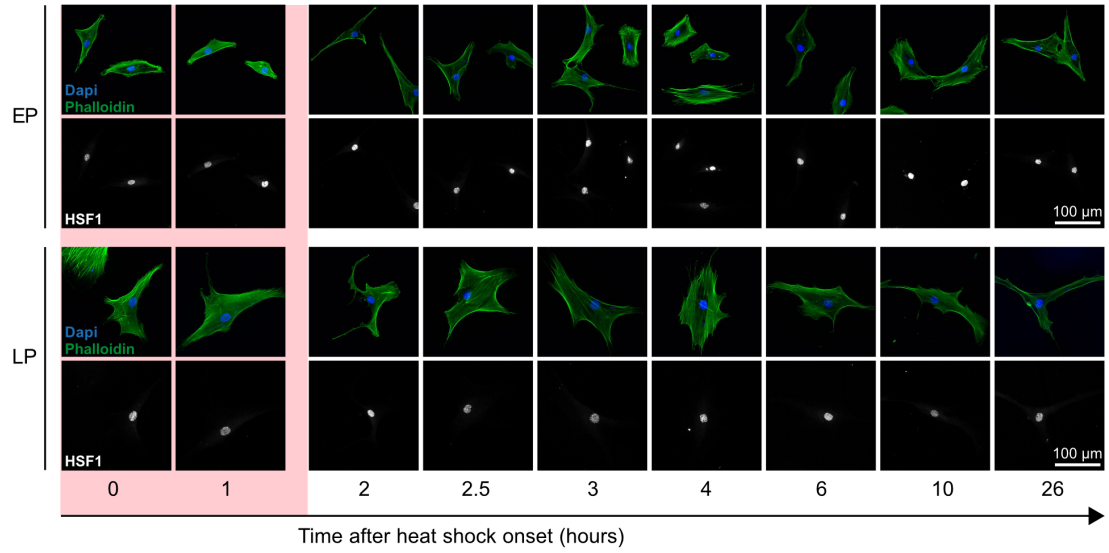

Figure 5.1: Representative images of HSF1 antibody staining in early- and late-passage cells, with DAPI and phalloidin tags used to identify nuclear and cellular regions, respectively.

In both EP and LP cells, HSF1 protein was almost completely localised to the nucleus throughout heat shock and recovery, suggesting a very high proportion of HSF1 may be transcriptionally active constitutively in hBM-MSCs *in vitro* (Figure 5.2a). In light of this, further HSF1 analysis in this section is restricted to nuclear HSF1. In both EP and LP cells, no consistent trends in HSF1 protein dynamics were seen. Figure 5.2b shows that, in EP cells, HSF1 protein concentration remained unchanged across a majority of the time points analysed. HSF1 briefly decreased significantly at the 2.5 hrs time point; and significantly increased across the 10 hrs and 26 hrs time points. The latter of these two results agrees with the elevated HSP70 protein after 26 hours seen in Section 4.5.2, and reinforces the conclusion that these cells acquire an enhanced level of thermotolerance. In LP cells, all time points are significantly decreased from the pre-stress time point in Figure 5.2b. As no clear mechanism is known by which cells down-regulate HSF1 in response to heat shock, the possibility that the pre-stress time point is anomalous should not be ruled out. Similarly, when the difference between EP and LP nuclear HSF1 concentration is fitted to a linear model, the only significant difference occurs at the pre-stress time point. As the current literature lacks a consensus on the mechanism behind heat-induced thermotolerance, and HSF1 regulation is not the focus of this study, HSF1 levels were regarded as constant for the purpose of modelling to reflect the relatively small changes seen in HSF1 dynamics. In agreement with Figure 5.2c, no change in HSF1 levels between EP and LP simulations was incorporated.

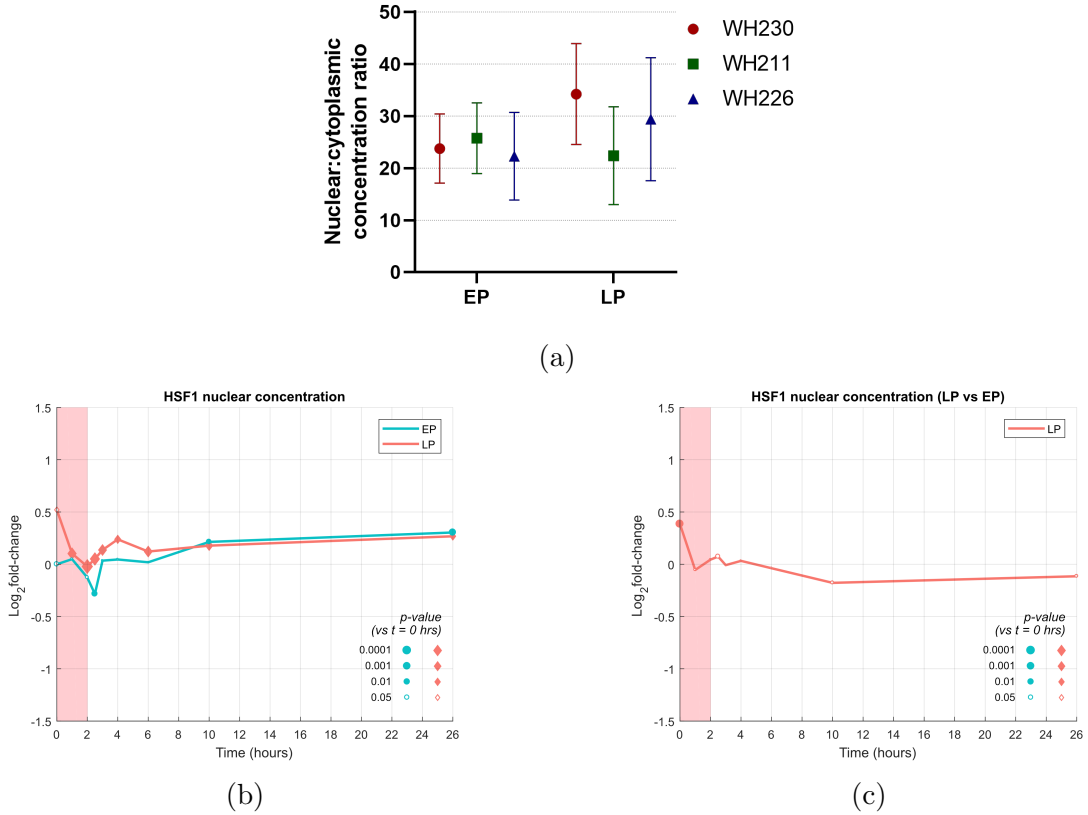

Figure 5.2: Immunofluorescence microscopy data tracking HSF1 protein concentration dynamics in early- (EP, blue) and late-passage (LP, red) populations ($n = 3$ donors). Populations are kept at 42°C from t = 0 hrs to t = 2 hrs and then kept at 37°C from t = 2 hrs to t = 26 hrs. Data is fit to a linear model assessing time point effects for each passage (5.2b); or passage effects for each time point (5.2c). (5.2a) Pre-stress ratio of nuclear-to-cytoplasmic mean HSF1 antibody fluorescence intensity per pixel. (5.2b/5.2c) Mean/Change in mean antibody fluorescence intensity per nuclear pixel. p-values are the statistical significance in linear model effect sizes (see Section 2.17). Marker sizes are proportional to the confidence of a significant change from the 0 hrs time point (5.2b); or from EP (5.2c) with filled markers representing significant changes at the 5% confidence level.

5.1.2 CHIP

Results in Chapters 3 and 4 have given strong evidence that a majority of HSP70 regulation in the short-term (of the order of hours) stress response is carried out downstream of transcription. As discussed in Section 1.6.2, the E3 ubiquitin ligase CHIP (the protein product of the STUB1 gene) dynamically regulates the ubiquitination of HSP70 as a function of quantities of misfolded proteins within the cell. With Figure 4.23 supporting the hypothesis that transcription takes hours to begin to dominate HSP70 regulation in response to stress, CHIP concentrations in EP and LP cells were analysed to investigate whether a change in CHIP-mediated turnover could be the limiting factor in the senescent stress response alluded to in Section 4.5.

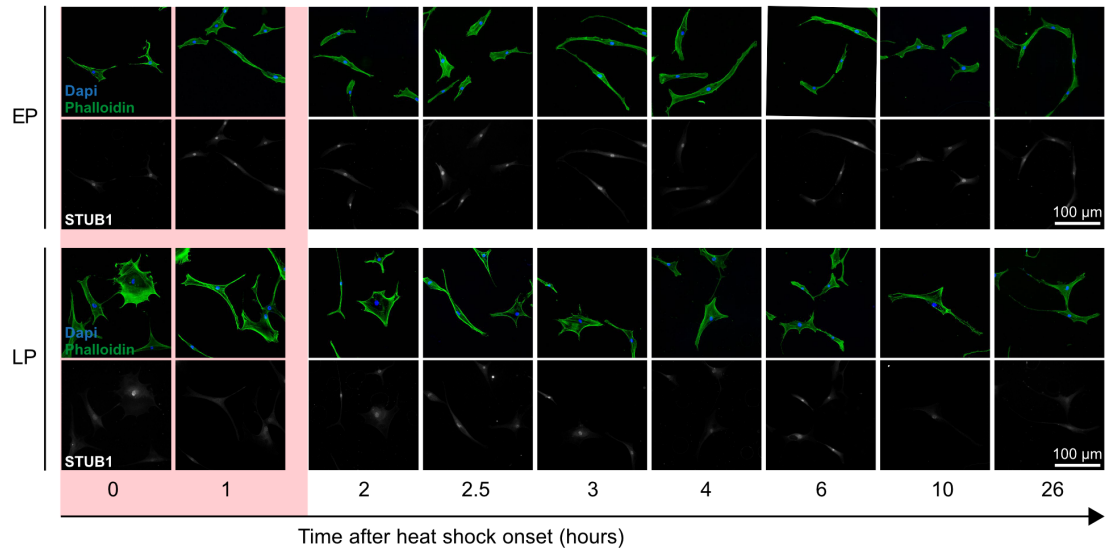

Figure 5.3: Representative images of CHIP antibody staining in early- and late-passage cells, with DAPI and phalloidin tags used to identify nuclear and cellular regions, respectively.

IF images of CHIP were taken at the same time points as in Section 5.1.1, under the same experimental conditions. Cellular CHIP also showed strong nuclear localisation in hBM-MSCs *in vitro*, but to a lesser extent than HSF1 (Figure 5.4a). Unlike HSF1, CHIP was also detected in hBM-MSCs by label-free mass spectrometry. Figure 5.4b shows the differences in CHIP levels at equilibrium between EP and LP cells. This was taken as an accurate reflection of changes to CHIP levels in LP cells and the difference between EP and LP CHIP levels pre-stress ($2^{-0.7799} = 0.5824$) was incorporated into the model.

In terms of dynamics, CHIP was unchanged at most time points in both EP and LP cells, and no consistent pattern was established. In EP cells, CHIP levels decreased significantly at the 6 hrs time point and in LP cells CHIP was significantly increased at the 3 hrs and 10 hrs time points, but was unchanged at all other time points in both cases. From these results it was concluded that no evidence supported the regulation of CHIP during heat shock, such that CHIP levels were also regarded as constant for the purposes of modelling.

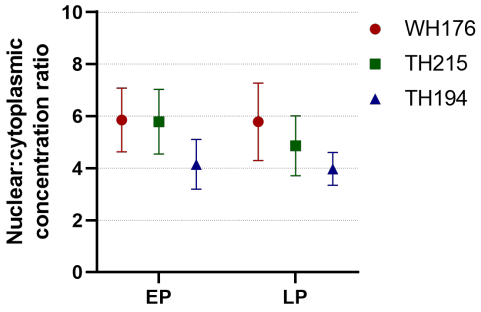

(a)

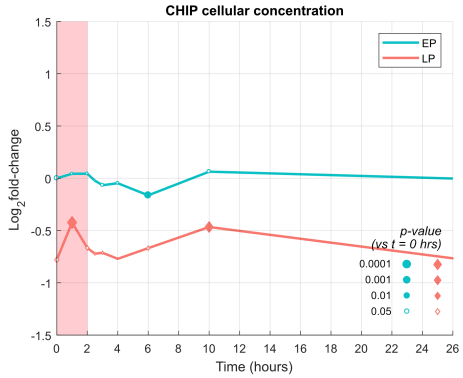

(b)

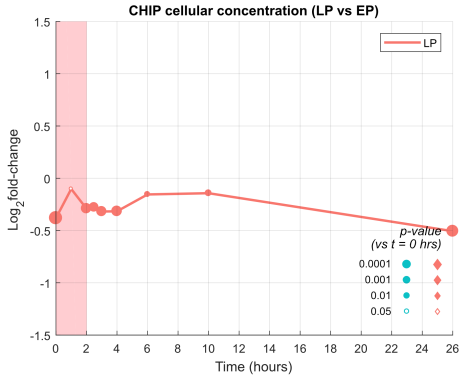

(c)

Figure 5.4: Immunofluorescence microscopy data tracking CHIP protein concentration dynamics in early- (EP, blue) and late-passage (LP, red) populations ($n = 3$ donors). Populations are kept at 42°C from t = 0 hrs to t = 2 hrs and then kept at 37°C from t = 2 hrs to t = 26 hrs. Data is fit to a linear model assessing time point effects for each passage (5.4b); or passage effects for each time point (5.4c). (5.4a) Pre-stress ratio of nuclear-to-cytoplasmic mean CHIP antibody fluorescence intensity per pixel. (5.4b/5.4c) Mean/Change in mean antibody fluorescence intensity per nuclear pixel. p-values are the statistical significance in linear model effect sizes (see Section 2.17). Marker sizes are proportional to the confidence of a significant change from the 0 hrs time point (5.4b); or from EP (5.4c) with filled markers representing significant changes at the 5% confidence level.

5.1.3 Ribosome

Following one of the main results from Chapter 4, namely that the limiting factor in the stress response of LP cells is downstream of chaperone transcription, this study sought to investigate chaperone translation. Studies of protein translation predominantly use *Saccharomyces cerevisiae* as a model organism due to its high ribosomal activity relative to human cells (Altmann & Linder, 2010). A lack of sample quantity has, for the most part (with the exception of Sabath et al., 2020, where a human cell line was used), restricted studies of protein translation in humans. In this particular case, a lack of ribosome-bound mRNA is exacerbated by the use of primary cells, cellular senescence, and global translation reduction in response to stress. Unfortunately these complications prevented a transcriptomic study of ribosome-bound mRNA. Instead, a relative quantification of the levels of ribosomal proteins via MS was used to gauge changes to protein translation in LP

cells. Rather than identifying the translation rates of specific proteins, this gives insight into how the maximal translational capacity changes due to senescence. 77 ribosomal proteins were detected and quantified across four matched donors. A significant decrease in representation was seen in LP populations (mean Log_2 fold-change -0.4873, $p < 0.0001$). In Figure 5.5, changes to the rest of the proteome have been underlayed for comparison - showing an apparent loss of translational capacity in LP cells. This was incorporated into the model as a change in the parameter k - representing the maximal rate of HSP70 synthesis - by a factor of $2^{-0.4873} = 0.7134$ in the simulations of LP cells.

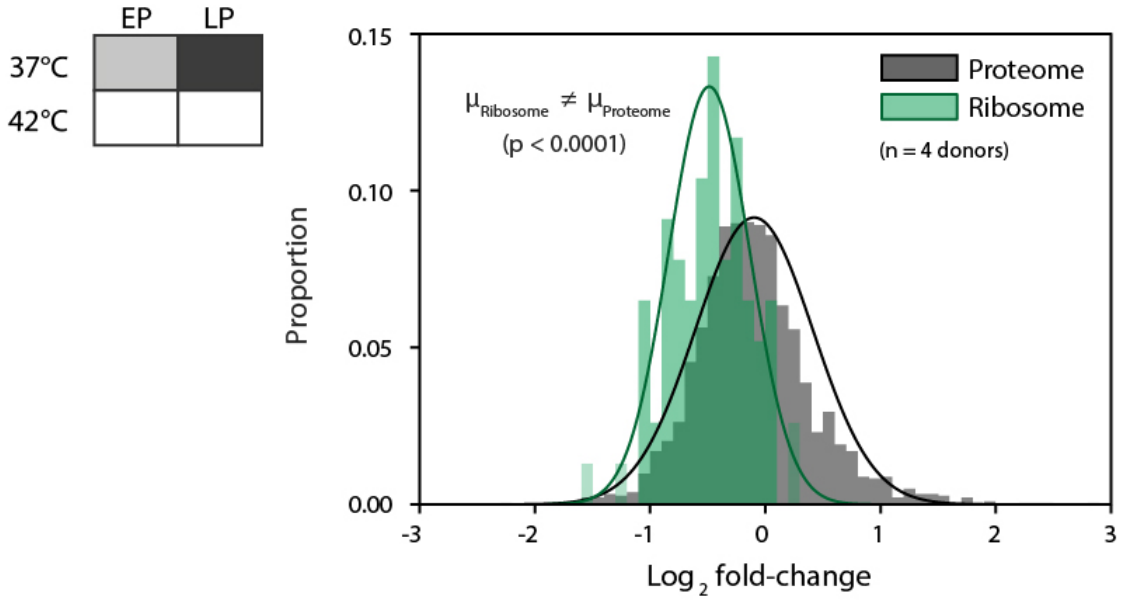

Figure 5.5: The Log_2 fold-changes of ribosomal proteins in mass spectrometry data in pre-stress late-passage (LP) cells compared to early-passage (EP). Data from the remainder of the proteomic dataset and fitted bell curves are also plotted for comparison. Significance is determined using a two-tailed, unpaired t-test.

5.2 Parameter constraints

Constraints were applied to the model based on experimental results and literature findings. The mean MS signal ratio between HSP70 (16 detected peptides) and CHIP (three detected peptides) across the four EP, pre-stress biological replicates: 3.10 (Figure 5.6), was used as the ratio of concentrations between HSP70 and CHIP at equilibrium. Practically, this was done by adjusting CHIP levels based on HSP70 at every time point until a stable equilibrium is reached. In agreement with previous findings (Jarnuczak et al., 2018; see Figure 4.23), the synthesis time of HSP70 from active HSF1 is drawn from a uniform distribution between one and three hours, $\tau \sim U[60, 180]$. For simplicity, it was assumed that there would be no substantial difference between the binding affinity of HSP70 to HSF1 or client proteins, such that $k_2 \approx k_3$. The turnover time for a protein via the proteasome was assumed to be linearly proportional to its length in amino acids. To incorporate this, the ratio of amino acid lengths between HSP70 and the median value of the human proteome

(Brocchieri, 2005) was used to reflect a difference in the time taken for turnover following ubiquitination, $\frac{k_6}{k_4} = \frac{641}{375}$.

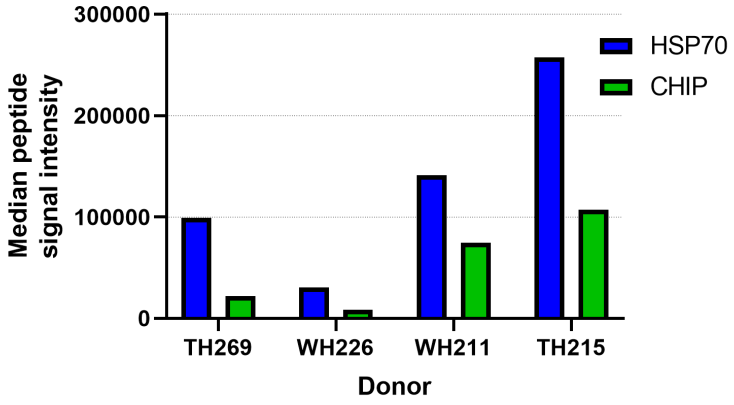

Figure 5.6: HSP70 and CHIP protein signal intensities quantified by mass spectrometry across four human donors in pre-stress early-passage samples.

5.3 Parameter optimisation

The seven remaining degrees of freedom – $k, K_d, k_2, k_4, k_5, k_7, \lambda$ – were optimised for the smallest sum-of-squared-errors (SSE) between HSP70 EP in vitro and HSP70 in silico results. A lower bound of 10^{-4} was set for the possible values of each parameter to ensure each reaction was represented within the model. The λ value used by Sivéry et al., 2016 was chosen as an initial condition, while several orders of magnitude were trialled for each remaining variable to obtain initial conditions for the optimisation, which was carried out using the built-in MATLAB function `fminsearch`. To demonstrate the seven-dimensional optimisation process whilst sparing the reader from an unwieldy amount of graphs, the mesh plots in Figure 5.7 illustrate the SSE minima found compared to several orders of magnitude for each parameter.

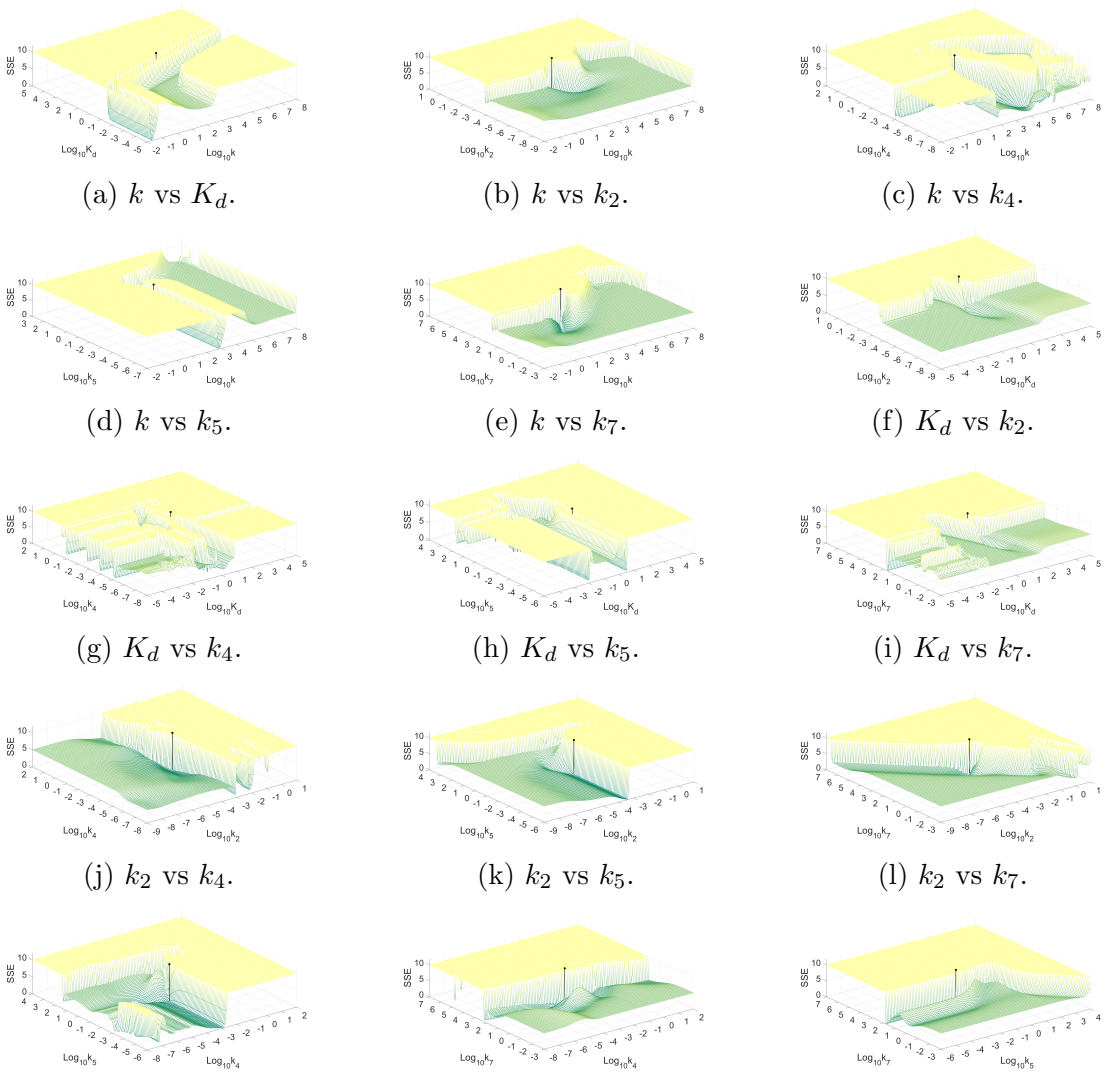

(a) k vs K_d. (b) k vs k_2. (c) k vs k_4.

(d) k vs k_5. (e) k vs k_7. (f) K_d vs k_2.

(g) K_d vs k_4. (h) K_d vs k_5. (i) K_d vs k_7.

(j) k_2 vs k_4. (k) k_2 vs k_5. (l) k_2 vs k_7.

(m) k_4 vs k_5. (n) k_4 vs k_7. (o) k_5 vs k_7.

Figure 5.7: Demonstration of the optimisation of free model parameters. The model of the stress response is simulated over a range of parameter values, and the sum of squared errors (SSE) compared to immunofluorescence microscopy *in vitro* data at each parameter value is collected. The parameter values chosen by optimisation are overlaid in black over the SSE values across several orders of magnitude.

5.4 Parameter modification for senescent cells

Two modifications to the system were made to reflect changes in senescent cells. The maximum transcription rate, k, of HSP70 was changed by a factor of 0.7134 in accordance with the observed mean change of ribosomal proteins in LP cells from MS results. In LP cells, levels of CHIP were significantly lower in MS data and all but one of the time points in IF microscopy time points. For the most accurate change in CHIP in LP cells, the change seen before heat shock in microscopy data was used, and multiplied CHIP by a factor of 0.5824. Table 5.1 gives a summary of all set variables within the model.

Parameter	Description	Value	Unit
k	Maximal HSP70 transcription rate	6.4294×10^2	$[min^{-1}]$
	(Modified value in late-passage cells)	4.5865×10^2	$[min^{-1}]$
n	Hill coefficient	3	[ ]
K_d	HSE · HSF dissociation constant	3.0534	$[\mu M]$
k_2	HSF1 · HSP70 binding rate	3.9827×10^{-4}	$[\mu M^{-1} min^{-1}]$
k_3	HSP70 · MFP binding rate	3.9827×10^{-4}	$[\mu M^{-1} min^{-1}]$
k_4	CHIP-mediated HSP70 turnover rate	1.240×10^{-3}	$[\mu M^{-1} min^{-1}]$
k_5	HSP70-mediated MFP refolding rate	5.0199×10^{-2}	$[min^{-1}]$
k_6	CHIP-mediated MFP turnover rate	2.120×10^{-3}	$[\mu M^{-1} min^{-1}]$
k_7	Rate of protein misfolding at 37°C	69.1068	$[\mu M min^{-1}]$
λ	Rate of protein misfolding at 42°C	4.2651×10^2	[ ]
t	Simulation time elapsed		$[min]$
τ	HSF1 activation/HSP70 synthesis delay	$\sim U[60, 180]$	$[min]$

Table 5.1: Optimised and approximated parameters for the ODE/DDE mathematical model of the heat shock response.

Using these parameters and arbitrarily chosen initial population concentrations relative to $[HSF1 \cdot HSP70] = 0.1\,\mu M$, *in silico* simulations were ran for sufficient time for the protein populations to settle to their steady state equilibrium, with the population concentrations detailed in Table 5.2. Figure 5.8 shows that each of the six population levels quickly deviates from its initial condition, before plateauing towards its predicted steady state concentration.

Population	Steady state concentration	Unit
Active $HSF1$	0.0998	$[\mu M]$
Total $HSP70$	300.2218	$[\mu M]$
$CHIP$	96.8457	$[\mu M]$
MFP	9708.1108	$[\mu M]$
$HSF1 \cdot HSP70$	0.0002	$[\mu M]$
$HSP70 \cdot MFP$	281.1222	$[\mu M]$

Table 5.2: *In silico* 37°C steady state concentrations.

As demonstrated by in Figure 5.8, the model converges to a steady state whereby the concentration of cellular HSP70 (blue) far outweighs HSF1 (black), roughly 500:1. This is in agreement with the mass spectrometry data introduced in Chapter 3, where 22 HSP70 peptides have been identified, whereas HSF1 did not meet the criteria for detection via mass spectrometry - suggesting a large difference in abundance between the two. Furthermore, a comparable ratio ($\sim$ 1000:1) was found in the model by Sivéry et al., 2016.

Figure 5.8 shows the model predicts a concentration of misfolded proteins (MFP, red) higher than HSP70. Combined with the low abundance of HSF1, this implies that HSP70-HSF1 binding is transient and surprisingly rare, with $\sim$ 90% of HSP70 bound to client proteins. This ratio is not in agreement with the model by Sivéry et al., 2016, wherein HSP:MFP was predicted to be $\approx$ 24:1 with $\sim$ 4% of HSP70 bound to client proteins at equilibrium. An intuitive explanation of this discrepancy is that the model by Sivéry et al., 2016 does not account for CHIP-mediated misfolded protein ubiquitination, considerably increasing the amount of HSP70 needed to chaperone an equal number of misfolded proteins. Misfolded proteins outnumbering cellular HSP70 would be a surprising result, however it should also be noted that due to the omission of co-chaperones and supporting chaperone systems in this model, the workload of HSP70 will be over-exaggerated.

Finally, Figure 5.8 demonstrates the model prediction that a vast majority of cellular HSF1 is in its active form (active HSF1, solid black versus HSF1-bound HSP70, dash-dotted blue). This is also supported by experimental findings. Immunofluorescence data in Figure 5.1 showed that HSF1 is almost entirely nuclear in hMSCs, in contrast to HSP70 in Figure 4.19. This suggests that almost the entireity of HSF1 may be transcriptionally active at equilibrium conditions in hMSCs *in vitro*.

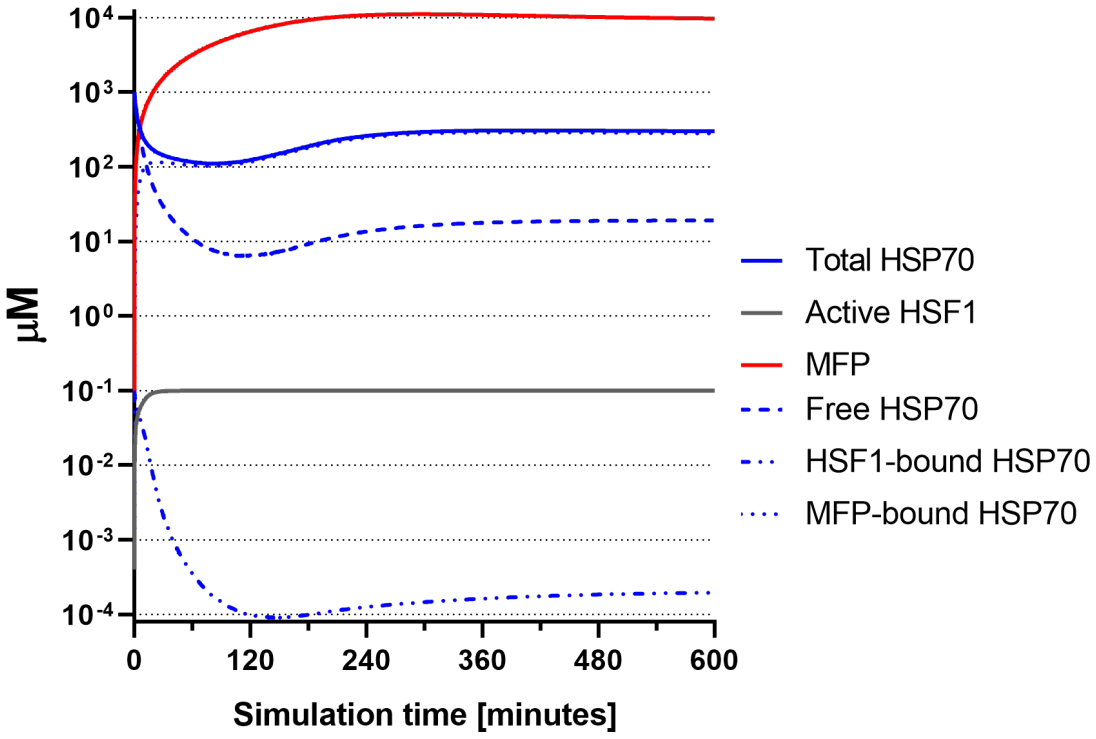

Figure 5.8: *In silico* convergence of populations within the heat shock response to a stable equilibrium given by the concentrations in Table 5.2 at 37°C. Arbitrary initial concentrations are chosen relative to 0.1 µM HSF1, and the model is simulated for sufficient time such that a stable equilibrium is reached.

5.5 A descriptive model of the ageing stress response

Using the parameters in Table 5.1, a two hour heat shock was simulated and the changes to the population concentrations from Table 5.2 were recorded. Figure 5.9 shows the dynamics of *in silico* HSP70 in both EP and LP cells with *in vitro* results overlaid. As we would expect, the simulation results closely follow EP IF data, as the model has been optimised against this dataset. HSP70 protein levels begin to increase immediately following heat stress, and continue to increase following a return to 37°C. Peak HSP70 levels are reached between the 4 hrs and 10 hrs time points - specifically a Log_2 fold-change from equilibrium of 1.2653 occurring 7 hours and 29 minutes following the onset of stress - following which HSP70 levels return toward pre-stress equilibrium. This demonstrates the functional accuracy of the model design. It is noteworthy, but not surprising, that the main source of error in the model is its inability to fit to the 26 hrs post-stress time point. While the prolonged up-regulation of HSP70 following stress has been previously shown (as reviewed by Park et al., 2005), it remains for a mechanism to be found that comprehensively explains this phenomenon. As a result it is not a feature the model is able to replicate, with HSP70 dynamics instead resembling a damped oscillator about the pre-stress equilibrium.

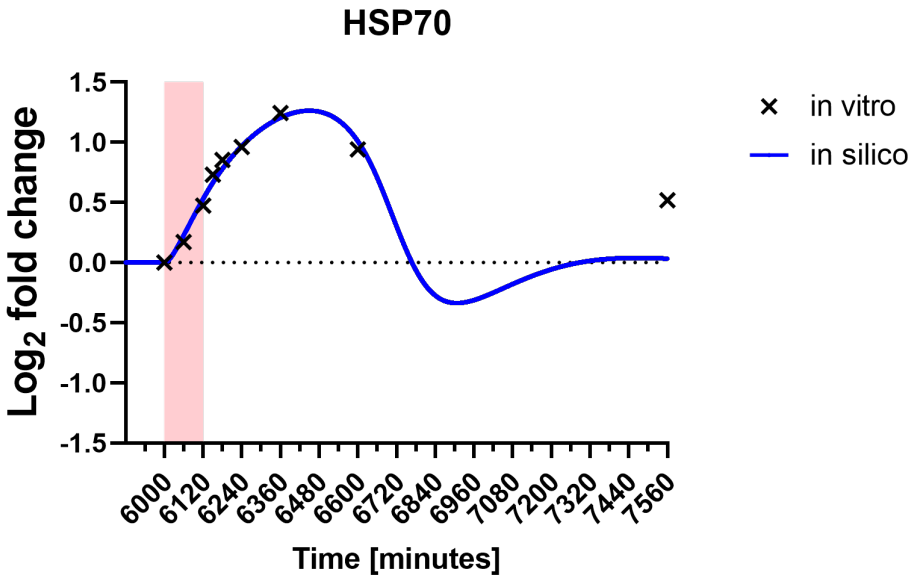

(a)

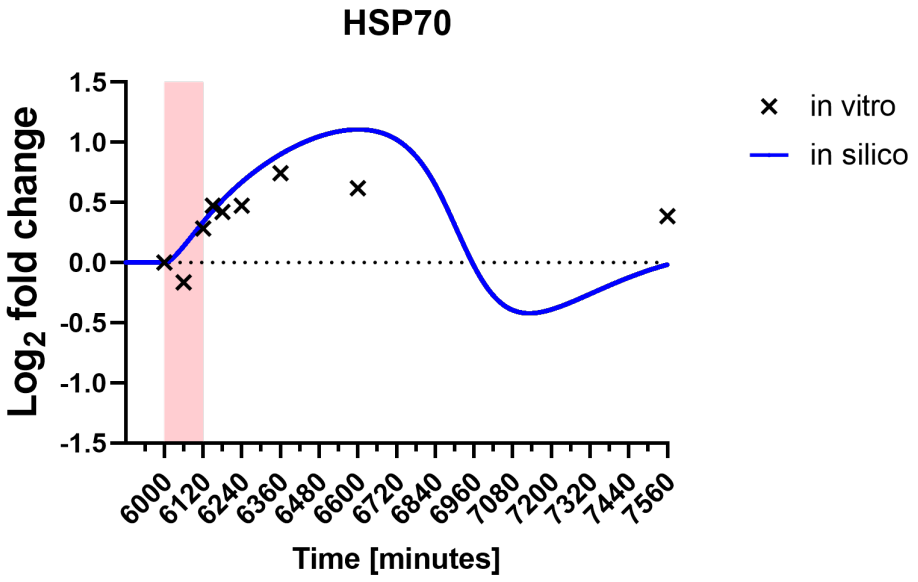

(b)

Figure 5.9: ODE/DDE model simulation of HSP70 levels in response to stress. *In silico* models of early- (5.9a) and late-passage (5.9b) cells are allowed to reach a stable equilibrium, before a proteotoxic stress is simulated by increasing the rate at which misfolded proteins are generated within the model for 120 minutes. At each time interval, the *in silico* concentration of HSP70 is recorded, with *in vitro* HSPA1A protein data from IF microscopy overlaid.

In Figure 5.9b, simulation of the model was repeated with the adjustments made factoring in differences seen in LP cells experimentally. While an objectively poorer fit is seen compared to Figure 5.9a, several *in vitro* findings are replicated by the model. Both the rate at which HSP70 increases (as plotted in Figure 5.10) and peak HSP70 levels are diminished in LP simulations, with the latter falling to a Log_2 fold-change of 1.1073, occurring 10 hours and 1 minute after the onset of stress.

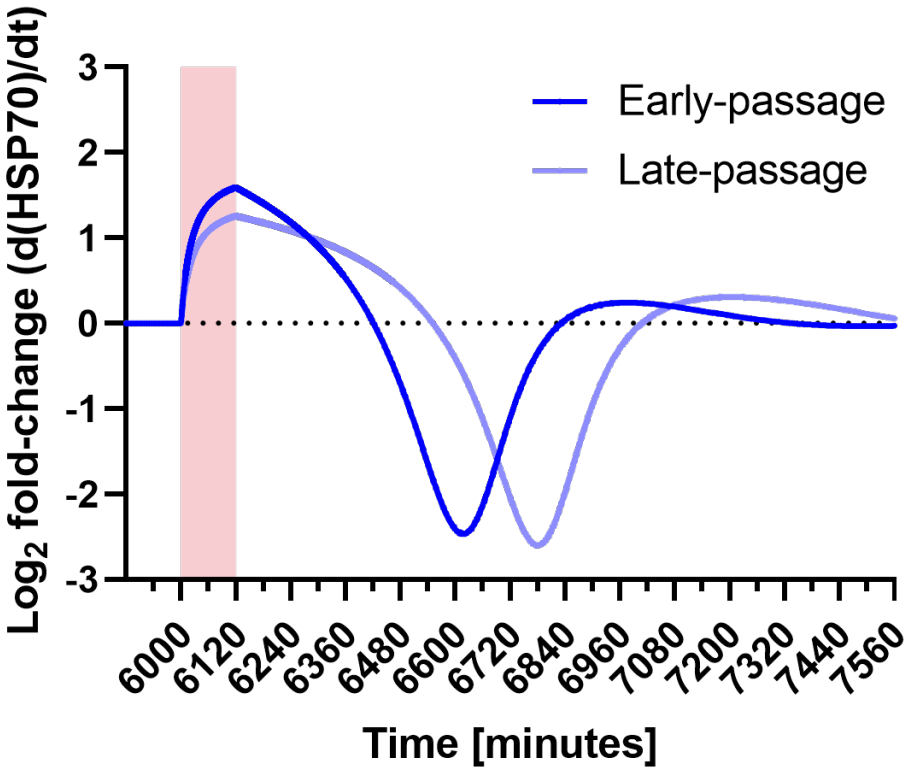

Figure 5.10: ODE/DDE model simulation of the rate of change of HSP70 levels in response to stress. *In silico* models of early- and late-passage cells are allowed to reach a stable equilibrium, before a proteotoxic stress is simulated by increasing the rate at which misfolded proteins are generated within the model for 120 minutes.

Judgement of the accuracy of the model is not limited to comparisons with *in vitro* HSP70 protein. If the model is accurately describing HSF1 activation dynamics, we would expect these to closely follow the dynamics of HSP70 mRNA, with an associated scale factor. Figure 5.11 shows the dynamics of *in silico* active HSF1 for EP and LP cells with the *in vitro* data for HSP70 mRNA overlaid with an adjusted scale. In EP cells, *in silico* active HSF1 and *in vitro* HSP70 mRNA dynamics are comparable with a scale factor of ~ 1500. Active HSF1 immediately rises at the onset of stress and quickly plateaus after approximately one hour. Active HSF1 levels then gradually decrease and, like *in vitro* HSP70 mRNA, levels drop below that of the pre-stress equilibrium at the 10 hrs time point before returning to equilibrium. To facilitate comparison between EP and LP, the same scale factor is used for LP cells. Here, active HSF1 reaches the same plateau as in EP simulations, and a drop

below pre-stress levels before returning to equilibrium is again observed. The time taken to return to equilibrium active HSF1 levels following the onset however, is 11 hours and 37 minutes in LP simulations as opposed to 9 hours and 9 minutes in EP simulations.

The most striking feature of the *in silico* data in Figure 5.11 is the pronounced decrease in transcriptionally active [free] HSF1 between the 10 hrs and 26 hrs time points. It should be considered that this may be a sign of over-fitting of the model to the experimental data available, with this large change in dynamics occurring in a region with scarce experimental data. The time-series experiments such as those shown in Figure 5.11 were designed with the hypothesis that a majority of chaperone regulation would occur immediately following culture temperature changes. To capture this regulation, logarithmically spaced time points were chosen, with significant regulation more than 10 hours post stress initially seeming unlikely. On the other hand, this time interval coincides with a decrease in HSP70 protein from peak values following stress (Figure 5.9), and a continual decrease in HSP70 mRNA from peak values following stress (Figure 5.11). Thus it is not counter-intuitive that HSP70 mRNA levels may continue to decrease further - as is predicted by the model - as cells down-regulate HSP70 following stress and return towards pre-stress concentrations. Biologically, this could be explained by an over-correction following the resolution of proteotoxic stress, whereby newly-surplus HSP70 is free to bind to the majority of HSF1, dramatically reducing HSP70 transcription.

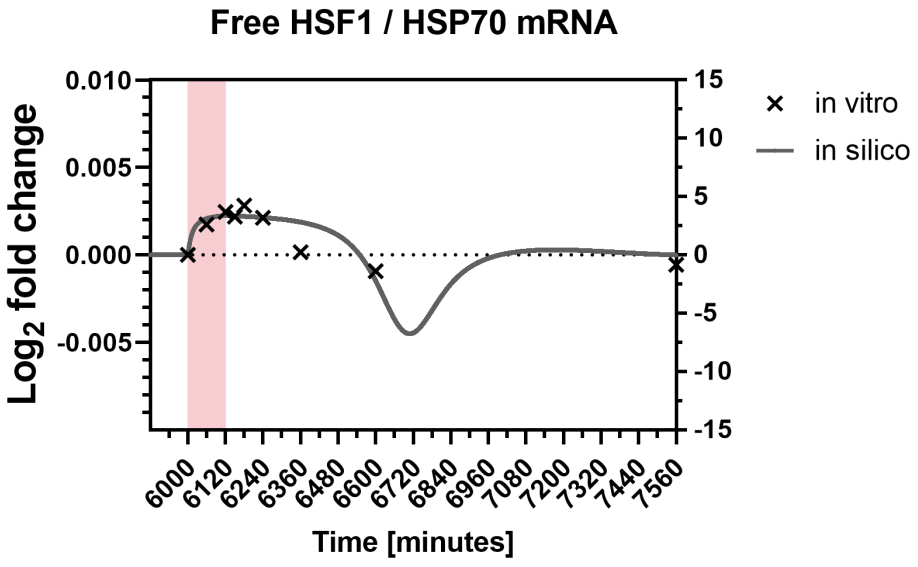

(a)

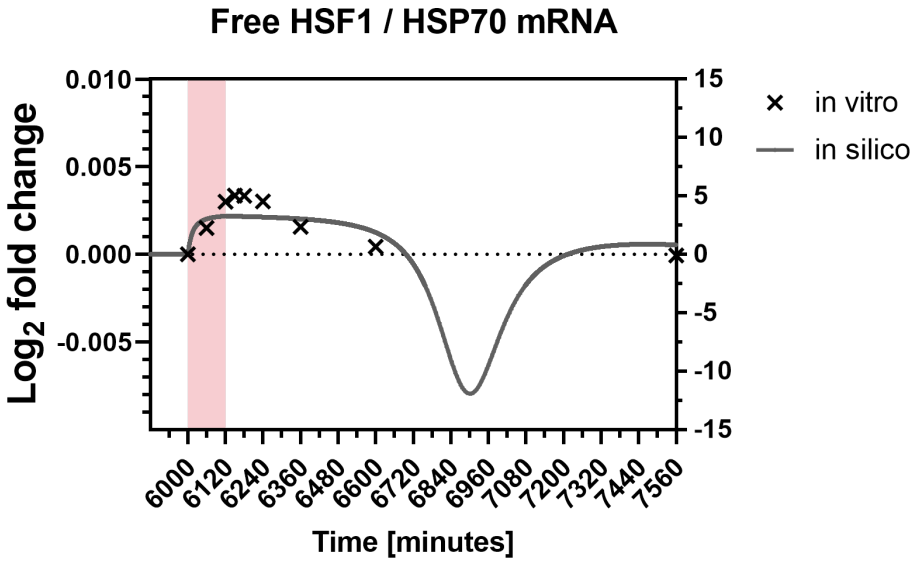

(b)

Figure 5.11: ODE/DDE model simulation of active HSF1 levels in response to stress. *In silico* models of early- (5.11a) and late-passage (5.11b) cells are allowed to reach a stable equilibrium, before a proteotoxic stress is simulated by increasing the rate at which misfolded proteins are generated within the model for 120 minutes. At each time interval, the *in silico* concentration of HSF1 is recorded (left axes), with *in vitro* HSPA1A mRNA data from RT-qPCR overlaid (right axes).

5.6 A predictive model of the ageing stress response

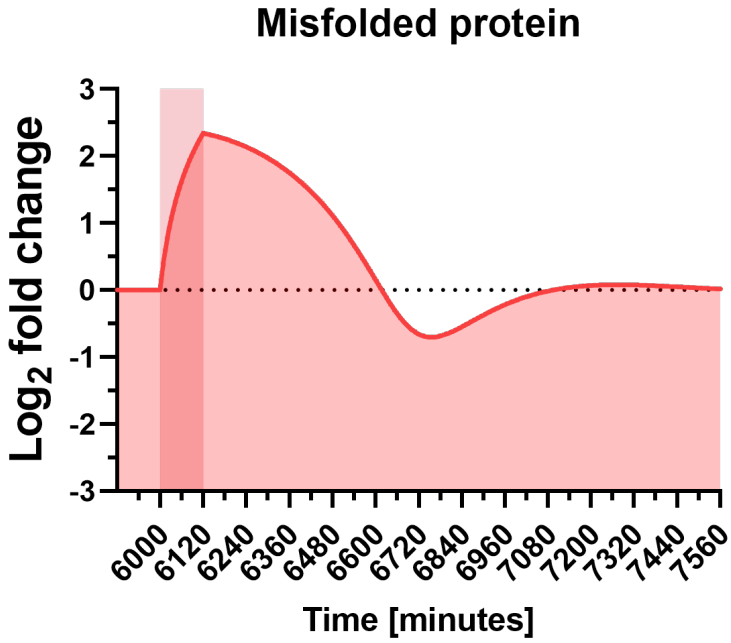

(a)

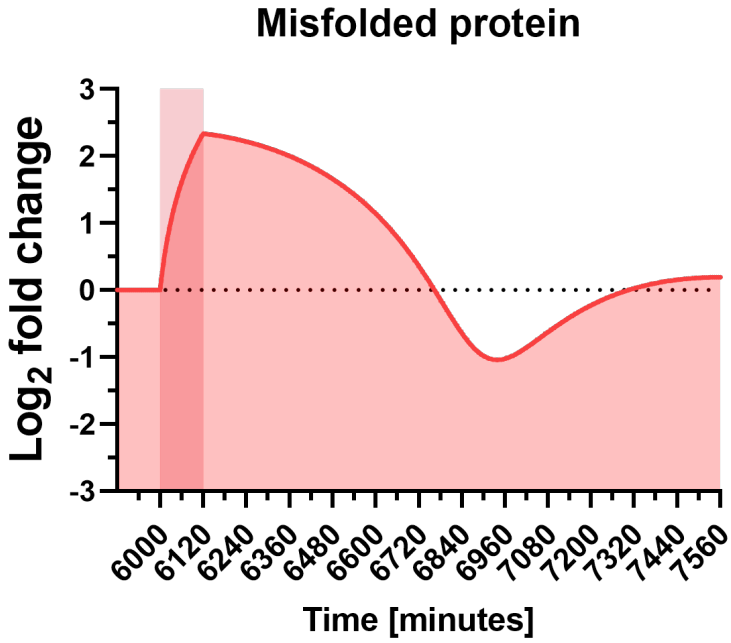

(b)

Figure 5.12: ODE/DDE model simulation of misfolded protein levels in response to stress. *In silico* models of early- (5.12a) and late-passage (5.12b) cells are allowed to reach a stable equilibrium, before a proteotoxic stress is simulated by increasing the rate at which misfolded proteins are generated within the model for 120 minutes.

With the accuracy of the model validated, it was next utilised to investigate properties of the stress response which are difficult to probe experimentally. Figure 5.12 plots the levels of misfolded protein in the EP and LP simulations. While there is little difference in the peak MFP Log_2 fold-changes between EP and LP cells (2.3406 in EP as opposed to 2.3362 in LP), the time taken for misfolded protein concentration to return to pre-stress levels is much more pronounced (10 hours and 17 minutes in EP as opposed to 12 hours and 44 minutes in LP). Figure 5.13 shows the absement of MFP from equilibrium, calculated from the areas under the plots in Figure 5.12 from the onset of stress until MFP returns to baseline levels, and thus gives a measure of how much MFP is induced due to stress and for how long. The Log_2 fold-change in misfolded protein absement from equilibrium was 0.3654 from EP and LP, therefore the model demonstrates that, in early- and LP cells exposed to an equally acute proteotoxic stress, the amount of misfolded protein accumulated will be greater in LP cells.

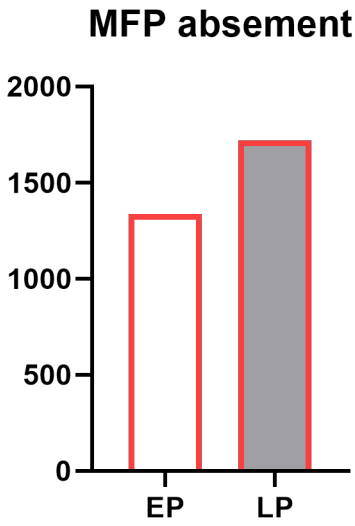

Figure 5.13: Absement of misfolded protein levels from equilibrium in simulations of the stress response in early- (EP) and late-passage (LP) cells. Calculated by taking the area-under-curve of MFP versus time dynamics, demonstrated in Figure 5.12 by the shaded region above baseline MFP level.

5.6.1 Reaction rates

Figure 5.14 depicts the *in silico* reaction rates that lead the model to replicate *in vitro* HSP70 protein dynamics. These graphs suggest that the majority of HSP70 regulation during stress is post-translational. While this would be a surprising result, it is not counter-intuitive given the high abundance of cellular HSPs. Both Beck et al., 2011 and Schwanhäusser et al., 2011 find HSPs among the most abundant proteins in mammalian cells. Increasing the quantity of HSP70 by the Log_2 fold change of 1.244 seen in Figure 4.22c via new protein translation would therefore require an immense diversion of energy and resources. Far more likely, as evidenced here, is that HSP70 up-regulation is achieved, for the most part, through an increase in its stability.

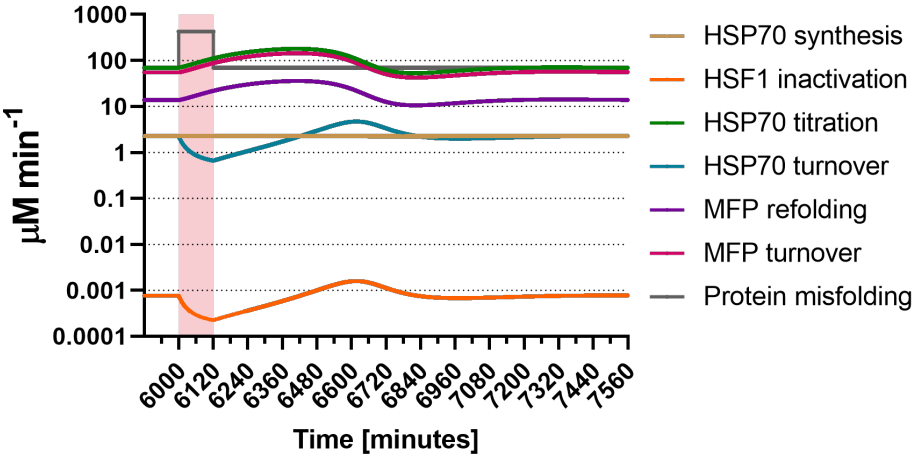

(a)

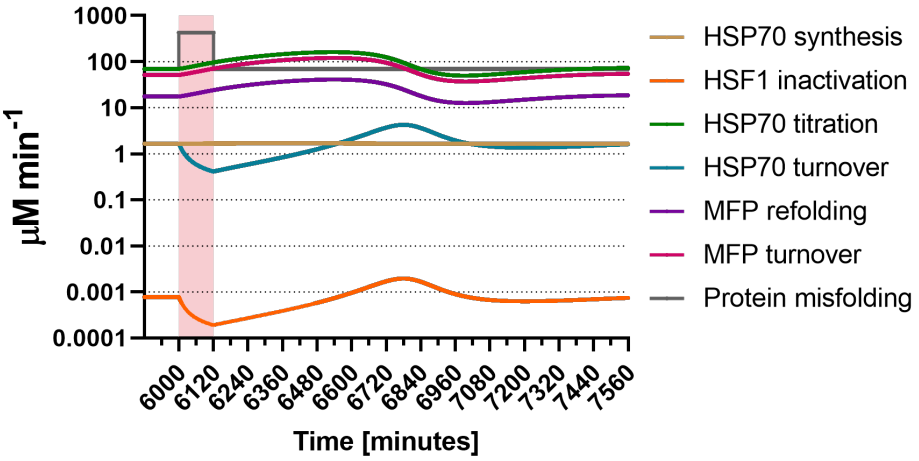

(b)

Figure 5.14: ODE/DDE model simulation of the rates of the reactions outlined in Table 2.8 in response to stress. *In silico* models of early- (5.14a) and late-passage (5.14b) cells are allowed to reach a stable equilibrium, before a proteotoxic stress is simulated by increasing the rate at which misfolded proteins are generated within the model for 120 minutes. At each time interval, the *in silico* rate of each reaction included in the model is recorded.

Similar results have been seen in human and mouse cell lines by Mao et al., 2013, who have shown an additional mechanism of HSP70 regulation beyond the desired complexity of this model. It was shown that the ATP-ase OLA1 is also capable of binding to the C-terminus of HSP70 and thus prevents CHIP-mediated HSP70 ubiquitination. To investigate the influence OLA1 has over HSP70 regulation, knockouts and knockdowns were performed in MEFs and the human breast cancer cell line MDA-MB-231 cells (respectively). In the human cell line, OLA1 knockdown cells experienced an $\sim$ 50% loss of HSP70, and a $\sim$ 67% loss of HSP70 induction during stress; while in the murine OLA1 knockout cell line these values were $\sim$ 80% and $\sim$ 67% respectively. In OLA1 knockout MEFs the stability of HSP70 following translation-blocking cycloheximide treatment was reduced from 69 minutes to 29

minutes, while in the human cell line the HSP70 half-life was reduced from 99 minutes to 58 minutes. In Figure 5.15, a remarkably similar half-life (100 minutes) of *in silico* HSP70 has been found in the present study by switching the rate of HSP70 synthesis to zero.

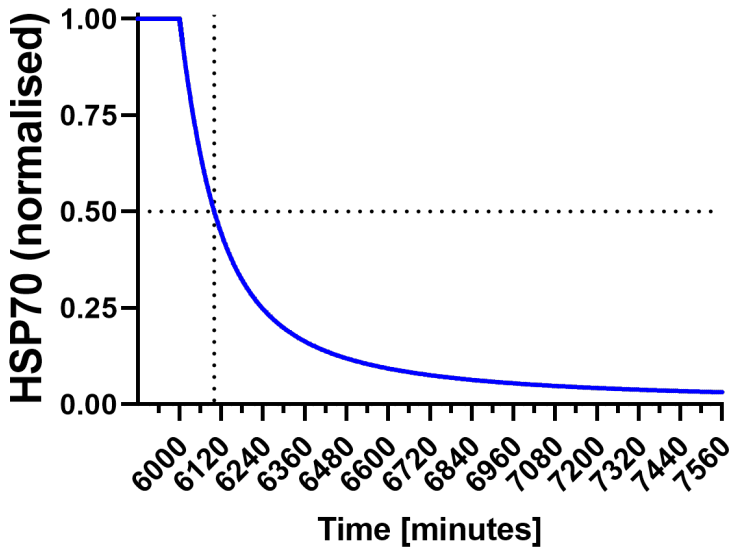

Figure 5.15: The half-life of *in silico* HSP70, 100 minutes, calculated by removing HSP70 synthesis from the model at equilibrium.

Regarding the triage of misfolded proteins, the ratio of degradation to refolding rates in Figure 5.14a is $\sim$ 4:1, and remains constant throughout stress. While Sivéry et al., 2016 places this ratio similarly, at 5:1, experimental evidence is lacking. It is likely that, with co-chaperones present as a finite resource in the cell, increasing amounts of HSP70-bound misfolded protein would trigger a transition from MFP refolding to MFP turnover and increase this ratio during stress.

5.6.2 Impact on the stress response of varying parameters

By varying each reaction rate in Table 2.8 independently, we can analyse the sensitivity of the response to each process, and hypothesise further processes which may be attenuated in senescent cells.

Intuitively, increasing the rate of HSP70 synthesis decreases MFP levels at equilibrium. Figure 5.16a demonstrates the effect of reduced HSP70 synthesis rates in the simulation of LP cells, attributed to underrepresented ribosomal proteins - with the response becoming both slower and smaller in magnitude. Modifying the rate at which HSP70 binds to misfolded proteins produces the same result (Figure 5.16b). This is expected, as more available HSP70 will also increase the rate of MFP binding.

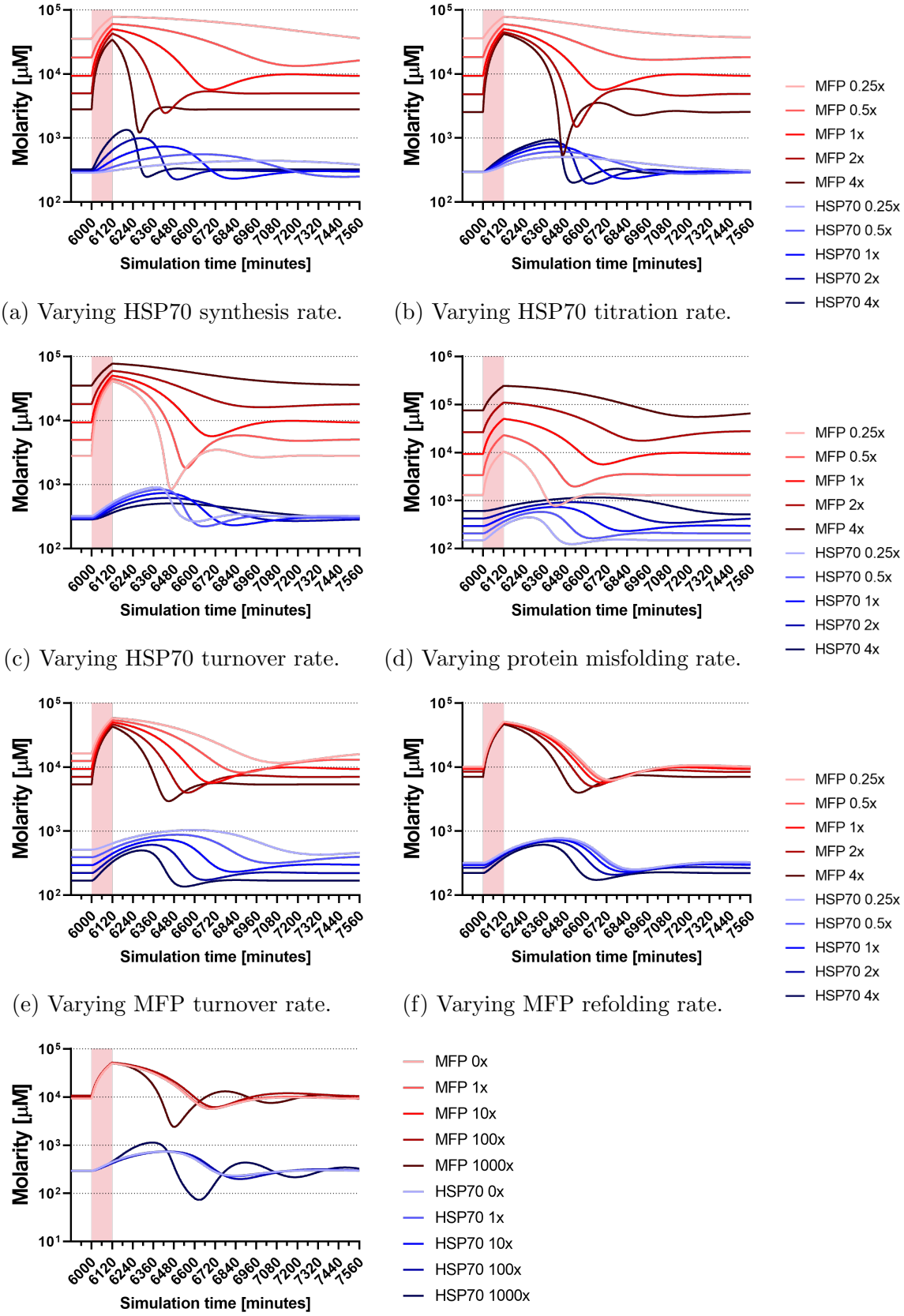

(a) Varying HSP70 synthesis rate.

(b) Varying HSP70 titration rate.

(c) Varying HSP70 turnover rate.

(d) Varying protein misfolding rate.

(e) Varying MFP turnover rate.

(f) Varying MFP refolding rate.

(g) Varying HSF1 inactivation rate.

Figure 5.16: Changes to misfolded protein (MFP) and HSP70 dynamics in response to modifying individual reaction rates from Table 2.8 across several values (e.g. '2x' indicates the corresponding reaction rate has been doubled).

Also intuitively, the concentration of misfolded proteins at equilibrium increases with increasing rates of HSP70 turnover (Figure 5.16c); and the time taken to return to equilibrium following stress also increases. This demonstrates the effect HSP70-stabilising agents such as OLA1 have on the stress response: suppressing HSP70 ubiquitination reduces the concentration of misfolded proteins at equilibrium and improves the efficacy of the stress response. In Figure 5.16f, increasing the protein misfolding rate has a similar effect on the dynamics of misfolded proteins. Interestingly, while varying the protein misfolding rate changes the steady-state HSP70 level accordingly, no effect on the steady-state of HSP70 was seen when varying the HSP70 turnover rate.

Reduced rates of MFP turnover demonstrate the behaviour of models which neglect to include post-translational regulatory mechanisms, with the up-regulation of HSP70 becoming much broader, and slower to return to equilibrium (Figure 5.16e). Conversely, increased rates of MFP turnover demonstrate how CHIP-HSP70/MFP binding is beneficial to the cell, reducing the concentration of misfolded proteins at equilibrium; reducing the amount of HSP70 needed to maintain proteostasis at equilibrium; and improving the efficacy of the stress response. A higher refolding rate (Figure 5.16d) has the same effect, and would correspond to increased availability of cellular ATP and co-chaperones to switch the HSP70 chaperone function from a holdase to a foldase.

Due to the relatively low concentration of HSF1 in the system, the rate of HSF1 inactivation (through binding to HSP70) is the least sensitive to change. Indeed, removing HSF1-HSP70 binding from the system altogether has markedly little effect on HSP70 or MFP dynamics. Fascinatingly, Figure 5.16g highlights that the rate of HSF1-HSP70 binding which best fits *in vitro* data is actually detrimental to the stress response compared with both lower and higher rates. A higher affinity for HSF1-HSP70 binding *in silico* causes the system to behave as an underdamped harmonic oscillator, with a majority of HSF1 repeatedly switching between its active and bound state. *In vitro*, several damping mechanisms exist (translocation time, monomerisation/trimerisation time, HSF1 post-translational modifications etc.) which increase the feasibility of a higher HSF1-HSP70 binding rate than predicted here.

The modifications in Figure 5.16 which cause HSP70 dynamics to more closely resemble LP *in vitro* results (see Figure 4.22c) are the attenuation of HSP70 synthesis, HSP70-MFP binding, HSP70-mediated protein refolding, and CHIP-mediated MFP turnover; a loss of HSP70 stability; and increased rates of protein misfolding. Thus the model predicts these changes to occur in senescent cells. Notably, *in silico* each of these modifications leads to an increased build-up of misfolded proteins.

5.7 Monobromobimane-labelling mass spectrometry

The ODE/DDE model of the stress response predicted that the perturbation of proteostasis due to stress is greater in LP cells than their EP counterparts (Figure 5.12. This was tested using mass spectrometry in conjunction with monobromobimane (mBBr) protein labelling. As utilised by Swift et al., 2013 and Gilbert et al., 2019, mBBr selectively labels reduced cysteine residues (see Figure 2.6) which are typically exposed in conformationally compromised proteins (Johnson et al., 2007). As such, an increase or decrease in mBBr-labelling from a stable state is an indicator of protein misfolding or aggregation, respectively.

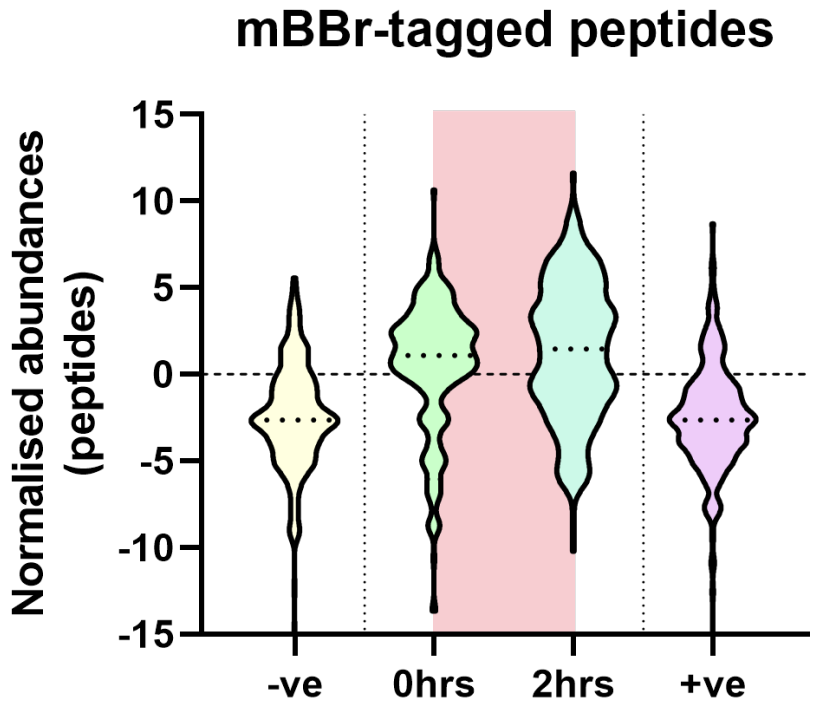

Figure 5.17: The abundances of monobromobimane (mBBr)-tagged peptides in mass spectrometry data pre-stress, immediately post-stress, as well as positive and negative controls. In the negative control, no mBBr has been applied, while in the positive control, mBBr is applied to a digested and reduced peptide sample. Dotted lines indicate sample medians.

mBBr-MS was carried out in EP and LP cells pre-stress, and immediately post-stress. Figure 5.17 also contains the results of an attempted positive control, whereby mBBr was applied to an already digested and reduced sample, such that all cysteines in the sample should be reduced and exposed to mBBr-binding. The benefit of the inclusion of a positive control is it provides a library of all possible labelling sites to improve the confidence of identifications. The results however, show little difference between the positive and negative controls. There are multiple possible reasons for

this, the first being a quenching of mBBr by the prior addition of the reducing agent, dithiothreitol (DTT). DTT has been shown to react with mBBr (Graham et al., 2003), and using the quantities outlined in Sections 2.27 and 2.34, this positive control sample contained $\sim 1.2 \times 10^{18}$ DTT molecules, and $\sim 1.8 \times 10^{14}$ mBBr molecules. In other words, this positive control sample contained $\sim$ 7000 non-peptide mBBr-binding sites per mBBr molecule. In comparison, even if the 50 µg peptide sample comprised of no amino acids other than reduced cysteines[1], this would still only amount to $\sim 2.5 \times 10^{17}$ mBBr binding sites. It is also possible that this quantity of mBBr added to samples halfway through the purification process was detrimental to sample quality. Figure 5.18 displays the ion intensity maps for the samples in Figure 5.17, which show the mass to charge ratios of ions over the course of a 90 minute run. The variation seen in Figure 5.18d, compared to the relatively homogeneous maps in Figures 5.18a, 5.18b, and 5.18c, illustrates the effect the addition of mBBr has on the sample. As a result, it was not possible to create the mBBr-labelling library desired for this experiment.

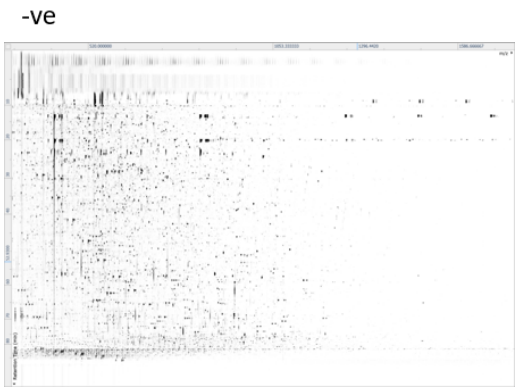

(a) Negative control.

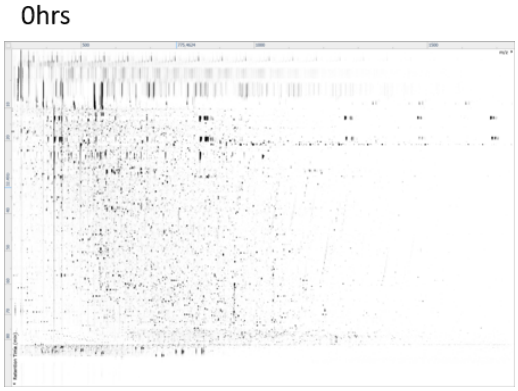

(b) Pre-stress.

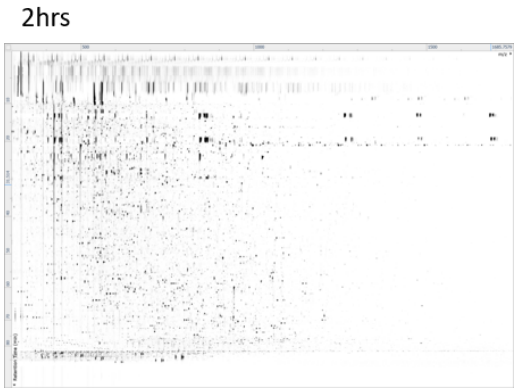

(c) Immediately post-stress.

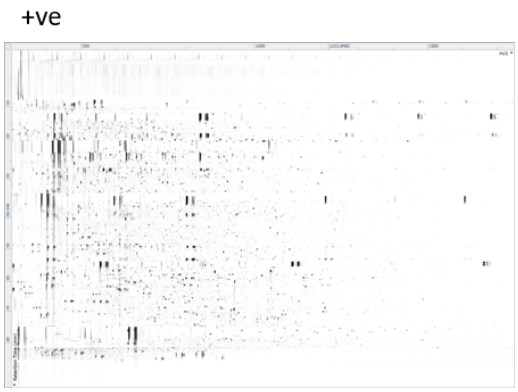

(d) Positive control.

Figure 5.18: Ion intensity maps from monobromobimane-labelling mass spectrometry samples in Figure 5.17, used to identify abnormality in samples from the same run. The x-axes show the mass to charge ratio of ions reaching the mass spectrometer detector, while the y-axes show the time each ion is detected across a 90 minute run. (5.18a) Negative control. (5.18b) Pre-stress. (5.18c) Immediately post-stress. (5.18d) Positive control.

[1]In fact, cystines have been found by Miseta and Csutora, 2000 to constitute roughly 2.3% of the mammalian proteome.

Figure 5.19 shows the data from 359 unique mBBr-labelled peptides from 252 proteins detected across four donors. Consistent with the *in silico* finding that proteostasis is increasingly perturbed by stress in LP cells, a significant change is seen in the mBBr-labelling profile of LP populations ($p < 0.0001$), compared with no significant change in EP populations ($p = 0.27$).

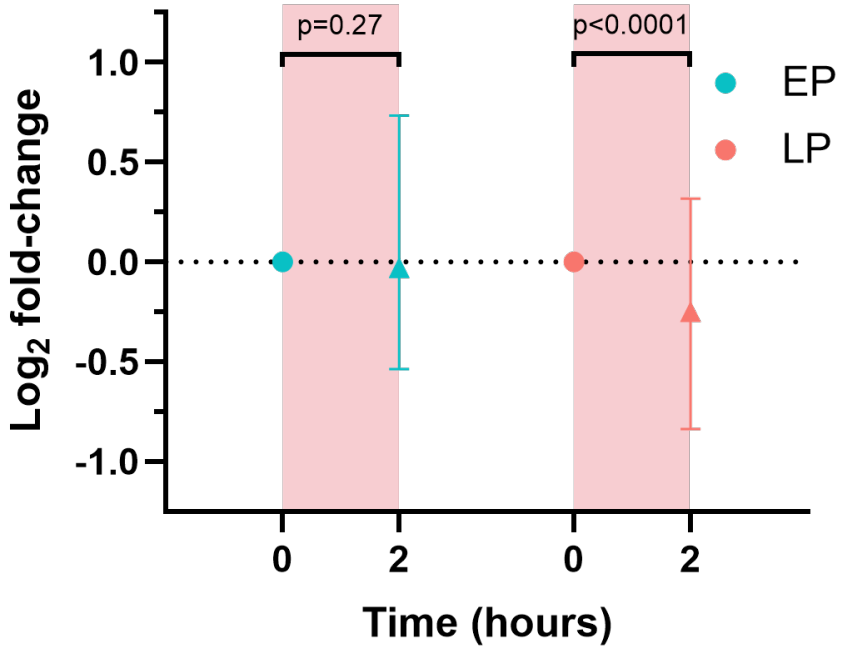

Figure 5.19: The distribution (median and interquartile range) of abundance changes of 359 monobromobimane (mBBr)-tagged peptides from 252 proteins in response to stress in early- (EP) and late-passage (LP) populations. As we are investigating whether mBBr labelling follows a non-parametric distribution, significance is evaluated via a non-parametric Wilcoxon signed-rank test.

To identify which proteins experience conformational changes specific to EP or LP cells, Figure 5.20 shows the individual peptides from Figure 5.19. Peptides where the absolute Log_2 fold-change was greater than 1 in just one of EP/LP populations, but not the other, are highlighted by the shaded regions in Figure 5.20. 49 proteins were identified as being differentially labelled in LP populations only (that is, proteins for which peptides were found in the red regions of Figure 5.20, but not the blue or white regions). A protein class analysis was performed on these proteins using PANTHER (Mi et al., 2021, version 16.0), with the results in Figure 5.21. Eight cytoskeletal proteins are found, with the details of these proteins shown in Table 5.3. This was in agreement with the finding in Chapter 3 that a functional module representing cytoskeletal-specific chaperones is downregulated in LP populations. Another class of interest is chaperone proteins themselves (note this is distinct from the class defined by Brehme et al., 2014). with proteins from the HSP70, HSP90, and CCT modules outlined in Chapter 3 represented in the orange region of Figure 5.20. Relating to impaired translation, the ribosomal protein RPS3 and translation elongation factor EEF2 also feature in this set.

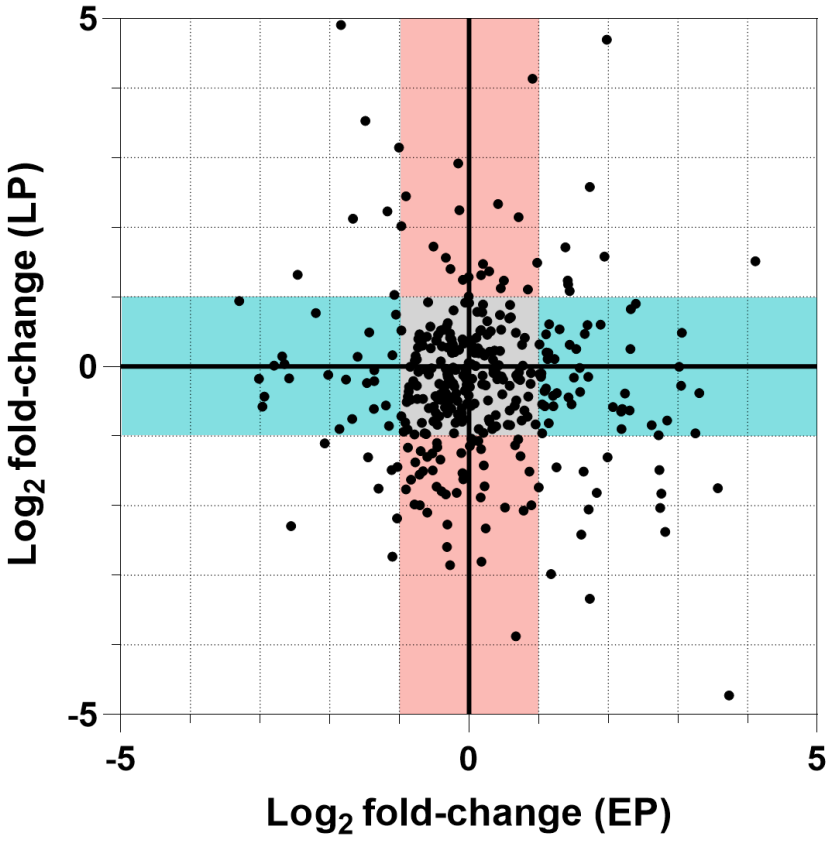

Figure 5.20: Median Log_2 fold-changes of monobromobimane (mBBr)-labelled peptides in response to stress in mass spectrometry data ($n = 4$ donors), normalised to protein level. Shaded blue regions indicate an absolute Log_2 fold-change > 1 in early-passage (EP) populations only, while shaded red regions indicate an absolute Log_2 fold-change > 1 in late-passage (LP) populations only. The shaded grey region indicates an absolute Log_2 fold-change < 1 in both EP and LP populations in response to stress.

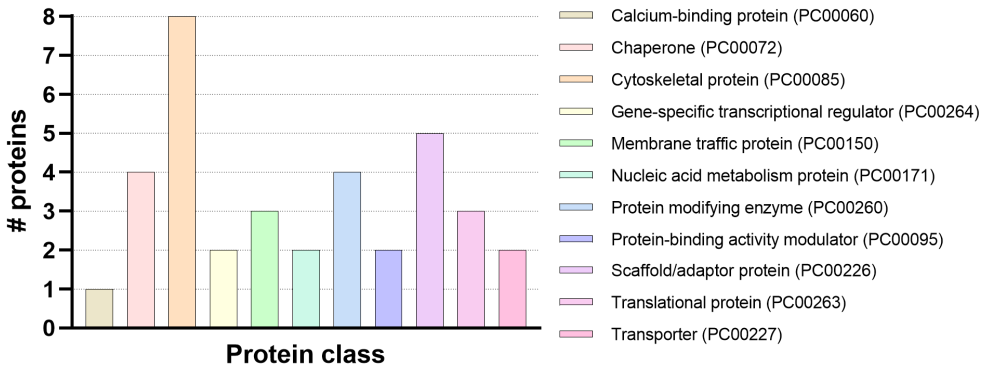

Figure 5.21: PANTHER Protein class analysis of the proteins which experience changes in monobromobimane labelling in response to stress in late-passage cells only.

Protein name	PANTHER protein subclass
Adenylyl cyclase-associated protein 1 (CAP1)	Actin or actin-binding cytoskeletal protein
Destrin (DEST)	Non-motor actin binding protein
LIM domain and actin-binding protein 1 (LIMA1)	Actin or actin-binding cytoskeletal protein
Microtubule-associated protein 1B (MAP1B)	Non-motor microtubule binding protein
Plastin-3 (PLST)	Non-motor actin binding protein
Supervillin (SVIL)	Non-motor actin binding protein
Tubulin alpha-4A chain (TBA4A)	Tubulin
Translationally controlled tumor protein (TCTP)	Non-motor microtubule binding protein

Table 5.3: Proteins identified by monobromobimane-labelling mass spectrometry as being conformationally compromised in late-passage populations only ($n = 4$ donors).

Several chaperones are known to undergo conformational changes during client folding. For example, ATP-binding to the HSP90 homodimer shifts the complex from an open to a closed structure (Krukenberg et al., 2011); similarly the HSPA1A protein has recently been shown to undergo conformational changes following HSP40 co-chaperone binding (Wu et al., 2020). Therefore, the conformational changes of proteins within this protein class may be evidence of an increased workload among chaperone proteins in response to stress in LP cells only. Such a result would be in line with the *in silico* prediction from Figure 5.12 that more protein misfolding occurs in response to stress in LP cells; and the *in vitro* finding from Figure 5.19 that the mBBr-labelling profile of the proteome changes in response to stress in LP cells only.

5.8 Summary

In this final results chapter, the effects of senescence on proteins which govern HSP70 regulation have been evaluated in order to determine why the proteotoxic stress response goes awry in senescent cells. In Section 5.1.1 using IF microscopy it was shown that HSF1, the main transcription factor controlling HSP70 synthesis, is almost entirely nuclear in hMSCs *in vitro*, suggesting that a majority of HSF1 is transcriptionally active even at 37°C. The E3 ubiquitin ligase CHIP, which marks unbound HSP70 for proteasomal turnover, was also analysed using IF microscopy (Section 5.1.2), and it was found that late-passage cells contain a significantly lower concentration of cellular CHIP than early-passage cells. This result suggests that there is less proteasomal turnover of HSP70 in late-passage cells, however in Chapter 4 we have seen that HSP70 concentration is unchanged between early- and

late-passage cells at 37°C. Following the findings from Chapters 3 and 4 that late-passage cells experience a loss of translational machinery, and thus exhibit a loss in the ratio of protein up-regulation to transcript up-regulation; Section 5.1.3 analysed mass spectrometry data from ribosomal proteins in isolation, finding significant under-representation of these proteins in the late-passage proteome. Thus these results show that late-passage populations lose the ability to regulate HSP70 both translationally and post-translationally.

Using the data gathered from HSP70, HSF1, and CHIP; a mathematical model of the stress response was designed to validate the hypothesis that a substantial amount of HSP70 regulation in response to stress is post-translational. The model was optimised using HSP70 early-passage IF microscopy data and replicated this with a high degree of accuracy (Figure 5.9a). This acts as a proof-of-principle showing that the model of HSP70 regulation presented here is sufficient to explain *in vitro* data. Moreover, the model replicated a number of *in vitro* findings, the data from which was not used in the model optimisation process. In particular, the model predicted a dampening of HSP70 up-regulation in late-passage cells (Figure 5.9), a majority of HSF1 being transcriptionally active (Figure 5.8), the time interval at which HSP70 mRNA returns to pre-stress levels in both early- and late-passage populations (Figure 5.11); as well as predicting the half-life of HSP70 to within one minute of a reference value (Figure 5.15).

Now verified, in Section 5.6 the model was next used to predict the toll of misfolded protein experienced due to proteotoxic stress in both early- and late-passage cells. It was predicted that following an identical stress, changes to levels of CHIP and ribosomal proteins cause late-passage cells to endure a greater amount of protein misfolding and take longer to return to equilibrium. Finally, in Section 5.7, mBBr-labelling mass spectrometry was used to identify proteins which undergo conformation changes in response to stress in early- and late-passage cells. Figure 5.19 shows that while no change was seen in the mBBr-labelling profile of early-passage populations following stress, a large significant change was seen in late-passage populations. Additionally, several cytoskeletal proteins were found to feature among the proteins conformationally compromised in late-passage populations only (Table 5.3,) in agreement with the finding in Chapter 3 that the cytoskeleton-specific CCT/TRiC chaperone complex is down-regulated in late-passage cells. These results demonstrate that senescent cells lose the capacity to regulate HSP70, which leads to a loss in the speed, magnitude, and efficacy of the proteotoxic stress response.

Chapter 6

Conclusions & future work

Late-passage hBM-MSC cultures consist of disproportionately high numbers of senescent cells

The results chapters of this study began by verifying LP hBM-MSC cultures predominantly consisted of cells which had undergone cellular senescence. Several markers of senescence have been verified in LP cells throughout this study, including up-regulation of β-galactosidase (Section 3.1), under-enrichment of cell cycle pathways (Section 3.4.2), loss of lamin B1 mRNA and protein (Sections 4.5.1 and 3.2 respectively), and changes in cell morphology (Section 4.5.2). Images of β-galactosidase staining demonstrate how senescence is not ubiquitous in LP populations (Figure 3.1), and invites the question of whether these markers could have been used to isolate senescent cells for the experiments in this study. Due to the increasing research being done on the SASP and the effects senescent cells can quickly have on surrounding cells (as reviewed in Section 1.8.5), it was decided to be of higher relevance to study late-passage populations of mixed senescent and proliferating cells.

Section 2.4 covers the acquisition of these cells, and it should not be ignored that this acquisition is a side-product of tissue replacement surgeries. As one would expect, these surgeries generally take place in aged patients, such that the early-passage populations used in this study do not necessarily reflect the properties of young tissues *in vivo*. This may therefore be best viewed as a study of the consequences of cellular ageing *in vitro*, rather than a study of the properties of young versus aged tissues *in vivo*.

This study of cellular ageing may be most pertinent to the field of regenerative medicine. As reviewed in Section 1.8.5, clinicians face a trade-off of prolonging MSC culture time to attain larger populations for stem cell therapies, at the expense of cellular ageing within cultures, the ill-effects of which have thus far been unexplored. Performing a pathway analysis on RNA-seq data (Section 3.5.2) demonstrated that during stress, LP populations disengage from DNA repair pathways and instead over-enrich cell death pathways compared with EP populations. Of further detriment to their application in stem cell therapies, LP populations also showed several significantly over-enriched pathways relating to the immune response. This finding may explain the literature discussed in Section 1.8.5, whereby extended passaging of cells has negatively affected treatment outcomes. The use of heat shock here

however is a crude model to reflect the compound of various cellular stresses in the post-transplant environment hMSCs experience, and a better representative model may be needed to conclusively implicate the attenuation of the stress response in the loss of efficacy in these therapies. Nonetheless, this study further emphasises the need for open-sourced, standardised culture protocols among stem cell therapies.

The early-passage response to proteotoxic stress goes awry in late-passage cells

This study aimed to quantitatively define the mechanisms behind a cellular age-associated vulnerability to proteotoxic stress. To this end, a comprehensive comparison of proliferating and senescent cells responding to proteotoxic stress at the -omic level has been carried out using high-throughput techniques. While there was a strong overlap between the EP and LP transcriptomic response to stress, no correlation was found in the protein regulation which takes place in the proteotoxic stress response between EP and LP populations (Section 3.4.1). Furthermore, a pathway analysis of these populations in response to stress demonstrated that the positive enrichment of the heat stress response pathway in EP populations was replaced by negative enrichment in LP populations (Section 3.4.2). As a result, Figure 3.17b shows LP populations are less equipped at the protein level to carry out the stress response over their EP counterparts. In a wider context, these results may indicate that increasing numbers of senescent cells within aged tissues changes the way these tissues respond to protein misfolding.

In Section 4.1, using a database of known human chaperone proteins (Brehme et al., 2014) and, borrowing tools from mathematical graph theory, these chaperones have been clustered into functional modules in order to identify functional trends in the proteotoxic stress response. This modular analysis demonstrated that in EP hMSCs, up-regulation of HSP70 machinery is the central feature in cellular management of proteotoxic heat shock, but that senescent hMSCs are no longer capable of this response. By inhibiting a key component of the HSP70 machinery, HSPA1A, in EP and LP hMSCs, it was investigated how senescence affects the ability of cells to respond to compromised HSP70 machinery both with and without thermal stress. In both EP and LP cells kept at 37°C, little proteomic difference is seen in comparison to control cells. In the presence of stress however, EP and LP populations displayed very different responses across the whole proteome, and a mechanism buffering against HSP70 inhibition seen in EP populations is lost in LP populations.

The human chaperone library curated by Brehme et al., 2014 is by no means conclusive, and new chaperone machineries are still being discovered. One example omitted here is the R2TP chaperone complex discovered by the Houry lab (R. Zhao et al., 2005), which is evolutionarily conserved and assists in the folding of a broad range of proteins in human cells (Jeronimo et al., 2007; Boulon et al., 2008; as reviewed by Houry et al., 2018). As more chaperone interactions are identified, future work may seek to produce an updated and more thorough library of human chaperone proteins. Moreover, the literature is still lacking comprehensive information regarding the clients of each chaperone machinery, or a defined mechanism of how clients are divided between chaperone machineries. This information would facili-

tate the creation of a human chaperone-client network, such as that developed in yeast by Jarnuczak et al., 2018, and would allow the much deeper analysis of the regulation of clients of each functional chaperone network in senescent cells and in response to stress. While the modularity approach taken here is as objective and systematic as possible, it should be noted that biases are still present in the network defined here, emerging from the STRING interaction database, whereby the most frequently researched proteins (such as those which support the survival of cancer cells, as reviewed by Calderwood and Murshid, 2017) are more likely to have higher interaction confidence scores.

A transcript-protein disparity indicates chaperone translation as a limiting factor of the late-passage stress response

A recurring theme throughout Chapter 3 has been that the changes in cells due to stress are far outweighed by the changes due to extended culture. The principal component analysis in Figure 3.4 showed that while differences between human donors were, as expected, the largest source of variation within the data ($> 49\%$), second were the differences between EP and LP cells ($> 27\%$), ahead of differences due to stress ($> 13\%$). Figure 3.6 showed that transcriptional regulation does not drive short-term (here defined as within two hours) changes to the proteome, rather Figure 3.13 showed that these changes take effect over weeks to months of extended passaging in culture. It remains that a majority of protein regulation in the proteotoxic stress response is governed at the post-transcriptional and post-translational levels. While the quantities of transcriptional regulation were similar in response to stress and in response to extended passaging, at the level of the proteome Figures 3.7 and 3.14 show a $>$ 9-fold increase in the number of proteins significantly regulated in extended passaging over those regulated during stress. In this respect, future work should seek to define the post-transcriptional post-translational mechanisms that drive rapid protein-level changes in cells responding to stress, and identify targets which dictate changes to these mechanisms in LP cells for potential treatments.

In order to build a mechanistic understanding of the difference between the stress response in EP and LP hMSCs, key components of the HSP70 machinery were examined with finer temporal resolution (Section 4.5). Quantification of HSPA1A transcript (Figure 4.18f) by RT-qPCR showed, like its main co-chaperone DNAJB1, a strong heat stress response in hMSCs which was remarkably similar between EP and LP populations, with greater transcriptional up-regulation seen in LP populations. It is unlikely that this result reflects an increased efficacy in the transcriptional stress response in senescent cells. More likely, the insult to proteostasis produced by stress may be greater in senescent cells as compared to healthy cells, but this has yet to be investigated *in vitro*.

RT-qPCR data also revealed that the time taken to resolve the proteotoxic stress induced by a 42°C, two hour heat shock is considerably longer in LP cells than in EP. IF microscopy data showed that this loss of efficacy of the LP stress response may be due to a dampened up-regulation of HSPA1A in response to stress. Analysing HSPA1A transcript and protein data in tandem, it became clear that this data aligned with a previously reported lag between the transcriptional and proteomic

stress response (Figure 4.23). Using this information, we may view the HSPA1A protein temporal dynamics presented in Section 4.5.2 as representing a dual-phase stress response.

In the first 2-3 hours following the onset of stress, the response of hBM-MSCs appears to be predominantly post-transcriptional, and in this region LP cells differ from EP only marginally. In the second phase, we may expect the transcriptionally driven stress response to dominate, and it is in this region where the disparity between the EP and LP stress responses becomes most evident - suggesting chaperone translation as an attenuated process in senescent cells. In support of this, down-regulation of large numbers of ribosomal proteins was seen in MS data (Section 5.1.3) which contributed to the under-enrichment of several protein translation pathways being seen in a pathway analysis of protein-level changes in LP populations (Section 3.5.2). These results suggest that a loss of translational capacity in senescent cells drives the attenuation of the stress response. A study of the EP and LP "translatomes" would therefore be of great interest, however performing techniques such as polysomal or ribosomal profiling on senescent primary human cells would require an excessive amount of cell cultures. Additionally, the acquired thermotolerance apparent at the 26 hrs post-stress time point in IF microscopy data (Figure 4.22c) supports previous studies (Sart et al., 2014; Choudhery et al., 2015) which suggest heat-shock pretreatment could enhance the success of MSC transplants.

Mathematical modelling identifies a loss of chaperone and misfolded protein turnover machinery as another limiting factor of the late-passage stress response

A mathematical model of the stress response was created with the primary aim of challenging the current understanding of HSP70 regulation in the proteotoxic stress response. Models attempting to describe the process thus far have been built around the theory of mass synthesis of an already highly abundant protein, and neglected post-translational regulation. Here it has been shown that the inclusion of the HSP70 and MFP regulator CHIP enables accurate fitting of *in vitro* data during both the stress response and the subsequent return to equilibrium. Furthermore, *in silico* results demonstrate these dynamics can be achieved mostly through post-translational regulation of HSP70, with transcriptional regulation playing a minor role. Predominantly stabilising HSP70 under stress rather than synthesising additional protein is supported in the literature by H. Chen et al., 2015 and would presumably conserve a considerable amount of energy during cellular stress. HSP70 up-regulation through a change in stability, rather than an increase in synthesis could be investigated through stable-isotope labelling by amino acids in cell culture (SILAC) mass spectrometry (as reviewed by Mann, 2006). Future experimental work may also seek to build upon the model predictions regarding mechanisms of HSP70 regulation. It would also be of interest to investigate whether these results are also seen in more specialised cell types, with Blanco et al., 2016 showing proliferating mammalian stem cells have surprisingly low rates of protein synthesis compared to differentiated cells.

A second aim of the model was to test if the changes observed in senescent cells

were sufficient to account for the attenuation of HSPA1A up-regulation seen in IF microscopy data. To this end, a loss of HSP70 synthesis proportional to the down-regulation of ribosomal proteins in LP cells, and a down-regulation of CHIP in LP cells were incorporated into the model. While these changes did result in a partial loss of HSP70 induction in response to stress, these changes alone were not sufficient to fully describe the attenuation of the stress response in LP cells. By varying the parameters included in the model, it was possible to predict mechanistic changes in senescent cells which would lead to the HSP70 dynamics observed *in vitro*. As it stands, this model paves the way for future work to investigate the factors predicted to influence the senescence-associated decline in the stress response.

Down-regulation of the CCT complex in late-passage cells drives the compromise of cytoskeletal proteins during proteotoxic stress

Following the dynamics of *in silico* concentrations of misfolded protein, the model predicted an increase of more than two hours in the time taken to resolve stress-induced protein misfolding in LP cells, and simulations suggested LP cells would sustain a greater attenuation to proteostasis than their EP counterparts when presented with an equal proteotoxic stress. This was tested using mBBr to quantify changes to the cysteine-labelling profile of cells following proteotoxic stress. mBBr-labelling revealed a significant ($p < 0.0001$) conformational change of proteins in LP cells compared to no change ($p = 0.27$) in EP cells. This was in agreement with the model prediction (Section 5.6) that an equal magnitude of stress will be more detrimental to proteostasis in LP cells than EP cells. In the context of ageing, this suggests that the maintenance of proteostasis within tissues becomes more finely balanced as aged cells accumulate in tissues.

Work in Chapter 4 identified the down-regulation of a functional module containing the CCT chaperone complex in LP cells. Evidence has been found that this complex serves client proteins related to both the cytoskeleton and the cell cycle. It is likely the cell cycle arrest in senescent cells drives the down-regulation of the CCT complex. In response to stress however, the chaperones in the CCT functional module are heavily transcribed (Section 4.2) in LP populations, suggesting a perturbation from proteostasis within the cytoskeleton. In agreement with this, work in Section 5.7 showed conformational changes to several cytoskeletal proteins in LP cells exposed to stress. This data could make way for a complementary study to investigate the mechanical stress response in senescent cells, with implications in age-associated diseases such as arthritis (Chalan et al., 2015; O. H. Jeon et al., 2018) and intervertebral disc degeneration (Gilbert, 2011; Feng et al., 2018; Patil et al., 2018).

Appendix A

MATLAB script

A.1 Titration model of proteotoxic stress

```
function [ HSF,totalHSP,totalMFP,sse ] = titration( B , K , k2 , k4 ,
    k5 , k7, stress )
% Jack Llewellyn 29/03/2021
% time is in minutes
% dt = time interval between evaluating abundances
% T = total simulation time [minutes]
% HS starts at T=6000, such that all populations are at equilibrium
% all populations are concentrations

% Set temporal resolution
dt=.01;
T=6000+26*60;

% Seed the rng for reproducible results
rng(0);

% Record sum-of-squared-errors for optimisation
sse=zeros( 1,max( [length(B(:)), length(K(:)), length(k2(:)), length(k4
    (:)), length(k5(:)), length(k7(:))] ) );

% Set passage
for senescent = 0:1

% initial population levels
HSP = 1000; % m.mole % = steady state lDoF
MFP = 0; % m.mole
HSP_HSF = 0.1; % m.mole
HSP_MFP = 0; % m.mole
% DDE to model translation delay
HSF = zeros(2+(T/dt),max( [length(B(:)), length(K(:)), length(k2(:)),
    length(k4(:)), length(k5(:)), length(k7(:))] ));
CHIP = (HSP+HSP_HSF+HSP_MFP)/3.1033; % m.mole

if senescent == 1
CHIP = 0.5824*CHIP;
end

% monitor abundances
totalHSP = zeros(1+(T/dt), max( [length(B(:)), length(K(:)), length(k2
    (:)), length(k4(:)), length(k5(:)), length(k7(:))] ) );
```

```
totaldHSP = zeros(1+(T/dt), max( [length(B(:)), length(K(:)), length(k2
    (:)), length(k4(:)), length(k5(:)), length(k7(:))] ) );
totalHSF = zeros(1+(T/dt),1);
totalMFP = zeros(1+(T/dt),max( [length(B(:)), length(K(:)), length(k2
    (:)), length(k4(:)), length(k5(:)), length(k7(:))] ));
rates = zeros(1+(T/dt),7); % reaction rates

% hill function
n = 3; % hill coefficient

if senescent == 1
B = 0.7134*B;
end

k3 = k2;

k6 = (641/375)*k4; % 1/(m.mole*min) % see notes



% initial rates
dHSF = k3.*HSP_HSF.*MFP + k4.*HSP_HSF.*CHIP - k2.*HSF(1,:).*HSP;
dHSP = B.*HSF(1,:)./((K.^n)+(HSF(1).^n)) + k5.*HSP_MFP + k6.*HSP_MFP.*
    CHIP - k2.*HSF(1,:).*HSP - k3.*HSP.*MFP - k4.*HSP.*CHIP;
dCHIP = 0;
dMFP = k7 - k3.*HSP.*MFP - k3.*HSP_HSF.*MFP;
dHSP_HSF = k2.*HSF(1,:).*HSP - k3.*HSP_HSF.*MFP - k4.*HSP_HSF.*CHIP;
dHSP_MFP = k3.*HSP_HSF.*MFP + k3.*HSP.*MFP - k5.*HSP_MFP - k6.*HSP_MFP
    .*CHIP;


for t = 0:dt:T % time

    % choose random transcription time between [1,3] hrs
    t_delay = randi([60 180]);

    % monitor abundances
     totalHSP(round(1+(t/dt)),:) = HSP + HSP_HSF + HSP_MFP;
     totaldHSP(round(1+(t/dt)),:) = dHSP + dHSP_HSF + dHSP_MFP;
     totalHSF(round(1+(t/dt))) = HSF(round(1+(t/dt))) + HSP_HSF;
     totalMFP(round(1+(t/dt)),:) = MFP + HSP_MFP;
      rates(round(1+(t/dt)),:) = [B.*HSF(max(1,round(1+(t/dt)) - (
          t_delay/dt)))/((K^n)+(HSF(max(1,round(1+(t/dt)) - (t_delay/dt
          )))^n)),...
                                  k2.*HSF(round(1+(t/dt))).*HSP,...
                                  k3.*HSP_HSF.*MFP + k3.*HSP.*MFP,...
                                  k4.*HSP_HSF.*CHIP + k4.*HSP.*CHIP
                                      ,...
                                  k5.*HSP_MFP,...
                                  k6.*HSP_MFP.*CHIP,...
                                  k7];

    if t == 6000 % "switch on" stress
       k7 = stress.*k7;

   %record baseline levels for overlaying experimental data
   HSPt0 = HSP+HSP_HSF+HSP_MFP;
    end
```

```
    if t == 6120 % "switch off" stress
        k7 = k7./stress;
    end

    % progress time
    HSF(round(2+(t/dt)),:) = max(0,HSF(round(1+(t/dt)),:) + dHSF.*dt);
    HSP = max(0,HSP + dHSP.*dt);

    % Match CHIP to steady state level of HSP
    if t < 6000
        CHIP = (HSP+HSP_HSF+HSP_MFP)/3.1033;
        if senescent == 1
        CHIP = 0.5824.*CHIP;
        end
    else
    CHIP = CHIP + dCHIP.*dt;
    end
    MFP = max(0,MFP + dMFP.*dt);
    HSP_HSF = max(0,HSP_HSF + dHSP_HSF.*dt);
    HSP_MFP = max(0,HSP_MFP + dHSP_MFP.*dt);

    % update rates for change at next time point
    dHSF = k3.*HSP_HSF.*MFP + k4.*HSP_HSF.*CHIP - k2.*HSF(round(1+(t/dt
        )),:).*HSP;
    dHSP = B.*HSF(max(1,round(1+(t/dt)) - (t_delay/dt)),:)./((K.^n)+(
        HSF(max(1,round(1+(t/dt)) - (t_delay/dt)),:).^n)) + k5.*HSP_MFP
         + k6.*HSP_MFP.*CHIP - k2.*HSF(round(1+(t/dt)),:).*HSP - k3.*
        HSP.*MFP - k4.*HSP.*CHIP;
    dCHIP = 0;
    dMFP = k7 - k3.*HSP.*MFP - k3.*HSP_HSF.*MFP;
    dHSP_HSF = k2.*HSF(round(1+(t/dt)),:).*HSP - k3.*HSP_HSF.*MFP - k4
        .*HSP_HSF.*CHIP;
    dHSP_MFP = k3.*HSP_HSF.*MFP + k3.*HSP.*MFP - k5.*HSP_MFP - k6.*
        HSP_MFP.*CHIP;

end

% calculate SSE in HSP vs experimental data
if senescent == 0
% low passage
sse = sse + ...
    (totalHSP(6000/dt +1,:)./HSPt0-2.^0).^2 +...
    (totalHSP(6060/dt +1,:)./HSPt0-2.^0.1721).^2 +...
    (totalHSP(6120/dt +1,:)./HSPt0-2.^0.4725).^2 +...
    (totalHSP(6150/dt +1,:)./HSPt0-2.^0.7322).^2 +...
    (totalHSP(6180/dt +1,:)./HSPt0-2.^0.8536).^2 +...
    (totalHSP(6240/dt +1,:)./HSPt0-2.^0.9621).^2 +...
    (totalHSP(6360/dt +1,:)./HSPt0-2.^1.244).^2 +...
    (totalHSP(6600/dt +1,:)./HSPt0-2.^0.9421).^2 +...
    (totalHSP(7560/dt +1,:)./HSPt0-2.^0.5177).^2;
 else
 high passage
  sse = sse + ...
      (totalHSP(6000/dt +1)./HSPt0-2.^-0.0747).^2 +...
      (totalHSP(6060/dt +1)./HSPt0-2.^-0.2382).^2 +...
      (totalHSP(6120/dt +1)./HSPt0-2.^0.2081).^2 +...
      (totalHSP(6150/dt +1)./HSPt0-2.^0.3995).^2 +...
```

```
        (totalHSP(6180/dt +1)./HSPt0-2.^0.3458).^2 +...
        (totalHSP(6240/dt +1)./HSPt0-2.^0.4000).^2 +...
        (totalHSP(6360/dt +1)./HSPt0-2.^0.6687).^2 +...
        (totalHSP(6600/dt +1)./HSPt0-2.^0.5430).^2 +...
        (totalHSP(7560/dt +1)./HSPt0-2.^0.3112).^2;
end

end
```

Bibliography

Abravaya, K., Phillips, B., & Morimoto, R. I. (1991). Attenuation of the heat shock response in HeLa cells is mediated by the release of bound heat shock transcription factor and is modulated by changes in growth and in heat shock temperatures. *Genes & Development*, *5*(11), 2117–2127. https://doi.org/10.1101/gad.5.11.2117

Acosta, J. C., O'Loghlen, A., Banito, A., Guijarro, M. V., Augert, A., Raguz, S., Fumagalli, M., Da Costa, M., Brown, C., Popov, N., Takatsu, Y., Melamed, J., d'Adda di Fagagna, F., Bernard, D., Hernando, E., & Gil, J. (2008). Chemokine Signaling via the CXCR2 Receptor Reinforces Senescence. *Cell*, *133*(6), 1006–1018. https://doi.org/10.1016/j.cell.2008.03.038

Acosta, J. C., Banito, A., Wuestefeld, T., Georgilis, A., Janich, P., Morton, J. P., Athineos, D., Kang, T.-W., Lasitschka, F., Andrulis, M., Pascual, G., Morris, K. J., Khan, S., Jin, H., Dharmalingam, G., Snijders, A. P., Carroll, T., Capper, D., Pritchard, C., … Gil, J. (2013). A complex secretory program orchestrated by the inflammasome controls paracrine senescence. *Nature Cell Biology*, *15*(8), 978–990. https://doi.org/10.1038/ncb2784

Acunzo, J., Katsogiannou, M., & Rocchi, P. (2012). Small heat shock proteins HSP27 (HspB1), B-crystallin (HspB5) and HSP22 (HspB8) as regulators of cell death. *The International Journal of Biochemistry & Cell Biology*, *44*(10), 1622–1631. https://doi.org/10.1016/j.biocel.2012.04.002

Adamo, H. P., Filoteo, A. G., Enyedi, A., & Penniston, J. T. (1995). Mutants in the Putative Nucleotide-binding Region of the Plasma Membrane Ca2+-Pump. *Journal of Biological Chemistry*, *270*(50), 30111–30114. https://doi.org/10.1074/jbc.270.50.30111

Adomavicius, T., Guaita, M., Zhou, Y., Jennings, M. D., Latif, Z., Roseman, A. M., & Pavitt, G. D. (2019). The structural basis of translational control by eIF2 phosphorylation. *Nature Communications*, *10*(1), 2136. https://doi.org/10.1038/s41467-019-10167-3

Advani, V. M., & Ivanov, P. (2019). Translational Control under Stress: Reshaping the Translatome. *BioEssays*, *41*(5), 1900009. https://doi.org/10.1002/bies.201900009

Ahn, S.-G. (2003). Redox regulation of mammalian heat shock factor 1 is essential for Hsp gene activation and protection from stress. *Genes & Development*, *17*(4), 516–528. https://doi.org/10.1101/gad.1044503

Aisha, M., Nor-Ashikin, M., Shaaniza, A., Nawawi, H., Kapitonova, M., & Froemming, G. (2014). Short-term moderate hypothermia stimulates alkaline phosphatase activity and osteocalcin expression in osteoblasts by upregulating Runx2 and osterix in vitro. *Experimental Cell Research*, *326*(1), 46–56. https://doi.org/10.1016/j.yexcr.2014.06.003

Åkerfelt, M., Morimoto, R. I., & Sistonen, L. (2010). Heat shock factors: Integrators of cell stress, development and lifespan. *Nature Reviews Molecular Cell Biology*, *11*(8), 545–555. https://doi.org/10.1038/nrm2938

Alekseenko, L. L., Shilina, M. A., Lyublinskaya, O. G., Kornienko, J. S., Anatskaya, O. V., Vinogradov, A. E., Grinchuk, T. M., Fridlyanskaya, I. I., & Nikolsky, N. N. (2018). Quiescent Human Mesenchymal Stem Cells Are More Resistant to Heat Stress than Cycling Cells. *Stem cells international*, *3753547*. https://doi.org/https://doi.org/10.1155/2018/3753547

Ali, A., Bharadwaj, S., O'Carroll, R., & Ovsenek, N. (1998). HSP90 Interacts with and Regulates the Activity of Heat Shock Factor 1 in Xenopus Oocytes. *Molecular and Cellular Biology*, *18*(9), 4949–4960. https://doi.org/10.1128/MCB.18.9.4949

Allard, J. S., Heilbronn, L. K., Smith, C., Hunt, N. D., Ingram, D. K., Ravussin, E., Team, P. C., & Cabo, R. d. (2008). In Vitro Cellular Adaptations of Indicators of Longevity in Response to Treatment with Serum Collected from Humans on Calorie Restricted Diets. *PLOS ONE*, *3*(9), e3211. https://doi.org/10.1371/journal.pone.0003211

Altmann, M., & Linder, P. (2010). Power of Yeast for Analysis of Eukaryotic Translation Initiation. *Journal of Biological Chemistry*, *285*(42), 31907–31912. https://doi.org/10.1074/jbc.R110.144196

Ambra, R., Mocchegiani, E., Giacconi, R., Canali, R., Rinna, A., Malavolta, M., & Virgili, F. (2004). Characterization of the hsp70 response in lymphoblasts from aged and centenarian subjects and differential effects of in vitro zinc supplementation. *Experimental Gerontology*, *39*(10), 1475–1484. https://doi.org/10.1016/j.exger.2004.07.009

Anckar, J., & Sistonen, L. (2011). Regulation of HSF1 Function in the Heat Stress Response: Implications in Aging and Disease. *Annual Review of Biochemistry*, *80*(1), 1089–1115. https://doi.org/10.1146/annurev-biochem-060809-095203

Anderson, R. M., Hadjichrysanthou, C., Evans, S., & Wong, M. M. (2017). Why do so many clinical trials of therapies for Alzheimer's disease fail? *The Lancet*, *390*(10110), 2327–2329. https://doi.org/10.1016/S0140-6736(17)32399-1

Ansari, M. Y., & Mande, S. C. (2018). A Glimpse Into the Structure and Function of Atypical Type I Chaperonins. *Frontiers in Molecular Biosciences*, *5*, 31. https://doi.org/10.3389/fmolb.2018.00031

Arakawa, A., Handa, N., Ohsawa, N., Shida, M., Kigawa, T., Hayashi, F., Shirouzu, M., & Yokoyama, S. (2010). The C-Terminal BAG Domain of BAG5 Induces Conformational Changes of the Hsp70 Nucleotide- Binding Domain for ADP-ATP Exchange. *Structure*, *18*(3), 309–319. https://doi.org/10.1016/j.str.2010.01.004

Backe, S. J., Sager, R. A., Woodford, M. R., Makedon, A. M., & Mollapour, M. (2020). Post-translational modifications of Hsp90 and translating the chaperone code. *Journal of Biological Chemistry*, *295*(32), 11099–11117. https://doi.org/10.1074/jbc.REV120.011833

Baker, D. J., Childs, B. G., Durik, M., Wijers, M. E., Sieben, C. J., Zhong, J., A. Saltness, R., Jeganathan, K. B., Verzosa, G. C., Pezeshki, A., Khazaie, K., Miller, J. D., & van Deursen, J. M. (2016). Naturally occurring p16 Ink4a

-positive cells shorten healthy lifespan. *Nature*, *530*(7589), 184–189. https://doi.org/10.1038/nature16932

Balchin, D., Hayer-Hartl, M., & Hartl, F. U. (2016). In vivo aspects of protein folding and quality control. *Science*, *353*(6294), aac4354. https://doi.org/10.1126/science.aac4354

Balogh, G., Horváth, I., Nagy, E., Hoyk, Z., Benkõ, S., Bensaude, O., & Vígh, L. (2005). The hyperfluidization of mammalian cell membranes acts as a signal to initiate the heat shock protein response. *The FEBS Journal*, *272*(23), 6077–6086. https://doi.org/https://doi.org/10.1111/j.1742-4658.2005.04999.x

Basha, E., O'Neill, H., & Vierling, E. (2012). Small heat shock proteins and alpha-crystallins: Dynamic proteins with flexible functions. *Trends in Biochemical Sciences*, *37*(3), 106–117. https://doi.org/10.1016/j.tibs.2011.11.005

Basisty, N., Kale, A., Jeon, O. H., Kuehnemann, C., Payne, T., Rao, C., Holtz, A., Shah, S., Sharma, V., Ferrucci, L., Campisi, J., & Schilling, B. (2020). A proteomic atlas of senescence-associated secretomes for aging biomarker development (M. Serrano, Ed.). *PLOS Biology*, *18*(1), e3000599. https://doi.org/10.1371/journal.pbio.3000599

Bassett, D. R. (2002). Scientific contributions of A. V. Hill: Exercise physiology pioneer. *Journal of Applied Physiology*, *93*(5), 1567–1582. https://doi.org/10.1152/japplphysiol.01246.2001

Beck, M., Schmidt, A., Malmstroem, J., Claassen, M., Ori, A., Szymborska, A., Herzog, F., Rinner, O., Ellenberg, J., & Aebersold, R. (2011). The quantitative proteome of a human cell line. *Molecular Systems Biology*, *7*(1), 549. https://doi.org/10.1038/msb.2011.82

Becker, R. E., Greig, N. H., & Giacobini, E. (2008). Why do so many drugs for {A}lzheimer's disease fail in development? Time for new methods and new practices? *Journal of Alzheimer's disease: JAD*, *15*(2), 303–325. https://doi.org/10.3233/jad-2008-15213

Behl, C. (2016). Breaking BAG: The Co-Chaperone BAG3 in Health and Disease. *Trends in Pharmacological Sciences*, *37*(8), 672–688. https://doi.org/10.1016/j.tips.2016.04.007

Benjamini, Y., & Hochberg, Y. (1995). Controlling the False Discovery Rate: A Practical and Powerful Approach to Multiple Testing. *Journal of the Royal Statistical Society. Series B (Methodological)*, *57*(1), 289–300. Retrieved January 9, 2021, from https://www.jstor.org/stable/2346101

Ben-Zvi, A., Miller, E. A., & Morimoto, R. I. (2009). Collapse of proteostasis represents an early molecular event in Caenorhabditis elegans aging. *Proceedings of the National Academy of Sciences*, *106*(35), 14914–14919. https://doi.org/10.1073/pnas.0902882106

Bhandari, V., & Houry, W. A. (2015). Substrate Interaction Networks of the Escherichia coli Chaperones: Trigger Factor, DnaK and GroEL. *Advances in Experimental Medicine and Biology*, *883*, 271–294. https://doi.org/10.1007/978-3-319-23603-2_15

Biran, A., Zada, L., Abou Karam, P., Vadai, E., Roitman, L., Ovadya, Y., Porat, Z., & Krizhanovsky, V. (2017). Quantitative identification of senescent cells in aging and disease. *Aging Cell*, *16*(4), 661–671. https://doi.org/10.1111/acel.12592

Blanco, S., Bandiera, R., Popis, M., Hussain, S., Lombard, P., Aleksic, J., Sajini, A., Tanna, H., Cortés-Garrido, R., Gkatza, N., Dietmann, S., & Frye, M. (2016). Stem cell function and stress response are controlled by protein synthesis. *Nature*, *534*(7607), 335–340. https://doi.org/10.1038/nature18282

Boja, E. S., & Fales, H. M. (2001). Overalkylation of a Protein Digest with Iodoacetamide. *Analytical Chemistry*, *73*(15), 3576–3582. https://doi.org/10.1021/ac0103423

Bolger, A. M., Lohse, M., & Usadel, B. (2014). Trimmomatic: A flexible trimmer for Illumina sequence data. *Bioinformatics (Oxford, England)*, *30*(15), 2114–2120. https://doi.org/10.1093/bioinformatics/btu170

Bonelli, M. A., Alfieri, R. R., Petronini, P. G., Brigotti, M., Campanini, C., & Borghetti, A. F. (1999). Attenuated Expression of 70-kDa Heat Shock Protein in WI-38 Human Fibroblasts during Aging in Vitro. *Experimental Cell Research*, *252*(1), 20–32. https://doi.org/10.1006/excr.1999.4614

Bottani, S., & Veitia, R. A. (2017). Hill function-based models of transcriptional switches: Impact of specific, nonspecific, functional and nonfunctional binding: Modeling of transcriptional switches. *Biological Reviews*, *92*(2), 953–963. https://doi.org/10.1111/brv.12262

Boulon, S., Marmier-Gourrier, N., Pradet-Balade, B., Wurth, L., Verheggen, C., Jády, B. E., Rothé, B., Pescia, C., Robert, M.-C., Kiss, T., Bardoni, B., Krol, A., Branlant, C., Allmang, C., Bertrand, E., & Charpentier, B. (2008). The Hsp90 chaperone controls the biogenesis of L7Ae RNPs through conserved machinery. *Journal of Cell Biology*, *180*(3), 579–595. https://doi.org/10.1083/jcb.200708110

Brehme, M., Voisine, C., Rolland, T., Wachi, S., Soper, J. H., Zhu, Y., Orton, K., Villella, A., Garza, D., Vidal, M., Ge, H., & Morimoto, R. I. (2014). A Chaperome Subnetwork Safeguards Proteostasis in Aging and Neurodegenerative Disease. *Cell Reports*, *9*(3), 1135–1150. https://doi.org/10.1016/j.celrep.2014.09.042

Brive, L., Takayama, S., Briknarová, K., Homma, S., Ishida, S. K., Reed, J. C., & Ely, K. R. (2001). The Carboxyl-Terminal Lobe of Hsc70 ATPase Domain Is Sufficient for Binding to BAG1. *Biochemical and Biophysical Research Communications*, *289*(5), 1099–1105. https://doi.org/10.1006/bbrc.2001.6087

Brocchieri, L. (2005). Protein length in eukaryotic and prokaryotic proteomes. *Nucleic Acids Research*, *33*(10), 3390–3400. https://doi.org/10.1093/nar/gki615

Brodin, P., Jojic, V., Gao, T., Bhattacharya, S., Angel, C. J. L., Furman, D., Shen-Orr, S., Dekker, C. L., Swan, G. E., Butte, A. J., Maecker, H. T., & Davis, M. M. (2015). Variation in the Human Immune System Is Largely Driven by Non-Heritable Influences. *Cell*, *160*(1-2), 37–47. https://doi.org/10.1016/j.cell.2014.12.020

Bromberg, Z., & Weiss, Y. (2016). The Role of the Membrane-Initiated Heat Shock Response in Cancer. *Frontiers in Molecular Biosciences*, *3*. https://doi.org/10.3389/fmolb.2016.00012

Bronzini, I., Patruno, M., Iacopetti, I., & Martinello, T. (2012). Influence of temperature, time and different media on mesenchymal stromal cells shipped for clinical application. *Veterinary Journal (London, England: 1997)*, *194*(1), 121–123. https://doi.org/10.1016/j.tvjl.2012.03.010

Brownridge, P., Lawless, C., Payapilly, A. B., Lanthaler, K., Holman, S. W., Harman, V. M., Grant, C. M., Beynon, R. J., & Hubbard, S. J. (2013). Quantitative analysis of chaperone network throughput in budding yeast. *PROTEOMICS*, *13*(8), 1276–1291. https://doi.org/10.1002/pmic.201200412

Budzyński, M. A., Puustinen, M. C., Joutsen, J., & Sistonen, L. (2015). Uncoupling Stress-Inducible Phosphorylation of Heat Shock Factor 1 from Its Activation. *Molecular and Cellular Biology*, *35*(14), 2530–2540. https://doi.org/10.1128/MCB.00816-14

Burrow, K. L., Hoyland, J. A., & Richardson, S. M. (2017). Human Adipose-Derived Stem Cells Exhibit Enhanced Proliferative Capacity and Retain Multipotency Longer than Donor-Matched Bone Marrow Mesenchymal Stem Cells during Expansion In Vitro. *Stem Cells International*, *2017*, 1–15. https://doi.org/10.1155/2017/2541275

Calderwood, S. K., & Murshid, A. (2017). Molecular Chaperone Accumulation in Cancer and Decrease in Alzheimer's Disease: The Potential Roles of HSF1. *Frontiers in Neuroscience*, *11*, 192. https://doi.org/10.3389/fnins.2017.00192

Calderwood, S. K., Murshid, A., & Prince, T. (2009). The Shock of Aging: Molecular Chaperones and the Heat Shock Response in Longevity and Aging; A Mini-Review. *Gerontology*, *55*(5), 550–558. https://doi.org/10.1159/000225957

Camasses, A., Bogdanova, A., Shevchenko, A., & Zachariae, W. (2003). The CCT Chaperonin Promotes Activation of the Anaphase-Promoting Complex through the Generation of Functional Cdc20. *Molecular Cell*, *12*(1), 87–100. https://doi.org/10.1016/S1097-2765(03)00244-2

Carra, S., Rusmini, P., Crippa, V., Giorgetti, E., Boncoraglio, A., Cristofani, R., Naujock, M., Meister, M., Minoia, M., Kampinga, H. H., & Poletti, A. (2013). Different anti-aggregation and pro-degradative functions of the members of the mammalian sHSP family in neurological disorders. *Philosophical Transactions of the Royal Society B: Biological Sciences*, *368*(1617), 20110409. https://doi.org/10.1098/rstb.2011.0409

Carrard, G., Dieu, M., Raes, M., Toussaint, O., & Friguet, B. (2003). Impact of ageing on proteasome structure and function in human lymphocytes. *The International Journal of Biochemistry & Cell Biology*, *35*(5), 728–739. https://doi.org/10.1016/S1357-2725(02)00356-4

Carver, J., Rekas, A., Thorn, D., & Wilson, M. (2003). Small Heat-shock Proteins and Clusterin: Intra- and Extracellular Molecular Chaperones with a Common Mechanism of Action and Function? *International Union of Biochemistry and Molecular Biology: Life*, *55*(12), 661–668. https://doi.org/10.1080/15216540310001640498

Chalan, P., van den Berg, A., Kroesen, B.-J., Brouwer, L., & Boots, A. (2015). Rheumatoid Arthritis, Immunosenescence and the Hallmarks of Aging. *Current Aging Science*, *8*(2), 131–146. https://doi.org/10.2174/1874609808666150727110744

Charmpilas, N., Kyriakakis, E., & Tavernarakis, N. (2017). Small heat shock proteins in ageing and age-related diseases. *Cell Stress and Chaperones*, *22*(4), 481–492. https://doi.org/10.1007/s12192-016-0761-x

Chen, H., Song, R., Wang, G., Ding, Z., Yang, C., Zhang, J., Zeng, Z., Rubio, V., Wang, L., Zu, N., Weiskoff, A. M., Minze, L. J., Jeyabal, P. V., Mansour, O. C., Bai, L., Merrick, W. C., Zheng, S., & Shi, Z.-Z. (2015). OLA1 regulates protein synthesis and integrated stress response by inhibiting eIF2 ternary

complex formation. *Scientific Reports*, *5*(1), 13241. https://doi.org/10.1038/srep13241

Chen, S., Wang, J., Peng, D., Li, G., Chen, J., & Gu, X. (2018). Exposure to heat-stress environment affects the physiology, circulation levels of cytokines, and microbiome in dairy cows. *Scientific Reports*, *8*(1), 14606. https://doi.org/10.1038/s41598-018-32886-1

Chen, X., Wang, L., Hou, J., Li, J., Chen, L., Xia, J., Wang, Z., Xiao, M., & Wang, Y. (2019). Study on the Dynamic Biological Characteristics of Human Bone Marrow Mesenchymal Stem Cell Senescence. *Stem Cells International*, *2019*, 1–9. https://doi.org/10.1155/2019/9271595

Cho, I., Jackson, M. R., & Swift, J. (2016). Roles of Cross-Membrane Transport and Signaling in the Maintenance of Cellular Homeostasis. *Cellular and Molecular Bioengineering*, *9*(2), 234–246. https://doi.org/10.1007/s12195-016-0439-6

Chondrogianni, N., Petropoulos, I., Franceschi, C., Friguet, B., & Gonos, E. (2000). Fibroblast cultures from healthy centenarians have an active proteasome. *Experimental Gerontology*, *35*(6-7), 721–728. https://doi.org/10.1016/S0531-5565(00)00137-6

Chondrogianni, N., Georgila, K., Kourtis, N., Tavernarakis, N., & Gonos, E. S. (2015). 20S proteasome activation promotes life span extension and resistance to proteotoxicity in *Caenorhabditis elegans*. *The FASEB Journal*, *29*(2), 611–622. https://doi.org/10.1096/fj.14-252189

Chondrogianni, N., Stratford, F. L. L., Trougakos, I. P., Friguet, B., Rivett, A. J., & Gonos, E. S. (2003). Central Role of the Proteasome in Senescence and Survival of Human Fibroblasts. *Journal of Biological Chemistry*, *278*(30), 28026–28037. https://doi.org/10.1074/jbc.M301048200

Chou, J. J. (2008). Dissecting the free energy of protein folding. *Harvard Medical School, Boston, Massachusetts*. Retrieved January 9, 2021, from http://www.biostat.jhsph.edu/~iruczins/teaching/260.655/notes/prigge3.1.pdf

Choudhery, M. S., Badowski, M., Muise, A., & Harris, D. T. (2015). Effect of mild heat stress on the proliferative and differentiative ability of human mesenchymal stromal cells. *Cytotherapy*, *17*(4), 359–368. https://doi.org/10.1016/j.jcyt.2014.11.003

Choudhery, M. S., Badowski, M., Muise, A., Pierce, J., & Harris, D. T. (2014). Donor age negatively impacts adipose tissue-derived mesenchymal stem cell expansion and differentiation. *Journal of Translational Medicine*, *12*(1), 8. https://doi.org/10.1186/1479-5876-12-8

Chung, H. Y., Kim, D. H., Lee, E. K., Chung, K. W., Chung, S., Lee, B., Seo, A. Y., Chung, J. H., Jung, Y. S., Im, E., Lee, J., Kim, N. D., Choi, Y. J., Im, D. S., & Yu, B. P. (2019). Redefining Chronic Inflammation in Aging and Age-Related Diseases: Proposal of the Senoinflammation Concept. *Aging and disease*, *10*(2), 367. https://doi.org/10.14336/AD.2018.0324

Chung, K. T., Shen, Y., & Hendershot, L. M. (2002). BAP, a mammalian BiP-associated protein, is a nucleotide exchange factor that regulates the ATPase activity of BiP. *The Journal of Biological Chemistry*, *277*(49), 47557–47563. https://doi.org/10.1074/jbc.M208377200

Ciborowski, P., & Silberring, J. (Eds.). (2016). *Proteomic profiling and analytical chemistry: The crossroads* (Second edition). Amsterdam ; Boston, Elsevier.

Cohen, A. A. (2018). Aging across the tree of life: The importance of a comparative perspective for the use of animal models in aging. *Biochimica et Biophysica Acta (BBA) - Molecular Basis of Disease*, *1864*(9), 2680–2689. https://doi.org/10.1016/j.bbadis.2017.05.028

Colotti, C., Cavallini, G., Vitale, R. L., Donati, A., Maltinti, M., Del Ry, S., Bergamini, E., & Giannessi, D. (2005). Effects of Aging and Anti-Aging Caloric Restrictions on Carbonyl and Heat Shock Protein Levels and Expression. *Biogerontology*, *6*(6), 397–406. https://doi.org/10.1007/s10522-005-4906-z

Cortopassi, G. A., & Arnheim, N. (1990). Detection of a specific mitochondrial DNA deletion in tissues of older humans. *Nucleic Acids Research*, *18*(23), 6927–6933. https://doi.org/10.1093/nar/18.23.6927

Cox, J., & Mann, M. (2008). MaxQuant enables high peptide identification rates, individualized p.p.b.-range mass accuracies and proteome-wide protein quantification. *Nature Biotechnology*, *26*(12), 1367–1372. https://doi.org/10.1038/nbt.1511

Crestfield, A. M., Moore, S., & Stein, W. H. (1963). The preparation and enzymatic hydrolysis of reduced and S-carboxymethylated proteins. *The Journal of Biological Chemistry*, *238*, 622–627.

Crippa, V., D'Agostino, V. G., Cristofani, R., Rusmini, P., Cicardi, M. E., Messi, E., Loffredo, R., Pancher, M., Piccolella, M., Galbiati, M., Meroni, M., Cereda, C., Carra, S., Provenzani, A., & Poletti, A. (2016). Transcriptional induction of the heat shock protein B8 mediates the clearance of misfolded proteins responsible for motor neuron diseases. *Scientific Reports*, *6*(1), 22827. https://doi.org/10.1038/srep22827

Csermely, P., & Vígh, L. (Eds.). (2007). *Molecular Aspects of the Stress Response: Chaperones, Membranes and Networks* (Vol. 594). New York, NY, Springer New York. https://doi.org/10.1007/978-0-387-39975-1

Cuervo, A. M., & Dice, J. F. (2000). Age-related Decline in Chaperone-mediated Autophagy. *Journal of Biological Chemistry*, *275*(40), 31505–31513. https://doi.org/10.1074/jbc.M002102200

Cui, X., Wang, L., Zuo, P., Han, Z., Fang, Z., Li, W., & Liu, J. (2004). D-galactose-caused life shortening in Drosophila melanogaster and Musca domestica is associated with oxidative stress. *Biogerontology*, *5*(5), 317–325. https://doi.org/10.1007/s10522-004-2570-3

Cummings, J. L., Morstorf, T., & Zhong, K. (2014). Alzheimer's disease drug-development pipeline: Few candidates, frequent failures. *Alzheimer's Research & Therapy*, *6*(4), 37. https://doi.org/10.1186/alzrt269

da Silva Meirelles, L. (2006). Mesenchymal stem cells reside in virtually all post-natal organs and tissues. *Journal of Cell Science*, *119*(11), 2204–2213. https://doi.org/10.1242/jcs.02932

Danielyan, L., Beer-Hammer, S., Stolzing, A., Schäfer, R., Siegel, G., Fabian, C., Kahle, P., Biedermann, T., Lourhmati, A., Buadze, M., Novakovic, A., Proksch, B., Gleiter, C. H., Frey, W. H., & Schwab, M. (2014). Intranasal Delivery of Bone Marrow-Derived Mesenchymal Stem Cells, Macrophages, and Microglia to the Brain in Mouse Models of Alzheimer's and Parkinson's Disease. *Cell Transplantation*, *23*(1_suppl), 123–139. https://doi.org/10.3727/096368914X684970

Dantuma, N. P., & Bott, L. C. (2014). The ubiquitin-proteasome system in neurodegenerative diseases: Precipitating factor, yet part of the solution. *Frontiers in Molecular Neuroscience*, *7*. https://doi.org/10.3389/fnmol.2014.00070

Danxi, L., & Duncan, R. F. (1995). Transient Acquired Thermotolerance in Drosophila, Correlated with Rapid Degradation of Hsp70 During Recovery. *European Journal of Biochemistry*, *231*(2), 454–465. https://doi.org/10.1111/j.1432-1033.1995.tb20719.x

Dawson, T. M., Golde, T. E., & Lagier-Tourenne, C. (2018). Animal models of neurodegenerative diseases. *Nature Neuroscience*, *21*(10), 1370–1379. https://doi.org/10.1038/s41593-018-0236-8

Dayalan Naidu, S., & Dinkova-Kostova, A. T. (2017). Regulation of the mammalian heat shock factor 1. *The FEBS Journal*, *284*(11), 1606–1627. https://doi.org/10.1111/febs.13999

de Andrade Mello, P., Bian, S., Savio, L. E. B., Zhang, H., Zhang, J., Junger, W., Wink, M. R., Lenz, G., Buffon, A., Wu, Y., & Robson, S. C. (2017). Hyperthermia and associated changes in membrane fluidity potentiate P2X7 activation to promote tumor cell death. *Oncotarget*, *8*(40), 67254–67268. https://doi.org/10.18632/oncotarget.18595

de Cabo, R., Fürer-Galbán, S., Anson, R., Gilman, C., Gorospe, M., & Lane, M. A. (2003). An in vitro model of caloric restriction. *Experimental Gerontology*, *38*(6), 631–639. https://doi.org/10.1016/S0531-5565(03)00055-X

de Mera-Rodríguez, J. A., Álvarez-Hernán, G., Gañán, Y., Martín-Partido, G., Rodríguez-León, J., & Francisco-Morcillo, J. (2021). Is Senescence-Associated -Galactosidase a Reliable in vivo Marker of Cellular Senescence During Embryonic Development? *Frontiers in Cell and Developmental Biology*, *9*, 623175. https://doi.org/10.3389/fcell.2021.623175

de Moraes, C. N., Maia, L., Dias, M. C., Dell'Aqua, C. P. F., da Mota, L. S. L. S., Chapwanya, A., Landim-Alvarenga, F. d. C., & Oba, E. (2016). Bovine endometrial cells: A source of mesenchymal stem/progenitor cells: Description and cryopreservation of bovine eMSCs. *Cell Biology International*, *40*(12), 1332–1339. https://doi.org/10.1002/cbin.10688

Dean, M. E., & Johnson, J. L. (2021). Human Hsp90 cochaperones: Perspectives on tissue-specific expression and identification of cochaperones with similar in vivo functions. *Cell Stress and Chaperones*, *26*(1), 3–13. https://doi.org/10.1007/s12192-020-01167-0

Debacq-Chainiaux, F., Erusalimsky, J. D., Campisi, J., & Toussaint, O. (2009). Protocols to detect senescence-associated beta-galactosidase (SA-betagal) activity, a biomarker of senescent cells in culture and in vivo. *Nature Protocols*, *4*(12), 1798–1806. https://doi.org/10.1038/nprot.2009.191

den Brave, F., Cairo, L. V., Jagadeesan, C., Ruger-Herreros, C., Mogk, A., Bukau, B., & Jentsch, S. (2020). Chaperone-Mediated Protein Disaggregation Triggers Proteolytic Clearance of Intra-nuclear Protein Inclusions. *Cell Reports*, *31*(9), 107680. https://doi.org/10.1016/j.celrep.2020.107680

Deschênes-Simard, X., Lessard, F., Gaumont-Leclerc, M.-F., Bardeesy, N., & Ferbeyre, G. (2014). Cellular senescence and protein degradation: Breaking down cancer. *Cell Cycle*, *13*(12), 1840–1858. https://doi.org/10.4161/cc.29335

Di Nicola, M., Carlo-Stella, C., Magni, M., Milanesi, M., Longoni, P. D., Matteucci, P., Grisanti, S., & Gianni, A. M. (2002). Human bone marrow stromal cells

suppress T-lymphocyte proliferation induced by cellular or nonspecific mitogenic stimuli. *Blood*, *99*(10), 3838–3843. https://doi.org/10.1182/blood.V99.10.3838

Dimri, G. P., Lee, X., Basile, G., Acosta, M., Scott, G., Roskelley, C., Medrano, E. E., Linskens, M., Rubelj, I., & Pereira-Smith, O. (1995). A biomarker that identifies senescent human cells in culture and in aging skin in vivo. *Proceedings of the National Academy of Sciences*, *92*(20), 9363–9367. https://doi.org/10.1073/pnas.92.20.9363

Dobin, A., Davis, C. A., Schlesinger, F., Drenkow, J., Zaleski, C., Jha, S., Batut, P., Chaisson, M., & Gingeras, T. R. (2013). STAR: Ultrafast universal RNA-seq aligner. *Bioinformatics*, *29*(1), 15–21. https://doi.org/10.1093/bioinformatics/bts635

Dobson, C. M. (2003). Protein folding and misfolding. *Nature*, *426*(6968), 884–890. https://doi.org/10.1038/nature02261

Duffy, D. J., Millane, R. C., & Frank, U. (2012). A heat shock protein and Wnt signaling crosstalk during axial patterning and stem cell proliferation. *Developmental Biology*, *362*(2), 271–281. https://doi.org/10.1016/j.ydbio.2011.11.014

Edelstein, A. D., Tsuchida, M. A., Amodaj, N., Pinkard, H., Vale, R. D., & Stuurman, N. (2014). Advanced methods of microscope control using Manager software. *Journal of Biological Methods*, *1*(2), 10. https://doi.org/10.14440/jbm.2014.36

Eftekharzadeh, B., Banduseela, V. C., Chiesa, G., Martínez-Cristóbal, P., Rauch, J. N., Nath, S. R., Schwarz, D. M. C., Shao, H., Marin-Argany, M., Di Sanza, C., Giorgetti, E., Yu, Z., Pierattelli, R., Felli, I. C., Brun-Heath, I., García, J., Nebreda, Á. R., Gestwicki, J. E., Lieberman, A. P., & Salvatella, X. (2019). Hsp70 and Hsp40 inhibit an inter-domain interaction necessary for transcriptional activity in the androgen receptor. *Nature Communications*, *10*(1), 3562. https://doi.org/10.1038/s41467-019-11594-y

Ehrenfried, J. A., Evers, B. M., Chu, K. U., Townsend, C. M., & Thompson, J. C. (1996). Caloric Restriction Increases the Expression of Heat Shock Protein in the Gut: *Annals of Surgery*, *223*(5), 592–599. https://doi.org/10.1097/00000658-199605000-00015

Elzi, D. J., Song, M., & Shiio, Y. (2016). Role of galactose in cellular senescence. *Experimental Gerontology*, *73*, 1–4. https://doi.org/10.1016/j.exger.2015.11.003

Evans, S. S., Repasky, E. A., & Fisher, D. T. (2015). Fever and the thermal regulation of immunity: The immune system feels the heat. *Nature Reviews Immunology*, *15*(6), 335–349. https://doi.org/10.1038/nri3843

Ewels, P., Magnusson, M., Lundin, S., & Käller, M. (2016). MultiQC: Summarize analysis results for multiple tools and samples in a single report. *Bioinformatics*, *32*(19), 3047–3048. https://doi.org/10.1093/bioinformatics/btw354

Ewing, B., & Green, P. (1998). Base-calling of automated sequencer traces using phred. II. Error probabilities. *Genome Research*, *8*(3), 186–194.

Fabregat, A., Sidiropoulos, K., Viteri, G., Forner, O., Marin-Garcia, P., Arnau, V., D'Eustachio, P., Stein, L., & Hermjakob, H. (2017). Reactome pathway analysis: A high-performance in-memory approach. *BMC Bioinformatics*, *18*(1), 142. https://doi.org/10.1186/s12859-017-1559-2

Faget, D. V., Ren, Q., & Stewart, S. A. (2019). Unmasking senescence: Context-dependent effects of SASP in cancer. *Nature Reviews Cancer*, *19*(8), 439–453. https://doi.org/10.1038/s41568-019-0156-2

Feng, C., Yang, M., Zhang, Y., Lan, M., Huang, B., Liu, H., & Zhou, Y. (2018). Cyclic mechanical tension reinforces DNA damage and activates the p53-p21-Rb pathway to induce premature senescence of nucleus pulposus cells. *International Journal of Molecular Medicine*. https://doi.org/10.3892/ijmm.2018.3522

Fernández-Fernández, M. R., Gragera, M., Ochoa-Ibarrola, L., Quintana-Gallardo, L., & Valpuesta, J. M. (2017). Hsp70 - a master regulator in protein degradation. *FEBS Letters*, *591*(17), 2648–2660. https://doi.org/10.1002/1873-3468.12751

Fong, K.-w., Leung, J. W.-c., Li, Y., Wang, W., Feng, L., Ma, W., Liu, D., Songyang, Z., & Chen, J. (2013). MTR120/KIAA1383, a novel microtubule-associated protein, promotes microtubule stability and ensures cytokinesis. *Journal of Cell Science*, *126*(Pt 3), 825–837. https://doi.org/10.1242/jcs.116137

Furuta, M., Kose, S., Koike, M., Shimi, T., Hiraoka, Y., Yoneda, Y., Haraguchi, T., & Imamoto, N. (2004). Heat-shock induced nuclear retention and recycling inhibition of importin alpha. *Genes to Cells*, *9*(5), 429–441. https://doi.org/10.1111/j.1356-9597.2004.00734.x

Gamerdinger, M., Hajieva, P., Kaya, A. M., Wolfrum, U., Hartl, F. U., & Behl, C. (2009). Protein quality control during aging involves recruitment of the macroautophagy pathway by BAG3. *The EMBO Journal*, *28*(7), 889–901. https://doi.org/10.1038/emboj.2009.29

Gao, F., Chiu, S. M., Motan, D. A. L., Zhang, Z., Chen, L., Ji, H.-L., Tse, H.-F., Fu, Q.-L., & Lian, Q. (2016). Mesenchymal stem cells and immunomodulation: Current status and future prospects. *Cell Death & Disease*, *7*(1), e2062–e2062. https://doi.org/10.1038/cddis.2015.327

Gao, Y., Zhu, Z., Zhao, Y., Hua, J., Ma, Y., & Guan, W. (2014). Multilineage Potential Research of Bovine Amniotic Fluid Mesenchymal Stem Cells. *International Journal of Molecular Sciences*, *15*(3), 3698–3710. https://doi.org/10.3390/ijms15033698

Garrido, C., Paul, C., Seigneuric, R., & Kampinga, H. (2012). The small heat shock proteins family: The long forgotten chaperones. *The International Journal of Biochemistry & Cell Biology*, *44*(10), 1588–1592. https://doi.org/10.1016/j.biocel.2012.02.022

Gavilán, E., Pintado, C., Gavilan, M. P., Daza, P., Sánchez-Aguayo, I., Castaño, A., & Ruano, D. (2015). Age-related dysfunctions of the autophagy lysosomal pathway in hippocampal pyramidal neurons under proteasome stress. *Neurobiology of Aging*, *36*(5), 1953–1963. https://doi.org/10.1016/j.neurobiolaging.2015.02.025

Ghosh, S., Dutta, K., & Basu, A. (2013). Chandipura Virus Induces Neuronal Death through Fas-Mediated Extrinsic Apoptotic Pathway. *Journal of Virology*, *87*(22), 12398–12406. https://doi.org/10.1128/JVI.01864-13

Ghosh, S., Kumar, G. V., Basu, A., & Banerjee, A. (2015). Graph theoretic network analysis reveals protein pathways underlying cell death following neurotropic viral infection. *Scientific Reports*, *5*(1), 14438. https://doi.org/10.1038/srep14438

Gilbert, H. T. J. (2011). *The response of human annulus fibrosus cells to cyclic tensile strain : Evidence for an altered mechanotransduction pathway with intervertebral disc degeneration.* (Print). The University of Manchester.

Gilbert, H. T. J., Mallikarjun, V., Dobre, O., Jackson, M. R., Pedley, R., Gilmore, A. P., Richardson, S. M., & Swift, J. (2019). Nuclear decoupling is part of a rapid protein-level cellular response to high-intensity mechanical loading. *Nature Communications*, *10*(1), 4149. https://doi.org/10.1038/s41467-019-11923-1

Goenka, A., Parihar, R., & Ganesh, S. (2018). Heat Shock-Induced Transcriptional and Translational Arrest in Mammalian Cells (A. A. A. Asea & P. Kaur, Eds.). In A. A. A. Asea & P. Kaur (Eds.), *Heat Shock Proteins and Stress*. Cham, Springer International Publishing. https://doi.org/10.1007/978-3-319-90725-3_12

Goldschmidt, R. (1935). Gen und Außeneigenschaft: (Untersuchungen anDrosophila) II. *Zeitschrift für Induktive Abstammungs- und Vererbungslehre*, *69*(1), 70–131. https://doi.org/10.1007/BF01762871

Gomez-Pastor, R., Burchfiel, E. T., Neef, D. W., Jaeger, A. M., Cabiscol, E., McKinstry, S. U., Doss, A., Aballay, A., Lo, D. C., Akimov, S. S., Ross, C. A., Eroglu, C., & Thiele, D. J. (2017). Abnormal degradation of the neuronal stress-protective transcription factor HSF1 in Huntington's disease. *Nature Communications*, *8*(1), 14405. https://doi.org/10.1038/ncomms14405

González-González, L., & Alonso, J. (2018). Periostin: A Matricellular Protein With Multiple Functions in Cancer Development and Progression. *Frontiers in Oncology*, *8*. https://doi.org/10.3389/fonc.2018.00225

Graham, D. E., Harich, K. C., & White, R. H. (2003). Reductive dehalogenation of monobromobimane by tris(2-carboxyethyl)phosphine. *Analytical Biochemistry*, *318*(2), 325–328. https://doi.org/10.1016/S0003-2697(03)00239-2

Graner, M. W., Cumming, R. I., & Bigner, D. D. (2007). The Heat Shock Response and Chaperones/Heat Shock Proteins in Brain Tumors: Surface Expression, Release, and Possible Immune Consequences. *Journal of Neuroscience*, *27*(42), 11214–11227. https://doi.org/10.1523/JNEUROSCI.3588-07.2007

Grantham, J. (2020). The Molecular Chaperone CCT/TRiC: An Essential Component of Proteostasis and a Potential Modulator of Protein Aggregation. *Frontiers in Genetics*, *11*. https://doi.org/10.3389/fgene.2020.00172

Guerrero, A., Guiho, R., Herranz, N., Uren, A., Withers, D. J., Martínez-Barbera, J. P., Tietze, L. F., & Gil, J. (2020). Galactose-modified duocarmycin prodrugs as senolytics. *Aging Cell*, *19*(4), e13133. https://doi.org/https://doi.org/10.1111/acel.13133

Gunawardena, J. (2012). Some lessons about models from Michaelis and Menten. *Molecular Biology of the Cell*, *23*(4), 517–519. https://doi.org/10.1091/mbc.E11-07-0643

Gunawardena, J. (2013). Biology is more theoretical than physics. *Molecular Biology of the Cell*, *24*(12), 1827–1829. https://doi.org/10.1091/mbc.E12-03-0227

Gunawardena, J. (2014). Models in biology:
accurate descriptions of our pathetic thinking'. *BMC Biology*, *12*(1), 29. https://doi.org/10.1186/1741-7007-12-29

Gundry, R. L., White, M. Y., Murray, C. I., Kane, L. A., Fu, Q., Stanley, B. A., & Van Eyk, J. E. (2009). Preparation of Proteins and Peptides for Mass Spectrometry Analysis in a Bottom-Up Proteomics Workflow, In *Current Protocols in Molecular Biology*. Hoboken, NJ, USA, John Wiley & Sons, Inc. https://doi.org/10.1002/0471142727.mb1025s88

Guo, M., Weng, G., Yin, D., Hu, X., Han, J., Du, Y., Liu, Y., Tang, D., & Pan, Y. (2015). Identification of the over alkylation sites of a protein by IAM in MALDI-TOF/TOF tandem mass spectrometry. *RSC Advances*, *5*(125), 103662–103668. https://doi.org/10.1039/C5RA18595E

Gutsmann-Conrad, A., Heydari, A. R., You, S., & Richardson, A. (1998). The Expression of Heat Shock Protein 70 Decreases with Cellular Senescencein Vitroand in Cells Derived from Young and Old Human Subjects. *Experimental Cell Research*, *241*(2), 404–413. https://doi.org/10.1006/excr.1998.4069

Hall, D. M., Oberley, T. D., Moseley, P. M., Buettner, G. R., Oberley, L. W., Weindruch, R., & Kregel, K. C. (2000). Caloric restriction improves thermotolerance and reduces hyperthermia-induced cellular damage in old rats. *The FASEB Journal*, *14*(1), 78–86. https://doi.org/https://doi.org/10.1096/fasebj.14.1.78

Harrison, C. (2003). GrpE, a nucleotide exchange factor for DnaK. *Cell Stress & Chaperones*, *8*(3), 218–224. https://doi.org/10.1379/1466-1268(2003)008⟨0218:ganeff⟩2.0.co;2

Hartl, F. U., Bracher, A., & Hayer-Hartl, M. (2011). Molecular chaperones in protein folding and proteostasis. *Nature*, *475*(7356), 324–332. https://doi.org/10.1038/nature10317

Haslbeck, M., Franzmann, T., Weinfurtner, D., & Buchner, J. (2005). Some like it hot: The structure and function of small heat-shock proteins. *Nature Structural & Molecular Biology*, *12*(10), 842–846. https://doi.org/10.1038/nsmb993

Hauser, M. A., Li, Y.-J., Xu, H., Noureddine, M. A., Shao, Y. S., Gullans, S. R., Scherzer, C. R., Jensen, R. V., McLaurin, A. C., Gibson, J. R., Scott, B. L., Jewett, R. M., Stenger, J. E., Schmechel, D. E., Hulette, C. M., & Vance, J. M. (2005). Expression Profiling of Substantia Nigra in Parkinson Disease, Progressive Supranuclear Palsy, and Frontotemporal Dementia With Parkinsonism. *Archives of Neurology*, *62*(6). https://doi.org/10.1001/archneur.62.6.917

Hein, M. Y., Hubner, N. C., Poser, I., Cox, J., Nagaraj, N., Toyoda, Y., Gak, I. A., Weisswange, I., Mansfeld, J., Buchholz, F., Hyman, A. A., & Mann, M. (2015). A human interactome in three quantitative dimensions organized by stoichiometries and abundances. *Cell*, *163*(3), 712–723. https://doi.org/10.1016/j.cell.2015.09.053

Hentze, N., Le Breton, L., Wiesner, J., Kempf, G., & Mayer, M. P. (2016). Molecular mechanism of thermosensory function of human heat shock transcription factor Hsf1. *eLife*, *5*, e11576. https://doi.org/10.7554/eLife.11576

Hernandez-Segura, A., Nehme, J., & Demaria, M. (2018). Hallmarks of Cellular Senescence. *Trends in Cell Biology*, *28*(6), 436–453. https://doi.org/10.1016/j.tcb.2018.02.001

Heuck, A., Schitter-Sollner, S., Suskiewicz, M. J., Kurzbauer, R., Kley, J., Schleiffer, A., Rombaut, P., Herzog, F., & Clausen, T. (2016). Structural basis for the

disaggregase activity and regulation of Hsp104 (M. Hayer-Hartl, Ed.). *eLife*, *5*, e21516. https://doi.org/10.7554/eLife.21516

Heuer, E., Rosen, R. F., Cintron, A., & Walker, L. C. (2012). Nonhuman primate models of Alzheimer-like cerebral proteopathy. *Current Pharmaceutical Design*, *18*(8), 1159–1169. https://doi.org/10.2174/138161212799315885

Hewitt, G., Jurk, D., Marques, F. D. M., Correia-Melo, C., Hardy, T., Gackowska, A., Anderson, R., Taschuk, M., Mann, J., & Passos, J. F. (2012). Telomeres are favoured targets of a persistent DNA damage response in ageing and stress-induced senescence. *Nature Communications*, *3*(1), 708. https://doi.org/10.1038/ncomms1708

Hill, A. B. T., Bressan, F. F., Murphy, B. D., & Garcia, J. M. (2019). Applications of mesenchymal stem cell technology in bovine species. *Stem Cell Research & Therapy*, *10*(1), 44. https://doi.org/10.1186/s13287-019-1145-9

Hipp, M. S., Kasturi, P., & Hartl, F. U. (2019). The proteostasis network and its decline in ageing. *Nature Reviews Molecular Cell Biology*, *20*(7), 421–435. https://doi.org/10.1038/s41580-019-0101-y

Hipp, M. S., Park, S.-H., & Hartl, F. U. (2014). Proteostasis impairment in protein-misfolding and -aggregation diseases. *Trends in Cell Biology*, *24*(9), 506–514. https://doi.org/10.1016/j.tcb.2014.05.003

Hirota, K., Nakamura, H., Masutani, H., & Yodoi, J. (2002). Thioredoxin Superfamily and Thioredoxin-Inducing Agents. *Annals of the New York Academy of Sciences*, *957*(1), 189–199. https://doi.org/https://doi.org/10.1111/j.1749-6632.2002.tb02916.x

Ho, S.-C., Liu, J.-H., & Wu, R.-Y. (2003). Establishment of the mimetic aging effect in mice caused by D-galactose. *Biogerontology*, *4*(1), 15–18. https://doi.org/10.1023/a:1022417102206

Houry, W. A., Bertrand, E., & Coulombe, B. (2018). The PAQosome, an R2TP-Based Chaperone for Quaternary Structure Formation. *Trends in Biochemical Sciences*, *43*(1), 4–9. https://doi.org/10.1016/j.tibs.2017.11.001

Hsu, A.-L. (2003). Regulation of Aging and Age-Related Disease by DAF-16 and Heat-Shock Factor. *Science*, *300*(5622), 1142–1145. https://doi.org/10.1126/science.1083701

Hu, G. (2006). A novel endothelial-specific heat shock protein HspA12B is required in both zebrafish development and endothelial functions in vitro. *Journal of Cell Science*, *119*(19), 4117–4126. https://doi.org/10.1242/jcs.03179

Iaccarino, H. F., Singer, A. C., Martorell, A. J., Rudenko, A., Gao, F., Gillingham, T. Z., Mathys, H., Seo, J., Kritskiy, O., Abdurrob, F., Adaikkan, C., Canter, R. G., Rueda, R., Brown, E. N., Boyden, E. S., & Tsai, L.-H. (2016). Gamma frequency entrainment attenuates amyloid load and modifies microglia. *Nature*, *540*(7632), 230–235. https://doi.org/10.1038/nature20587

Ichhaporia, V. P., & Hendershot, L. M. (2021). Role of the HSP70 Co-Chaperone SIL1 in Health and Disease. *International Journal of Molecular Sciences*, *22*(4), 1564. https://doi.org/10.3390/ijms22041564

Jarnuczak, A. F., Albornoz, M. G., Eyers, C. E., Grant, C. M., & Hubbard, S. J. (2018). A quantitative and temporal map of proteostasis during heat shock in *Saccharomyces cerevisiae*. *Molecular Omics*, *14*(1), 37–52. https://doi.org/10.1039/C7MO00050B

Jayaraj, G. G., Hipp, M. S., & Hartl, F. U. (2020). Functional Modules of the Proteostasis Network. *Cold Spring Harbor Perspectives in Biology*, *12*(1), a033951. https://doi.org/10.1101/cshperspect.a033951

Jeon, O. H., David, N., Campisi, J., & Elisseeff, J. H. (2018). Senescent cells and osteoarthritis: A painful connection. *Journal of Clinical Investigation*, *128*(4), 1229–1237. https://doi.org/10.1172/JCI95147

Jeon, R.-H., Lee, W.-J., Son, Y.-B., Bharti, D., Shivakumar, S. B., Lee, S.-L., & Rho, G.-J. (2019). PPIA, HPRT1, and YWHAZ Genes Are Suitable for Normalization of mRNA Expression in Long-Term Expanded Human Mesenchymal Stem Cells. *BioMed Research International*, *2019*, 3093545. https://doi.org/10.1155/2019/3093545

Jeong, S., Lim, S., Schevzov, G., Gunning, P. W., & Helfman, D. M. (2017). Loss of Tpm4.1 leads to disruption of cell-cell adhesions and invasive behavior in breast epithelial cells via increased Rac1 signaling. *Oncotarget*, *8*(20), 33544–33559. https://doi.org/10.18632/oncotarget.16825

Jeronimo, C., Forget, D., Bouchard, A., Li, Q., Chua, G., Poitras, C., Thérien, C., Bergeron, D., Bourassa, S., Greenblatt, J., Chabot, B., Poirier, G. G., Hughes, T. R., Blanchette, M., Price, D. H., & Coulombe, B. (2007). Systematic Analysis of the Protein Interaction Network for the Human Transcription Machinery Reveals the Identity of the 7SK Capping Enzyme. *Molecular Cell*, *27*(2), 262–274. https://doi.org/10.1016/j.molcel.2007.06.027

Jiang, J., Maes, E. G., Taylor, A. B., Wang, L., Hinck, A. P., Lafer, E. M., & Sousa, R. (2007). Structural basis of J cochaperone binding and regulation of Hsp70. *Molecular Cell*, *28*(3), 422–433. https://doi.org/10.1016/j.molcel.2007.08.022

Johnson, C. P., Tang, H.-Y., Carag, C., Speicher, D. W., & Discher, D. E. (2007). Forced Unfolding of Proteins Within Cells. *Science*, *317*(5838), 663–666. https://doi.org/10.1126/science.1139857

Jolly, C., Konecny, L., Grady, D. L., Kutskova, Y. A., Cotto, J. J., Morimoto, R. I., & Vourc'h, C. (2002). In vivo binding of active heat shock transcription factor 1 to human chromosome 9 heterochromatin during stress. *Journal of Cell Biology*, *156*(5), 775–781. https://doi.org/10.1083/jcb.200109018

Jones, M. C., Zha, J., & Humphries, M. J. (2019). Connections between the cell cycle, cell adhesion and the cytoskeleton. *Philosophical Transactions of the Royal Society B: Biological Sciences*, *374*(1779), 20180227. https://doi.org/10.1098/rstb.2018.0227

Kabat, M., Bobkov, I., Kumar, S., & Grumet, M. (2020). Trends in mesenchymal stem cell clinical trials 2004-2018: Is efficacy optimal in a narrow dose range? *STEM CELLS Translational Medicine*, *9*(1), 17–27. https://doi.org/https://doi.org/10.1002/sctm.19-0202

Kabbage, M., & Dickman, M. B. (2008). The BAG proteins: A ubiquitous family of chaperone regulators. *Cellular and Molecular Life Sciences*, *65*(9), 1390–1402. https://doi.org/10.1007/s00018-008-7535-2

Kaisari, S., Sitry-Shevah, D., Miniowitz-Shemtov, S., Teichner, A., & Hershko, A. (2017). Role of CCT chaperonin in the disassembly of mitotic checkpoint complexes. *Proceedings of the National Academy of Sciences*, *114*(5), 956–961. https://doi.org/10.1073/pnas.1620451114

Kamentsky, L., Jones, T. R., Fraser, A., Bray, M.-A., Logan, D. J., Madden, K. L., Ljosa, V., Rueden, C., Eliceiri, K. W., & Carpenter, A. E. (2011). Im-

proved structure, function and compatibility for CellProfiler: Modular high-throughput image analysis software. *Bioinformatics*, *27*(8), 1179–1180. https://doi.org/10.1093/bioinformatics/btr095

Kampinga, H. H., & Craig, E. A. (2010). The HSP70 chaperone machinery: J proteins as drivers of functional specificity. *Nature Reviews Molecular Cell Biology*, *11*(8), 579–592. https://doi.org/10.1038/nrm2941

Kampinga, H., Brunsting, J., Stege, G., Konings, A., & Landry, J. (1994). Cells Overexpressing Hsp27 Show Accelerated Recovery from Heat-Induced Nuclear-Protein Aggregation. *Biochemical and Biophysical Research Communications*, *204*(3), 1170–1177. https://doi.org/10.1006/bbrc.1994.2586

Kantidze, O. L., Velichko, A. K., & Razin, S. V. (2015). Heat stress-induced transcriptional repression. *Biochemistry (Moscow)*, *80*(8), 990–993. https://doi.org/10.1134/S0006297915080039

Kaushik, S., & Cuervo, A. M. (2015). Proteostasis and aging. *Nature Medicine*, *21*(12), 1406–1415. https://doi.org/10.1038/nm.4001

Khan, M., Mohsin, S., Khan, S. N., & Riazuddin, S. (2011). Repair of senescent myocardium by mesenchymal stem cells is dependent on the age of donor mice. *Journal of Cellular and Molecular Medicine*, *15*(7), 1515–1527. https://doi.org/10.1111/j.1582-4934.2009.00998.x

Kiernan, J. A. (2007). Indigogenic substrates for detection and localization of enzymes. *Biotechnic & Histochemistry: Official Publication of the Biological Stain Commission*, *82*(2), 73–103. https://doi.org/10.1080/10520290701375278

Kim, G., Meriin, A. B., Gabai, V. L., Christians, E., Benjamin, I., Wilson, A., Wolozin, B., & Sherman, M. Y. (2012). The heat shock transcription factor Hsf1 is downregulated in DNA damage-associated senescence, contributing to the maintenance of senescence phenotype: Role of Hsf1 in senescence. *Aging Cell*, *11*(4), 617–627. https://doi.org/10.1111/j.1474-9726.2012.00827.x

Kim, H. Y., Kim, H. V., Jo, S., Lee, C. J., Choi, S. Y., Kim, D. J., & Kim, Y. (2015). EPPS rescues hippocampus-dependent cognitive deficits in APP/PS1 mice by disaggregation of amyloid- oligomers and plaques. *Nature Communications*, *6*(1), 8997. https://doi.org/10.1038/ncomms9997

Kim, Y. E., Hipp, M. S., Bracher, A., Hayer-Hartl, M., & Ulrich Hartl, F. (2013). Molecular Chaperone Functions in Protein Folding and Proteostasis. *Annual Review of Biochemistry*, *82*(1), 323–355. https://doi.org/10.1146/annurev-biochem-060208-092442

King, A. (2018). The search for better animal models of Alzheimer's disease. *Nature*, *559*(7715), S13–S15. https://doi.org/10.1038/d41586-018-05722-9

Klaips, C. L., Jayaraj, G. G., & Hartl, F. U. (2017). Pathways of cellular proteostasis in aging and disease. *Journal of Cell Biology*, *217*(1), 51–63. https://doi.org/10.1083/jcb.201709072

Klyushnenkova, E., Mosca, J. D., Zernetkina, V., Majumdar, M. K., Beggs, K. J., Simonetti, D. W., Deans, R. J., & McIntosh, K. R. (2005). T cell responses to allogeneic human mesenchymal stem cells: Immunogenicity, tolerance, and suppression. *Journal of Biomedical Science*, *12*(1), 47–57. https://doi.org/10.1007/s11373-004-8183-7

Kmiecik, S. W., Le Breton, L., & Mayer, M. P. (2020). Feedback regulation of heat shock factor 1 (Hsf1) activity by Hsp70-mediated trimer unzipping and

dissociation from DNA. *The EMBO Journal*, *39*(14). https://doi.org/10.15252/embj.2019104096

Koga, H., Kaushik, S., & Cuervo, A. M. (2011). Protein homeostasis and aging: The importance of exquisite quality control. *Ageing Research Reviews*, *10*(2), 205–215. https://doi.org/10.1016/j.arr.2010.02.001

Komatsu, M., Waguri, S., Chiba, T., Murata, S., Iwata, J.-i., Tanida, I., Ueno, T., Koike, M., Uchiyama, Y., Kominami, E., & Tanaka, K. (2006). Loss of autophagy in the central nervous system causes neurodegeneration in mice. *Nature*, *441*(7095), 880–884. https://doi.org/10.1038/nature04723

Kose, S., Furuta, M., & Imamoto, N. (2012). Hikeshi, a Nuclear Import Carrier for Hsp70s, Protects Cells from Heat Shock-Induced Nuclear Damage. *Cell*, *149*(3), 578–589. https://doi.org/10.1016/j.cell.2012.02.058

Kotoglou, P., Kalaitzakis, A., Vezyraki, P., Tzavaras, T., Michalis, L. K., Dantzer, F., Jung, J. U., & Angelidis, C. (2009). Hsp70 translocates to the nuclei and nucleoli, binds to XRCC1 and PARP-1, and protects HeLa cells from single-strand DNA breaks. *Cell Stress and Chaperones*, *14*(4), 391–406. https://doi.org/10.1007/s12192-008-0093-6

Kotormán, M., Laczkó, I., Szabó, A., & Simon, L. (2003). Effects of Ca2+ on catalytic activity and conformation of trypsin and -chymotrypsin in aqueous ethanol. *Biochemical and Biophysical Research Communications*, *304*(1), 18–21. https://doi.org/10.1016/S0006-291X(03)00534-5

Krakowiak, J., Zheng, X., Patel, N., Feder, Z. A., Anandhakumar, J., Valerius, K., Gross, D. S., Khalil, A. S., & Pincus, D. (2018). Hsf1 and Hsp70 constitute a two-component feedback loop that regulates the yeast heat shock response. *eLife*, *7*, e31668. https://doi.org/10.7554/eLife.31668

Krasnodembskaya, A., Song, Y., Fang, X., Gupta, N., Serikov, V., Lee, J.-W., & Matthay, M. A. (2010). Antibacterial effect of human mesenchymal stem cells is mediated in part from secretion of the antimicrobial peptide LL-37. *Stem Cells (Dayton, Ohio)*, *28*(12), 2229–2238. https://doi.org/10.1002/stem.544

Kriegenburg, F., Jakopec, V., Poulsen, E. G., Nielsen, S. V., Roguev, A., Krogan, N., Gordon, C., Fleig, U., & Hartmann-Petersen, R. (2014). A Chaperone-Assisted Degradation Pathway Targets Kinetochore Proteins to Ensure Genome Stability (J. L. Brodsky, Ed.). *PLoS Genetics*, *10*(1), e1004140. https://doi.org/10.1371/journal.pgen.1004140

Krishna, S., Jensen, M. H., & Sneppen, K. (2006). Minimal model of spiky oscillations in NF- B signaling. *Proceedings of the National Academy of Sciences*, *103*(29), 10840–10845. https://doi.org/10.1073/pnas.0604085103

Krukenberg, K. A., Street, T. O., Lavery, L. A., & Agard, D. A. (2011). Conformational dynamics of the molecular chaperone Hsp90. *Quarterly Reviews of Biophysics*, *44*(2), 229–255. https://doi.org/10.1017/S0033583510000314

Kundrat, L., & Regan, L. (2010). Balance between Folding and Degradation for Hsp90-Dependent Client Proteins: A Key Role for CHIP. *Biochemistry*, *49*(35), 7428–7438. https://doi.org/10.1021/bi100386w

Kurz, D. J., Decary, S., Hong, Y., & Erusalimsky, J. D. (2000). Senescence-associated (beta)-galactosidase reflects an increase in lysosomal mass during replicative ageing of human endothelial cells. *Journal of Cell Science*, *113 (Pt 20)*, 3613–3622.

Labbadia, J., & Morimoto, R. I. (2015). The Biology of Proteostasis in Aging and Disease. *Annual Review of Biochemistry*, *84*(1), 435–464. https://doi.org/10.1146/annurev-biochem-060614-033955

Lackie, R. E., Maciejewski, A., Ostapchenko, V. G., Marques-Lopes, J., Choy, W.-Y., Duennwald, M. L., Prado, V. F., & Prado, M. A. M. (2017). The Hsp70/Hsp90 Chaperone Machinery in Neurodegenerative Diseases. *Frontiers in Neuroscience*, *11*, 254. https://doi.org/10.3389/fnins.2017.00254

Lau, E., Kluger, H., Varsano, T., Lee, K., Scheffler, I., Rimm, D. L., Ideker, T., & Ronai, Z. A. (2012). PKC promotes oncogenic functions of ATF2 in the nucleus while blocking its apoptotic function at mitochondria. *Cell*, *148*(3), 543–555. https://doi.org/10.1016/j.cell.2012.01.016

Lazarus, H. M., Koc, O. N., Devine, S. M., Curtin, P., Maziarz, R. T., Holland, H. K., Shpall, E. J., McCarthy, P., Atkinson, K., Cooper, B. W., Gerson, S. L., Laughlin, M. J., Loberiza, F. R., Moseley, A. B., & Bacigalupo, A. (2005). Cotransplantation of HLA-identical sibling culture-expanded mesenchymal stem cells and hematopoietic stem cells in hematologic malignancy patients. *Biology of Blood and Marrow Transplantation: Journal of the American Society for Blood and Marrow Transplantation*, *11*(5), 389–398. https://doi.org/10.1016/j.bbmt.2005.02.001

Lee, B. Y., Han, J. A., Im, J. S., Morrone, A., Johung, K., Goodwin, E. C., Kleijer, W. J., DiMaio, D., & Hwang, E. S. (2006). Senescence-associated beta-galactosidase is lysosomal beta-galactosidase. *Aging Cell*, *5*(2), 187–195. https://doi.org/10.1111/j.1474-9726.2006.00199.x

Lee, D., Hokinson, D., Park, S., Elvira, R., Kusuma, F., Lee, J.-M., Yun, M., Lee, S.-G., & Han, J. (2019). ER Stress Induces Cell Cycle Arrest at the G2/M Phase Through eIF2 Phosphorylation and GADD45. *International Journal of Molecular Sciences*, *20*(24), 6309. https://doi.org/10.3390/ijms20246309

Lee, J.-H., Gao, J., Kosinski, P. A., Elliman, S. J., Hughes, T. E., Gromada, J., & Kemp, D. M. (2013). Heat shock protein 90 (HSP90) inhibitors activate the heat shock factor 1 (HSF1) stress response pathway and improve glucose regulation in diabetic mice. *Biochemical and Biophysical Research Communications*, *430*(3), 1109–1113. https://doi.org/10.1016/j.bbrc.2012.12.029

Lee, J. S., Hong, J. M., Moon, G. J., Lee, P. H., Ahn, Y. H., & Bang, O. Y. (2010). A Long-Term Follow-Up Study of Intravenous Autologous Mesenchymal Stem Cell Transplantation in Patients With Ischemic Stroke. *STEM CELLS*, *28*(6), 1099–1106. https://doi.org/https://doi.org/10.1002/stem.430

Lee, J., Sung, N., Yeo, L., Chang, C., Lee, S., & Tsai, F. T. (2017). Structural determinants for protein unfolding and translocation by the Hsp104 protein disaggregase. *Bioscience Reports*, *37*(6), BSR20171399. https://doi.org/10.1042/BSR20171399

Leu, J. I.-J., Pimkina, J., Frank, A., Murphy, M. E., & George, D. L. (2009). A Small Molecule Inhibitor of Inducible Heat Shock Protein 70. *Molecular Cell*, *36*(1), 15–27. https://doi.org/10.1016/j.molcel.2009.09.023

Leu, J. I.-J., Pimkina, J., Pandey, P., Murphy, M. E., & George, D. L. (2011). HSP70 Inhibition by the Small-Molecule 2-Phenylethynesulfonamide Impairs Protein Clearance Pathways in Tumor Cells. *Molecular Cancer Research*, *9*(7), 936–947. https://doi.org/10.1158/1541-7786.MCR-11-0019

Leu, J. I.-J., Barnoud, T., Zhang, G., Tian, T., Wei, Z., Herlyn, M., Murphy, M. E., & George, D. L. (2017). Inhibition of stress-inducible HSP70 impairs mitochondrial proteostasis and function. *Oncotarget*, *8*(28), 45656–45669. https://doi.org/10.18632/oncotarget.17321

Lever, J., Krzywinski, M., & Altman, N. (2017). Principal component analysis. *Nature Methods*, *14*(7), 641–642. https://doi.org/10.1038/nmeth.4346

Li, X., Yang, Q., Bai, J., Xuan, Y., & Wang, Y. (2015). Identification of appropriate reference genes for human mesenchymal stem cell analysis by quantitative real-time PCR. *Biotechnology Letters*, *37*(1), 67–73. https://doi.org/10.1007/s10529-014-1652-9

Li, Y., Yan, M., Wang, Z., Zheng, Y., Li, J., Ma, S., Liu, G., & Yu, J. (2014). 17beta-estradiol promotes the odonto/osteogenic differentiation of stem cells from apical papilla via mitogen-activated protein kinase pathway. *Stem Cell Research & Therapy*, *5*(6), 125. https://doi.org/10.1186/scrt515

Lim, J., & Yue, Z. (2015). Neuronal Aggregates: Formation, Clearance, and Spreading. *Developmental Cell*, *32*(4), 491–501. https://doi.org/10.1016/j.devcel.2015.02.002

Lin, Y., Huo, L., Liu, Z., Li, J., Liu, Y., He, Q., Wang, X., & Liang, S. (2013). Sodium Laurate, a Novel Protease- and Mass Spectrometry-Compatible Detergent for Mass Spectrometry-Based Membrane Proteomics (M. Massiah, Ed.). *PLoS ONE*, *8*(3), e59779. https://doi.org/10.1371/journal.pone.0059779

Lin, Y., Zhou, J., Bi, D., Chen, P., Wang, X., & Liang, S. (2008). Sodium-deoxycholate-assisted tryptic digestion and identification of proteolytically resistant proteins. *Analytical Biochemistry*, *377*(2), 259–266. https://doi.org/10.1016/j.ab.2008.03.009

Lin, Y.-H., Zhen, Y.-Y., Chien, K.-Y., Lee, I.-C., Lin, W.-C., Chen, M.-Y., & Pai, L.-M. (2017). LIMCH1 regulates nonmuscle myosin-II activity and suppresses cell migration (L. Blanchoin, Ed.). *Molecular Biology of the Cell*, *28*(8), 1054–1065. https://doi.org/10.1091/mbc.e15-04-0218

Liu, J., Ding, Y., Liu, Z., & Liang, X. (2020). Senescence in Mesenchymal Stem Cells: Functional Alterations, Molecular Mechanisms, and Rejuvenation Strategies. *Frontiers in Cell and Developmental Biology*, *8*. https://doi.org/10.3389/fcell.2020.00258

Liu, Q., Liang, C., & Zhou, L. (2020). Structural and functional analysis of the Hsp70/Hsp40 chaperone system. *Protein Science*, *29*(2), 378–390. https://doi.org/10.1002/pro.3725

Liu, S.-Q., Ji, X.-L., Tao, Y., Tan, D.-Y., Zhang, K.-Q., & Fu, Y.-X. (2012). Protein Folding, Binding and Energy Landscape: A Synthesis (P. Kaumaya, Ed.). In P. Kaumaya (Ed.), *Protein Engineering*. InTech. https://doi.org/10.5772/30440

Liu, X., Lin, C.-Y., Lei, M., Yan, S., Zhou, T., & Erikson, R. L. (2005). CCT Chaperonin Complex Is Required for the Biogenesis of Functional Plk1. *Molecular and Cellular Biology*, *25*(12), 4993–5010. https://doi.org/10.1128/MCB.25.12.4993-5010.2005

Livak, K. J., & Schmittgen, T. D. (2001). Analysis of Relative Gene Expression Data Using Real-Time Quantitative PCR and the 2CT Method. *Methods*, *25*(4), 402–408. https://doi.org/10.1006/meth.2001.1262

Livingston, G., Sommerlad, A., Orgeta, V., Costafreda, S. G., Huntley, J., Ames, D., Ballard, C., Banerjee, S., Burns, A., Cohen-Mansfield, J., Cooper, C., Fox, N., Gitlin, L. N., Howard, R., Kales, H. C., Larson, E. B., Ritchie, K., Rockwood, K., Sampson, E. L., ... Mukadam, N. (2017). Dementia prevention, intervention, and care. *The Lancet*, *390*(10113), 2673–2734. https://doi.org/10.1016/S0140-6736(17)31363-6

López-Otín, C., Blasco, M. A., Partridge, L., Serrano, M., & Kroemer, G. (2013). The Hallmarks of Aging. *Cell*, *153*(6), 1194–1217. https://doi.org/10.1016/j.cell.2013.05.039

Love, M. I., Huber, W., & Anders, S. (2014). Moderated estimation of fold change and dispersion for RNA-seq data with DESeq2. *Genome Biology*, *15*(12), 550. https://doi.org/10.1186/s13059-014-0550-8

Lukomska, B., Stanaszek, L., Zuba-Surma, E., Legosz, P., Sarzynska, S., & Drela, K. (2019). Challenges and Controversies in Human Mesenchymal Stem Cell Therapy. https://doi.org/https://doi.org/10.1155/2019/9628536

Mackenzie, R. (2017). *Investigating the Heat Shock Response of the Yeast Proteome via Quantitative Proteomics* (Print). The University of Manchester. Manchester, England.

Madeo, F., Zimmermann, A., Maiuri, M. C., & Kroemer, G. (2015). Essential role for autophagy in life span extension. *Journal of Clinical Investigation*, *125*(1), 85–93. https://doi.org/10.1172/JCI73946

Magalhães, J. P., & Passos, J. F. (2018). Stress, cell senescence and organismal ageing. *Mechanisms of Ageing and Development*, *170*, 2–9. https://doi.org/10.1016/j.mad.2017.07.001

Magalhães, J. (2004). From cells to ageing: A review of models and mechanisms of cellular senescence and their impact on human ageing. *Experimental Cell Research*, *300*(1), 1–10. https://doi.org/10.1016/j.yexcr.2004.07.006

Magni, S., Succurro, A., Skupin, A., & Ebenhöh, O. (2018). Data-driven dynamical model indicates that the heat shock response in Chlamydomonas reinhardtii is tailored to handle natural temperature variation. *Journal of The Royal Society Interface*, *15*(142), 20170965. https://doi.org/10.1098/rsif.2017.0965

Mahat, D. B., Salamanca, H. H., Duarte, F. M., Danko, C. G., & Lis, J. T. (2016). Mammalian Heat Shock Response and Mechanisms Underlying Its Genome-wide Transcriptional Regulation. *Molecular Cell*, *62*(1), 63–78. https://doi.org/10.1016/j.molcel.2016.02.025

Mallikarjun, V., Richardson, S. M., & Swift, J. (2020). BayesENproteomics: Bayesian Elastic Nets for Quantification of Peptidoforms in Complex Samples. *Journal of Proteome Research*, *19*(6), 2167–2184. https://doi.org/10.1021/acs.jproteome.9b00468

Malyshev, I. (2013). *Immunity, Tumors and Aging: The Role of HSP70* (Vol. 6). Dordrecht, Springer Netherlands. https://doi.org/10.1007/978-94-007-5943-5

Mann, M. (2006). Functional and quantitative proteomics using SILAC. *Nature Reviews Molecular Cell Biology*, *7*(12), 952–958. https://doi.org/10.1038/nrm2067

Mao, R.-F., Rubio, V., Chen, H., Bai, L., Mansour, O. C., & Shi, Z.-Z. (2013). OLA1 protects cells in heat shock by stabilizing HSP70. *Cell Death & Disease*, *4*(2), e491–e491. https://doi.org/10.1038/cddis.2013.23

Markoski, M. M. (2016). Advances in the Use of Stem Cells in Veterinary Medicine: From Basic Research to Clinical Practice. *Scientifica*, *2016*(4516920). https://doi.org/https://doi.org/10.1155/2016/4516920

Marroquin, L. D., Hynes, J., Dykens, J. A., Jamieson, J. D., & Will, Y. (2007). Circumventing the Crabtree effect: Replacing media glucose with galactose increases susceptibility of HepG2 cells to mitochondrial toxicants. *Toxicological Sciences: An Official Journal of the Society of Toxicology*, *97*(2), 539–547. https://doi.org/10.1093/toxsci/kfm052

Martinello, T., Bronzini, I., Maccatrozzo, L., Mollo, A., Sampaolesi, M., Mascarello, F., Decaminada, M., & Patruno, M. (2011). Canine adipose-derived-mesenchymal stem cells do not lose stem features after a long-term cryopreservation. *Research in Veterinary Science*, *91*(1), 18–24. https://doi.org/10.1016/j.rvsc.2010.07.024

Martínez de Toda, I., Maté, I., Vida, C., Cruces, J., & De la Fuente, M. (2016). Immune function parameters as markers of biological age and predictors of longevity. *Aging*, *8*(11), 3110–3119. https://doi.org/10.18632/aging.101116

Martinez Guimera, A., Welsh, C., Dalle Pezze, P., Fullard, N., Nelson, G., Roger, M. F., Przyborski, S. A., & Shanley, D. P. (2017). Systems modelling ageing: From single senescent cells to simple multi-cellular models (T. B. Kirkwood & V. I. Korolchuk, Eds.). *Essays in Biochemistry*, *61*(3), 369–377. https://doi.org/10.1042/EBC20160087

Marx, C., Silveira, M. D., Selbach, I., da Silva, A. S., Braga, L. M. G. d. M., Camassola, M., & Nardi, N. B. (2014). Acupoint Injection of Autologous Stromal Vascular Fraction and Allogeneic Adipose-Derived Stem Cells to Treat Hip Dysplasia in Dogs. *Stem Cells International*, *2014*(391274). https://doi.org/https://doi.org/10.1155/2014/391274

McArdle, A., H. Dillmann, W., Mestril, R., A. Faulkner, J., & J. Jackson, M. (2004). Overexpression of HSP70 in mouse skeletal muscle protects against muscle damage and age-related muscle dysfunction. *The FASEB Journal*, *18*(2), 1–12. https://doi.org/10.1096/fj.03-0395fje

Mendillo, M. L., Santagata, S., Koeva, M., Bell, G. W., Hu, R., Tamimi, R. M., Fraenkel, E., Ince, T. A., Whitesell, L., & Lindquist, S. (2012). HSF1 Drives a Transcriptional Program Distinct from Heat Shock to Support Highly Malignant Human Cancers. *Cell*, *150*(3), 549–562. https://doi.org/10.1016/j.cell.2012.06.031

Metzler, B., Abia, R., Ahmad, M., Wernig, F., Pachinger, O., Hu, Y., & Xu, Q. (2003). Activation of Heat Shock Transcription Factor 1 in Atherosclerosis. *The American Journal of Pathology*, *162*(5), 1669–1676. https://doi.org/10.1016/S0002-9440(10)64301-5

Meyer, K., & Selbach, M. (2015). Quantitative affinity purification mass spectrometry: A versatile technology to study protein–protein interactions. *Frontiers in Genetics*, *6*. https://doi.org/10.3389/fgene.2015.00237

Mi, H., Ebert, D., Muruganujan, A., Mills, C., Albou, L.-P., Mushayamaha, T., & Thomas, P. D. (2021). PANTHER version 16: A revised family classification, tree-based classification tool, enhancer regions and extensive API. *Nucleic Acids Research*, *49*(D1), D394–D403. https://doi.org/10.1093/nar/gkaa1106

Mikhailov, A., & Rieder, C. L. (2002). Cell cycle: Stressed out of mitosis. *Current biology: CB*, *12*(9), R331–333. https://doi.org/10.1016/s0960-9822(02)00833-3

Milisav, I. (2011). Cellular Stress Responses (S. Wislet-Gendebien, Ed.). In S. Wislet-Gendebien (Ed.), *Advances in Regenerative Medicine*. InTech. https://doi.org/10.5772/26118

Milo, R. (2013). What is the total number of protein molecules per cell volume? A call to rethink some published values. *BioEssays*, *35*(12), 1050–1055. https://doi.org/10.1002/bies.201300066

Mine, S., Fortunel, N. O., Pageon, H., & Asselineau, D. (2008). Aging Alters Functionally Human Dermal Papillary Fibroblasts but Not Reticular Fibroblasts: A New View of Skin Morphogenesis and Aging. *PLOS ONE*, *3*(12), e4066. https://doi.org/10.1371/journal.pone.0004066

Miseta, A., & Csutora, P. (2000). Relationship Between the Occurrence of Cysteine in Proteins and the Complexity of Organisms. *Molecular Biology and Evolution*, *17*(8), 1232–1239. https://doi.org/10.1093/oxfordjournals.molbev.a026406

Miyamoto, Y., Saiwaki, T., Yamashita, J., Yasuda, Y., Kotera, I., Shibata, S., Shigeta, M., Hiraoka, Y., Haraguchi, T., & Yoneda, Y. (2004). Cellular stresses induce the nuclear accumulation of importin and cause a conventional nuclear import block. *Journal of Cell Biology*, *165*(5), 617–623. https://doi.org/10.1083/jcb.200312008

Mohyeddin Bonab, M., Ali Sahraian, M., Aghsaie, A., Ahmadi Karvigh, S., Massoud Hosseinian, S., Nikbin, B., Lotfi, J., Khorramnia, S., Reza Motamed, M., Togha, M., Hossien Harirchian, M., Beladi Moghadam, N., Alikhani, K., Yadegari, S., Jafarian, S., & Reza Gheini, M. (2012). Autologous Mesenchymal Stem Cell Therapy in Progressive Multiple Sclerosis: An Open Label Study. *Current Stem Cell Research & Therapy*, *7*(6), 407–414. https://doi.org/10.2174/157488812804484648

Montague, J. (2019). The 'unwarranted hype' of stem cell therapies. Retrieved January 21, 2021, from https://www.bbc.com/future/article/20190819-the-unwarranted-hype-of-stem-cell-therapies-for-autism-ms

Morimoto, R. I. (1998). Regulation of the heat shock transcriptional response: Cross talk between a family of heat shock factors, molecular chaperones, and negative regulators. *Genes & Development*, *12*(24), 3788–3796. https://doi.org/10.1101/gad.12.24.3788

Morimoto, R. I. (2008). Proteotoxic stress and inducible chaperone networks in neurodegenerative disease and aging. *Genes & Development*, *22*(11), 1427–1438. https://doi.org/10.1101/gad.1657108

Morishima, Y., Wang, A. M., Yu, Z., Pratt, W. B., Osawa, Y., & Lieberman, A. P. (2008). CHIP deletion reveals functional redundancy of E3 ligases in promoting degradation of both signaling proteins and expanded glutamine proteins. *Human Molecular Genetics*, *17*(24), 3942–3952. https://doi.org/10.1093/hmg/ddn296

Mosser, D. D., Ho, S., & Glover, J. R. (2004). Saccharomyces cerevisiae Hsp104 Enhances the Chaperone Capacity of Human Cells and Inhibits Heat Stress-Induced Proapoptotic Signaling. *Biochemistry*, *43*(25), 8107–8115. https://doi.org/10.1021/bi0493766

Motojima, F. (2015). How do chaperonins fold protein? *BIOPHYSICS*, *11*(0), 93–102. https://doi.org/10.2142/biophysics.11.93

Motta, S., & Pappalardo, F. (2013). Mathematical modeling of biological systems. *Briefings in Bioinformatics*, *14*(4), 411–422. https://doi.org/10.1093/bib/bbs061

MS Society UK. (2019). First results of new stem cell therapy trial announced. Retrieved January 27, 2021, from https://www.mssociety.org.uk/research/latest-research/latest-research-news-and-blogs/first-results-of-new-stem-cell-therapy-trial-announced

Munneke, J. M., Spruit, M. J., Cornelissen, A. S., van Hoeven, V., Voermans, C., & Hazenberg, M. D. (2016). The Potential of Mesenchymal Stromal Cells as Treatment for Severe Steroid-Refractory Acute Graft-Versus-Host Disease: A Critical Review of the Literature. *Transplantation*, *100*(11), 2309–2314. https://doi.org/10.1097/TP.0000000000001029

Nadeau, S. I., & Landry, J. (2007). Mechanisms of Activation and Regulation of the Heat Shock-Sensitive Signaling Pathways (P. Csermely & L. Vígh, Eds.). In P. Csermely & L. Vígh (Eds.), *Molecular Aspects of the Stress Response: Chaperones, Membranes and Networks*. New York, NY, Springer New York. https://doi.org/10.1007/978-0-387-39975-1_10

Nader, M., Khalil, B., Kattuah, W., Dzimiri, N., & Bakheet, D. (2020). Striatin translocates to the cytosol of apoptotic cells and is proteolytically cleaved in a caspase 3-dependent manner. *Heliyon*, *6*(9), e04990. https://doi.org/10.1016/j.heliyon.2020.e04990

Naesens, M. (2011). Replicative senescence in kidney aging, renal disease, and renal transplantation. *Discovery Medicine*, *11*(56), 65–75.

Neef, D. W., Jaeger, A. M., Gomez-Pastor, R., Willmund, F., Frydman, J., & Thiele, D. J. (2014). A direct regulatory interaction between chaperonin TRiC and stress-responsive transcription factor HSF1. *Cell Reports*, *9*(3), 955–966. https://doi.org/10.1016/j.celrep.2014.09.056

Németh, K., Leelahavanichkul, A., Yuen, P. S. T., Mayer, B., Parmelee, A., Doi, K., Robey, P. G., Leelahavanichkul, K., Koller, B. H., Brown, J. M., Hu, X., Jelinek, I., Star, R. A., & Mezey, E. (2009). Bone marrow stromal cells attenuate sepsis via prostaglandin E(2)-dependent reprogramming of host macrophages to increase their interleukin-10 production. *Nature Medicine*, *15*(1), 42–49. https://doi.org/10.1038/nm.1905

Neves, J., Demaria, M., Campisi, J., & Jasper, H. (2015). Of Flies, Mice, and Men: Evolutionarily Conserved Tissue Damage Responses and Aging. *Developmental Cell*, *32*(1), 9–18. https://doi.org/10.1016/j.devcel.2014.11.028

Newman, M. E. J. (2006a). Finding community structure in networks using the eigenvectors of matrices. *Physical Review E*, *74*(3), 036104. https://doi.org/10.1103/PhysRevE.74.036104

Newman, M. E. J. (2006b). Modularity and community structure in networks. *Proceedings of the National Academy of Sciences*, *103*(23), 8577–8582. https://doi.org/10.1073/pnas.0601602103

Nillegoda, N. B., Kirstein, J., Szlachcic, A., Berynskyy, M., Stank, A., Stengel, F., Arnsburg, K., Gao, X., Scior, A., Aebersold, R., Guilbride, D. L., Wade, R. C., Morimoto, R. I., Mayer, M. P., & Bukau, B. (2015). Crucial HSP70 co-

chaperone complex unlocks metazoan protein disaggregation. *Nature*, *524*(7564), 247–251. https://doi.org/10.1038/nature14884

Njemini, R., Bautmans, I., Onyema, O. O., Van Puyvelde, K., Demanet, C., & Mets, T. (2011). Circulating Heat Shock Protein 70 in Health, Aging and Disease. *BMC Immunology*, *12*(1), 24. https://doi.org/10.1186/1471-2172-12-24

Nollen, E. A. A., Garcia, S. M., van Haaften, G., Kim, S., Chavez, A., Morimoto, R. I., & Plasterk, R. H. A. (2004). From The Cover: Genome-wide RNA interference screen identifies previously undescribed regulators of polyglutamine aggregation. *Proceedings of the National Academy of Sciences*, *101*(17), 6403–6408. https://doi.org/10.1073/pnas.0307697101

Novelle, M. G., Davis, A., Price, N. L., Ali, A., Fürer-Galvan, S., Zhang, Y., Becker, K., Bernier, M., & de Cabo, R. (2015). Caloric restriction induces heat shock response and inhibits B16F10 cell tumorigenesis both in vitro and in vivo. *Aging*, *7*(4), 233–240. https://doi.org/10.18632/aging.100732

O'Connor, C. M., & Adams, J. U. (2010). *Essentials of Cell Biology*. Cambridge, MA, NPG Education.

Ogrodnik, M., Miwa, S., Tchkonia, T., Tiniakos, D., Wilson, C. L., Lahat, A., Day, C. P., Burt, A., Palmer, A., Anstee, Q. M., Grellscheid, S. N., Hoeijmakers, J. H. J., Barnhoorn, S., Mann, D. A., Bird, T. G., Vermeij, W. P., Kirkland, J. L., Passos, J. F., von Zglinicki, T., & Jurk, D. (2017). Cellular senescence drives age-dependent hepatic steatosis. *Nature Communications*, *8*(1), 15691. https://doi.org/10.1038/ncomms15691

Oh, K.-W., Moon, C., Kim, H. Y., Oh, S.-i., Park, J., Lee, J. H., Chang, I. Y., Kim, K. S., & Kim, S. H. (2015). Phase I Trial of Repeated Intrathecal Autologous Bone Marrow-Derived Mesenchymal Stromal Cells in Amyotrophic Lateral Sclerosis. *STEM CELLS Translational Medicine*, *4*(6), 590–597. https://doi.org/https://doi.org/10.5966/sctm.2014-0212

Olde Riekerink, R. G. M., Barkema, H. W., & Stryhn, H. (2007). The effect of season on somatic cell count and the incidence of clinical mastitis. *Journal of Dairy Science*, *90*(4), 1704–1715. https://doi.org/10.3168/jds.2006-567

Pal, S., & Sharma, R. (2020). A mathematical model of heat shock response to study the competition between protein folding and aggregation. *bioRxiv*, 2020.04.13.039123. https://doi.org/10.1101/2020.04.13.039123

Park, H. G., Han, S. I., Oh, S. Y., & Kang, H. S. (2005). Cellular responses to mild heat stress. *Cellular and Molecular Life Sciences*, *62*(1), 10–23. https://doi.org/10.1007/s00018-004-4208-7

Passos, J. F., Saretzki, G., Ahmed, S., Nelson, G., Richter, T., Peters, H., Wappler, I., Birket, M. J., Harold, G., Schaeuble, K., Birch-Machin, M. A., Kirkwood, T. B. L., & von Zglinicki, T. (2007). Mitochondrial Dysfunction Accounts for the Stochastic Heterogeneity in Telomere-Dependent Senescence (T. De Lange, Ed.). *PLoS Biology*, *5*(5), e110. https://doi.org/10.1371/journal.pbio.0050110

Patil, P., Niedernhofer, L. J., Robbins, P. D., Lee, J., Sowa, G., & Vo, N. (2018). Cellular Senescence in Intervertebral Disc Aging and Degeneration. *Current Molecular Biology Reports*, *4*(4), 180–190. https://doi.org/10.1007/s40610-018-0108-8

Pavel, M., Imarisio, S., Menzies, F. M., Jimenez-Sanchez, M., Siddiqi, F. H., Wu, X., Renna, M., O'Kane, C. J., Crowther, D. C., & Rubinsztein, D. C. (2016).

CCT complex restricts neuropathogenic protein aggregation via autophagy. *Nature Communications*, *7*(1), 13821. https://doi.org/10.1038/ncomms13821

Petersen, K. F. (2003). Mitochondrial Dysfunction in the Elderly: Possible Role in Insulin Resistance. *Science*, *300*(5622), 1140–1142. https://doi.org/10.1126/science.1082889

Petre, I., Mizera, A., Hyder, C. L., Meinander, A., Mikhailov, A., Morimoto, R. I., Sistonen, L., Eriksson, J. E., & Back, R.-J. (2011). A simple mass-action model for the eukaryotic heat shock response and its mathematical validation. *Natural Computing*, *10*(1), 595–612. https://doi.org/10.1007/s11047-010-9216-y

Petsko, G. A., & Ringe, D. (2009). *Protein structure and function* [OCLC: 845361937]. London, Oxford Univ. Press [u.a.]

Petta, I., Bougarne, N., Vandewalle, J., Dejager, L., Vandevyver, S., Ballegeer, M., Desmet, S., Thommis, J., De Cauwer, L., Lievens, S., Libert, C., Tavernier, J., & De Bosscher, K. (2017). Glucocorticoid Receptor-mediated transactivation is hampered by Striatin-3, a novel interaction partner of the receptor. *Scientific Reports*, *7*(1), 8941. https://doi.org/10.1038/s41598-017-09246-6

Phillip, J. M., Aifuwa, I., Walston, J., & Wirtz, D. (2015). The Mechanobiology of Aging. *Annual Review of Biomedical Engineering*, *17*(1), 113–141. https://doi.org/10.1146/annurev-bioeng-071114-040829

Phipps, S. M. O., Berletch, J. B., Andrews, L. G., & Tollefsbol, T. O. (2007). Aging Cell Culture (T. O. Tollefsbol, Ed.). In T. O. Tollefsbol (Ed.), *Biological Aging*. Totowa, NJ, Humana Press. https://doi.org/10.1007/978-1-59745-361-5_2

Piechota, M., Sunderland, P., Wysocka, A., Nalberczak, M., Sliwinska, M. A., Radwanska, K., & Sikora, E. (2016). Is senescence-associated -galactosidase a marker of neuronal senescence? *Oncotarget*, *7*(49), 81099–81109. https://doi.org/10.18632/oncotarget.12752

Pignolo, R. J., Passos, J. F., Khosla, S., Tchkonia, T., & Kirkland, J. L. (2020). Reducing Senescent Cell Burden in Aging and Disease. *Trends in Molecular Medicine*, *26*(7), 630–638. https://doi.org/10.1016/j.molmed.2020.03.005

Pittenger, M. F., Discher, D. E., Péault, B. M., Phinney, D. G., Hare, J. M., & Caplan, A. I. (2019). Mesenchymal stem cell perspective: Cell biology to clinical progress. *npj Regenerative Medicine*, *4*(1), 1–15. https://doi.org/10.1038/s41536-019-0083-6

Powers, E. T., Morimoto, R. I., Dillin, A., Kelly, J. W., & Balch, W. E. (2009). Biological and Chemical Approaches to Diseases of Proteostasis Deficiency. *Annual Review of Biochemistry*, *78*(1), 959–991. https://doi.org/10.1146/annurev.biochem.052308.114844

Pratt, W. B., & Toft, D. O. (2003). Regulation of Signaling Protein Function and Trafficking by the hsp90/hsp70-Based Chaperone Machinery. *Experimental Biology and Medicine*, *228*(2), 111–133. https://doi.org/10.1177/153537020322800201

Pyo, J.-O., Yoo, S.-M., Ahn, H.-H., Nah, J., Hong, S.-H., Kam, T.-I., Jung, S., & Jung, Y.-K. (2013). Overexpression of Atg5 in mice activates autophagy and extends lifespan. *Nature Communications*, *4*(1), 2300. https://doi.org/10.1038/ncomms3300

Qian, S.-B., McDonough, H., Boellmann, F., Cyr, D. M., & Patterson, C. (2006). CHIP-mediated stress recovery by sequential ubiquitination of substrates and Hsp70. *Nature*, *440*(7083), 551–555. https://doi.org/10.1038/nature04600

Qiu, X.-B., Shao, Y.-M., Miao, S., & Wang, L. (2006). The diversity of the DnaJ/Hsp40 family, the crucial partners for Hsp70 chaperones. *Cellular and Molecular Life Sciences*, *63*(22), 2560–2570. https://doi.org/10.1007/s00018-006-6192-6

Qu, Z., Titus, A. S. C. L. S., Xuan, Z., & D'Mello, S. R. (2018). Neuroprotection by Heat Shock Factor-1 (HSF1) and Trimerization-Deficient Mutant Identifies Novel Alterations in Gene Expression. *Scientific Reports*, *8*(1), 17255. https://doi.org/10.1038/s41598-018-35610-1

Quintana-Gallardo, L., Martín-Benito, J., Marcilla, M., Espadas, G., Sabidó, E., & Valpuesta, J. M. (2019). The cochaperone CHIP marks Hsp70- and Hsp90-bound substrates for degradation through a very flexible mechanism. *Scientific Reports*, *9*(1), 5102. https://doi.org/10.1038/s41598-019-41060-0

Radons, J. (2016). The human HSP70 family of chaperones: Where do we stand? *Cell Stress and Chaperones*, *21*(3), 379–404. https://doi.org/10.1007/s12192-016-0676-6

Rampelt, H., Kirstein-Miles, J., Nillegoda, N. B., Chi, K., Scholz, S. R., Morimoto, R. I., & Bukau, B. (2012). Metazoan Hsp70 machines use Hsp110 to power protein disaggregation: Disaggregation by animal Hsp110-Hsp70-Hsp40. *The EMBO Journal*, *31*(21), 4221–4235. https://doi.org/10.1038/emboj.2012.264

Rand, J. D., & Grant, C. M. (2006). The Thioredoxin System Protects Ribosomes against Stress-induced Aggregation. *Molecular Biology of the Cell*, *17*(1), 387–401. https://doi.org/10.1091/mbc.e05-06-0520

Raychaudhuri, S., Loew, C., Körner, R., Pinkert, S., Theis, M., Hayer-Hartl, M., Buchholz, F., & Hartl, F. U. (2014). Interplay of Acetyltransferase EP300 and the Proteasome System in Regulating Heat Shock Transcription Factor 1. *Cell*, *156*(5), 975–985. https://doi.org/10.1016/j.cell.2014.01.055

Raynes, D. A., & Guerriero, V. (1998). Inhibition of Hsp70 ATPase activity and protein renaturation by a novel Hsp70-binding protein. *The Journal of Biological Chemistry*, *273*(49), 32883–32888. https://doi.org/10.1074/jbc.273.49.32883

Retraction: Spontaneous Human Adult Stem Cell Transformation. (2010). *Cancer Research*, *70*(16), 6682–6682. https://doi.org/10.1158/0008-5472.CAN-10-2451

Richardson, S. M., Kalamegam, G., Pushparaj, P. N., Matta, C., Memic, A., Khademhosseini, A., Mobasheri, R., Poletti, F. L., Hoyland, J. A., & Mobasheri, A. (2016). Mesenchymal stem cells in regenerative medicine: Focus on articular cartilage and intervertebral disc regeneration. *Methods*, *99*, 69–80. https://doi.org/10.1016/j.ymeth.2015.09.015

Rieger, T. R., Morimoto, R. I., & Hatzimanikatis, V. (2005). Mathematical Modeling of the Eukaryotic Heat-Shock Response: Dynamics of the hsp70 Promoter. *Biophysical Journal*, *88*(3), 1646–1658. https://doi.org/10.1529/biophysj.104.055301

Robbins, E., Levine, E. M., & Eagle, H. (1970). Morphologic changes accompanying senescence of cultured human diploid cells. *The Journal of Experimental Medicine*, *131*(6), 1211–1222. https://doi.org/10.1084/jem.131.6.1211

Roberts, R. M., Smith, G. W., Bazer, F. W., Cibelli, J., Seidel, G. E., Bauman, D. E., Reynolds, L. P., & Ireland, J. J. (2009). Farm Animal Research in Crisis. *Science*, *324*(5926), 468–469. https://doi.org/10.1126/science.1168521

Roncarati, D., & Scarlato, V. (2017). Regulation of heat-shock genes in bacteria: From signal sensing to gene expression output. *FEMS microbiology reviews*, *41*(4), 549–574. https://doi.org/10.1093/femsre/fux015

Roodveldt, C., Bertoncini, C. W., Andersson, A., van der Goot, A. T., Hsu, S.-T., Fernández-Montesinos, R., de Jong, J., van Ham, T. J., Nollen, E. A., Pozo, D., Christodoulou, J., & Dobson, C. M. (2009). Chaperone proteostasis in Parkinson's disease: Stabilization of the Hsp70/-synuclein complex by Hip. *The EMBO Journal*, *28*(23), 3758–3770. https://doi.org/10.1038/emboj.2009.298

Rossignol, R., Gilkerson, R., Aggeler, R., Yamagata, K., Remington, S. J., & Capaldi, R. A. (2004). Energy substrate modulates mitochondrial structure and oxidative capacity in cancer cells. *Cancer Research*, *64*(3), 985–993. https://doi.org/10.1158/0008-5472.can-03-1101

Rubinov, M., & Sporns, O. (2010). Complex network measures of brain connectivity: Uses and interpretations. *NeuroImage*, *52*(3), 1059–1069. https://doi.org/10.1016/j.neuroimage.2009.10.003

Rubio, D., Garcia-Castro, J., Martín, M. C., de la Fuente, R., Cigudosa, J. C., Lloyd, A. C., & Bernad, A. (2005). Spontaneous Human Adult Stem Cell Transformation. *Cancer Research*, *65*(8), 3035–3039. https://doi.org/10.1158/0008-5472.CAN-04-4194

Rühle, A., Thomsen, A., Saffrich, R., Voglstätter, M., Bieber, B., Sprave, T., Wuchter, P., Vaupel, P., Huber, P. E., Grosu, A.-L., & Nicolay, N. H. (2020). Multipotent mesenchymal stromal cells are sensitive to thermic stress – potential implications for therapeutic hyperthermia. *International Journal of Hyperthermia*, *37*(1), 430–441. https://doi.org/10.1080/02656736.2020.1758350

Ryan, M. T., & Pfanner, N. (2001). Hsp70 proteins in protein translocation, In *Advances in Protein Chemistry*. Elsevier. https://doi.org/10.1016/S0065-3233(01)59007-5

Sabath, N., Levy-Adam, F., Younis, A., Rozales, K., Meller, A., Hadar, S., Soueid-Baumgarten, S., & Shalgi, R. (2020). Cellular proteostasis decline in human senescence. *Proceedings of the National Academy of Sciences*, *117*(50), 31902–31913. https://doi.org/10.1073/pnas.2018138117

Saez, I., & Vilchez, D. (2014). The Mechanistic Links Between Proteasome Activity, Aging and Age-related Diseases. *Current Genomics*, *15*(1), 38–51. https://doi.org/10.2174/1389202915011403061133 44

Sala, A. J., Bott, L. C., & Morimoto, R. I. (2017). Shaping proteostasis at the cellular, tissue, and organismal level. *Journal of Cell Biology*, *216*(5), 1231–1241. https://doi.org/10.1083/jcb.201612111

Sart, S., Ma, T., & Li, Y. (2014). Preconditioning Stem Cells for *In Vivo* Delivery. *BioResearch Open Access*, *3*(4), 137–149. https://doi.org/10.1089/biores.2014.0012

Scheff, J. D., Stallings, J. D., Reifman, J., & Rakesh, V. (2015). Mathematical Modeling of the Heat-Shock Response in HeLa Cells. *Biophysical Journal*, *109*(2), 182–193. https://doi.org/10.1016/j.bpj.2015.06.027

Scherz-Shouval, R., Santagata, S., Mendillo, M. L., Sholl, L. M., Ben-Aharon, I., Beck, A. H., Dias-Santagata, D., Koeva, M., Stemmer, S. M., Whitesell, L., & Lindquist, S. (2014). The Reprogramming of Tumor Stroma by HSF1 Is a Potent Enabler of Malignancy. *Cell*, *158*(3), 564–578. https://doi.org/10.1016/j.cell.2014.05.045

Schimke, M. M., Marozin, S., & Lepperdinger, G. (2015). Patient-Specific Age: The Other Side of the Coin in Advanced Mesenchymal Stem Cell Therapy. *Frontiers in Physiology*, *6*. https://doi.org/10.3389/fphys.2015.00362

Schindelin, J., Arganda-Carreras, I., Frise, E., Kaynig, V., Longair, M., Pietzsch, T., Preibisch, S., Rueden, C., Saalfeld, S., Schmid, B., Tinevez, J.-Y., White, D. J., Hartenstein, V., Eliceiri, K., Tomancak, P., & Cardona, A. (2012). Fiji: An open-source platform for biological-image analysis. *Nature Methods*, *9*(7), 676–682. https://doi.org/10.1038/nmeth.2019

Schmidt, M., & Finley, D. (2014). Regulation of proteasome activity in health and disease. *Biochimica et Biophysica Acta (BBA) - Molecular Cell Research*, *1843*(1), 13–25. https://doi.org/10.1016/j.bbamcr.2013.08.012

Schmittgen, T. D., & Livak, K. J. (2008). Analyzing real-time PCR data by the comparative C T method. *Nature Protocols*, *3*(6), 1101–1108. https://doi.org/10.1038/nprot.2008.73

Schopf, F. H., Biebl, M. M., & Buchner, J. (2017). The HSP90 chaperone machinery. *Nature Reviews Molecular Cell Biology*, *18*(6), 345–360. https://doi.org/10.1038/nrm.2017.20

Schwanhäusser, B., Busse, D., Li, N., Dittmar, G., Schuchhardt, J., Wolf, J., Chen, W., & Selbach, M. (2011). Global quantification of mammalian gene expression control. *Nature*, *473*(7347), 337–342. https://doi.org/10.1038/nature10098

Servick, K. (2019). Another major drug candidate targeting the brain plaques of Alzheimer's disease has failed. What's left? *Science*. https://doi.org/10.1126/science.aax4236

Shannon, P. (2003). Cytoscape: A Software Environment for Integrated Models of Biomolecular Interaction Networks. *Genome Research*, *13*(11), 2498–2504. https://doi.org/10.1101/gr.1239303

Sharma, N., & Jeong, D. K. (2013). Stem cell research: A novel boulevard towards improved bovine mastitis management. *International Journal of Biological Sciences*, *9*(8), 818–829. https://doi.org/10.7150/ijbs.6901

Shatrova, A. N., Lyublinskaya, O. G., Borodkina, A. V., & Burova, E. B. (2016). Oxidative stress response of human fibroblasts and endometrial mesenchymal stem cells. *Cell and Tissue Biology*, *10*(1), 18–28. https://doi.org/10.1134/S1990519X16010090

Shemesh, N., Shai, N., & Ben-Zvi, A. (2013). Germline stem cell arrest inhibits the collapse of somatic proteostasis early in *Caenorhabditis elegans* adulthood. *Aging Cell*, *12*(5), 814–822. https://doi.org/10.1111/acel.12110

Shi, Y., Mosser, D. D., & Morimoto, R. I. (1998). Molecularchaperones as HSF1-specific transcriptional repressors. *Genes & Development*, *12*(5), 654–666. https://doi.org/10.1101/gad.12.5.654

Shibata, Y., & Morimoto, R. I. (2014). How the Nucleus Copes with Proteotoxic Stress. *Current Biology*, *24*(10), R463–R474. https://doi.org/10.1016/j.cub.2014.03.033

Shimi, T., Butin-Israeli, V., Adam, S. A., Hamanaka, R. B., Goldman, A. E., Lucas, C. A., Shumaker, D. K., Kosak, S. T., Chandel, N. S., & Goldman, R. D. (2011). The role of nuclear lamin B1 in cell proliferation and senescence. *Genes & Development*, *25*(24), 2579–2593. https://doi.org/10.1101/gad.179515.111

Shimoni, C., Goldstein, M., Ribarski-Chorev, I., Schauten, I., Nir, D., Strauss, C., & Schlesinger, S. (2020). Heat Shock Alters Mesenchymal Stem Cell Identity and Induces Premature Senescence. *Frontiers in Cell and Developmental Biology*, *8*. https://doi.org/10.3389/fcell.2020.565970

Shin, J. Y., Park, H. J., Kim, H. N., Oh, S. H., Bae, J.-S., Ha, H.-J., & Lee, P. H. (2014). Mesenchymal stem cells enhance autophagy and increase -amyloid clearance in Alzheimer disease models. *Autophagy*, *10*(1), 32–44. https://doi.org/10.4161/auto.26508

Shomura, Y., Dragovic, Z., Chang, H.-C., Tzvetkov, N., Young, J. C., Brodsky, J. L., Guerriero, V., Hartl, F. U., & Bracher, A. (2005). Regulation of Hsp70 function by HspBP1: Structural analysis reveals an alternate mechanism for Hsp70 nucleotide exchange. *Molecular Cell*, *17*(3), 367–379. https://doi.org/10.1016/j.molcel.2004.12.023

Shorter, J. (2016). Engineering therapeutic protein disaggregases (D. G. Drubin, Ed.). *Molecular Biology of the Cell*, *27*(10), 1556–1560. https://doi.org/10.1091/mbc.E15-10-0693

Siegel, G., Kluba, T., Hermanutz-Klein, U., Bieback, K., Northoff, H., & Schäfer, R. (2013). Phenotype, donor age and gender affect function of human bone marrow-derived mesenchymal stromal cells. *BMC Medicine*, *11*(1), 146. https://doi.org/10.1186/1741-7015-11-146

Silva, C. F., Sartorelli, E. S., Castilho, A. C. S., Satrapa, R. A., Puelker, R. Z., Razza, E. M., Ticianelli, J. S., Eduardo, H. P., Loureiro, B., & Barros, C. M. (2013). Effects of heat stress on development, quality and survival of Bos indicus and Bos taurus embryos produced in vitro. *Theriogenology*, *79*(2), 351–357. https://doi.org/10.1016/j.theriogenology.2012.10.003

Sisoula, C., & Gonos, E. S. (2011). CHIP E3 ligase regulates mammalian senescence by modulating the levels of oxidized proteins. *Mechanisms of Ageing and Development*, *132*(5), 269–272. https://doi.org/10.1016/j.mad.2011.04.003

Sivéry, A., Courtade, E., & Thommen, Q. (2016). A minimal titration model of the mammalian dynamical heat shock response. *Physical Biology*, *13*(6), 066008. https://doi.org/10.1088/1478-3975/13/6/066008

Smith, R. K. W., Werling, N. J., Dakin, S. G., Alam, R., Goodship, A. E., & Dudhia, J. (2013). Beneficial Effects of Autologous Bone Marrow-Derived Mesenchymal Stem Cells in Naturally Occurring Tendinopathy. *PLOS ONE*, *8*(9), e75697. https://doi.org/10.1371/journal.pone.0075697

Son, H. N., Chi, H. N. Q., Chung, D. C., & Long, L. T. (2019). Morphological changes during replicative senescence in bovine ovarian granulosa cells. *Cell Cycle*, *18*(13), 1490–1497. https://doi.org/10.1080/15384101.2019.1624108

Song, J., & Singh, M. (2013). From hub proteins to hub modules: The relationship between essentiality and centrality in the yeast interactome at different scales of organization. *PLoS computational biology*, *9*(2), e1002910. https://doi.org/10.1371/journal.pcbi.1002910

Soria, B., Martin-Montalvo, A., Aguilera, Y., Mellado-Damas, N., López-Beas, J., Herrera-Herrera, I., López, E., Barcia, J. A., Alvarez-Dolado, M., Hmadcha, A., & Capilla-González, V. (2019). Human Mesenchymal Stem Cells Prevent Neurological Complications of Radiotherapy. *Frontiers in Cellular Neuroscience*, *13*, 204. https://doi.org/10.3389/fncel.2019.00204

Sousa, R. (2014). Structural mechanisms of chaperone mediated protein disaggregation. *Frontiers in Molecular Biosciences*, *1*. https://doi.org/10.3389/fmolb.2014.00012

Spiess, C., Meyer, A. S., Reissmann, S., & Frydman, J. (2004). Mechanism of the eukaryotic chaperonin: Protein folding in the chamber of secrets. *Trends in Cell Biology*, *14*(11), 598–604. https://doi.org/10.1016/j.tcb.2004.09.015

Srivastava, S., Savanur, M. A., Sinha, D., Birje, A., R, V., Saha, P. P., & D'Silva, P. (2017). Regulation of mitochondrial protein import by the nucleotide exchange factors GrpEL1 and GrpEL2 in human cells. *The Journal of Biological Chemistry*, *292*(44), 18075–18090. https://doi.org/10.1074/jbc.M117.788463

Strassburg, S., Richardson, S. M., Freemont, A. J., & Hoyland, J. A. (2010). Co-culture induces mesenchymal stem cell differentiation and modulation of the degenerate human nucleus pulposus cell phenotype. *Regenerative Medicine*, *5*(5), 701–711. https://doi.org/10.2217/rme.10.59

Straus, D., Walter, W., & Gross, C. A. (1990). DnaK, DnaJ, and GrpE heat shock proteins negatively regulate heat shock gene expression by controlling the synthesis and stability of sigma 32. *Genes & Development*, *4*(12A), 2202–2209. https://doi.org/10.1101/gad.4.12a.2202

Suzuki, M., McHugh, J., Tork, C., Shelley, B., Hayes, A., Bellantuono, I., Aebischer, P., & Svendsen, C. N. (2008). Direct Muscle Delivery of GDNF With Human Mesenchymal Stem Cells Improves Motor Neuron Survival and Function in a Rat Model of Familial ALS. *Molecular Therapy*, *16*(12), 2002–2010. https://doi.org/10.1038/mt.2008.197

Swift, J., Ivanovska, I. L., Buxboim, A., Harada, T., Dingal, P. C. D. P., Pinter, J., Pajerowski, J. D., Spinler, K. R., Shin, J.-W., Tewari, M., Rehfeldt, F., Speicher, D. W., & Discher, D. E. (2013). Nuclear Lamin-A Scales with Tissue Stiffness and Enhances Matrix-Directed Differentiation. *Science*, *341*(6149), 1240104. https://doi.org/10.1126/science.1240104

Szklarczyk, D., Gable, A. L., Lyon, D., Junge, A., Wyder, S., Huerta-Cepas, J., Simonovic, M., Doncheva, N. T., Morris, J. H., Bork, P., Jensen, L. J., & Mering, C. v. (2019). STRING v11: Protein–protein association networks with increased coverage, supporting functional discovery in genome-wide experimental datasets. *Nucleic Acids Research*, *47*(D1), D607–D613. https://doi.org/10.1093/nar/gky1131

Szymańska, Z., & Zylicz, M. (2009). Mathematical modeling of heat shock protein synthesis in response to temperature change. *Journal of Theoretical Biology*, *259*(3), 562–569. https://doi.org/10.1016/j.jtbi.2009.03.021

Tajiri, N., Duncan, K., Borlongan, M., Pabon, M., Acosta, S., de la Pena, I., Hernadez-Ontiveros, D., Lozano, D., Aguirre, D., Reyes, S., Sanberg, P., Eve, D., Borlongan, C., & Kaneko, Y. (2014). Adult Stem Cell Transplantation: Is Gender a Factor in Stemness? *International Journal of Molecular Sciences*, *15*(9), 15225–15243. https://doi.org/10.3390/ijms150915225

Takaki, E., & Nakai, A. (2016). Regulation of HSF Activation and Repression (A. Nakai, Ed.). In A. Nakai (Ed.), *Heat Shock Factor*. Tokyo, Springer Japan. https://doi.org/10.1007/978-4-431-55852-1_3

Tam, S., Geller, R., Spiess, C., & Frydman, J. (2006). The chaperonin TRiC controls polyglutamine aggregation and toxicity through subunit-specific interactions. *Nature Cell Biology*, *8*(10), 1155–1162. https://doi.org/10.1038/ncb1477

Tanaka, K., & Matsuda, N. (2014). Proteostasis and neurodegeneration: The roles of proteasomal degradation and autophagy. *Biochimica et Biophysica Acta (BBA) - Molecular Cell Research*, *1843*(1), 197–204. https://doi.org/10.1016/j.bbamcr.2013.03.012

Tang, Y., Liu, L., Wang, P., Chen, D., Wu, Z., & Tang, C. (2017). Periostin promotes migration and osteogenic differentiation of human periodontal ligament mesenchymal stem cells *via* the Jun amino-terminal kinases (JNK) pathway under inflammatory conditions. *Cell Proliferation*, *50*(6), e12369. https://doi.org/10.1111/cpr.12369

Tanguay, R. M., & Hightower, L. E. (Eds.). (2015). *The Big Book on Small Heat Shock Proteins* (Vol. 8). Cham, Springer International Publishing. https://doi.org/10.1007/978-3-319-16077-1

Tawo, R., Pokrzywa, W., Kevei, É., Akyuz, M. E., Balaji, V., Adrian, S., Höhfeld, J., & Hoppe, T. (2017). The Ubiquitin Ligase CHIP Integrates Proteostasis and Aging by Regulation of Insulin Receptor Turnover. *Cell*, *169*(3), 470–482.e13. https://doi.org/10.1016/j.cell.2017.04.003

The UniProt Consortium. (2019). UniProt: A worldwide hub of protein knowledge. *Nucleic Acids Research*, *47*(D1), D506–D515. https://doi.org/10.1093/nar/gky1049

Thermo Fisher Scientific. (2017). Protein Sample Preparation for Mass Spectrometry. Retrieved January 15, 2021, from https://www.thermofisher.com/uk/en/home/life-science/protein-biology/protein-biology-learning-center/protein-biology-resource-library/pierce-protein-methods/sample-preparation-mass-spectrometry.html

Tomlin, C. J., & Axelrod, J. D. (2007). Biology by numbers: Mathematical modelling in developmental biology. *Nature Reviews Genetics*, *8*(5), 331–340. https://doi.org/10.1038/nrg2098

Török, Z., Tsvetkova, N. M., Balogh, G., Horváth, I., Nagy, E., Pénzes, Z., Hargitai, J., Bensaude, O., Csermely, P., Crowe, J. H., Maresca, B., & Vígh, L. (2003). Heat shock protein coinducers with no effect on protein denaturation specifically modulate the membrane lipid phase. *Proceedings of the National Academy of Sciences*, *100*(6), 3131–3136. https://doi.org/10.1073/pnas.0438003100

Torres, N. V., & Santos, G. (2015). The (Mathematical) Modeling Process in Biosciences. *Frontiers in Genetics*, *6*. https://doi.org/10.3389/fgene.2015.00354

Uhlen, M., Fagerberg, L., Hallstrom, B. M., Lindskog, C., Oksvold, P., Mardinoglu, A., Sivertsson, A., Kampf, C., Sjostedt, E., Asplund, A., Olsson, I., Edlund, K., Lundberg, E., Navani, S., Szigyarto, C. A.-K., Odeberg, J., Djureinovic, D., Takanen, J. O., Hober, S., ... Ponten, F. (2015). Tissue-based map of the human proteome. *Science*, *347*(6220), 1260419–1260419. https://doi.org/10.1126/science.1260419

Ullah, I., Subbarao, R. B., & Rho, G. J. (2015). Human mesenchymal stem cells - current trends and future prospective. *Bioscience Reports*, *35*(2), e00191. https://doi.org/10.1042/BSR20150025

Urbaniak, A., Jablonska, K., Podhorska-Okolow, M., Ugorski, M., & Dziegiel, P. (2018). Prolactin-induced protein (PIP)-characterization and role in breast cancer progression. *American Journal of Cancer Research*, *8*(11), 2150–2164.

Valenzano, D. R., Aboobaker, A., Seluanov, A., & Gorbunova, V. (2017). Non-canonical aging model systems and why we need them. *The EMBO Journal*, *36*(8), 959–963. https://doi.org/10.15252/embj.201796837

Vallin, J., & Grantham, J. (2019). The role of the molecular chaperone CCT in protein folding and mediation of cytoskeleton-associated processes: Implications for cancer cell biology. *Cell Stress and Chaperones*, *24*(1), 17–27. https://doi.org/10.1007/s12192-018-0949-3

van Deursen, J. M. (2014). The role of senescent cells in ageing. *Nature*, *509*(7501), 439–446. https://doi.org/10.1038/nature13193

Velazquez, J. M., & Lindquist, S. (1984). Hsp70: Nuclear concentration during environmental stress and cytoplasmic storage during recovery. *Cell*, *36*(3), 655–662. https://doi.org/10.1016/0092-8674(84)90345-3

Verghese, J., Abrams, J., Wang, Y., & Morano, K. A. (2012). Biology of the heat shock response and protein chaperones: Budding yeast (Saccharomyces cerevisiae) as a model system. *Microbiology and molecular biology reviews: MMBR*, *76*(2), 115–158. https://doi.org/10.1128/MMBR.05018-11

Verma, P., Pfister, J. A., Mallick, S., & D'Mello, S. R. (2014). HSF1 Protects Neurons through a Novel Trimerization- and HSP-Independent Mechanism. *Journal of Neuroscience*, *34*(5), 1599–1612. https://doi.org/10.1523/JNEUROSCI.3039-13.2014

Vetter, I. R., Nowak, C., Nishimoto, T., Kuhlmann, J., & Wittinghofer, A. (1999). Structure of a Ran-binding domain complexed with Ran bound to a GTP analogue: Implications for nuclear transport. *Nature*, *398*(6722), 39–46. https://doi.org/10.1038/17969

Vilasi, S., Carrotta, R., Mangione, M. R., Campanella, C., Librizzi, F., Randazzo, L., Martorana, V., Marino Gammazza, A., Ortore, M. G., Vilasi, A., Pocsfalvi, G., Burgio, G., Corona, D., Palumbo Piccionello, A., Zummo, G., Bulone, D., Conway de Macario, E., Macario, A. J. L., San Biagio, P. L., & Cappello, F. (2014). Human Hsp60 with its mitochondrial import signal occurs in solution as heptamers and tetradecamers remarkably stable over a wide range of concentrations. *PloS One*, *9*(5), e97657. https://doi.org/10.1371/journal.pone.0097657

Vilchez, D., Saez, I., & Dillin, A. (2014). The role of protein clearance mechanisms in organismal ageing and age-related diseases. *Nature Communications*, *5*(1), 5659. https://doi.org/10.1038/ncomms6659

Volk, S. W., Wang, Y., & Hankenson, K. D. (2012). Effects of Donor Characteristics and Ex Vivo Expansion on Canine Mesenchymal Stem Cell Properties: Implications for MSC-Based Therapies. *Cell Transplantation*, *21*(10), 2189–2200. https://doi.org/10.3727/096368912X636821

Wang, J., Liao, L., Wang, S., & Tan, J. (2013). Cell therapy with autologous mesenchymal stem cells—how the disease process impacts clinical considerations. *Cytotherapy*, *15*(8), 893–904. https://doi.org/10.1016/j.jcyt.2013.01.218

Wang, Q., Li, X., Wang, Q., Xie, J., Xie, C., & Fu, X. (2019). Heat shock pretreatment improves mesenchymal stem cell viability by heat shock proteins and autophagy to prevent cisplatin-induced granulosa cell apoptosis. *Stem Cell Research & Therapy*, *10*(1), 348. https://doi.org/10.1186/s13287-019-1425-4

Weinmüllner, R., Zbiral, B., Becirovic, A., Stelzer, E. M., Nagelreiter, F., Schosserer, M., Lämmermann, I., Liendl, L., Lang, M., Terlecki-Zaniewicz, L., Andriotis, O., Mildner, M., Golabi, B., Waidhofer-Söllner, P., Schedle, K., Emsenhuber, G., Thurner, P. J., Tschachler, E., Gruber, F., & Grillari, J. (2020). Organotypic human skin culture models constructed with senescent fibroblasts show hallmarks of skin aging. *npj Aging and Mechanisms of Disease*, *6*(1), 1–7. https://doi.org/10.1038/s41514-020-0042-x

Welch, W. J., & Feramisco, J. R. (1984). Nuclear and nucleolar localization of the 72,000-dalton heat shock protein in heat-shocked mammalian cells. *The Journal of Biological Chemistry*, *259*(7), 4501–4513.

Wenk, M., Ba, Q., Erichsen, V., MacInnes, K., Wiese, H., Warscheid, B., & Koch, H.-G. (2012). A Universally Conserved ATPase Regulates the Oxidative Stress Response in *Escherichia coli*. *Journal of Biological Chemistry*, *287*(52), 43585–43598. https://doi.org/10.1074/jbc.M112.413070

Westerheide, S. D., Anckar, J., Stevens, S. M., Sistonen, L., & Morimoto, R. I. (2009). Stress-Inducible Regulation of Heat Shock Factor 1 by the Deacetylase SIRT1. *Science*, *323*(5917), 1063–1066. https://doi.org/10.1126/science.1165946

Willison, K. R. (2018). The substrate specificity of eukaryotic cytosolic chaperonin CCT. *Philosophical Transactions of the Royal Society B: Biological Sciences*, *373*(1749), 20170192. https://doi.org/10.1098/rstb.2017.0192

Wu, S., Hong, L., Wang, Y., Yu, J., Yang, J., Yang, J., Zhang, H., & Perrett, S. (2020). Kinetics of the conformational cycle of Hsp70 reveals the importance of the dynamic and heterogeneous nature of Hsp70 for its function. *Proceedings of the National Academy of Sciences*, *117*(14), 7814–7823. https://doi.org/10.1073/pnas.1914376117

Xia, C., Braunstein, Z., Toomey, A. C., Zhong, J., & Rao, X. (2018). S100 Proteins As an Important Regulator of Macrophage Inflammation. *Frontiers in Immunology*, *8*. https://doi.org/10.3389/fimmu.2017.01908

Yako, Y., Hayashi, T., Takeuchi, Y., Ishibashi, K., Kasai, N., Sato, N., Kuromiya, K., Ishikawa, S., & Fujita, Y. (2018). ADAM-like Decysin-1 (ADAMDEC1) is a positive regulator of Epithelial Defense Against Cancer (EDAC) that promotes apical extrusion of RasV12-transformed cells. *Scientific Reports*, *8*(1), 9639. https://doi.org/10.1038/s41598-018-27469-z

Yang, G., Heisenberger, C., Kos-Braun, I. C., Polacek, N., Grillari, J., Schosserer, M., & Koš, M. (2020). Cellular senescence and quiescence are associated with altered ribosomal RNA methylation and processing. *bioRxiv*, 2020.04.01.019653. https://doi.org/10.1101/2020.04.01.019653

Yang, R., Zheng, G., Ren, D., Chen, C., Zeng, C., Lu, W., & Li, H. (2018). The clinical significance and biological function of tropomyosin 4 in colon cancer. *Biomedicine & Pharmacotherapy*, *101*, 1–7. https://doi.org/10.1016/j.biopha.2018.01.166

Youn, D.-Y., Lee, D.-H., Lim, M.-H., Yoon, J.-S., Lim, J. H., Jung, S. E., Yeum, C. E., Park, C. W., Youn, H.-J., Lee, J.-S., Lee, S.-B., Ikawa, M., Okabe, M.,

Tsujimoto, Y., & Lee, J.-H. (2008). Bis deficiency results in early lethality with metabolic deterioration and involution of spleen and thymus. *American Journal of Physiology-Endocrinology and Metabolism*, *295*(6), E1349–E1357. https://doi.org/10.1152/ajpendo.90704.2008

Young, J. C., Hoogenraad, N. J., & Hartl, F. U. (2003). Molecular chaperones Hsp90 and Hsp70 deliver preproteins to the mitochondrial import receptor Tom70. *Cell*, *112*(1), 41–50. https://doi.org/10.1016/s0092-8674(02)01250-3

Zanotti, S., Kalajzic, I., Aguila, H. L., & Canalis, E. (2014). Sex and Genetic Factors Determine Osteoblastic Differentiation Potential of Murine Bone Marrow Stromal Cells (L. Malaval, Ed.). *PLoS ONE*, *9*(1), e86757. https://doi.org/10.1371/journal.pone.0086757

Zhang, H., Amick, J., Chakravarti, R., Santarriaga, S., Schlanger, S., McGlone, C., Dare, M., Nix, J. C., Scaglione, K. M., Stuehr, D. J., Misra, S., & Page, R. C. (2015). A Bipartite Interaction between Hsp70 and CHIP Regulates Ubiquitination of Chaperoned Client Proteins. *Structure*, *23*(3), 472–482. https://doi.org/10.1016/j.str.2015.01.003

Zhang, W., Xue, D., Yin, H., Wang, S., Li, C., Chen, E., Hu, D., Tao, Y., Yu, J., Zheng, Q., Gao, X., & Pan, Z. (2016). Overexpression of HSPA1A enhances the osteogenic differentiation of bone marrow mesenchymal stem cells via activation of the Wnt/-catenin signaling pathway. *Scientific Reports*, *6*(1), 27622. https://doi.org/10.1038/srep27622

Zhao, R., Davey, M., Hsu, Y.-C., Kaplanek, P., Tong, A., Parsons, A. B., Krogan, N., Cagney, G., Mai, D., Greenblatt, J., Boone, C., Emili, A., & Houry, W. A. (2005). Navigating the Chaperone Network: An Integrative Map of Physical and Genetic Interactions Mediated by the Hsp90 Chaperone. *Cell*, *120*(5), 715–727. https://doi.org/10.1016/j.cell.2004.12.024

Zhao, X., Jiang, M., & Wang, Z. (2019). TPM4 promotes cell migration by modulating F-actin formation in lung cancer. *OncoTargets and Therapy*, *12*, 4055–4063. https://doi.org/10.2147/OTT.S198542

Zheng, X., Krakowiak, J., Patel, N., Beyzavi, A., Ezike, J., Khalil, A. S., & Pincus, D. (2016). Dynamic control of Hsf1 during heat shock by a chaperone switch and phosphorylation. *eLife*, *5*, e18638. https://doi.org/10.7554/eLife.18638